Finger Vein Biometrics - An Analysis from Different Perspectives

by
Bernhard Prommegger

Cumulative dissertation submitted to the
Faculty of Natural Sciences, University of Salzburg
in partial fulfillment of the requirements
for the Doctoral Degree.

Thesis Supervisor
Univ.-Prof. Mag. Dr. Andreas Uhl

Department of Computer Sciences
University of Salzburg
Jakob Haringer Str. 2
5020 Salzburg, AUSTRIA

Salzburg, January 2021

Abstract

In our society, access to many activities or applications is restricted to authorized persons only, or at least it is necessary to keep track of who performed or accessed them. For this it is necessary to know or determine the identity of the persons involved. This can happen in different ways. Classic methods for this are, e.g. a handwritten signature, the presentation of an identification document or the query of passwords and PIN codes. Alternatively, biometric characteristics can also be used for authentication.

Biometric systems make it possible to recognize a person based on their behavioural and biological characteristics. The characteristics used for this must be differentiable, reproducible and usable for automated processing. Biometric systems have already found their way into our everyday life and are widely used, e.g. to unlock smartphones or for verifying the identity of a person at borders or at other access systems. The most widespread modalities are probably fingerprint and facial recognition. Other biometric recognition system utilize iris, voice, gait or the vascular pattern inside the human body for authentication.

This dissertation deals with the recognition of people based on the structure of the blood vessels inside the human finger, commonly referred to as finger vein biometrics. It is based on the assumption that the structure of the blood vessels within the finger is unique for every person and can thus be used for biometric recognition. Up to now, in finger vein biometrics the palm side (or palmar view) of the finger has been used nearly exclusively. There is little work that also use the opposite side of the finger (dorsal view), but all other perspectives are ignored completely. This is exactly the topic to which this work is tailored. It evaluates whether these additional views show similar or even better recognition rates than the commonly used perspectives or if they at least provide enough information to increase the recognition rates when they are used together with the currently used ones. Since there exists neither appropriate data sets nor suitable capturing devices to acquire different perspectives, such devices needs to get developed and built and data from a sufficient amount of subject needs to be acquired to enable scientific evaluations. Another focus of the work is the evaluation of the effect of longitudinal finger rotation (the finger is subject to rotation around the longitudinal axis of the finger) on the recognition rates and how such a rotation can be compensated or corrected. Finally, four different rotation invariant multi-camera systems are presented.

Abstract (German)

In unserem Leben gibt es viele Tätigkeiten oder Anwendungen bei denen es wichtig ist zu wissen wer diese ausführt bzw. dass diese nur von berechtigten Personen ausgeführt werden. Dafür ist es notwendig die Identität der handelnden Personen zu kennen bzw. festzustellen. Dies kann auf unterschiedliche Weise passieren. Klassische Methoden dafür sind z.B. die handschriftliche Unterschrift, das Vorlegen eines Ausweisdokuments oder das Abfragen von Passwörtern und PIN Codes. Alternativ dazu können auch biometrischen Merkmale für die Authentifizierung verwendet werden.

Biometrische Systeme ermöglichen es eine Person anhand seines Verhaltens und seiner biologischen Charakteristika zu erkennen. Die dafür verwendeten Charakteristika müssen zur Unterscheidung geeignet, reproduzierbar und für die automatisierte Bearbeitung einsetzbar sein. Biometrische Systeme haben längst den Einzug in unser Alltagsleben gefunden und werden weit verbreitet z.B. für das Entsperren von Smartphones, an Grenzen oder bei Zutrittssystemen eingesetzt. Die am weitesten verbreiteten Modalitäten sind wohl der Fingerabdruck und die Gesichtserkennung. Man kann aber auch andere Merkmale wie z.B. Iris, Stimme und Gang aber auch die Struktur der Blutgefäße für die Erkennung verwenden.

Diese Dissertation beschäftigt sich mit der Wiedererkennung von Personen anhand der Blutgefäße in den Fingern. Diese Modalität wird im allgemeinen als Fingervenenbiometrie bezeichnet und beruht auf der Annahme, dass die Struktur der Blutgefäße innerhalb des Körpers eindeutig ist und so einer einzelnen Person zugewiesen werden kann. Bis jetzt werden für die Fingervenebiometrie hauptsächlich die Innenseite des Fingers (palmare Sicht) verwendet. Es gibt zwar einige Arbeiten die auch die Außenseite verwenden (dorsale Ansicht), alle anderen Perspektiven werden aber ignoriert. Genau hier setzt diese Arbeit an. Es wird evaluiert ob diese Ansichten ähnlich gute oder sogar bessere Wiedererkennungsraten zulassen und ob eine gemeinsame Auswertung mehrerer Perspektiven zu einer höheren Genauigkeit führt. Da es für diese Auswertungen weder entsprechende Datensätze noch geeignete Aufnahmegeräte gibt müssen die dazu benötigten Geräte entwickelt und gebaut, sowie Daten aufgenommen und ausgewertet werden. Ein weiterer Schwerpunkt der Arbeit liegt in der Evaluierung der Auswirkung von längsseitiger Fingerrotation (der Finger wird um die Längsachse des Fingers gedreht) auf die Wiedererkennungsraten von Fingervenensystemen und wie man diese kompensieren bzw. korrigieren kann. Weiters werden vier Mehrkamerasysteme vorgestellt die invariant gegen längsseitige Fingerrotation sind.

Acknowledgments

I would like to thank all people who supported me throughout my studies and work at the University of Salzburg. In particular, I wish to to thank my advisor Andreas Uhl, who supported me throughout my PhD degree. Furthermore, I would like to thank all people of my research group, the Multimedia Signal Processing and Security Lab (WaveLab) at the University of Salzburg, in particular my colleagues and co-authors Christof Kauba, Michael Linortner and Georg Wimmer (in alphabetical order) for the fruitful collaboration.

This thesis would not have been possible without funding from the European Union's Horizon 2020 research and innovation program under grant agreement No. 700259 ("*PROTECT - Pervasive and UseR Focused BiomeTrics BordEr ProjeCT*"), the FFG KIRAS Project under grant 864785 ("*AUTFingerATM - Finger-based Biometrics for Austrian ATMs*") and the Austrian Science Fund (FWF) project no. P32201 ("*Advanced Methods and Applications for Fingervein Recognition*") which was co-funded by the Salzburg state government.

Last but not least, I would like to thank my wife Lola for the invaluable support she has always given me. It's just great when you can go through life with your love.

Salzburg, March 2021 *Bernhard Prommegger*

Contents

1. Introduction

In our society it is normal that you have to authenticate yourself for many activities or applications. Common situations are e.g. signing a contract, unlocking a phone, boarding on an aircraft or withdrawing money from a cash machine. Classical authentication techniques are handwritten signatures, identification documents, smart cards, passwords and pin codes. Besides these classical methods, biometrics offers a vital alternative. Biometric systems try to recognize individuals based on their behavioural and biological characteristics in an automated manner [21]. Biometrics will not replace classical authentication methods, but is a valuable addition to them.

1.1. Biometrics and Biometric Systems

Biometrics, or biometric recognition, is the automated recognition of human subjects based on their biological (physiological) characteristics and their behaviour utilizing biometric systems [21]. Besides other properties, biometric traits must be unique (all persons need to differ in terms of the characteristics), universal (everybody should have it), permanent (invariant over time), collectable (it must be possible to acquire the characteristic in real world applications) and accepted throughout the targeted user group (there should be no strong objections to the biometric) [11]. In general, biometric systems work as two-step processes: First the users have to be enrolled (registered) in the system so that they can be recognized in a second step. Figure 1.1 shows a generic model of biometric recognition system. It consists of four major building blocks: the capturing device, a feature extractor, an enrolment database and a comparison module. The capturing device is responsible for acquiring the biometric characteristics. It provides the captured biometric samples to the feature extractor. In case of the enrolment of a user, the extracted features are stored in the enrolment database for future use. Depending on the use-case, the enrolment databases can be either centralized or distributed (e.g. on smartcards). With recognition attempts, the biometric features are compared to those of the enrolment database. Recognition can be operated in two different modes: (1) verification and (2) identification. For verification the user of the system needs to lay claim of his identity. This reduces the enrolled users to a single entity. The system compares the acquired probe sample to the enrolled one and decides, e.g. based on a threshold, if the claim is correct (accept/reject decision). In contrast to this, biometric identification is based only on the biometric characteristics itself. Therefore, the probe sample needs to be compared to all subjects contained in the enrolment database. The return of such a search can be a list of candidates which finally needs be reduced to size 1 [6].

Commonly used biometric characteristics are face, fingerprint or iris, but there are also systems that use other characteristics such as voice, gait, keystroke dynamics or vascular patterns of different parts of the body. This thesis deals mainly with finger vein recognition, in particular with the effects of longitudinal finger rotation.

1.2. Finger Vein Recognition

Vascular pattern based recognition, commonly denoted as vein recognition, deals with the authentication of subjects based on the structure of the blood vessels inside the human body. There are several vascular pattern based systems. The majority of them uses either the human eye or

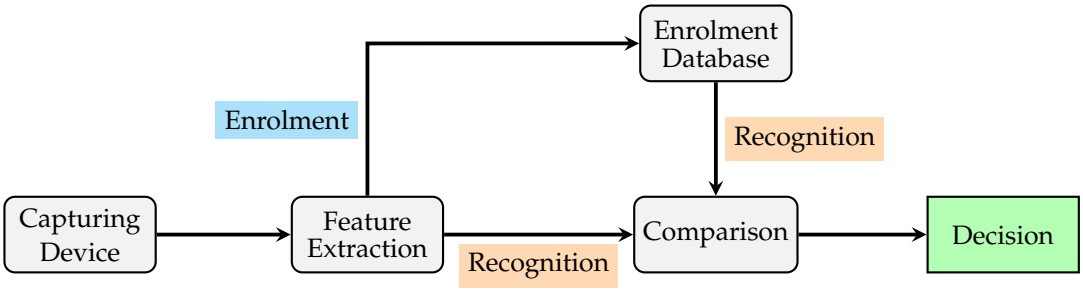

Figure 1.1.: Exemplary generic biometric system

the human hand (including its finger) as source for data acquisition. However, recently, in particular hand and finger based system have been attracting a lot of attention. A major difference to other biometric modalities like face or fingerprint is, that hand and finger veins are inside the human body and are therefore not visible under normal conditions (visible light). But as the haemoglobin in the blood absorbs more near-infraread (NIR) light than the surrounding tissue, they become visible as dark structures under NIR illumination [54]. The first hand based recognition system called "Veincheck" has been patented by Joe Rice in 1985 [49], the first finger based system was presented by Kono *et al.* in 2002 [30]. Currently finger vein authentication is used in several commercial products, e.g. at cash machines in Japan [4], for online banking in the UK [2] or for authentication of bank customers also in the UK [3].

1.3. Longitudinal Finger Rotation

Typical commercial and scientific finger vein sensors capture the vein pattern from a single finger using a single camera where the finger is placed directly on the device (non-contactless acquisition). Different types of finger misplacements, including in-planar shifts and rotations, finger tilt and bending and rotations around the longitudinal axis of the finger, can easily occur with such scanners. Some of these misplacements can be reduced or prevented with the help of a suitable design in the first place, e.g. by adding support structures or guiding walls. Other possible solutions for this problem are a supervised acquisition or software based solutions during pre-processing, feature extraction or comparison. But in particular longitudinal finger rotation has proven to be a difficult problem [39].

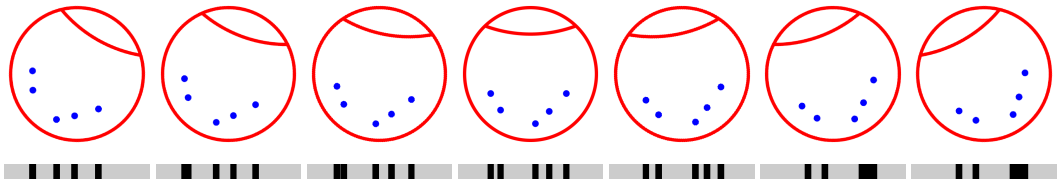

Figure 1.2.: Longitudinal finger rotation principle: A schematic finger cross section showing five veins (blue dots) rotated from -30° (left) to +30° (right) in 10° steps. The projection (bottom row) of the vein pattern is different according to the rotation angle following a non-linear transformation (originally published in [39]).

When capturing finger vein images, the vein structure inside the finger (3D space) is projected onto a 2D plane. The resulting vein pattern differs depending on the relative positioning of the veins to each other and the rotation angle at which the vein image has been captured. Figure 1.2 visualizes the influence of longitudinal rotation to the vein pattern. The top row shows schematic cross sections of a finger rotated from -30° to 30°, the bottom row the corresponding vein patterns. It can be clearly seen that some vein patterns differ considerably, particularly those acquired at -30° (left), 0° (middle) and +30° (right). One can imagine that such deformations, that follow a non-linear transformation, cause major problems for vein recognition systems [39].

2. Contribution

The work published in the scope of this thesis can be divided into three major areas: design and creation of finger vein capturing devices together with the acquisition of publicly available finger vein data sets, analysis of finger vein recognition for different perspectives and rotation invariant (multi-perspective) finger vein recognition.

2.1. Finger Vein Capturing Devices and Data Set Creation

In biometrics the availability of appropriate data sets is a prerequisite for every research. Especially in finger vein biometrics there is a lack of large high quality data sets. The reason for this is that almost all commercially available systems do not provide the original raw images, but only already processed images (templates) in a proprietary format. As a result of this, such devices cannot be used to collect scientifically useful data sets and research groups (including our group) are forced to built their own capturing devices.

The quality of the input data is a crucial factor for any image based system. In finger vein biometrics, the quality of the acquired images is influenced by the capturing device itself (design of the device and quality of the used components [26]), environmental conditions (e.g. ambient light, humidity, temperatures, etc.) [29] and the subject to be captured itself (biological factors of the subject [32, 29] as well as the presentation of the finger during acquisition). The most important components of the capturing device are the illumination and camera module as well as the protection against unwanted exposure, e.g. from the NIR portion of daylight. When designing our sensors, we pursued two goals: (1) Acquisition and evaluation of high-quality data sets in a contact (which was standard when the work on this theses started) as well as in a contactless manner, and (2) the acquisition of perspectives other than the commonly used palmar (e.g. [58, 32, 53]) and dorsal (e.g. [48]) perspective, respectively. All together, we proposed three capturing devices and acquired three data sets which are all available to the scientific public free of charge.

The first device, the *PLUS OpenVein Open Source Finger-Vein Scanner* [23, 24, 26], is a multi-purpose capturing device that supports the acquisition of finger veins from the two major perspectives (palmar and dorsal view) using different illumination types. The used illumination types not only differ in their set-up (reflected light vs transillumination), but also in the used technology. Reflected light and transillumination are distinguished based on the relative positioning of the light source, the finger and the used image sensor to each other. In case of reflected light, camera and illumination module are both placed on the same side of the finger. The camera captures only that portion of the emitted NIR light that was reflected by the finger. In case of transillumination, also called light transmission, light source and camera are on opposite sides of the finger. The NIR light penetrates the skin and tissue of the finger. The camera captures only that portion of the light that passes through the finger. Figure 2.1 visualizes both illumination set-ups. In finger vein recognition, transillumination is used almost exclusively. The modular designed scanner supports as light source the commonly used NIR LEDs as well as NIR lasers. NIR lasers have first been proposed by Kim *et al.* [28] and have been hardly used since. Their main advantage over LEDs is that they have a narrower radiation angle than NIR LEDs. This property is beneficial for contactless acquisition [23]. Typical commercial and scientific finger vein sensors acquire vein images from a single finger using a single camera ideally

always from the same perspective. Contrary to this, the proposed *PLUS OpenVein Finger vein scanner* acquires three fingers at the same time. In [26] all details such as technical drawings, control board schematics or the necessary software of those sensors are published. All designed components as well as the required software are open source, and can therefore be used by other scientists. If many institutions acquire finger veins data with the same scanner, these data sets could theoretically be merged into a larger data set. This happened e.g. in [14] with the *PLUSVein-FV3 Finger Vein Data Set* [23] and *PROTECT Multimodal Dataset* [15] (both were acquired with the PLUS OpenVein sensor). A prototype fo this sensor has been used in the land boarder demonstrator of the PROTECT[1] Project.

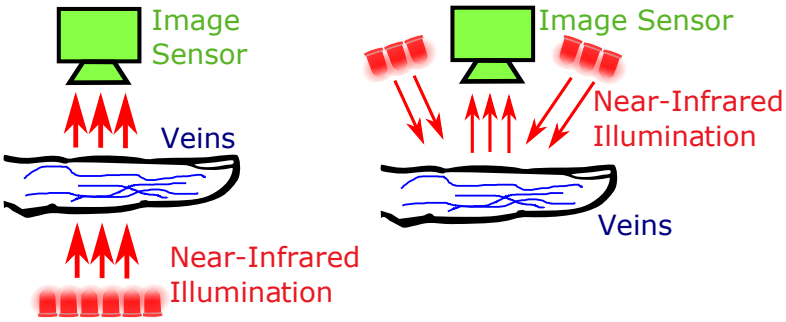

Figure 2.1.: Light source and camera positioning, left: transillumination, right: reflected light (originally published in [26])

The second device is a multi-perspective finger vein scanner [40]. It is capable of acquiring the vascular pattern all around the finger. It's working principle is, that the camera and illumination module, which are placed on opposite sides of the finger (transillumination principle), rotate around the finger. During this rotation a video of the vein pattern is acquired. The speed of the rotation and the video frame rate are coordinated in such way that every frame of the video corresponds to a rotation of 1°. The acquisition of the vein pattern all around the finger allows not only the evaluation of the performance of the different perspectives, but also the combination (fusion) of them. Due to the distance between the illumination module and the acquired finger, NIR laser modules were used as light source [40].

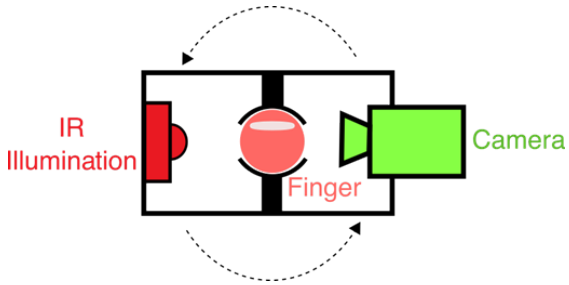

Figure 2.2.: Principle of multi perspective acquisition using rotating camera and illumination modules (originally published in [40], © 2018 IEEE)

The last device, the *Combined Fully Contact-Less Finger and Hand Vein Acquisition Device* [25], is capable of acquiring hand and finger vein samples from the palmar view in a contactless

[1] Pervasive and UseR Focused BiomeTrics BordEr ProjeCT, http://projectprotect.eu/

scenario. While finger vein images are captured in a light transmission mode utilizing LED laser diodes, the hand veins are acquired using reflected light from NIR LED diodes with two different wavelengths [25]. This is the first combined contactless hand and finger vein capturing device.

The following datasets have been acquired and are also available for download:

- ***PLUSVein-FV3 Finger Vein Data Set*[2]:** The data set includes 4 subsets acquired from the palmar and dorsal view using the LED and laser version of the *PLUS OpenVein finger vein sensor*. It contains 6 fingers (left and right index, middle and ring finger) of 60 subjects. Each of the 360 unique fingers have been acquired 5 times, which sums up to 7.200 unique finger vein samples [23, 24].
- ***PLUSVein Finger Rotation Data Set*[3]:** It consists of 252 unique fingers from 63 subjects, each presenting its left and right middle and index finger, acquired from 361 perspectives all around the finger (0° and 360° have been acquired separately), each finger 5 times. This results in a total number of 454.860 finger vein images [40]. For our analysis, several subsets have been established. The first subset, *±45° around the palmar view* [38], consist of the perspectives of ±45° around the palmar view in steps of 1°. It can be used e.g. for the analysis and development of rotation tolerant finger vein recognition systems. The second subset, *Longitudinal finger rotation validation data set* [43], has been developed to test the robustness of recognition schemes with respect to longitudinal finger rotation. It provides data for two different scenarios: The PLUSVein-FR-ED contains vein images in the range of ±45° where the rotation angles are equally distributed. This should correspond to the unconstrained placement of the finger in a contactless acquisition scenario. The rotation angles of the second set, PLUSVein-FR-ND, are normally distributed over the same range. This data set models a realistic real world scenario of a classical unsupervised single perspective acquisition system. The standard deviation of the distribution is based on our analysis of publicly available data sets in [41] and corresponds to the one of the challenging SDUMLA-HMT data set [58].
- ***PLUSVein-Contactless Finger and Hand Vein Data Set*[4]:** For this data set, palmar hand and finger vein images were recorded from 42 people. The finger vein samples were taken using transmitted light, whereas for palm veins reflected light utilizing two different wavelengths was used. The acquisition for one subject consists of 5 samples from 6 fingers (left and right index, middle and ring finger) and both palms (left and right). This results in a total of 1.260 finger vein and 840 hand vein images [25].

Publications (sorted chronologically)

[23] C. Kauba, B. Prommegger, and A. Uhl. Focussing the beam - a new laser illumination based data set providing insights to finger-vein recognition. In *2018 IEEE 9th International Conference on Biometrics Theory, Applications and Systems (BTAS)*, pages 1–9, 2018

[40] B. Prommegger, C. Kauba, and A. Uhl. Multi-perspective finger-vein biometrics. In *2018 IEEE 9th International Conference on Biometrics Theory, Applications and Systems (BTAS)*, 2018

[24] C. Kauba, B. Prommegger, and A. Uhl. The two sides of the finger - an evaluation on the recognition performance of dorsal vs. palmar finger-veins. In A. Brömme, C. Busch,

[2] http://wavelab.at/sources/PLUSVein-FR/
[3] http://wavelab.at/sources/PLUSVein-FV3/
[4] http://wavelab.at/sources/PLUSVein-Contactless/

A. Dantcheva, C. Rathgeb, and A. Uhl, editors, *BIOSIG 2018 - Proceedings of the 17th International Conference of the Biometrics Special Interest Group*, Bonn, 2018. Köllen Druck+Verlag GmbH

[25] C. Kauba, B. Prommegger, and A. Uhl. Combined fully contactless finger and hand vein capturing device with a corresponding dataset. *Sensors*, 19(22)(5014), 2019

[26] C. Kauba, B. Prommegger, and A. Uhl. *OpenVein—An Open-Source Modular Multipurpose Finger Vein Scanner Design*, pages 77–111. Springer International Publishing, Cham, 2020

2.2. Finger Vein Recognition from different perspectives

When the work on this theses started, finger vein recognition focused mainly on the palmar view of the finger (from the inside of the hand). There was only little to no work for other perspectives. Raghavendra and Bush [48] proposed a system that utilizes dorsal finger vein images. Lu *et al*. fused images from two different views [34]. Since then, other scientists have also dealt with this topic, but always in connection with multi-perspective recognition systems [7, 52, 22]. In our work we do not limit ourselves to systems acquiring certain (pre-defined) perspectives, but examined the performance of the perspectives all around the finger in general. The aim is to evaluate if perspectives other than the commonly used once (especially the palmar view) achieve similar or even better recognition results or at least provide enough additional information to improve the performance when fusing them. We also analyse the robustness of various recognition schemes to longitudinal rotations and how the performance - with respect to longitudinal finger rotation - can be improved.

The PLUSVein-FV3 can be split into four subsets with respect to the illumination type (LED vs laser) and acquired perspective (palmar vs dorsal). In [24] the four subsets are evaluated independently of each other using four well established recognition systems, namely three vein pattern based once, *Maximum Curvature* (MC) [37], *Principal Curvature* (PC) [10] and *Garbor Filter* (GF) [32], and a SIFT based approach [27]. The experimental results reveal, that vein pattern based approaches, especially GF, not only extract the vein lines itself, but also parts of the finger texture and wrinkles. Therefore there is actually an implicit fusion of finger veins with the finger texture. It's worth noting that the dorsal view has more wrinkles than the palmar view. In particular, the dorsal finger knuckles should be mentioned as these are also used as a separate biometric modality [31, 59]. For MC and PC, the palmar view achieves better recognition rates, for GF and SIFT the dorsal one, respectively.

In [40] the PLUSVein-FR data set is utilized to analyse the performance of finger vein recognition systems all around the finger (360°). In this context, every perspective of the data set is considered as an independent data set. This means that in principle every perspective represents its own, independent single camera recognition system. Just as in [24], these evaluations have been executed using the same well established recognition systems, MC, PC, GF and SIFT. Again, for MC and PC, the best recognition results are achieved for the widely used palmar view (0°) followed by the dorsal region (180°). With SIFT, the dorsal region achieves better results than the palmar one, while for GF both perspectives achieve approximately the same recognition rates. All four recognition systems have in common that the perspectives inbetween the palmar and dorsal view show inferior but still acceptable recognition rates. The worst results are achieved around 90° and 270°.

Finger vein images from different perspectives do not necessarily have to be evaluated independently from each other. Therefore, we also investigate different fusion strategies [40, 42]. Namely multi-perspective fusion, multi-algorithm fusion and combinations of both. In [40]

up to 72 perspectives are combined together, [42] evaluates all possible pairs and triplets. The results show, that already a fusion of two perspectives significantly improves the recognition performance, especially if the palmar and/or dorsal perspective are included. Adding further perspectives still improves the results, but not to the same extent. For multi-algorithm fusion it turned out, that the best results are achieved when different types of feature extraction schemes (vein pattern based vs key-point based systems) are used. The fusion experiments have been executed using three vein pattern systems (MC, PC and GF) and two key-point based recognition systems (SIFT and *Deformation Tolerant Feature-Point Matching* (DTFPM) [35]).

Furthermore, we systematically analyse the effect of longitudinal finger rotation on the performance of single camera recognition systems and how the negative impact can be reduced [39, 38, 46]. As nearly all finger vein recognition systems acquire the vein pattern from the palmar view, our experiments focus on the region around this view ($\pm 90°$ in [39] and $\pm 45°$ in [38, 46]). The experiments are carried out using the PLUSVein-FR data set, which provides finger vein samples all around the finger with a resolution of 1°. The evaluations in [39] show, that key-point based recognition schemes (SIFT, DTFPM) are more robust to longitudinal rotations than vein pattern based ones (MC, PC, GF) and that for rotational distances between the enrolment and probe sample larger than $\pm 30°$ biometric recognition is not possible at all. In our further work these observations get confirmed for other recognition schemes, namely the (*Wide Line Detector* (WLD) [20] and *Finger Vein Recognition with Anatomy Structure Analysis* (ASAVE) [57] in [38] and *Deformable Finger Vein Recognition* (DFVR) [9] and a CNN based approach [55] in [46]). The overall best performing recognition system with respect to its tolerance to longitudinal finger rotation is DFVR.

As longitudinal finger rotation obviously poses a severe problem to finger vein recognition systems, we investigate how to counter this problem. In [38] we propose two rotation correction and compensation schemes, evaluate their impact on the recognition performance and compare the results to other rotation tolerant approaches, i.e. *Elliptic Pattern Normalization* (EPN) [20] and *Geometric Shape Analysis based Finger Vein Deformation Detection and Correction* (GADC) [8]. The first approach corrects the deformation by rotating the vein pattern back into its desired position using the actual angle of rotation. It assumes a circular finger shape and that the acquired veins are located close to the finger surface. This "*known angle*" approach is only applicable if the rotation angle is known or can be detected or estimated. In case of the used data set, the PLUSVein-FR, the rotation angle is known. The second approach ("*fixed angle*") does not correct the rotation but tries to reduce the rotational distance of the probe and enrolment sample by introducing two additional samples for comparisons. The new images are generated by rotating the enrolment sample with a pre-defined angle in both directions. The probe sample is compared to all three enrolment samples, the original and the two rotated ones. The final score is calculated using a maximum rule score level fusion (MaxSLF). This way, the rotational distance between the enrolment and recognition sample is reduced and the achieved biometric candidate score is improved. The analysis was executed for several vein pattern based methods (MC, PC, WLD, GF, ASAVE) and two key-point based ones (SIFT, DTFPM). Both proposed methods show better performance than the two existing methods (EPN and GADC). The overall best results are achieved when the "*fixed angle*" approach is combined with EPN. The experiments reveal the general trend, that simple vein-pattern-based methods (MC, PC, WLD, GF) benefit more from rotation compensation than approaches that are already tolerant to longitudinal misalignments by design (ASAVE, SIFT, DTFPM). After applying rotation compensation, the simple methods outperform the more sophisticated once.

Furthermore, we analyse four publicly available finger vein data sets, namely SDUMLA-HMT [58], UTFVP [53], FV-USM [5] and the PLUSVein-FV3 [23], with respect to the extent to which they contain longitudinal finger rotation [41, 47]. In [41] the rotation angle be-

tween two samples of the same subject is estimated based on an empirical approach using the correlation of the extracted vein patterns. This is done by pre-rotating all samples in steps of 1° between ±45°. After this, all versions of the images are compared to the first non rotated sample of the same finger. The rotation angle is estimated as the angle of the image that shows the highest similarity (correlation) to the not rotated reference image, i.e. where the comparison score reaches its maximum. The results show that all data sets contain longitudinal rotation, although to different extents. While the PLUSVein-FV3, due to the design of the device that prevents the rotation in the first place, contains nearly no rotation, the other data sets contain a good portion of longitudinal rotation. SDUMLA-HMT exhibits the highest amount with an average of nearly 20° and a maximum of 77° (!) between two samples. By correcting the rotation contained in the data set using the *known angle* approach as presented in [38], the performance can be increased by up to 350%. As this empirical approach is computational expensive, it is not applicable to real-time systems. Therefore, a second CNN based rotation detector is presented in [47]. It is trained on data from the *PROTECT Multimodal Dataset* (PMMDB) [15] and evaluated on the PLUSVein-FR. Due to the use of the CNN, the detection of rotation angles is very fast and can be executed, followed by a rotation correction, prior to every biometric comparison. Due to the rotational pre-alignment the recognition performance can be increased. Further experiments show, that the trained CNN is not limited to the PMMDB and PLUSVein-FR data sets. We applied our rotation detector to other data sets (SDUMLA-HMT, UTFVP, FV-USM and the PLUSVein-FV3) without any additional training achieving similar results as the empirical approach of [41]. The only prerequisite for re-using the CNN is that the ROI is extracted as described in [47]. Since the CNN based approach allows rotation detection in real-time, the "*known angle*" approach presented by us in [38] can now be applied to real-world applications.

Publications (sorted chronologically)

[40] B. Prommegger, C. Kauba, and A. Uhl. Multi-perspective finger-vein biometrics. In *2018 IEEE 9th International Conference on Biometrics Theory, Applications and Systems (BTAS)*, 2018

[24] C. Kauba, B. Prommegger, and A. Uhl. The two sides of the finger - an evaluation on the recognition performance of dorsal vs. palmar finger-veins. In A. Brömme, C. Busch, A. Dantcheva, C. Rathgeb, and A. Uhl, editors, *BIOSIG 2018 - Proceedings of the 17th International Conference of the Biometrics Special Interest Group*, Bonn, 2018. Köllen Druck+Verlag GmbH

[39] B. Prommegger, C. Kauba, and A. Uhl. Longitudinal finger rotation - problems and effects in finger-vein recognition. In A. Brömme, C. Busch, A. Dantcheva, C. Rathgeb, and A. Uhl, editors, *BIOSIG 2018 - Proceedings of the 17th International Conference of the Biometrics Special Interest Group*, Bonn, 2018. Köllen Druck+Verlag GmbH

[38] B. Prommegger, C. Kauba, M. Linortner, and A. Uhl. Longitudinal finger rotation—deformation detection and correction. *IEEE Transactions on Biometrics, Behavior, and Identity Science*, 1(2):123–138, 2019

[41] B. Prommegger, C. Kauba, and A. Uhl. On the extent of longitudinal finger rotation in publicly available finger vein data sets. In *2019 International Conference on Biometrics (ICB)*, pages 1–8, 2019

[42] B. Prommegger, C. Kauba, and A. Uhl. *Different Views on the Finger - Score-Level Fusion in Multi-Perspective Finger Vein Recognition*, pages 261–305. Springer International Publishing, Cham, 2020

[47] B. Prommegger, G. Wimmer, and A. Uhl. Rotation detection in finger vein biometrics using cnns. In *Proceedings of the 25th International Conference on Pattern Recognition (ICPR)*, pages 1–7, 2020

[46] B. Prommegger and A. Uhl. A fully rotation invariant multi-camera finger vein recognition system. *IET Biometrics*, pages 1–15, 2021

2.3. Rotation Invariant Finger Vein Recognition

Classical finger vein recognition systems acquire the vein pattern of a single finger using a single camera typically from the palmar view. As a result of this, such systems acquire only a limited part of the vein pattern information. If fingers are not always placed in the same (correct) way, this might lead to a degradation of the systems recognition performance. In particular, misplacements due to longitudinal finger rotations poses a severe problem. As finger vein recognition devices evolve towards contactless and on-the-move acquisition [36, 25, 33], problems cause by longitudinal rotations will become more important. One way to solve this problem is to acquire the vein pattern from different perspectives. This increases the range for which the vein pattern is available. Ideally, finger vein recognition can thereby become even invariant to such misplacements of the finger. Multi-perspective finger vein recognition has only recently received more attention. E.g. Bunda [7] and Sonna Momo *et al.* [52] presented systems that acquire the vein pattern from three different perspectives and Kang *et al.* [22] applies finger vein recognition in the 3D space. In our work we propose four novel rotation invariant multi-camera finger vein recognition systems:

1. *Perspective Cumulative Finger Vein Templates* (PCT) [44] requires the acquisition of the vein pattern from multiple perspectives during enrolment and from a single perspective for recognition. The rotation angles of the captured enrolment samples are spread linearly over the desired acquisition range and are combined to a large single template. This is done in the feature space after applying *Circular Pattern Normalization* (CPN) [38] using MC features. The achieved recognition rates with EERs of 4-8% for the best performing set-up are noticeably inferior to those of state-of-the-art single camera systems, but they are stable over the whole rotational range under investigation. These results indicate that this approach has potential but needs further development in order to be applicable in real applications.

2. As for PCT, also *Multi-Perspective Enrolment (MPE) [44]* acquires multiple perspectives during enrolment but still a single one for recognition. Again, the rotation angles of the enrolment samples are spaced linearly of the desired acquisition range. In contrast to PCT, for MPE the enrolment samples are not combined to a single template but evaluated separately. For authentication, the probe sample is compared to every enrolment sample. The final biometric comparison score is calculated with the help of a *Maximum Rule Score Level Fusion* (MaxSLF) of the individual comparison results. The best setting (MPE 15°, rotational distance of 15° between the enrolment samples) achieves EERs $< 1.4\%$ all around the finger. These results are better than those achieved if every perspective is considered as its own single camera recognition system (intra-perspective recognition performance, IPP). In order to achieve similar recognition rates than those of IPP, the distance between two enrolment samples can be increased to 45° (MPE 45°). If the vein pattern is acquired all around the finger (360°) during enrolment, the method is invariant to longitudinal finger rotation. A drawback of the system is, that the number of the needed enrolment perspectives is relatively high. This leads to complex and expensive capturing devices.

3. *Perspective Multiplication for Multi-Perspective Enrolment (PM-MPE) [43]* is an advanced version of MPE. It's aim is to reduce the number of involved perspectives while the recognition rates are kept on a high level. The reduction is achieved by combining MPE with the "*fixed angle*" approach we presented in [38]: PM-MPE adds two so called pseudo perspectives inbetween two adjacent enrolment perspectives. This is done by rotating every enrolment sample in both directions with a defined angle α, where α is a third of the rotational distance between the enrolment cameras. This way, the actually acquired perspectives and the generated pseudo perspectives are again spread linearly over the acquisition range. Just as for MPE, the probe samples are compared to all enrolment samples (original image as well as the generated pseudo perspectives). The final biometric candidate score is again calculated using MaxSLF. To achieve similar recognition results as for MPE, the rotational distance between the enrolment cameras of PM-MPE can be increased by at least 15°. Rotational distances of more than 60° between the enrolment cameras are still not useful.

4. In comparison to the three previous methods, *Combinde Multi-Perspective Enrolment and Recognition (MPER) [46]* acquires multiple perspectives for both, enrolment and recognition. Contrary to other multi-camera recognition systems like [7, 52, 22], where the same capturing devices are used for enrolment and recognition, the capturing devices for MPER differ. While the MPER enrolment device covers the vein pattern all around the finger, the one for recognition acquires only the range between two adjacent enrolment cameras. The two devices are designed in such way that the rotational distance between the closest enrolment and recognition perspective as well as that the number of involved cameras is kept to a minimum. Similar to MPR, all acquired probe samples are compared to all enrolment samples. The final biometric candidate score is calculated using MaxSLF. Just like the systems presented above, MPER is also rotationally invariant.

In [45] MPE and PM-MPE are further investigated. While the original publications uses MC features, this work analyses the applicability of other recognition schemes (i.e. WLD, SIFT, ASAVE) to (PM-)MPE. Furthermore we investigate if changing the positions of the enrolment cameras increases the performance of MPE, as well as if introducing even more pseudo perspectives is beneficial for PM-MPE. It turned out that simple vein pattern based methods such as MC and WLD are more suited for (PM-)MPE than more sophisticated methods or methods that are already tolerant to rotation by design. Changing the camera positions or introducing more pseudo perspectives did not increase the recognition performance for MPE and PM-MPE, respectively.

Publications (sorted chronologically)

[44] B. Prommegger and A. Uhl. Rotation invariant finger vein recognition. In *2019 IEEE 10th International Conference on Biometrics Theory, Applications and Systems (BTAS)*, pages 1–9, 2019

[43] B. Prommegger and A. Uhl. Perspective multiplication for multi-perspective enrolment in finger vein recognition. In A. Brömme, C. Busch, A. Dantcheva, C. Rathgeb, and A. Uhl, editors, *BIOSIG 2019 - Proceedings of the 18th International Conference of the Biometrics Special Interest Group*, pages 107–117, Bonn, 2019. Gesellschaft für Informatik e.V

[45] B. Prommegger and A. Uhl. Advanced multi-perspective enrolment in finger vein recognition. In *2020 8th International Workshop on Biometrics and Forensics (IWBF)*, pages 1–6, 2020

[46] B. Prommegger and A. Uhl. A fully rotation invariant multi-camera finger vein recognition system. *IET Biometrics*, pages 1–15, 2021

3. Publications

This chapter presents the publications as originally published, reprinted with permission from the corresponding copyright holders. The copyright of the original publications is held by the respective copyright holders, see the following copyright notices. In order to fit the paper dimension, reprinted publications may be scaled in size and/or cropped.

Focussing the Beam - A New Laser Illumination Based Data Set Providing Insights to Finger-Vein Recognition

Christof Kauba, Bernhard Prommegger and Andreas Uhl
University of Salzburg
Jakob-Haringer-Str. 2, 5020 Salzburg, AUSTRIA
{ckauba, bprommeg, uhl}@cosy.sbg.ac.at

Abstract

The vascular pattern inside human fingers has become an emerging biometric trait during the last years, commonly denoted as finger vein recognition. However, the number of publicly available data sets is limited. In order to capture a finger vein data set, a suitable scanner device is needed. The design of such a scanner device is crucial if it comes to image quality, robustness against external influences during the capturing process and consequently to a good recognition performance. In this paper we propose two novel, modular designed, multi-purpose finger vein scanners, both able to capture three fingers at once, together with a publicly available finger-vein data set captured with these scanners. One scanner uses common near-infrared LEDs as a light source. The second one is based on a new concept using near-infrared lasers. Near-infrared lasers are not common in finger-vein recognition before despite their advantages especially in touchless operation. Our recognition performance evaluation confirm the good recognition performance that can be achieved using our proposed scanner design and provides some new insights by conducting sex and age-group specific analysis.

1. Introduction

Vascular pattern based recognition (commonly denoted as vein recognition), as a promising new biometric, gains more and more attention and can help to overcome some of the problems existing biometric recognition systems have. Vein based systems rely on the structure of the vascular pattern formed by the blood vessels inside the human body tissue. This pattern only becomes visible in near-infrared (NIR) light. Thus, vein based biometrics provide a good resistance to spoofing and are insensitive to abrasion and skin surface conditions. They achieve good recognition performance while the user convenience is at the same level as for fingerprint systems as long as the scanner is designed in an open manner. Moreover, a contactless operation is possible and liveness detection can be performed easily [6].

Although, especially hand- and finger-vein based systems are already equipped in commercial products, there is still a lack of comprehensive, public available data sets, which is one of the key factors in order to facilitate research in vascular pattern based biometrics. A major reason for this lack of available data sets is that almost all commercial off-the-shelf finger- and hand-vein scanners do not provide access to the raw vein images they capture. They only output some kind of template in a proprietary format specified by the manufacturer, which is of little use in research. Prior to establishing such a data set, two important things are needed. Most important are the volunteers, who are willing to participate in the data collection, present their fingers to the scanner and donate some of their time while their fingers are scanned. The second most important thing is a scanner device, which provides access to the raw vein images.

A deliberately designed scanner device is crucial for the image quality of the vascular pattern images and consequently, the recognition performance. The first contribution of this paper is our proposed design of two novel multi-purpose finger-vein scanners. Both of our proposed scanners are equipped with transillumination as well as reflected light illumination and are able to capture dorsal and palmar images. They are designed to capture three fingers at a time to speed up the data acquisition process. The scanners differ in the type of their NIR light source: the first one is based on NIR LEDs, while the second one uses NIR lasers. NIR lasers have hardly been used in finger-vein recognition since they were first proposed by Kim et al. [5] in 2009. The main advantage of lasers over LEDs is an increased range of possible vertical finger movement without impacting the image quality. This becomes important as soon as the finger is desired not to touch the sensor's surface and thus especially if it comes to touchless operation. This paper covers the main aspects of our scanner design. The details of the scanner design, including all construction plans, schematics, parts lists and the software will be

978-1-5386-7180-1/18/$31.00 ©2018 IEEE

made publicly available as an open-hardware project. Other researchers interested in finger-vein biometrics can benefit from our open-source scanner design, build a scanner on their own and capture finger-vein images. By providing their captured data, they can help in establishing an extensive, publicly available finger-vein data set and thus help in stimulating research on vascular biometrics. Such an extensive data set is especially vital in order to develop efficient (in terms of runtime) finger-vein identification and finger-vein indexing schemes.

The main contribution of this paper is the data set itself, which was captured utilising our two finger-vein scanners. This new, publicly available, dorsal finger-vein data set consists of two sub sets: one for each of our proposed two scanners. To the best of our knowledge there is neither a finger-vein data set which was acquired using NIR laser illumination nor an extensive, publicly available, data set containing dorsal images. Our data set provides high resolution dorsal finger-vein images of 360 individual fingers together with additional information about the 60 subjects. It is currently being extended by capturing additional subjects and is expected to grow further due to our plans to make the scanner hardware an open-source project.

The performance evaluation based on some well-established finger-vein recognition algorithms confirms the good recognition performance that can be achieved using our data set, both the LED and the laser scanner one. Beyond the baseline performance results, a subgroup specific analysis of the recognition performance is carried out. The whole data set is divided into 2 sex specific subgroups as well as 3 age specific ones. We did not come across any other finger-vein recognition paper that covers such a subgroup specific performance evaluation so far. The subgroup specific results indicate that there is no significant difference in the recognition performance for male and female subjects as well as among the different age groups. Finally, the cross-sensor (LED vs. laser) recognition performance is evaluated and an image quality analysis using several no reference image quality metrics is performed.

The rest of this paper is organised as follows: Section 2 explains the principle of a finger-vein scanner in general, followed by the details about the two proposed finger-vein scanning devices. In Section 3 at first an overview of available finger-vein data sets, including all important details, is given. This is followed by a detailed description of our new finger-vein data set. Section 4 outlines the experimental setup, including the recognition tool-chain as well as the evaluation protocol and gives the performance evaluation results together with a results discussion. Section 5 concludes this paper along with an outlook on future work.

2. Finger-Vein Scanners

Finger-vein biometrics rely on the structure of the vascular pattern inside the fingers of a human. To be able to extract meaningful features of this vascular structure at first the blood vessels inside the human body tissue have to be made visible. The blood vessels can be rendered visible (as dark lines in the images) due to the fact that the haemoglobin contained in the blood flowing through the vessels absorbs NIR light while the surrounding tissue is semi-permeable. Hence, the crucial components of a finger-vein scanner are an NIR sensitive camera and some kind of NIR light source, the latter typically consists of NIR LEDs with wavelengths between 750 nm and 950 nm. Usually either an NIR pass-through filter is added to the camera or the scanner is enclosed in an optically opaque box in order to reduce the influence of ambient light.

Based on the positioning of the illuminator relative to the camera and the finger, there are two types of illumination:

1. Transillumination, where the camera and the illuminator are positioned on opposite sides of the finger. The light penetrates the skin and tissue of the finger and gets captured by the camera as it emerges.

2. Reflected light, where the camera and the illuminator are positioned on the same side of the finger. The light originates from the light source, gets reflected at the finger's surface and tissue and is captured by the camera.

A further distinction can be made based on the side of the finger where the camera is positioned or the images is taken from, respectively: palmar (also called ventral), where the images are taken from the palm side of the hand and dorsal, where the images are taken from the back side of the hand.

In finger-vein recognition usually palmar images are captured using transillumination. Our proposed scanners are multi-purpose finger-vein scanners, i.e. they are able to capture dorsal as well as palmar images and apply transillumination as well as reflected light illumination. Thanks to its modular design it is easy to change, replace, modify or improve individual parts of the scanner while keeping its basic structure.

2.1. PLUS OpenVein LED Based Scanner

The LED based version of the PLUS OpenVein finger-vein scanner can be seen in Figure 1. The image sensor is an NIR enhanced industrial camera (IDS Imaging UI-ML1240-NIR) equipped with a Fujifilm HF9HA-1B 9 mm lens in combination with a MIDOPT FIL LP830/27 NIR pass-through filter. The transillumination light source consists of 3 stripes (one underneath each finger) of 8 Osram SFH-4253-Z LEDs each. An LED ring consisting of 8 850

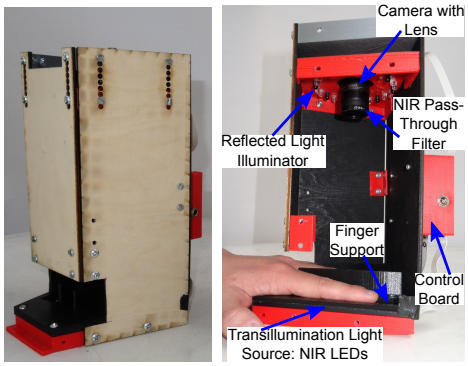

Figure 1. PLUS OpenVein three-finger vein scanner LED version

nm LEDs, 8 950 nm LEDs and 8 daylight LEDs for capturing reflected light images is situated on top of the device. To assist in positioning of the finger, the lower part contains a custom 3D printed finger support which serves as a bracket for the 3 LED stripes too. The control board is located on the back plate of the scanner. This scanner is designed to capture 3 fingers (index, middle and ring finger) at once. It is able to capture both palmar and dorsal (by rotating the hand) as well as transillumination and reflected light finger vein images. The whole scanner is built into a wooden housing to improve stability. The outside dimensions of the scanner are $146 \times 175 \times 258\,mm$. All the housing parts, the 3D printed parts and the control boards were designed by ourselves. The acquisition time for one image is about 3 s (containing three fingers). Figure 6 bottom shows some example images captured with this scanner.

The scanner has an integrated control board which enables the individual brightness control of each of the transillumination LEDs. The capturing software uses an automatic brightness control algorithm to achieve an optimal image contrast and quality. This is done iteratively by comparing the average grey level of the image area around each LED centre ($GL_{current}$) with a pre-configured target value (GL_{target}). Initially all LEDs are set to half of the maximum intensity (I_{max}). The intensity correction is then done according to: $corr = \frac{GL_{target}-GL_{current}}{GL_{max}} \cdot \frac{I_{max}}{2 \cdot n}$, where GL_{max} is the maximum grey value and n is the current iteration. The LED centre positions are pre-configured too. Each of the 3 reflected light illuminators can be brightness controlled as a whole as well (not the individual LEDs).

2.2. PLUS OpenVein Laser Based Scanner

This scanner is the first finger-vein scanner that uses NIR laser diodes instead of NIR LEDs for transillumination. The main parts (camera, reflected light source, finger support and housing) of the laser based scanner are the same as for the LED version except the illuminator and the control board. The transillumination light source consists of 3x 5 DLC-180-500-9T5 808 nm 300 mW laser diodes including a control PCB and a housing with an adjustable lens to focus the laser beam (subsequently called laser module). An image of the scanner can be seen in Figure 1. The height of laser based scanner is larger than the LED version (outside dimension are: $146 \times 175 \times 306\,mm$) because the laser modules are bigger than the LEDs.

An NIR illuminator based on laser modules instead of LEDs exhibits several advantages in the transillumination setting. First of all the laser modules have a very narrow radiation angle. If LEDs are used, the finger has to be placed close to the light source. As soon as the finger does not directly touch the sensor surface most of the light emission passes alongside and outside the finger, not through the finger. Thus, the finger boundaries appear too bright while the interesting regions of the finger containing the blood vessels exhibit little contrast leading to a lower vein image quality in general, which can be seen in the bottom row of Figure 6 and in detail in Figure 3. Depending on the radiation angle of the LED this gets worse the farther away the finger is from the illuminator, implying problems especially if the distance between illuminator and finger cannot be easily controlled. Figure 5 shows some example images captured with our scanners. The distance between the finger and the scanner surface varies from 0mm (directly on the scanner surface), 20 mm and 40 mm. The images captured with the LED based scanner (left part of the figure) clearly show more bright areas around the finger boundaries and less image contrast of the vein region the further away the finger is from the scanner surface, while the laser based scanner (images in right part of the figure) is still able to maintain a good image contrast in the vein region. This is one of the main problems if it comes to touchless finger-vein scanners. The narrow radiation angle of the laser modules enables an increased range of vertical finger movement (see Figure 4 for an illustration) without lowering the overall vein image contrast and quality. This is a key requirement for real touchless operation of a finger-vein scanner. Thus, the design of a touchless finger-vein scanner becomes feasible or at least less complex by utilising laser modules. Kim et al. [5] were the first to propose the use of NIR lasers instead of NIR LEDs in 2009. They exploited the increased range of vertical finger movement and higher illuminous flux compared to LEDs in their touchless finger-vein scanner. In contrast to our design they used only one NIR laser in combination with a laser line generator lens. They made a real-time camera control software to achieve an optimal image contrast instead of controlling the laser's illumination intensity. Their acquired data set consisting of 200 images

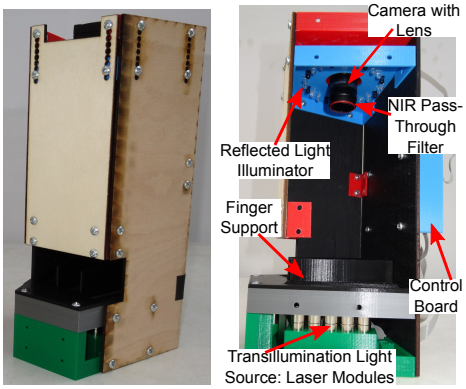

Figure 2. PLUS OpenVein three-finger vein scanner laser version

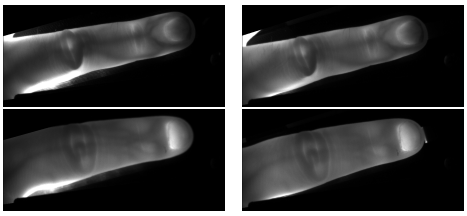

Figure 3. Comparison of LED (left) and laser (right) illumination. Note the bright spots along the left bottom part of the finger for the LED scanner images which are reduced using the laser illumination.

captured from 10 different subjects has not been published. Another advantage of NIR laser modules is that the emission spectrum of the laser modules is narrower compared to LEDs. This enables the use of narrow band-pass filters instead of NIR long-pass filters (filters all wavelengths below the cut-off frequency but all frequencies above it will pass unaffected) to further reduce the influence of ambient illumination. The disadvantages of laser modules include the higher current consumption (400 mA compared to 70 mA for an LED), bigger size and the higher costs compared to LEDs.

3. PLUSVein-FV3 Dorsal Finger-Vein Data Set

Table 1 lists some details of the the 8 publicly available finger vein data sets we found so far, including the number of subjects (subjs), the number of fingers per subject that were captured (fings), the total number of images (imgs) as well as if the images are captured from the palmar or dorsal side (dors/palm). Furthermore, the number of sessions (sess), the image resolution and more important the effective resolution of the visible finger area inside the images (finger w*h) as well as the type of camera and the illumination type is given if this information was available. The last row lists our new finger-vein data set.

This table clearly shows that all of these data sets except the PROTECT Multimodal Database [16] are palmar finger-vein data sets. Raghavendra and Busch [13] did some experiments on dorsal finger veins but their data set has never been published. Moreover, for all of these data sets, NIR

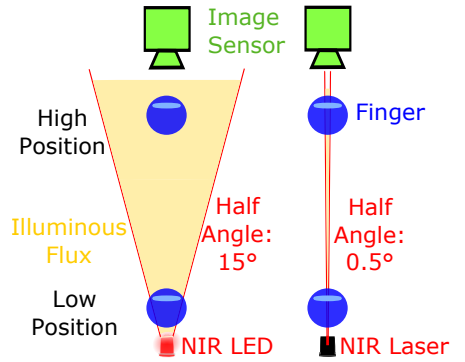

Figure 4. Illumination issues due to vertical finger movement: for usual LEDs (depicted here is an LED with a radiation half angle of 15°) the further away the finger is from the illuminator, the higher the amount of illuminous flux that is outside the finger. The more illuminous flux outside the finger, the less image contrast and vein visibility. Laser modules have a narrow radiation angle, thus the illuminous flux outside the finger remains 0 if the finger is moved in y-direction.

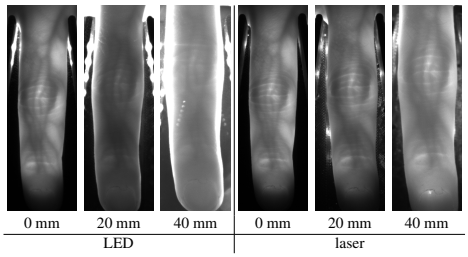

Figure 5. Finger-vein images captured with our scanners showing illumination issues due to vertical finger movement: note the bright areas along the finger boundaries and the reduced contrast of the vein region the further away the finger gets from the scanner surface for the LED scanner images (left) compared to the laser scannes ones (right) which still exhibit enough image contrast.

name	subjs	fings	imgs	dors/palm	sess	resolution	finger w*h	camera	illumination
UTFVP [15]	60	6	1440	palmar	2	672×380	672×240	C-Cam BCi5	850 nm LEDs
SDUMLA-HMT [19]	106	6	3816	palmar	1	320×240	320×130	NIR CCD 900nm	890 nm LEDs
FV-USM [1]	123	4	5940	palmar	2	640×480	170×450	Sony PSEye cam	850 nm LEDs
VERA FingerVein [14]	110	2	440	palmar	2	665×250	650×240	C-Cam BCi5	850 nm LEDs
MMCBNU_6000 [9]	100	6	6000	palmar	1	640×480	640×240	-	850 nm LEDs
THU-FVFDT [18]	610	2	6540	palmar	2	720×576	200×500	camera + NIR filter	890 nm LEDs
HKPU-FID [6]	156	2	3132	palmar	2	512×256	512×190	NIR camera	850 nm LEDs
PMMDB-FV [16]	20	4	240	dorsal	1	1280×440	1120×400	UI-ML1240-NIR	850 nm LEDs
PLUSVein-FV3	60	6	3600	dorsal	1	1280×1024	200×750	UI-ML1240-NIR	LEDs/laser

Table 1. Available finger-vein data sets

LEDs were used as light source. The main contributions of our data set are:

1. A comprehensive dorsal finger-vein data set. We aimed at optimising the acquisition set-up to achieve a high and consistent image quality in order to obtain a good recognition performance.

2. Images captured using two scanners: one with NIR LED based illumination and one with NIR laser module based illumination.

3. Subjects' metadata enabling sub-group specific analysis (e.g. sex and age group as we performed in this paper).

3.1. Data Set Description

The PLUSVein-FV3 finger-vein data set consists of 2 subsets: one dorsal finger-vein subset captured with the LED based scanner and one dorsal finger-vein subset captured with the laser module based scanner. There are the same 60 subjects in each of the 2 subsets. 6 fingers (left and right index, middle and ring finger) and 5 images per finger in 1 session were captured. So each subset consists of 360 individual fingers. Each scanner captures 3 fingers at a time. Thus, each subset contains 600 raw finger-vein images. Some of these example images can be seen in Figure 6. The images are then separated into 3 parts, corresponding to index, middle and ring finger, respectively. Hence, there are effectively 1800 images in each subset and 3600 images in the data set in total. 25 of the subjects are female, 35 are male. The youngest subject was 18, the oldest one 79. The subjects are from 11 different countries.

The raw images have a resolution of 1280×1024 pixels and are stored in 8 bit greyscale png format. The separated images have a resolution of 420×1024 pixels and the visible area of the finger inside the images is about 200×750 pixels per finger. The data set is publicly available for research purposes and can be downloaded at: `http://www.wavelab.at/sources/PLUSVein-FV3`. It is still being extended and is expected to contain more than 100 subjects until the end of 2018.

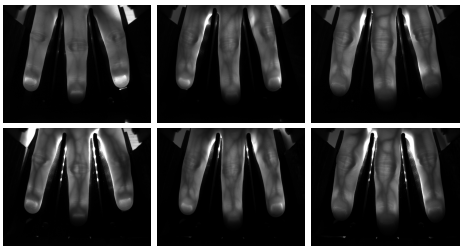

Figure 6. Scanner example images, laser (top) and LED (bottom)

4. Performance Evaluation

In the following the finger-vein processing tool-chain and the evaluation protocol are described. Then the experimental results are given and discussed.

4.1. Processing Tool-Chain

The finger-vein processing tool-chain consists of ROI (region of interest) extraction, preprocessing, feature extraction and comparison. We opted for simple binarisation type feature extraction methods as well as one key-point based method (SIFT based) to have a complimentary feature type too. If these simple recognition schemes perform well on our data set, more recent and more sophisticated recognition schemes will certainly perform even better. Implementations of all of the methods we used are publicly available.

ROI Extraction At first the input image is split into 3 parts, corresponding to index, middle and ring finger, respectively. This can be done using fixed boundary lines. Afterwards each image is processed individually. Prior to the extraction of the ROI, the finger outline is detected by the help of edge detection algorithms. Then a straight centre line is fitted into the finger. Based on this centre line, the finger is aligned (rotated and shifted) such that it is in upright position in the middle of the image. Then the area outside the finger is masked out (pixels set to black). Then a rectangular ROI is fit inside the finger area. The ROI images

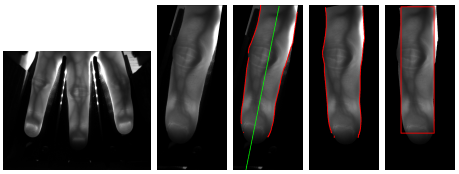

Figure 7. ROI extraction process, from left to right: input image, left finger separated, finger outline and centre line detection, finger aligned and masked, ROI boundary

have a size of 192×736 pixels. The single steps of the ROI extraction are depicted in Figure 7.

Preprocessing To improve the image contrast and the visibility of the vein pattern **CLAHE** [22], which is the most prevalent and simple technique, in combination with **High Frequency Emphasis Filtering (HFE)** [21] and filtering with a **Circular Gabor Filter** (**CGF**) as proposed by Zhang and Yang [20] are applied. Furthermore, the images are resized to half of its original size, which not only speeds up the comparison process but further improves the results due to intrinsic denoising. For more details on the preprocessing methods the interested reader is referred to the authors' original publications..

Feature Extraction and Comparison The first three of the following techniques aim to extract the vein pattern from the background resulting in a binary template image followed by a comparison of these binary templates using a correlation measure.

Maximum Curvature (MC [12]) aims to emphasise only the centre lines of the veins, making it insensitive to varying vein widths. The first step is the extraction of the centre positions of the veins. Afterwards a score according to the width and curvature of the vein region is assigned to each centre position and recorded in a matrix called locus space. Due to noise or other distortions some pixels may not have been classified correctly at the first step, thus the centre positions of the veins are connected using a filtering operation. Finally binarisation is done by thresholding using the median of the locus space.

Principal Curvature (PC [2]): At first the gradient field of the image is calculated. Hard thresholding is done to filter out small noise components and then the gradient at each pixel is normalised to 1 to get a normalised gradient field. This is smoothed by applying a Gaussian filter. The next step is the actual principal curvature calculation, obtained from the Eigenvalues of the Hessian matrix at each pixel. Only the bigger Eigenvalue, corresponding to the maximum curvature, is used. The last step is a binarisation of the principal curvature values to get the binary vein output image.

Gabor Filter (GF [6]): The image is filtered using a filter bank consisting of several 2D even symmetric Gabor filters with different orientations, resulting in several feature images. The final vein feature image is obtained by fusing all these single images, which is then post-processed using morphological operations to remove noise.

For comparing the binary feature images we adopted the approach of Miura et al. [12]. As the input images are neither registered to each other nor aligned vertically, the correlation between the input image and x- and y-direction shifted versions of the reference image is calculated. The maximum of these correlation values is normalised and then used as final comparison score.

In addition to the techniques described above, the fourth technique is a key-point based one. Key-point based techniques try to use information from the most discriminative points as well as considering the neighbourhood and context information of these points by extracting key-points and assigning a descriptor to each key-point. We used a **SIFT** [8] based technique with additional key-point filtering along the finger boundaries as proposed by Kauba et al. [4].

4.2. Evaluation Protocol

To quantify the performance, the EER as well as the FMR1000 (the lowest $FNMR$ for $FMR <= 0.1\%$) and the ZeroFMR (the lowest $FNMR$ for $FMR = 0\%$) are used. We followed the test protocol of the FVC2004 [10]. For calculating the genuine scores, all possible genuine comparisons are performed, which are $62 \cdot 6 \cdot \frac{5 \cdot 4}{2} = 3600$ comparisons. For calculating the impostor scores, only the first image of a finger is compared against the first image of all other fingers, resulting in $6 \cdot \frac{60 \cdot 59}{2} = 10620$ comparisons, so 14220 comparisons in total. All result values are given in percentage terms, e.g. 1.43 means 1.43%. A public implementation of the complete processing tool-chain as well as the score and detailed results are available at: `http://www.wavelab.at/sources/Kauba18c`.

4.3. Baseline Performance Results

Table 2 shows the baseline recognition performance results for all 4 tested finger-vein recognition schemes and both scanner types, laser and LED. All of the 4 quite simple finger-vein recognition schemes achieve a competitive recognition performance in terms of EER, FMR1000 as well as ZeroFMR on both, the laser and the LED scanner data set. The DET plots for the laser and the LED scanner can be found in Figure 8 left and right, respectively. Regarding the laser scanner data set, MC performs best achieving an EER of 0.028%, followed by SIFT and PC while GF performs worst. On the LED scanner data set, PC performs slightly better than MC (in terms of ZeroFMR), both having an EER of 0.028%. SIFT is ranked third while GF again performs

		MC	PC	SIFT	GF
laser	EER	**0.028**	0.331	0.111	0.523
	FMR1000	**0.028**	0.444	0.111	0.694
	ZeroFMR	**0.028**	0.694	0.361	1.306
LED	EER	**0.028**	0.028	0.117	0.336
	FMR1000	**0.028**	0.028	0.139	0.444
	ZeroFMR	0.083	**0.056**	0.361	0.917

Table 2. Baseline performance results (the best results per illumination type are highlighted **bold**)

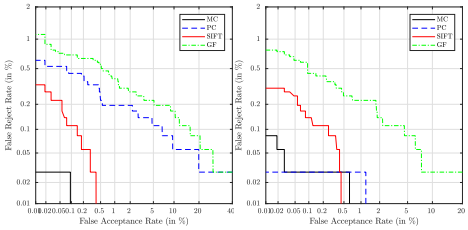

Figure 8. DET plot for laser scanner (left) and LED (right)

worst. Note that due to the limited number of comparison scores (14220) the resolution of the DET curve is limited. Thus, the DET curve of MC and the one of PC for the LED scanner shows a straight line between 0.01% and 0.1% (0.6% for MC on the LED scanner and 1.2% for PC on the LED scanner, respectively). Consequently, the EER could be any value in between 0.028% and 0.1%/0.6%/1.2%, respectively. We decided to report the lowest possible FRR as EER in those cases. In our scanner set-up, where the fingers are placed directly above the illumination source, the tested recognition schemes perform slightly better on the LED scanner data set than on the laser one, especially PC and GF. However, the laser based scanner has its main advantage in terms of recognition performance if the finger is not placed directly on the scanner surface but located a few centimetres away from it (touchless operation).

4.4. Cross-Sensor Comparison Performance

The cross-sensor recognition performance results are given in Tab. 3. MC performs best if it comes to cross-sensor comparison achieving a competitive EER of 0.288%. This time GF performs second best, followed by PC while SIFT performs worst. In terms of relative performance degradation ($\frac{EER_{i,cross}-EER_{i,single}}{EER_{i,single}} \cdot 100\%$, where $EER_{i,cross}$ is the cross-sensor comparison EER for the i-th recognition scheme and $EER_{i,single}$ is the lower of the two single sensor performances for the corresponding recognition scheme), MC's performance dropped by about 930%. PC's performance dropped by 740%, the one of SIFT by 2340% and the one of GF only by 160% in terms of relative EER increase. According to these relative performance drops GF can handle the cross-sensor comparison best. However, MC still performs best in terms of absolute performance values in the cross-sensor comparison. Summing up, the cross-sensor comparison lowers the recognition performance but is still usable in practical deployments of finger-vein scanners, especially if it comes to MC.

	MC	PC	SIFT	GF
EER	0.288	2.775	2.86	1.353
FMR1000	0.478	5.078	5.622	3.522
ZeroFMR	1.267	6.522	7.689	8.144

Table 3. Cross-sensor (LED vs. laser) comparison performance results

		male		female	
		MC	SIFT	MC	SIFT
nr. of subjects		35		25	
laser	EER	0.0	0.038	0.061	0.122
	FMR1000	0.0	0.286	0.067	0.2
	ZeroFMR	0.0	0.429	0.067	0.4
LED	EER	0.089	0.052	0.0	0.211
	FMR1000	0.048	0.048	0.0	0.267
	ZeroFMR	0.95	0.048	0.0	0.533

Table 4. Sex subgroup specific results

4.5. Sex and Age Group Specific Analysis

In addition to the baseline performance evaluation we also conducted a subset specific analysis. Therefore, we divided the total data set into 2 sex (male/female) and 3 age group (< 30 / $\geq 30 < 40$ /≥ 40) specific subsets. To keep the tables and plots clear, only the results of MC and SIFT are depicted. PC and GF follow the same trend. The sex subgroup specific results are given in table 4. While the general performance (including male and female subjects) in terms of EER for MC using the LED scanner data is 0.028%, for the male subset it is 0.089%, whereas for the female one it is 0%. For SIFT the situation is completely opposite: the baseline EER for the LED scanner data is 0.117%, for the male subset it is 0.052% and for the female one it is 0.211%. Regarding the laser scanner, male subjects achieve a slightly better recognition performance than female ones for both, MC and SIFT. Overall, there is no substantial difference between male and female subjects regarding the recognition performance using our finger-vein recognition system including the scanner hardware and the recognition tool-chain.

The age-group specific results are listed in table 5. It can be seen that for the LED scanner the EER as well as the FMR1000 and the ZeroFMR are all 0%, i.e. the best recognition performance that can be achieved. Consequently, there is no difference between the three age subgroups, i.e. the finger-vein recognition system's performance is inde-

		< 30		$\geq 30 < 40$		≥ 40	
		MC	SIFT	MC	SIFT	MC	SIFT
nr. of subjects		19		21		20	
laser	EER	0.0	0.0	0.0	0.0	0.0	0.0
	FMR1000	0.0	0.0	0.0	0.0	0.0	0.0
	ZeroFMR	0.0	0.0	0.0	0.0	0.0	0.0
LED	EER	0.0	0.0	0.0	0.0	0.0	0.0
	FMR1000	0.0	0.0	0.0	0.0	0.0	0.0
	ZeroFMR	0.0	0.0	0.0	0.0	0.0	0.0

Table 5. Age subgroup specific results

metric	BIQAA	SSEQ	GCF	Wang17
laser	0.00461	28.5888	1.289	0.32679
LED	0.00423	36.4295	1.419	0.30035

Table 6. Image quality evaluation results, BIQAA values are in the range of [0, 1], SSEQ in [0, 100], GCF in [0, 8] and Wang17 in [0, 1]. Higher values correspond to higher image quality, except for SSEQ where 0 is the best quality.

pendent of the subject's age. The results for the laser scanner are in line with the LED ones. Note that this is only a first indicator as the number of subjects/fingers in each of the subgroups is low. In order to arrive at a more profound statement, a larger data set is needed.

4.6. Image Quality Assessment

The finger-vein images were analysed using 2 general image quality metrics (BIQAA [3] and SSEQ [7]). BIQAA and SSEQ were selected as they have been proved to be well suited for natural scene images. As they are based on image entropies they should perform well using arbitrary, not necessarily natural scene images, too. Moreover, GCF [11] was selected as it is a general image contast metric and thus independent of the image content. With the help of GCF the image contrast can be quantified exclusively disregearding the actual image content. As we aim to quantify the image quality of finger-vein images, of course a vein specific NIR image quality metric, Wang17 [17] was included as well. The image quality assessment results, listed in Tab. 6 are diverse. The recognition performance of the LED scanner is superior compared to the laser one. However, only GCF indicated that the LED images exhibit a higher image quality while BIQAA, SSEQ and Wang17 indicate the contrary. Hence, a reliable prediction of the recognition performance based on the assessed image quality is not possible.

5. Conclusion and Future Work

Two new, modular designed, multi-purpose finger-vein scanners have been proposed. The first one is based on widely used NIR LED illumination while the second one uses NIR lasers. NIR lasers have hardly been used in finger-vein recognition despite their advantages over LEDs, especially if it comes to touchless operation. Due to the narrow radiation angle of the lasers they enable an increased range of vertical finger movement without lowering the image contrast and overall image quality. A new dorsal finger-vein data set captured by utilising our two proposed scanners has been established. This data set contains 360 individual fingers (60 subjects and 6 fingers each), is publicly available for research purposes and can be downloaded at: `http://www.wavelab.at/sources/PLUSVein-FV3`.

The performance evaluation on our new data set confirms the decent recognition performance that can be achieved using our proposed scanner design, both the LED and the laser version and in the cross-sensor comparison scenario as well. Even the selected simple but well-established finger-vein recognition schemes arrived at quite a remarkable performance. In our set-up, where the finger is placed directly on top of the illumination source, the LED based scanner is able to compete and even slightly outperform the laser based version. However, this situation changes if the finger is placed a few centimetres away from the illuminator, then the laser scanner will outperform the LED one.

Moreover, a sex and age group specific subset analysis has been carried out which indicates that there is no substantial difference in terms of recognition performance for male and female subjects as well as among the different age groups of the subjects. Such a subgroup specific analysis has not been performed before. These results need further investigation and confirmation based on a larger data set.

As mentioned in the introduction, all the details about the scanner and its design will be made available as an open-hardware documentation together with an open-source repository where construction plans, schematics, parts lists, firmware, etc. can be found. Researchers can benefit from our open-source design, as it enables them to build a scanner based on our design on their own. By capturing and providing finger-vein images using a scanner based on our design, i.e. having essentially the same structure as we proposed, they can contribute to a large, open, publicly available finger-vein data set. The whole finger-vein research community will benefit from such a data set.

Together with our partners as well as other researchers building a scanner device based on our design, we are confident that our data set will continue to grow in the future. We are currently capturing further subjects in-house and our finger-vein data set is expected to contain more than 100 subjects by the end of 2018. Furthermore, we are extending our data set by capturing palmar finger-vein images as well, which will be released soon.

Acknowledgements

This project has received funding from the European Union's Horizon 2020 research and innovation program under grant agreement No. 700259.

References

[1] M. S. M. Asaari, S. A. Suandi, and B. A. Rosdi. Fusion of band limited phase only correlation and width centroid contour distance for finger based biometrics. *Expert Systems with Applications*, 41(7):3367–3382, 2014.

[2] J. H. Choi, W. Song, T. Kim, S.-R. Lee, and H. C. Kim. Finger vein extraction using gradient normalization and principal curvature. volume 7251, pages 7251 – 7251 – 9, 2009.

[3] S. Gabarda and G. Cristóbal. Blind image quality assessment through anisotropy. *JOSA A*, 24(12):B42–B51, 2007.

[4] C. Kauba, J. Reissig, and A. Uhl. Pre-processing cascades and fusion in finger vein recognition. In *Proceedings of the International Conference of the Biometrics Special Interest Group (BIOSIG'14)*, Darmstadt, Germany, Sept. 2014.

[5] J. Kim, H.-J. Kong, S. Park, S. Noh, S.-R. Lee, T. Kim, and H. C. Kim. Non-contact finger vein acquisition system using nir laser. In *Sensors, Cameras, and Systems for Industrial/Scientific Applications X*, volume 7249. International Society for Optics and Photonics, 2009.

[6] A. Kumar and Y. Zhou. Human identification using finger images. *Image Processing, IEEE Transactions on*, 21(4):2228–2244, 2012.

[7] L. Liu, B. Liu, H. Huang, and A. C. Bovik. No-reference image quality assessment based on spatial and spectral entropies. *Signal Processing: Image Communication*, 29(8):856–863, 2014.

[8] D. G. Lowe. Object recognition from local scale-invariant features. In *Proceedings of the Seventh IEEE International Conference on Computer Vision (CVPR'99)*, volume 2, pages 1150 – 1157. IEEE, 1999.

[9] Y. Lu, S. J. Xie, S. Yoon, Z. Wang, and D. S. Park. An available database for the research of finger vein recognition. In *Image and Signal Processing (CISP), 2013 6th International Congress on*, volume 1, pages 410–415. IEEE, 2013.

[10] D. Maio, D. Maltoni, R. Cappelli, J. L. Wayman, and A. K. Jain. FVC2004: Third Fingerprint Verification Competition. In *ICBA*, volume 3072 of *LNCS*, pages 1–7. Springer Verlag, 2004.

[11] K. Matkovic, L. Neumann, A. Neumann, T. Psik, and W. Purgathofer. Global contrast factor-a new approach to image contrast. *Computational Aesthetics*, 2005:159–168, 2005.

[12] N. Miura, A. Nagasaka, and T. Miyatake. Extraction of finger-vein patterns using maximum curvature points in image profiles. *IEICE transactions on information and systems*, 90(8):1185–1194, 2007.

[13] R. Raghavendra and C. Busch. Exploring dorsal finger vein pattern for robust person recognition. In *2015 International Conference on Biometrics (ICB)*, pages 341–348, May 2015.

[14] P. Tome, M. Vanoni, and S. Marcel. On the vulnerability of finger vein recognition to spoofing. In *IEEE International Conference of the Biometrics Special Interest Group (BIOSIG)*, Sept. 2014.

[15] B. Ton and R. Veldhuis. A high quality finger vascular pattern dataset collected using a custom designed capturing device. In *International Conference on Biometrics, ICB 2013*. IEEE, 2013.

[16] University of Reading. PROTECT Multimodal DB Dataset, June 2017. Available by request at http://projectprotect.eu/dataset/.

[17] C. Wang, X. Zeng, X. Sun, W. Dong, and Z. Zhu. Quality assessment on near infrared palm vein image. In *Automation (YAC), 2017 32nd Youth Academic Annual Conference of Chinese Association of*, pages 1127–1130. IEEE, 2017.

[18] W. Yang, X. Yu, and Q. Liao. Personal authentication using finger vein pattern and finger-dorsa texture fusion. In *Proceedings of the 17th ACM international conference on Multimedia*, pages 905–908. ACM, 2009.

[19] Y. Yin, L. Liu, and X. Sun. Sdumla-hmt: a multimodal biometric database. *Biometric Recognition*, pages 260–268, 2011.

[20] J. Zhang and J. Yang. Finger-vein image enhancement based on combination of gray-level grouping and circular gabor filter. In *Information Engineering and Computer Science, 2009. ICIECS 2009. International Conference on*, pages 1–4. IEEE, 2009.

[21] J. Zhao, H. Tian, W. Xu, and X. Li. A new approach to hand vein image enhancement. In *Intelligent Computation Technology and Automation, 2009. ICICTA'09. Second International Conference on*, volume 1, pages 499–501. IEEE, 2009.

[22] K. Zuiderveld. Contrast limited adaptive histogram equalization. In P. S. Heckbert, editor, *Graphics Gems IV*, pages 474–485. Morgan Kaufmann, 1994.

Multi-Perspective Finger-Vein Biometrics

Bernhard Prommegger and Christof Kauba and Andreas Uhl
University of Salzburg
Jakob-Haringer-Str. 2
5020 Salzburg, AUSTRIA
{bprommeg, ckauba, uhl}@cosy.sbg.ac.at

Abstract

Most finger vein recognition systems use palmar finger images. There is some work on the dorsal view, but the remaining views have not been sufficiently investigated yet. All major public available finger-vein databases contain only images from the palmar view and only one smaller database has images from the dorsal view. We aim to fill this gap and evaluate the performance using other perspectives than dorsal and palmar. Therefore, we established a new finger vein data set that consists of videos showing the vein structure all around the finger. We carried out several experiments utilizing common finger-vein recognition algorithms to quantify the recognition performance of each single projection. We further analyzed if a fusion of different views can improve the recognition performance of the system.

1. Introduction

Biometric authentication systems are well established today as they exhibit many advantages over traditional password and token based ones. The most prominent examples are fingerprint and face recognition systems. In recent times authentication based on finger- and hand-veins has gained more attention as they provide several advantages over the well established fingerprint ones. Finger-vein recognition utilizes the pattern of the blood vessels inside the hand of a human which is captured using near infrared (NIR) illumination. Finger-vein recognition is more resistant against forgery because the veins are underneath the skin and only visible in infrared light. In addition the vein patterns are neither susceptible to abrasion nor skin surface conditions. The drawbacks of finger-vein based recognition systems include relatively big capturing devices compared to fingerprint sensors, images having low contrast and quality in general and that the vein structure may be influenced by temperature, physical activity and certain injuries and diseases.

978-1-5386-7180-1/18/$31.00 ©2018 IEEE

Currently there has only been little research on finger-veins biometric recognition systems using images from different viewpoints. Most works focus on the analysis of the palmar perspective [1, 7, 15, 16, 18, 19]. Raghavendra and Busch [12] proposed a vein recognition system for the dorsal perspective, Lu et al. [8] fused images from two different views which are positioned quite close to each other. Zhang et al. [22] applied point cloud matching on hand-veins using two cameras. All major publicly available finger-vein databases contain only images from the palmar or dorsal perspective. Table 1 lists these available data sets. The only dorsal database has just been released and was not used in any publication so far. To the best of our knowledge, there is no work analyzing finger-veins using perspectives all around the finger. Hence, it is not clear if there are other perspectives that provides better or enough additional information to improve the performance of the recognition system. Another advantage of using several perspectives is an increased robustness against spoofing attacks. It has been shown that finger- as well as hand-vein recognition systems are susceptible to spoofing [15, 14]. The proposed spoofing technique is based on a simple paper printout of the vein pattern. Capturing the vein images from different perspectives will prevent such simple kinds of spoofing attacks.

Name	Subjects	Finger	Images	View
UTFVP [16]	60	6	1440	palmar
FV-USM [1]	123	4	5940	palmar
MMCBNU 6000 [7]	100	6	6000	palmar
SDUMLA HMT [19]	106	6	3816	palmar
VERA FV DB [15]	110	2	440	palmar
THU-FVFDT [18]	610	2	6540	palmar
PROTECT MM DB [17]	20	4	240	dorsal
HKPU-FID [5]	156	2	3132	palmar

Table 1. Publicly available finger-vein data sets

The main goal of this work is to evaluate the recognition performance of finger-vein images taken from different perspectives. We evaluate the performance of these additional perspectives in order to find out if they exhibit a better or similar performance compared to the palmar one or

at least provide enough information to improve the recognition performance when fusing them. The provided data set can also be used to evaluate the robustness of finger recognition systems against longitudinal finger rotation. Based on this data set, the different projections' individual recognition performances are evaluated utilizing some well established vein recognition schemes, compared and ranked. In addition, we conducted experiments using score-level fusion of selected projections in order to find out if the recognition performance can be increased further.

The rest of the paper is organized as follows: Section 2 describes the used finger vein recognition system. At first the image acquisition is explained, then the algorithms for ROI extraction, preprocessing, feature extraction and comparison are briefly outlined. Section 3 contains informations about the custom build multi-perspective finger-vein scanner hardware used to acquire the new data set as well as a description of the data set itself. Section 4 presents the experimental protocol and discusses the results. Section 5 concludes this paper.

2. Finger-Vein Recognition System

2.1. Image Acquisition

A hand-vein scanner consists of 2 basic components: a near-infrared (NIR) sensitive camera and a NIR light source. Usually there is some automatic illumination intensity control to achieve an optimal contrast of the vein images. The wavelength of the NIR light source is typically between 730 and 950 nm. The near-infrared light is absorbed by the haemoglobin in the blood flowing through the veins and arteries. Thus, they appear as dark lines in the captured images. The camera should be equipped with an NIR pass-through filter to block the ambient light and further enhance the image contrast.

2.2. Preprocessing, Feature Extraction and Comparison

ROI Extraction Prior to the extraction of the region of interest (ROI), the finger is aligned and normalized. The alignment should place the finger always in the same position - independent of the relative position of the finger during the acquisition. To achieve this, we detected the finger lines (edge between finger and the background of the image) and calculate the center line (in the middle of the two finger lines). Next we rotate and translate the center line of the finger in a way that it is placed in the middle of the image and mask the image outside of the finger region. The final step is to extract a rectangular ROI. In order to keep the whole information of the vein structure, we first adjust the finger region to fit into a rectangle of defined height and just cut off some pixels on the border. The three steps are visualized in Figure 1.

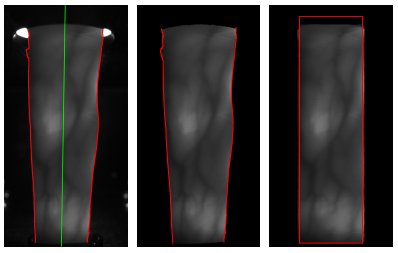

Figure 1. ROI Extraction

Preprocessing Preprocessing tries to enhance the low contrast and improve the image quality. Simple **CLAHE** [24] or other local histogram equalization techniques are most prevalent according to the literature for this purpose. We used **High Frequency Emphasis Filtering (HFE)** which was originally proposed for hand vein image enhancement [23]. In addition, filtering using a **Circular Gabor Filter** (**CGF**) as proposed by Zhang and Yang [20] was applied. Furthermore, the images were resized to half of their original size, which not only speed up the comparison process but also improved the results. For more details on the preprocessing methods the interested reader is referred to the authors' original publication [3].

Feature Extraction and Comparison We used two different types of feature extraction and comparison methods. The first three techniques discussed aim to extract the vein pattern from the background resulting in a binary image followed by a comparison of these binary images using a correlation measure. All algorithms are well established and therefore deliver reproducible results. We used the publicly available implementations published in [4].

Maximum Curvature (MC [11]) aims to emphasize only the center lines of the veins and is therefore insensitive to varying vein widths. The first step is the extraction of the center positions of the veins. Afterwards, a score according to the width and curvature of the vein region is assigned to each center position which is recorded in a matrix called locus space. Due to noise or other distortions some pixels may not have been classified correctly at the first step, thus the center positions of the veins are connected using a filtering operation. Finally binarization is done by thresholding using the median of the locus space.

Principal Curvature (PC [2]): At first the gradient field of the image is calculated. Hard thresholding is done to filter out small noise components and then the gradient at each pixel is normalized to 1 to get a normalized gradient field.

This is smoothed by applying a Gaussian filter. The next step is the actual principal curvature calculation. It is obtained from the Eigenvalues of the Hessian matrix at each pixel. The two Eigenvectors of the Hessian matrix represent the directions of the maximum and minimum curvature and the corresponding Eigenvalues are the principal curvatures. Only the bigger one which corresponds to the maximum curvature is used. The last step is a binarization of the principal curvature values to get the binary vein output image.

Gabor Filter (GF [5]): A filter bank consisting of several 2D even symmetric Gabor filters with different orientations (in $\frac{\pi}{k}$ steps where k is the number of orientations) is created. Several features images are extracted by filtering the vein image using the different filter kernels of the Gabor filter bank. The final feature image is obtained by fusing all the single images from the previous step. This final vein output image is then post-processing using morphological operations to remove noise.

For comparison the binary feature images we extended the approach in [10] and [11]. As the input images are neither registered to each other nor aligned, the correlation between the input image in x- and y-direction shifted versions of the reference image is calculated. The maximum of these correlation values is normalized and then used as final comparison score.

In contrast to the techniques described above, key-point based techniques try to use information from the most discriminative points as well as considering the neighborhood and context information of these points by extracting key-points and assigning a descriptor to each key-point. We used a **SIFT** [6] based technique with additional key-point filtering. Details are described in [3].

3. Multi-Perspective Finger-Vein Data Set

Due to the lack of an existing data set consisting of finger-vein images from different perspectives, we established a new data set which will be made publicly available. The images have been acquired using a custom build scanner. The different projection angles are achieved by rotating a NIR camera and the illumination unit around the finger. The principle is shown in Figure 2: The finger is positioned at the axis of rotation, whereas the camera and the illumination module are placed on the opposite sides, rotating around the finger, i.e. the scanner is based on the transillumination principle. The rotation of camera and light source enables the scanner to acquire images from different views.

3.1. Multi-Perspective Finger-Vein Scanner

Our custom build sensor is based on the above mentioned principle. All non-commercially available parts were engineered and manufactured by ourselves using a 3D printer and a laser cutter for the wooden parts. Figure 3 shows the unwrapped scanner with all its components. In the middle of

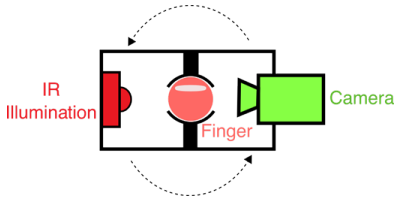

Figure 2. Basic principle of our finger vein scanner

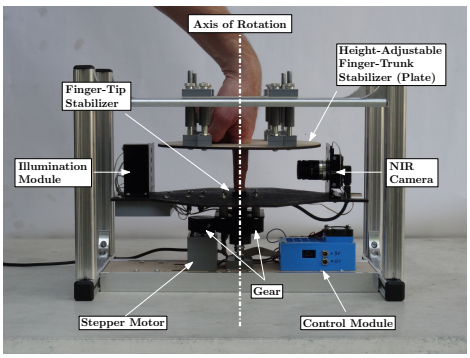

Figure 3. Custom build multi-perspective finger-vein scanner

the image you can see the finger. In order to keep the movement of the finger during the acquisition to a minimum, we added two parts to help to stabilize the finger. For the finger-tip, we constructed a part that has a finger-tip shaped hole. Putting the finger into this hole keeps it in its position. For the hand we added a height-adjustable wooden plate. Placing the hand on this plate stabilizes the trunk of the finger. The height of the plate is adjusted according to the length of the captured finger. The illumination module on the left side consists of 5 NIR laser diodes (808 nm) placed on a strip. The illumination intensity of each laser diode is controlled separately. The plane of focus is set at the axis of rotation where the center of the finger is located. This results in a uniform illumination of the finger. During data acquisition, the intensity of the different laser diodes is set automatically. This is achieved by individually setting the intensity value (controlled by the operating current) for each laser. The best value is selected by evaluating the image contrast in the corresponding section of the image. The images are captured by a NIR enhanced industrial camera (IDS Imaging UI-1240ML-NIR, max. resolution 1280x1024 pixels) with a 9 mm wide-angle-lens (Fujifilm, HF9HA-1b, 9mm, 2/3"). An additional NIR longpass filter (Midopt LP780, useful range: 800-1100mm) mounted on the lens blocks visible light up to a wavelength 780 nm. The rotation is ac-

complished using a stepping motor (SY42STH47-1684A). The stepper and the rotor are connected via self printed cogwheels having a gear ratio of 1:5/3 (motor to rotor). One step corresponds to $0.0675°$, thus it is possible to capture a maximum of 5.333 different projections. The sensor has a size of 25.8 x 32.5 x 45.5 cm (width x height x depth). The rotor has a length of 38 cm.

The acquisition process is semi-automated. After the finger is put into the device and the capture process is initiated, the illumination for the finger is set automatically in order to achieve an optimal image contrast with the help of a contrast measure. After this, the video acquisition is started. To achieve a defined resolution (in degrees) of images (video frames), the speed of the rotation and the video frame rate are coordinated with each other. All perspectives are captured in one run using the same illumination conditions to ensure the comparability of the different projections.

The automated illumination algorithm evaluates the average gray level of the image around in the center of each laser diode ($GL_{i,current}$)) and tries to achieve a preconfigured target gray value ($GL_{i,target}$). The centers of the diodes are arranged along the longitudinal axis of the finger. The individual intensity values of all diodes are set at once. Initially all diodes are set to half of its max intensity (I_{max}). The intensity is corrected by:

$$correction_i = \frac{GL_{i,target} - GL_{i,current}}{GL_{max}} * \frac{I_{max}}{2 * n} \quad (1)$$

where GL_{max} is the maximum gray value and n is the number of the current iteration. The maximum number of iterations is $\log_2(I_{max})$.

3.2. Data Set

The data set currently contains of a total of 252 unique fingers from 63 different subjects, 4 fingers per subject. We acquired videos from the index and middle finger of both hands where the target resolution is $1°$. As acquiring of the ring finger would be ergonomically uncomfortable for our volunteers, we skipped capturing of this finger.

We extracted the video frames as images which leads to 361 different perspectives (361 as we captured one frame for $0°$ and $360°$). Due to some variations in the video frame rate and the speed of the rotation during the capturing, we got between 357 and 362 frames for a full rotation (ideal would be 361 frames). To get 361 perspectives for every finger, we mapped the frame with the minimum deviation to the desired position for every perspective. This results in a maximum deviation of $0.5042°$ to its desired position.

Every finger was acquired 5 times - each time removing the finger from the scanner and putting it in again. This results in $252 * 361 * 5 = 454.860$ images in total. One projections consists of $252 * 5 = 1260$ images. The extracted frames are 8-bit gray scale images with a resolution of 1024*1280 pixels. Due to the fact that the finger is always positioned in the middle of the scanner, we cut of the borders. This results in to a final image resolution of 650x1280. Figure 4 shows our sensor during data acquisition. Recording a single person with 4 fingers and 5 iterations takes approximately 15 minutes.

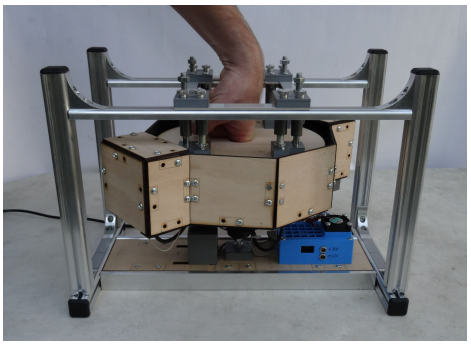

Figure 4. Data capturing

Figure 5 shows 6 example images ($0°$ - $300°$ in $60°$ steps, $0°$ corresponding to palmar view and $180°$ corresponding to dorsal view, respectively). It is apparent, that the number of visible veins in the images differ among the different projections. The black area at the top results from the hand stabilization plate. Depending on the length of the finger, the plate is pushed in further or less far.

The gender distribution of the volunteers is balanced. Among the 63 subjects, 27 are female (43%) and 36 men (57%). The dataset represents a good cross section among all age groups with a slight overhang among the 20-40 year olds. The youngest participant was 18, the oldest 79 years. Due to national law, we were not allowed to acquire data from people younger than 18. The actual distribution is shown in Figure 6. Our subjects are from 11 different countries[1] where the majority is white Europeans (73%).

4. Experiments

The experiments are split into two main parts: in the first part we analyze the recognition performance of the different projections. Every perspective is considered as a separate data set. We did not perform cross-projection comparison. We processed the images as described in section 2. As we aim for analyzing the recognition performance from views all around the finger, we used 73 perspectives extracted in $5°$ steps. To quantify the performance we used the EER as well as the FMR100 (the lowest $FNMR$ for $FMR \leq 1\%$), the

[1] Austria, Brazil, China, Ethiopia, Germany, Hungary, Iran, Italy, Russia, Slovenia, USA

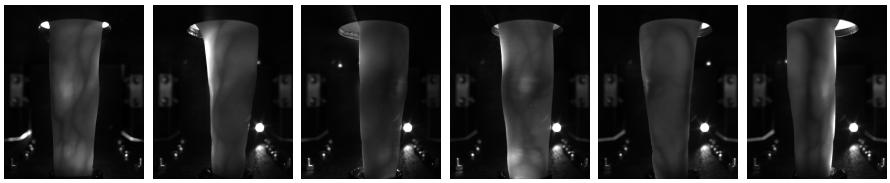

Figure 5. Example images of the data set acquired from 0° to 360° in 5° steps

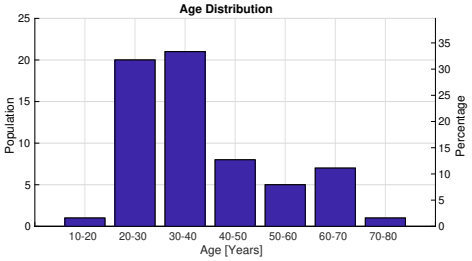

Figure 6. Age distribution among all subjects

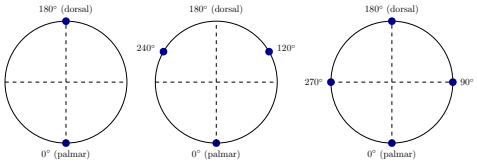

Figure 7. Selection of view angles for fusion with 2, 3 and 4 perspectives

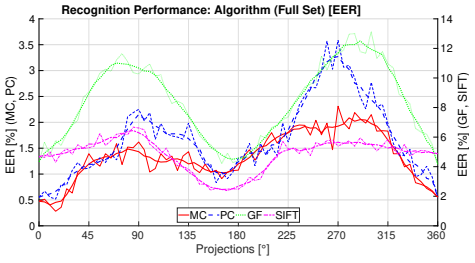

Figure 8. Recognition performance for different projections (EER)

FMR1000 (the lowest $FNMR$ for $FMR \leq 0.1\%$) and the ZeroFMR (the lowest $FNMR$ for $FMR = 0\%$). For their calculation we followed the test protocol of the FVC2004 [9]: for calculating the genuine scores for each projection, all possible genuine matches are done, which are $63 * 4 * \frac{5*4}{2} = 2520$ matches. For calculating the impostor scores, only the first image of a finger is matched against the first image of all other fingers, resulting in $4 * \frac{63*62}{2} = 7812$ matches, so together 10332 matches in total. All values are given in percentage terms, e.g. 2.35 means 2.35%.

In the second part of our experiments, we apply score-level fusion [13] to selected projections in order to improve the recognition performance. We start with the fusion of two views and increase the number to the maximum of 72 views. The perspectives used are evenly distributed over the whole circle. The step width of 5° of the selected images allows us to fuse 2, 3, 4, 6, 8, 9, 12, 18, 24, 36 and 72 different projections. Figure 7 shows the principle for the first 3 options. In addition, we fuse certain angles in a 2-view-fusion against all other perspectives. Since all scores are from the same modality using the same feature extraction method (we do not fuse results from different feature extraction algorithms), a score normalization was not necessary. For the fusion we used the simple sum rule.

4.1. Recognition Performance Results

Figure 8 visualizes the results for the evaluation of the recognition performance using MC, PC, GF and SIFT based on the EER. For every method there are two lines: the thin line shows the actual EER values of the relevant view, the thicker line is calculated from the EER values using a moving average filter of size 5 and should highlight the trend of the recognition performance. As the step between two projections is only 5°, the acquired images of neighboring perspectives show similar vein structures. This results in similar recognition performances. The best results are obtained around the palmar (0°) and dorsal (180°) region. The inferior results of the perspectives between those two view

can be explained by the fact that they contain fewer vein information, as it can be seen in Figure 9. It shows the original ROI, the ROI after preprocessing, and the extracted veins (using MC) for the views at 0°, 90°, 180° and 270°. It reveals, that the palmar and dorsal perspectives contain more vein information than the other two views. Moreover, it turns out that vein extraction - especially at 180° - compromises some features related with the knuckles of the finger. This features can be recognized as horizontal lines in the feature image.

For SIFT, the best performance is achieved around the dorsal region. The palmar region exhibits better performance than the remaining perspectives as well, but it is inferior compared to the dorsal one. This is due to the applied preprocessing: for SIFT we only apply algorithms that enhance the vein structure, but not a vein extraction algorithm (binarization) ahead of the SIFT point calculation. This prevails the texture of the finger. Especially the structure of finger knuckles seem to contain a lot of information in it. Finger knuckles have been introduced by Zhang et al. [21] as its own biometric modality. This could explain the better performance at the dorsal view. Yang [18] et al. experienced similar behavior. They fused the finger vein structure of the palmar view and the finger texture of the dorsal view which improved the recognition performance.

The EERs for the best projections are in accordance with the rates achieved in well-established implementations. For projections other than palmar/dorsal no comparisons are available. The best/worst rates are shown in Table 2.

	Worst Result		Best Result	
	View	EER	View	EER
MC	270°	2.31	15°	0.28
PC	270°	3.59	15°	0.52
GF	300°	13.12	360°	4.16
SIFT	85°	6.67	170°	2.38

Table 2. Recognition performance (EER) for single views

The results for FMR100 (Figure 10), FMR1000 (Figure 11) and ZeroFMR (Figure 12) show the same trend as the EER. Again, the best performance is achieved around 0° and 180°.

To ensure that two opposing views do not contain the same (just mirrored) information, we further investigated the palmar and dorsal perspective. We mirrored the images of the dorsal view along the longitudinal axis of the finger and matched them against the palmar ones. If both perspectives show the same blood vessels, they should - due to the mirroring - be registered to each other, and a comparison against each other would show similar performance as comparing the single views itself. Our results show exactly the opposite behavior: The EER of all four used algorithms is close to 50% which means that the vein structure of the two perspectives is not related to each other. Figure 9 shows the original ROI, the ROI after preprocessing, and the extracted veins (using MC) for both projections. It is obvious that the vessel structure differs between the palmar and dorsal view. Table 3 shows the results in detail.

	EER for Perspective		
	0°	180°	0° vs 180°
MC	0.47	1.08	47.28
PC	0.55	1.31	49.41
GF	4.33	4.38	50.04
SIFT	4.68	2.48	46.74

Table 3. Recognition performance (EER) for palmar vs dorsal view

4.2. Score-Level Fusion Results

In the second part of our experiments we analyze the impact of fusing selected perspectives. In the first experiment we fuse an increasing number of views which are, as described in section 4, evenly distributed over the whole circle. As starting angles we used 0° (palmar view), 45°, 90°, 180° (dorsal view) and 270°.

Figure 13 visualizes the results for start angle 0°. The fusion results for MC, PC, GF and SIFT are similar: Fusing the palmar with dorsal view improves the result. With the fusion of 3 views (60°, 180° and 300°), the result is slightly inferior to the one with two views. This can be explained by the fact that we removed the well performing palmar view and replaced it with two less performing ones. When adding additional views, the recognition performance further increases and stabilizes at a high level.

As the remaining 4 start angles show - in principle - the same general trend, we do not discuss them in detail. Figure 14 shows the results of the other reference angles. Table 4 holds detailed results for the multi-perspective fusion. For every method/reference angle combination it shows the EER for the reference view and the worst/best fusion result. The number of views is always the minimum number of needed perspectives to achieve the stated EER. We achieved a clear performance increase for all combinations.

In our second fusion experiment we applied a 2-view-fusion of a certain perspective against all others. This was done for every feature extraction and comparison algorithm. As reference views we selected a good performing (0°) and an inferior performing view (270°).

Figure 15 shows the results for MC: The solid red line shows the recognition performance without fusion and serves as reference for the other lines. The dotted green line represents the fusion results for 270°. None of the fused values has a worse performance than the single-view performance of 270°. The dashed blue line for 0° shows the same behavior, although not as distinctive.

PC, GF and SIFT (not visualized) show similar behavior.

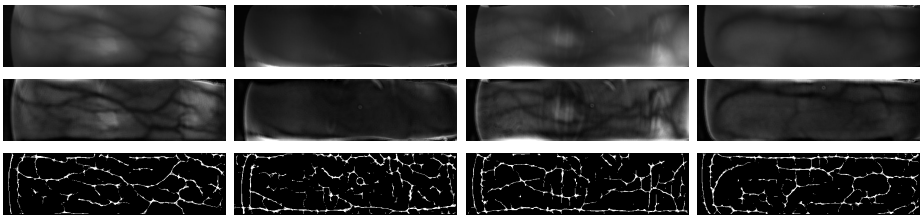

Figure 9. ROI, enhanced image and extracted features (MC) for different projections

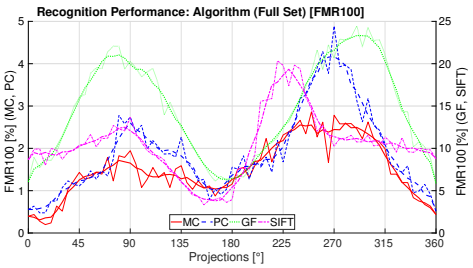

Figure 10. Recognition performance for different projections (FMR100)

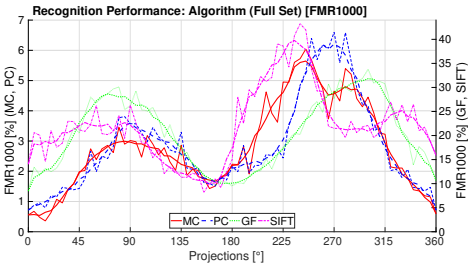

Figure 11. Recognition performance for different projections (FMR1000)

Note that the fusion of two views can result in an inferior recognition performance than the better of the two used views. E.g. this occurs for PC and reference view 0° when fusing it with the 305° perspective. Table 5 holds detailed results for the 2-view-fusion. It shows the EER for the reference view and the worst/best fusion result for every method/reference angle combination.

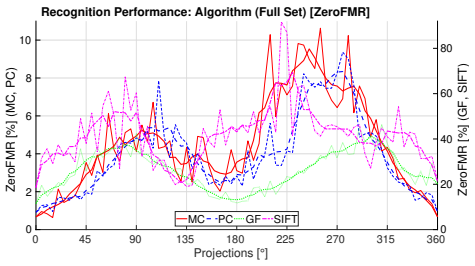

Figure 12. Recognition performance for different projections (ZeroFMR)

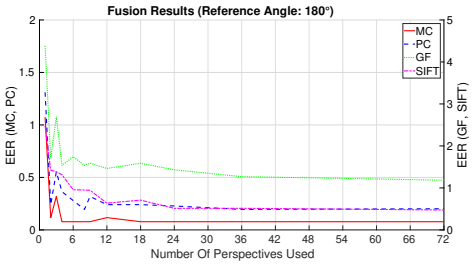

Figure 13. Recognition performance for fusion of different number of perspectives

4.3. Results Discussion

Our analysis of the recognition performance for different projections showed, that the widely used perspectives, palmar and dorsal, perform best. We also showed, that the vein structure of palmar and dorsal view are not connected to each other. The angles inbetween show a slightly worse performance, but it is still acceptable. For further in-depth analysis - e.g. on the individual performance of left/right hand or single fingers - the data set has to be extended by acquiring further subjects.

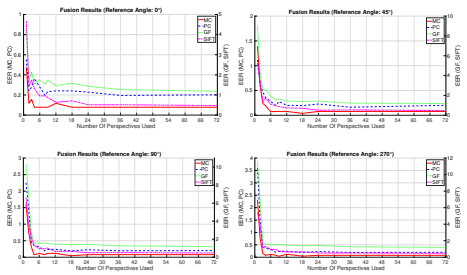

Figure 14. Recognition performance for fusion of different number of perspectives

	Reference		Worst Result		Best Result	
	View	EER	#	EER	#	EER
MC	0°	0.47	3	0.16	4	0.08
	45°	1.39	2	0.59	18	0.04
	90°	1.62	2	0.75	18	0.05
	180°	1.08	3	0.32	4	0.08
	270°	2.31	2	0.75	9	0.04
PC	0°	0.55	4	0.36	8	0.20
	45°	1.11	2	0.62	36	0.16
	90°	2.25	2	1.47	8	0.20
	180°	1.31	3	0.55	8	0.20
	270°	3.59	2	1.47	8	0.20
GF	0°	4.33	3	2.15	72	1.18
	45°	9.04	2	4.17	72	1.18
	90°	10.27	2	6.81	72	1.18
	180°	4.38	3	2.69	72	1.18
	270°	11.65	2	6.81	72	1.18
SIFT	0°	4.68	3	1.74	72	0.47
	45°	5.27	2	3.22	72	0.47
	90°	6.62	2	3.73	72	0.47
	180°	2.48	2	1.42	72	0.47
	270°	5.40	2	3.73	72	0.47

Table 4. Detailed performance results for multi-perspective fusion

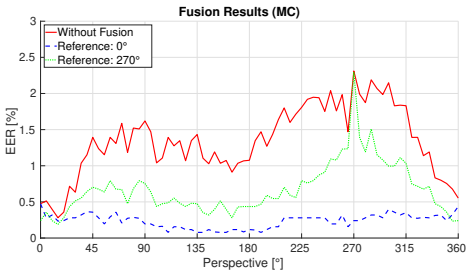

Figure 15. Recognition performance for fusion of two perspectives (MC)

The results indicate that the presence of finger texture has a positive influence on the recognition performance. As it can be seen in Figure 9, regularly used feature extraction algorithms also recognize the texture of the finger and thereby implicitly fuse vein structure and texture. This happens especially in the dorsal region with finger knuckles.

Additionally we showed, that the fusion of multiple perspectives improves the recognition performance. The fusion of two opposite views achieves is already sufficient to achieve superior results compared to a single-view evaluation.

	Reference		Worst Result		Best Result	
	View	EER	View	EER	View	EER
MC	0°	0.47	5°	0.47	110°	0.08
	270°	2.31	275°	2.30	15°	0.19
PC	0°	0.55	305°	0.68	170°	0.15
	270°	3.59	275°	3.58	360°	0.59
GF	0°	4.33	5°	4.33	170°	1.63
	270°	11.65	275°	11.64	165°	3.25
SIFT	0°	4.68	5°	4.68	170°	1.27
	270°	5.40	275°	5.39	175°	1.59

Table 5. Detailed performance results for reference view fusion

5. Conclusion

We established a new finger vein data set containing videos that capture the vein structure all around the finger. The videos allow us to extract frames in steps of 1°. Based on this data set, we evaluated the recognition performance using several common finger-vein recognition algorithms on each of the projections which enabled a direct comparison in terms of their accuracy. According to our experimental results, the best performance was achieved around 0° and 180° which corresponds to the palmar and dorsal view. We further showed that a fusion of two or more perspectives can improve the recognition results.

Our future work includes further analysis of the data we acquired using our custom made finger-vein scanner. We will use the data acquired in 1° steps to verify the robustness of existing algorithms with respect to the finger tilt. We aim to further improve recognition performance by fusing the information from different perspectives (further experiments with vein structure only and vein fused with texture are planned). Our final goal is to achieve a complete 3D reconstruction of the finger-vein structure. Our work will also include performance improvements in our scanner hardware.

6. Acknowledgements

This project has received funding from the European Union's Horizon 2020 research and innovation program under grant agreement No. 700259.

References

[1] M. S. M. Asaari, S. A. Suandi, and B. A. Rosdi. Fusion of band limited phase only correlation and width centroid contour distance for finger based biometrics. *Expert Systems with Applications*, 41(7):3367–3382, 2014.

[2] J. H. Choi, W. Song, T. Kim, S.-R. Lee, and H. C. Kim. Finger vein extraction using gradient normalization and principal curvature. In *IS&T/SPIE Electronic Imaging*, pages 725111–725111. International Society for Optics and Photonics, 2009.

[3] C. Kauba, J. Reissig, and A. Uhl. Pre-processing cascades and fusion in finger vein recognition. In *Proceedings of the International Conference of the Biometrics Special Interest Group (BIOSIG'14)*, Darmstadt, Germany, Sept. 2014.

[4] C. Kauba and A. Uhl. Shedding light on the veins - reflected light or transillumination in hand-vein recognition. In *Proceedings of the 11th IAPR/IEEE International Conference on Biometrics (ICB'18)*, pages 1–8, 2018.

[5] A. Kumar and Y. Zhou. Human identification using finger images. *Image Processing, IEEE Transactions on*, 21(4):2228–2244, 2012.

[6] D. G. Lowe. Object recognition from local scale-invariant features. In *Proceedings of the Seventh IEEE International Conference on Computer Vision (CVPR'99)*, volume 2, pages 1150 – 1157. IEEE, 1999.

[7] Y. Lu, S. J. Xie, S. Yoon, Z. Wang, and D. S. Park. An available database for the research of finger vein recognition. In *Image and Signal Processing (CISP), 2013 6th International Congress on*, volume 1, pages 410–415. IEEE, 2013.

[8] Y. Lu, S. Yoon, and D. S. Park. Finger vein identification system using two cameras. *Electronics Letters*, 50(22):1591–1593, 2014.

[9] D. Maio, D. Maltoni, R. Cappelli, J. L. Wayman, and A. K. Jain. FVC2004: Third Fingerprint Verification Competition. In *ICBA*, volume 3072 of *LNCS*, pages 1–7. Springer Verlag, 2004.

[10] N. Miura, A. Nagasaka, and T. Miyatake. Feature extraction of finger-vein patterns based on repeated line tracking and its application to personal identification. *Machine Vision and Applications*, 15(4):194–203, 2004.

[11] N. Miura, A. Nagasaka, and T. Miyatake. Extraction of finger-vein patterns using maximum curvature points in image profiles. *IEICE transactions on information and systems*, 90(8):1185–1194, 2007.

[12] R. Raghavendra and C. Busch. Exploring dorsal finger vein pattern for robust person recognition. In *Biometrics (ICB), 2015 International Conference on*, pages 341–348. IEEE, 2015.

[13] A. Ross and K. Nandakumar. *Encyclopedia of Biometrics: Fusion, Score-Level*, pages 611–616. Springer US, Boston, MA, 2009.

[14] P. Tome and S. Marcel. On the vulnerability of palm vein recognition to spoofing attacks. In *The 8th IAPR International Conference on Biometrics (ICB)*, May 2015.

[15] P. Tome, M. Vanoni, and S. Marcel. On the vulnerability of finger vein recognition to spoofing. In *IEEE International Conference of the Biometrics Special Interest Group (BIOSIG)*, Sept. 2014.

[16] B. T. Ton and R. N. J. Veldhuis. A high quality finger vascular pattern dataset collected using a custom designed capturing device. In *Proceedings of the 2013 International Conference on Biometrics (ICB), Madrid, Spain*, pages 1–5, 2013.

[17] University of Reading. PROTECT Multimodal DB Dataset, June 2017. Available by request at projectprotect.eu/dataset.

[18] W. Yang, X. Yu, and Q. Liao. Personal authentication using finger vein pattern and finger-dorsa texture fusion. In *Proceedings of the 17th ACM international conference on Multimedia*, pages 905–908. ACM, 2009.

[19] Y. Yin, L. Liu, and X. Sun. Sdumla-hmt: a multimodal biometric database. *Biometric Recognition*, pages 260–268, 2011.

[20] J. Zhang and J. Yang. Finger-vein image enhancement based on combination of gray-level grouping and circular gabor filter. In *Information Engineering and Computer Science, 2009. ICIECS 2009. International Conference on*, pages 1–4. IEEE, 2009.

[21] L. Zhang, L. Zhang, and D. Zhang. Finger-knuckle-print: a new biometric identifier. In *Image Processing (ICIP), 2009 16th IEEE International Conference on*, pages 1981–1984. IEEE, 2009.

[22] Q. Zhang, Y. Zhou, D. Wang, and X. Hu. Personal authentication using hand vein and knuckle shape point cloud matching. In *Biometrics: Theory, Applications and Systems (BTAS), 2013 IEEE Sixth International Conference on*, pages 1–6. IEEE, 2013.

[23] J. Zhao, H. Tian, W. Xu, and X. Li. A new approach to hand vein image enhancement. In *Intelligent Computation Technology and Automation, 2009. ICICTA'09. Second International Conference on*, volume 1, pages 499–501. IEEE, 2009.

[24] K. Zuiderveld. Contrast limited adaptive histogram equalization. In P. S. Heckbert, editor, *Graphics Gems IV*, pages 474–485. Morgan Kaufmann, 1994.

On the Extent of Longitudinal Finger Rotation in Publicly Available Finger Vein Data Sets

Bernhard Prommegger and Christof Kauba and Andreas Uhl
University of Salzburg
Jakob-Haringer-Str. 2
5020 Salzburg, AUSTRIA
{bprommeg, ckauba, uhl}@cs.sbg.ac.at

Abstract

Finger vein recognition deals with the identification of a subjects based on its venous pattern within the fingers. The majority of the publicly available finger vein data sets has been acquired with the help of scanner devices that capture a single finger from the palmar side using light transmission. Some of them are equipped with a contact surface or other structures to support in finger placement. However, these means are not able to prevent all possible types of finger misplacements, in particular longitudinal finger rotation can not be averted. It has been shown that this type of finger rotation results in a non-linear deformation of the vein structure, causing severe problems to finger vein recognition systems. So far it is not known if and to which extent this longitudinal finger rotation is present in publicly available finger vein data sets. This paper evaluates the presence of longitudinal finger rotation and its extent in four publicly available finger vein data sets and provides the estimated rotation angles to the scientific public. This additional information will increase the value of the evaluated data sets. To verify the correctness of the estimated rotation angles, we furthermore demonstrate that employing a simple rotation correction, using those rotation angles, improves the recognition performance.

1. Introduction

Biometric authentication systems have become well established nowadays. The most prominent examples are iris, face and fingerprint recognition systems. Recently, some emerging, new biometrics gain more attraction, especially hand and finger vein based systems as they provide several advantages over e.g. fingerprint based ones. Vein based systems utilize the patterns of the blood vessels inside the human body which are only visible in near infrared (NIR) light. This makes vein recognition systems more resistant against forgery. Moreover, the vein patterns are insensible to abrasion and skin surface conditions and a liveness detection can be performed easily [6]. The drawbacks of such systems compared to fingerprint based ones are the relatively large capturing devices and the low contrast and quality of the captured images. Furthermore, it is not clear if the blood vessel structure might be influenced by e.g. physical activity, temperature changes, certain injuries or diseases.

The performance of finger vein recognition systems is highly dependent on the quality of the acquired images. The acquisition quality is influenced by different internal and external factors, e.g. the quality of the illumination and camera module, ambient light or the presentation of the finger during acquisition. The later includes unintended finger movement during acquisition and finger misplacement in general. The influence of some kind of misplacements can be reduced by adding components to the scanner device, for example by adding a finger-shaped guiding surface to prevent a shift of the finger. However, finger tilt and longitudinal rotation of the finger are hard to avoid and pose severe problems for most finger vein recognition schemes. As finger vein systems evolve towards contact-less operation, problems due to finger misplacements will receive more attention in the future.

Performance degradations caused by various types of finger misplacement are not new and have been addressed in several publications. Kumar and Zhou [6] addressed the need for robust finger vein image normalization, including rotational alignment, already in 2012. Chen et al. [2] stated that deformations caused by a misplacement of the finger can be corrected either during pre-processing, feature extraction or comparison. Moreover, the design of the finger vein sensor helps to avoid or reduce misplacements of the finger as well. In [13] the authors showed, that longitudinal finger rotation has a severe influence on the recognition performance of a finger vein recognition system. There are several approaches that try to handle these issues during the

978-1-7281-3640-0/19/$31.00 ©2019 IEEE

processing of the vein patterns. Recognition schemes that claim to be resistant against finger misplacements to a certain extent are e.g. [7, 10, 15]. Huang et al. [3] improved the resistance against longitudinal rotation by applying an elliptical normalization to the input images. Chen et al. [2] tried to tackle the problem by detecting the deformation based on an analysis of the shape of the finger, e.g. around its longitudinal axis, and corrects the detected deformations using linear and non-linear transformations. However, none of theses approaches quantifies the extent (e.g. the rotation angle or the tilt angle) of the misplacement on which the deformation is based on. Besides these software based solutions, there are some hardware-based ones which aim to prevent finger misplacements during acquisition rather than correcting them. For example, Kauba et al. [5] presented a finger vein scanner that captures three fingers at once and requires the subject to place the fingers in an aligned position on a finger shaped guiding surface. This reduces longitudinal finger rotation, planar finger rotation as well as finger shifts to a minimum.

The main contribution of this work is the analysis of four public finger vein data sets on the presence of longitudinal finger rotation. Our analysis does not only indicate if longitudinal finger rotation is present, but also estimates the longitudinal rotation angle. This increases the value of those data sets for the scientific public as future evaluations on longitudinal finger rotation detection and correction can use the provided information as a reference. To verify our rotation detection results, we apply a simple rotation correction based on the estimated rotation angle and compare the recognition results of the original data set. The four finger vein data sets are UTFVP [14], SDUMLA-HMT [16], FV-USM [1] and PLUSVein-FV3 [4]. In contrast to the first three data sets, PLUSVein-FV3 should exhibit hardly any longitudinal finger rotation due to the design of the scanner device.

The rest of this paper is organized as follows: Section 2 describes longitudinal finger rotation and its impact on the recognition performance. Section 3 presents our proposed approach to detect and determine the longitudinal finger rotation present in a data set. Section 4 explains the processing tool-chain, the analysed data sets, the experimental set-up and discusses the results. Section 5 concludes this paper and gives an outlook on our future work.

2. Longitudinal Finger Rotation

Typically, finger vein scanners are designed to acquire only a single finger at a time. Different types of finger misplacement can easily occur with these scanners and pose a severe problem. Figure 1 shows the orientations of the x, y and z axis with respect to the finger. The different types of finger misplacement include planar shifts and rotation (shifts and rotations in the xy-plane) , shifts of the finger in z-direction (distance to the camera, scaling), finger bending, finger tilt (finger tip and root are not in the same xy-plane) and longitudinal finger rotation around the y-axis. As described in [13], the influence of some of these problematic misplacements can be reduced or even prevented completely during acquisition by adding simple support structures for finger positioning (e.g. guiding walls to prevent planar shifts) or corrected during pre-processing, feature extraction or comparison. Almost all currently available sensors are equipped with such support structures, but most of them still do not prevent a rotation around the y-axis (longitudinal finger rotation). Thus, longitudinal finger rotation cannot be ruled out and poses a severe problem to finger vein recognition systems.

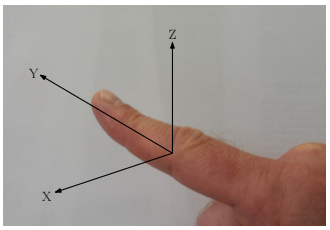

Figure 1. Definition of the axes of a finger in a three-dimensional space

The captured vein structure is a projection of the vessel structure in the 3D space onto a 2D plane. If the finger is rotated along its longitudinal axis, the vein pattern is deformed according to a non-linear transformation. Figure 2 shows the effect of longitudinal finger rotation on the vein pattern. The finger cross section (top row) is rotated from -30° to +30°. As a result of the rotation the projected pattern of the veins (bottom row) changes as well. Depending on the relative position of the veins to each other and the rotation angle, some of the captured veins might merge into a single one. The vein structures of -30° (left), 0° (middle) and 30° (right) are completely different. Widely used vein recognition schemes can handle such deformations only to a certain extent [13]. If the deformations caused by the longitudinal rotation are corrected, the negative effect can be reduced but not completely prevented.

3. Finger Rotation Detection

All publicly available finger vein data sets provide only images captured from one perspective. But a single image does not provide enough information to reliably calculate or estimate the longitudinal rotation angle. Therefore, we propose an empirical approach to estimate the rotation angle: All images in the data set are rotated in steps of 1° within the range of $\pm 45°$. Then the rotated images of a finger are

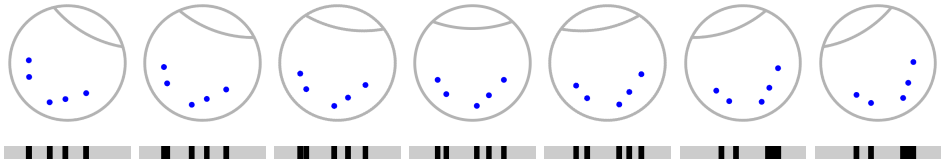

Figure 2. Longitudinal finger rotation principle: a schematic finger cross section showing five veins (blue dots) rotated from -30° (left) to +30° (right) in 10° steps. The projection (bottom row) of the vein pattern is different depending on the rotation angle according to a non-linear transformation (originally published in [13]).

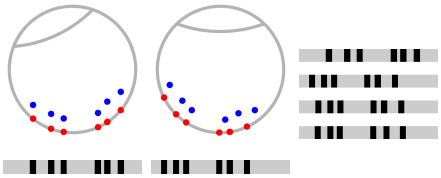

Figure 3. Principle of rotation correction. Left: finger rotated with 25°. The blue points depict the veins inside the finger, the cyan points the veins projected on the finger shape. The bar below is the projected vein pattern. Middle: the cyan points represent the rotation corrected vein pattern on the skin, the blue points represent the veins in the finger in its original position from the palmar view. The bar below is the rotation corrected vein pattern. On the right side the vein patterns are visualized below each other. From top to bottom: rotated vein pattern, corrected vein pattern, corrected pattern shifted for the highest correlation to the palmar pattern (bottom row).

compared to the first non rotated sample of this finger. The rotation angle is the angle, where the rotated an non rotated image shows the highest similarity, i.e. where the comparison score reaches its maximum. As more advanced vein recognition schemes, e.g. deformation tolerant feature point matching [10], try to compensate longitudinal rotation, they are not suitable for our approach. Thus, we opted to utilise Maxium Curvature (MC) [12], a simple vein pattern based feature extraction method and the comparison method proposed by Miura et al. in [11].

For an accurate correction of the vein pattern, in addition to the position of the veins in the 2D image, the shape of the finger and the depth of the veins within the finger must also be known. As this information is not available, both need to be estimated. We approximate the shape of the finger as a circle like Matsuda et al. did in [10]. We further assume, that the veins are located on the skin surface. Therefore, the vein pattern is projected back on the outer circle of the finger. Figure 3 depicts this principle. The left image shows a schematic cross section of a finger acquired under a longitudinal rotation of $\varphi_{rotate} = 25°$. The blue dots represent the veins in their proper position, the red ones those that are projected onto the skin. The bar below is a visualization of the vein pattern where the black areas correspond to the veins. In the middle image, the finger is rotated back into the ideal palmar position ($\varphi_{rotate} = 0°$). It is clearly visible, that the blue and red dots are not perfectly aligned with each other. The right side shows from top to bottom the vein patterns of the acquired image (same as on the left side), the rotated pattern (same as in the middle), a shifted version of the rotated pattern and the original pattern that would have been acquired without the presence of longitudinal rotation. It is clearly visible that the rotation corrected pattern is more similar to the original pattern than the acquired one. The additional shift is applied to achieve the highest possible correlation between the corrected and the original pattern.

The rotation of the veins by an angle of φ_{rotate} is calculated by applying a rotation matrix given in (1).

$$\begin{bmatrix} x_r \\ y_r \end{bmatrix} = \begin{bmatrix} cos(-\varphi_{rotate}) & -sin(-\varphi_{rotate}) \\ sin(-\varphi_{rotate}) & cos(-\varphi_{rotate}) \end{bmatrix} * \begin{bmatrix} x \\ y \end{bmatrix} \quad (1)$$

x and y are the coordinates of the vein pixel in the acquired image, x_r and y_r the ones in the rotated image. x is the position of the pixel in the vein pattern, y is calculated by (2)

$$y = \sqrt{r^2 - x^2} \quad (2)$$

where r is the approximated radius of the finger.

The rotation angle $\varphi_{i,j}$ between two samples of the same finger is calculated by (3). $score(i, j, \varphi_{rotate})$ is the score, obtained by applying the Miura matcher [11] on the extracted MC features, of the i^{th} sample rotated by φ_{rotate} and the non rotated j^{th} sample.

$$\varphi_{i,j} = \underset{-45° \leq \varphi_{rotate} \leq +45°}{\arg\max} score(i, j, \varphi_{rotate}) \quad (3)$$

To achieve a more robust result, the final rotation angle $\Phi_{i,1}$ is calculated as the average of $\varphi_{i,1}$ (the calculated angle of

the rotated i^{th} sample against the non rotated 1^{st} sample) and $\varphi_{1,i}$ (the calculated angle of the rotated 1^{st} sample against the non rotated i^{th} sample):

$$\Phi_{i,1} = \text{avg}\left(\varphi_{i,1}.\varphi_{1,i}\right) \quad (4)$$

4. Experiments

The rotation angle is estimated based on the approach described in Section 3. We used Maximum Curvature as feature extractor as it usually achieves accurate results in extracting the vein patterns. The rotation angle of the samples is always calculated with respect to the first sample of the respective finger. In order to confirm the obtained rotation angles, we evaluate the recognition performance of the original data sets as well as on the rotation corrected ones and compare the results. The rotation correction has been done in two different ways: with respect to the first sample of the respective finger and with respect to the mean of the determined rotation angles of each finger.

4.1. Data Sets

We evaluate the longitudinal finger rotation of four different publicly available finger vein data sets:

- **SDUMLA-HMT [16]** is a multimodal biometric database that contains samples for face, gait, iris, fingerprint and finger veins from 106 individuals. The finger vein subset contains six fingers (ring, middle and index finger from both hands) per subject, captured in one session taking six images of each finger.
- **UTFVP [14]** contains six fingers (ring, middle and index finger from both hands) from 60 volunteers in two sessions. At each session two samples per finger were captured.
- **FV-USM [1]** was acquired from 123 volunteers, four fingers each (left and right index and middle finger). The data was captured in two different sessions, capturing six samples per finger in each session.
- **PLUSVein-FV3 [4]** contains palmar and dorsal images of 360 fingers from 60 different subjects (ring, middle and index finger from both hands) captured in one session with five samples per finger using two different variants of the same sensor: One utilizing NIR laser modules for illumination, the other one using NIR LEDs. The sensor was built in a way that requires the subject to place the whole hand flat on the sensor. Therefore, the data set is expected contain little to no longitudinal rotation. We only evaluate the dorsal images acquired by the laser version of the sensor.

Table 1 contains an overview on the statistics of the data sets.

Name	Subjects	Finger	Samples	Images	View
SDUMLA-HMT	106	6	6	3816	palmar
UTFVP	60	6	4	1440	palmar
FV-USM	123	4	12	5904	palmar
PLUSVein-FV3	60	6	5	1800	dorsal

Table 1. Evaluated finger-vein data sets

Name	Genuine	Impostor	Total
SDUMLA-HMT	9540	200340	209880
UTFVP	2160	63720	65880
FV-USM	32472	120048	152520
PLUSVein-FV3	3600	63720	67320

Table 2. Number of comparisons for each data set

4.2. Recognition Tool-Chain

The finger vein recognition tool-chain consists of the following components:

1. For **finger region detection** and **finger alignment** we use an implementation that is based on [8].
2. The **ROI extraction** differs from [8]. We do not cut a defined rectangle within the finger, but similar to [3], normalize the finger to a fixed width.
3. To improve the visibility of the vein pattern we use **High Frequency Emphasis Filtering** (HFE) [18], **Circular Gabor Filter** (CGF) [17] and simple **CLAHE** (local histogram equalisation) [19] as **preprocessing**.
4. As **feature extraction** method we employ the well-established vein-pattern based **Maximum Curvature** method [12].
5. The **comparison** of the binary feature images is done using a correlation measure, calculated between the input images and in x- and y-direction shifted and rotated versions of the reference image as described in [11].

An implementation of the recognition tool-chain is available for download on our website[1].

4.3. Experimental Protocol

To quantify the performance, the EER, the FMR100 (the lowest FNMR for FMR $\leq$ 1%), the FMR1000 (the lowest FNMR for FMR $\leq$ 0,1%) as well as the ZeroFMR (the lowest FNMR for FMR = 0%) are used. We follow the test protocol of the FVC2004 [9]: For calculating the genuine scores, all possible genuine comparisons are performed. For calculating the impostor scores, only the first image of a finger is compared against the first image of all other fingers. The resulting numbers of comparisons for all data sets are listed in Table 2. To quantify the increase of the performance, the relative performance increase (RPI) is used, which

[1] http://wavelab.at/sources/Prommegger19c

is calculated as stated in (5):

$$RPI_{x,ref} = \frac{EER_{ref} - EER_x}{EER_x}, \quad (5)$$

EER_{ref} is the EER of the reference data set and EER_x the EER of the evaluated data set.

4.4. Results

Table 3 shows the detected longitudinal rotation angles with respect to the reference image (first sample of every finger) as a histogram distribution with 5° bins. As expected, the PLUSVein-FV3 data set exhibits little to no rotation. 98.4% of the fingers lay within 0-5° of rotation. There is no sample that is rotated more than 10° from its reference. The detected rotation on the UTFVP is small as well. 85% of the samples are within 5°, 99.1% within 10° of rotation. Only 0.9% of the images exceed a rotation of 10°. FV-USM exhibits a slightly higher degree of longitudinal rotation than UTFVP. 80% of the samples are within 5°, 95.3% are within 10° and 4.7% of the samples are rotated more than 10°. SDUMLA-HMT shows the largest deviations caused by longitudinal finger rotation. Only 56.4% of the images are rotated less than 5°, whereas 5.6% exceeds a rotation of more than 20°. The largest rotation detected is 44.5°.

Table 4 contains statistical data regarding the longitudinal rotation of the different data sets, i.e. the distance of the rotation angles with respect to the mean rotation angle of each finger and the maximum rotation distance between two samples of the same finger. PLUSVein-FV3 shows the smallest deviations. In average, there is a rotation of 1.37° between two samples. The maximum distance to the mean value is 8.6°, the maximum rotation between two samples is 12.5°. For UTFVP, the average distance to the mean rotation angle is 2.65°. The maximum rotation between two samples is 29.5°. The results for FV-USM are slightly worse than for UTFVP. Also Table 4 confirms that the level of longitudinal rotation present in the SDUMLA-HMT is high. On average, two samples are rotated 6.43° against each other. The maximum rotation angle between two samples is 77°, which is astonishingly high.

In order to ensure that the determined 77° did not occur due to an calculation error, we examined the respective sample images visually. The mentioned rotation was determined between sample #4 and #6 of the left ring finger of subject #96. Figure 4 shows the samples: on the left #1 as reference image, #4 in the middle and #6 on the right. The top row shows the original images as contained the data set. It is clearly visible that the three samples are rotated versions of the same finger. The second row shows the extracted ROIs and the third row shows the rotation corrected version of the ROI using the determined rotation anlge $\Phi_{i,1}$. Sample #4 (middle column) is corrected by 44.5° and sample #6 (left column) by -32.5°. One can easy see that the rotation corrected ROIs are better aligned with respect to longitudinal rotation.

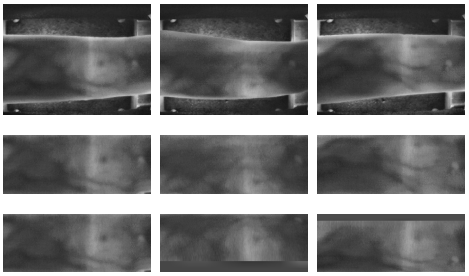

Figure 4. Three samples from the same finger (left ring finger of subject #96) of the SDUMLA-HTM data set. Top row: original images from data set, row 2: extracted ROI not rotated, row 3: corrected ROI. The left column shows sample #1 (reference image), the middle sample #4 (rotation angle: 44°) and the right sample #6 (rotation angle: -32°). All images are enhanced using CLAHE.

To verify the estimated rotation angles, the recognition performance for the original data sets (ORI) and the two corrected versions of the data sets have been evaluated: In the first version (ROT), all samples are corrected with respect to the first sample of each finger, in the second one (ROT Mean), all samples of a finger are corrected with respect to the calculated mean rotation angle of this finger. The rotation correction is done by applying the rotation matrix of Equation (1). The recognition performance results are given in Table 5. It also gives some statistics on the comparison score values, including the mean, minimum and maximum values for the genuine as well as for the impostor scores. The EER, FMR100, FMR1000 and ZeroFMR decreased for both correction scenarios. For SDUMLA-HMT, FV-USM and PLUSVein-FV3, the correction with respect to the first sample of a finger achieves the best result, for UTFVP the correction with respect to the mean rotation angle attains a superior performance. To point out the performance increase that can be gained by applying this simple rotation correction, the RPI as stated in Equation (5) is calculated too. For SDUMLA-HMT and UTFVP we arrive at a RPI of nearly 350%, for FV-USM of 120%. The lowest RPI is achieved for PLUSVein-FV3, which directly corresponds to the low level of longitudinal finger rotation present in this data set.

The improvement in terms of recognition performance is mainly due to a better separation of genuine and impostor scores. In Figure 5 the score distribution for the original SDUMLA-HMT data set (blue lines) and its corrected version (version 1, rotated to the first sample of a finger, red

Data Set	Rotation to mean								
	0° - 5°	5° - 10°	10° - 15°	15° - 20°	20° - 25°	25° - 30°	30° - 35°	35° - 40°	40° - 45°
SDUMLA-HMT	56.4%	21.5%	10.4%	6.2%	2.7%	1.6%	0.8%	0.4%	0.1%
UTFVP	85.2%	13.9%	0.8%	0.1%	-	-	-	-	-
FV-USM	80.0%	15.3%	3.7%	0.8%	0.2%	-	-	-	-
PLUSVein-FV3	98.4%	1.6%	-	-	-	-	-	-	-

Table 3. Distribution of longitudinal finger rotation in classes of size 5°.

Data Set	Absolute Distance to Mean			Maximum Distance		
	Mean	Max	Std	Mean	Max	Std
SDUMLA-HMT	6.43	44.83	6.90	19.40	77.00	15.73
UTFVP	2.65	16.50	2.29	7.95	29.50	4.41
FV-USM	3.04	23.83	3.23	11.32	41.00	7.75
PLUSVein-FV3	1.37	8.60	1.24	4.46	12.50	2.44

Table 4. Statistical data on the degree of rotation present in the data sets.

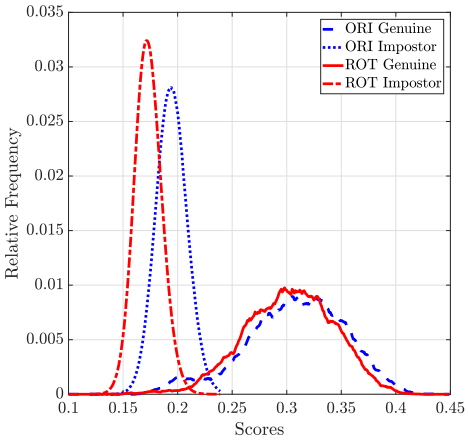

Figure 5. Distribution of genuine and impostor scores for SDUMLA-HMT: ORI = oiriginal data set, ROT = rotation corrected to 1st image

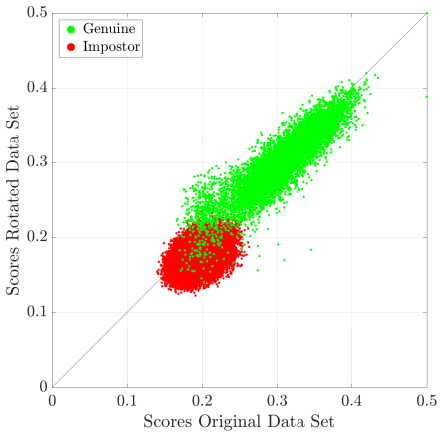

Figure 6. Changes in scores from the original data set to the rotation corrected data set

lines) is visualized. The impostor scores of the rotated images are lower in general compared to the scores obtained from the original data set. This is mainly due to the reduced extent of vertical shift that has to be applied during comparison for the corrected data set. In our set up, the shift range is reduced by a third compared to the value necessary to achieve the best results for the original data set. The reduction of the vertical shift also leads to a slight decrease in the genuine score values. However, this decrease is lower than for the impostor ones, which leads to a better separation of the scores in general. Moreover, the genuine scores of samples exhibiting a high degree of rotation are increased too (the accumulation of the original genuine scores around the score of 0.2 disappears after the correction). Figure 6 presents the shift in the score distributions in a different way by showing the change in their values. The score values of the original data set are plotted on the x axis while the ones of the corrected data set are plotted on the y axis. Due to the reduction of the individual impostor score values, the cluster corresponding to the impostor scores (red) moves slightly downwards. The genuine scores (green) move downwards too, but to a lower extent. The interesting part of the plot are those genuine scores that overlap with the impostor ones in the evaluation of the original data set. Most of these originally low genuine score are increased above the level of the impostor scores after the rotation correction. This becomes visible by the raise of the green genuine scores above the red impostor ones around the score of 0.2. Again, this visualises the better separation of genuine and impostor scores. The statistical values of the genuine and impostor scores in Table 5 confirm these visual observation.

Data Set	Version	Performance Indicators					Genuine Scores				Impostor Scores			
		EER	FMR100	FMR1000	ZeroFMR	RPI	Min	Mean	Max	Std	Min	Mean	Max	Std
SDUMLA-HMT	ORI	4.73 (±0.22)	6.12	8.09	63.25	-	0.17	0.31	0.44	0.05	0.14	0.19	0.33	0.01
	ROT	**1.07** (±0.11)	1.13	1.72	59.91	**341.6**	0.15	0.30	0.42	0.04	0.12	0.17	0.32	0.01
	ROT Mean	1.14 (±0.11)	1.18	1.82	47.77	315.8	0.14	0.30	0.42	0.04	0.12	0.17	0.30	0.01
UTFVP	ORI	0.42 (±0.12)	0.23	0.65	3.11	-	0.12	0.26	0.38	0.04	0.07	0.12	0.18	0.01
	ROT	0.19 (±0.09)	0.19	0.23	1.62	124.5	0.09	0.25	0.36	0.04	0.06	0.09	0.16	0.01
	ROT Mean	**0.09** (±0.06)	0.05	0.09	1.30	**349.1**	0.10	0.25	0.37	0.04	0.07	0.10	0.15	0.01
FV-USM	ORI	1.23 (±0.08)	1.30	2.34	5.27	-	0.13	0.25	0.36	0.03	0.11	0.15	0.19	0.01
	ROT	**0.56** (±0.05)	0.48	0.93	2.47	**120.1**	0.13	0.24	0.50	0.03	0.11	0.14	0.18	0.01
	ROT Mean	0.77 (±0.06)	0.69	1.42	3.93	59.4	0.13	0.24	0.40	0.03	0.11	0.14	0.19	0.01
PLUSVein-FV3	ORI	0.08 (±0.05)	0.03	0.08	0.39	-	0.08	0.20	0.32	0.04	0.05	0.07	0.09	0.00
	ROT	**0.06** (±0.04)	0.00	0.06	0.25	**50.0**	0.08	0.20	0.31	0.04	0.05	0.07	0.09	0.00
	ROT Mean	0.08 (±0.05)	0.00	0.08	0.22	0.9	0.08	0.20	0.32	0.04	0.05	0.07	0.09	0.00

Table 5. Recognition performance on the evaluated data sets and its corrected versions: ORI = original data set, ROT = rotation corrected to 1st image, ROT Mean = rotation corrected to mean of finger. Best achieved EER and RPI values are highlighted in bold.

5. Conclusion

It has been shown previously that longitudinal finger rotation poses a significant problem for many well-established recognition schemes [13]. This paper investigated on the presence and degree of longitudinal finger rotation in four publicly available finger vein data sets. The rotation angle between different samples of the same finger has been estimated based on an empirical approach using a correlation based comparison of the extracted vein patterns.

PLUSVein-FV3 showed the lowest degree of longitudinal finger rotation, followed by UTFVP and FV-USM, while SDUMLA-HMT exhibited the highest amount. The degree of longitudinal finger rotation present in the data set strongly depends on the design of the scanner device, the acquisition protocol and its supervision. In the PLUSVein-FV3 data set, the rotation is reduced to a minimum by requiring the subject to place the whole hand flat on the scanner device. The scanners used to acquire UTFVP, FV-USM, and SDUMLA-HMT were not built to avoid longitudinal finger rotation. Nevertheless, the small rotation present in UTFVP and FV-USM suggests that the acquisition protocol and supervision was very good.

Moreover, we applied a simple rotation correction and verified the determined rotation angles by comparing the recognition performance of the original data sets and their rotation corrected versions. It turned out that the recognition performance could be improved for all four data sets. The highest improvement could be achieved for SDUMLA-HMT and UTFVP with a performance increase of 350%. Even the correction of the low longitudinal rotation in PLUSVein-FV3 lead to a performance increase of 50%.

We provide the determined rotation angles for all four data sets in order to increase the value of those data sets by augmenting them with this additional information. These can be download at: `http://wavelab.at/sources/Prommegger19c`.

In our future work we will evaluate the presence of longitudinal finger rotation and its extent for further data sets as well as an inter-session analysis of data sets acquired in multiple sessions.

6. Acknowledgements

This project has received funding from the European Union's Horizon 2020 research and innovation program under grant agreement No. 700259.

References

[1] M. S. M. Asaari, S. A. Suandi, and B. A. Rosdi. Fusion of band limited phase only correlation and width centroid contour distance for finger based biometrics. *Expert Systems with Applications*, 41(7):3367–3382, 2014.

[2] Q. Chen, L. Yang, G. Yang, and Y. Yin. Geometric shape analysis based finger vein deformation detection and correction. *Neurocomputing*, 2018.

[3] B. Huang, Y. Dai, R. Li, D. Tang, and W. Li. Finger-vein authentication based on wide line detector and pattern normalization. In *Pattern Recognition (ICPR), 2010 20th International Conference on*, pages 1269–1272. IEEE, 2010.

[4] C. Kauba, B. Prommegger, and A. Uhl. Focussing the beam - a new laser illumination based data set providing insights to finger-vein recognition. In *Proceedings of the IEEE 9th International Conference on Biometrics: Theory, Applications, and Systems (BTAS2018)*, pages 1–9, Los Angeles, California, USA, 2018. accepted.

[5] C. Kauba, B. Prommegger, and A. Uhl. The two sides of the finger - dorsal or palmar - which one is better in finger-vein recognition? In *Proceedings of the International Conference of the Biometrics Special Interest Group (BIOSIG'18)*, Darmstadt, Germany, 2018.

[6] A. Kumar and Y. Zhou. Human identification using finger images. *Image Processing, IEEE Transactions on*, 21(4):2228–2244, 2012.

[7] E. C. Lee, H. C. Lee, and K. R. Park. Finger vein recognition using minutia-based alignment and local binary pattern-based feature extraction. *International Journal of Imaging Systems and Technology*, 19(3):179–186, 2009.

[8] Y. Lu, S. J. Xie, S. Yoon, J. Yang, and D. S. Park. Robust finger vein roi localization based on flexible segmentation. *Sensors*, 13(11):14339–14366, 2013.

[9] D. Maio, D. Maltoni, R. Cappelli, J. L. Wayman, and A. K. Jain. FVC2004: Third Fingerprint Verification Competition. In *ICBA*, volume 3072 of *LNCS*, pages 1–7. Springer Verlag, 2004.

[10] Y. Matsuda, N. Miura, A. Nagasaka, H. Kiyomiu, and T. Miyatake. Finger-vein authentication based on deformation-tolerant feature-point matching. *Machine Vision and Applications*, 27(2):237–250, 2016.

[11] N. Miura, A. Nagasaka, and T. Miyatake. Feature extraction of finger-vein patterns based on repeated line tracking and its application to personal identification. *Machine Vision and Applications*, 15(4):194–203, 2004.

[12] N. Miura, A. Nagasaka, and T. Miyatake. Extraction of finger-vein patterns using maximum curvature points in image profiles. *IEICE transactions on information and systems*, 90(8):1185–1194, 2007.

[13] B. Prommegger, C. Kauba, and A. Uhl. Longitudinal finger rotation - problems and effects in finger-vein recognition. In *Proceedings of the International Conference of the Biometrics Special Interest Group (BIOSIG'18)*, Darmstadt, Germany, 2018.

[14] B. Ton and R. Veldhuis. A high quality finger vascular pattern dataset collected using a custom designed capturing device. In *International Conference on Biometrics, ICB 2013*. IEEE, 2013.

[15] L. Yang, G. Yang, Y. Yin, and X. Xi. Finger vein recognition with anatomy structure analysis. *IEEE Transactions on Circuits and Systems for Video Technology*, 2017.

[16] Y. Yin, L. Liu, and X. Sun. Sdumla-hmt: a multimodal biometric database. *Biometric Recognition*, pages 260–268, 2011.

[17] J. Zhang and J. Yang. Finger-vein image enhancement based on combination of gray-level grouping and circular gabor filter. In *Information Engineering and Computer Science, 2009. ICIECS 2009. International Conference on*, pages 1–4. IEEE, 2009.

[18] J. Zhao, H. Tian, W. Xu, and X. Li. A new approach to hand vein image enhancement. In *Intelligent Computation Technology and Automation, 2009. ICICTA'09. Second International Conference on*, volume 1, pages 499–501. IEEE, 2009.

[19] K. Zuiderveld. Contrast limited adaptive histogram equalization. In P. S. Heckbert, editor, *Graphics Gems IV*, pages 474–485. Morgan Kaufmann, 1994.

Rotation Invariant Finger Vein Recognition

Bernhard Prommegger and Andreas Uhl
University of Salzburg
Jakob-Haringer-Str. 2, 5020 Salzburg, AUSTRIA
{bprommeg, uhl}@cs.sbg.ac.at

Abstract

Finger vein recognition deals with the identification of subjects based on its venous pattern within the fingers. The majority of the scanner devices capture a single finger from the palmar side using light transmission. Some of them are equipped with a contact surface or other structures to support in finger placement. However, these means are not able to prevent all possible types of finger misplacements, in particular longitudinal finger rotation can not be averted. It has been shown that this type of deformation causes severe problems to finger vein recognition systems. This paper proposes two new methods in which finger vein images from different perspectives are captured during enrolment and, but only one during authentication. In the first method, the authentication image is compared to all enrolment images, whereas in the second method they are linked together to form a perspective cumulative finger vein template. As the enrolled finger vein images depict the vein structure of a larger range of the finger, the longitudinal positioning of the finger during the acquisition for the biometric recognition is less critical. The experimental results confirm the applicability especially of the first approach.

1. Introduction

Vascular pattern based biometric systems, commonly denoted as vein biometrics, offer several advantages over other well-established biometric recognition systems. In particular, hand and finger vein systems have become a serious alternative to fingerprint based ones for several applications. Vein based systems use the structure of the blood vessels inside the human body, which becomes visible under near-infrared (NIR) light. As the vein structure is located inside the human body, it is resistant to abrasion and external influences on the skin. Furthermore, a lifeness detection to detect presentation attacks can be performed easily [4].

The performance of finger vein recognition systems suffers from different internal and external factors. Internal factors include the design and configuration of the sensor itself, especially the NIR light source and the camera module. External factors include environmental conditions (e.g. temperature and humidity) and deformations due to misplacement of the finger, typically including shifts, tilt, bending and longitudinal rotation.

Performance degradations caused by various types of finger misplacement are not new and have been addressed in several publications. The need for a robust finger vein image normalisation has already been mentioned by Kumar and Zhou in 2012 [4]. Chen *et al*. [1] state that deformation correction can be done either during pre-processing, feature extraction or comparison. Moreover, the physical design of the sensor can help to avoid misplacements of the finger. In [12] the authors showed, that longitudinal finger rotation has a severe influence on the performance of a finger vein recognition system. There are several approaches that try to reduce the influence of these issues during the processing of the vein patterns. Kumar and Zhou [4] introduced a finger alignment based on the finger boundary to overcome finger translation and rotation. Lee *et al*. [5] proposed a system utilizing a minutia based alignment together with local binary patterns as feature extraction method. Huang *et al*. [2] improved the resistance against longitudinal rotation by applying an elliptic pattern normalization to the input images. Matsuda *et al*. [8] proposed a feature-point based recognition system introducing a finger-shape model and a non-rigid registration method. Yang *et al*. [16] introduced a finger vein recognition framework including an anatomy structure analysis based vein extraction algorithm and integration matching strategy. Chen *et al*. [1] detects different types of finger deformation by analysing the shape of the finger and corrects them using linear and non-linear transformations. Prommegger *et al*. [11] proposed a method that applies a rotation correction on the enrolled templates in both directions using a pre-defined angle for additional comparisons combined with score level fusion. Besides these software based solutions, there are some hardware-based ones which aim to prevent finger misplacements in the first place, during acquisition, rather than correcting them afterwards. Kauba *et al*. [3] presented a finger vein

978-1-7281-1522-1/19/$31.00 ©2019 IEEE

scanner that requires the subject to place the fingers in a flat, aligned position on a finger shaped guiding surface. This reduces finger misplacements to a minimum. Problems resulting from finger misplacements will receive more attention in the future as finger vein systems evolve towards contact-less operation.

The main contribution of this work is the analysis of two novel rotation invariant finger vein recognition methods and the provision of two new data sets that are designed to allow a thorough analysis of the robustness of finger vein recognition systems against longitudinal finger rotation. Both methods aim to improve the recognition performance by enrolling multiple finger vein images from different perspectives and compare them, just as in current system, against a single sample acquired during authentication. This results in a more complex and expensive enrolment device, whereas the capturing device for authentication remains inexpensive. The first method, multi-perspective enrolment (MPE), uses the acquired enrolment perspectives after applying circular pattern normalization (CPN), the second one combines the different perspectives to form a perspective cumulative finger vein template (PCT). The experiments are carried out using the *PLUSVein finger rotation data set* (PLUSVein-FR) [13]. To show the effectiveness of the proposed approaches, their recognition results are compared to the results of other methods, that claim to be robust against longitudinal finger rotation, utilizing the new data sets.

The rest of this paper is organized as follows: Longitudinal finger rotation and its problems caused for finger vein recognition systems are described in more detail in section 2. Section 3 explains the MPE method and section 4 all details of the generation of the PCT, respectively. The experimental set-up together with its results are described in section 6. Section 7 concludes the paper along with an outlook on future work.

2. Longitudinal Finger Rotation

Typically, finger vein scanners are designed to acquire only a single finger at a time. Different types of finger misplacement can easily occur with these scanners and pose a severe problem. Figure 1 shows the orientations of the x, y and z axis with respect to the finger. The different types of finger misplacement include planar shifts and rotation in the xy-plane, shifts of the finger in z-direction (distance to the camera, scaling), finger bending, finger tilt (finger tip and root are not in the same xy-plane) and longitudinal finger rotation around the y-axis. As described in [12], the influence of some of these problematic misplacements can be reduced or even prevented completely during acquisition by adding support structures for finger positioning or a correction during pre-processing, feature extraction or comparison. Almost all currently available sensors use such support structures, but most of them still do not prevent a rotation around

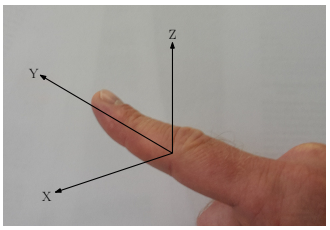

Figure 1. Definition of the axes of a finger in a three-dimensional space (originally published in [11])

the y-axis (longitudinal finger rotation). Thus, longitudinal finger rotation cannot be ruled out and poses a severe problem to finger vein recognition systems.

The captured vein structure is a projection of the vessel structure in the 3D space onto a 2D plane. If the finger is rotated along its longitudinal axis, the vein pattern is deformed according to a non-linear transformation. Figure 2 shows the effect of longitudinal finger rotation on the vein pattern. The finger cross section (top row) is rotated from -30° to +30°. As a result of the rotation the projected pattern of the veins (bottom row) changes as well. Depending on the relative position of the veins to each other and the rotation angle, some of the captured veins might merge into a single one. The vein structures of -30° (left), 0° (middle) and 30° (right) are completely different. Widely used vein recognition schemes can handle such deformations only to a certain extent [12]. If the deformations caused by the longitudinal rotation are corrected, the negative effect can be reduced but not completely prevented [11].

3. Multi-Perspective Enrolment

MPE requires the acquisition of multiple perspectives during enrolment. The acquisition angles of the different perspectives are linearly spaced over the desired acquisition range. For authentication, only a single perspective is acquired and compared to all enrolment samples together with a maximum rule score level fusion. As shown in [11], elliptic pattern normalization (EPN) [2] increases the robustness against longitudinal finger rotation. EPN is based on the hypothesis, that the cross section of a finger approximately resembles an ellipsis and that the veins which are captured by the finger vein scanner are located close to the finger surface. The normalization essentially corresponds to a rolling of the finger, which reduces the non-linear deformation of the vein structure across the entire width of the finger. After this correction is applied, a horizontal shift of the images during comparison corresponds to a rotation of the finger. The elliptic shape normalization proposed by Huang *et al*. holds only true for the palmar and dorsal perspect-

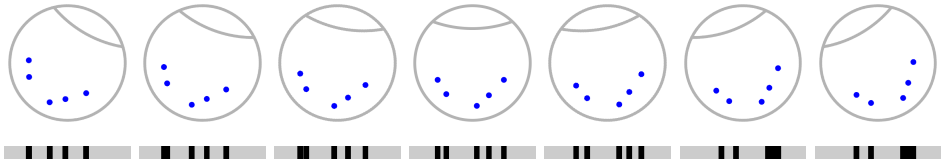

Figure 2. Longitudinal finger rotation principle: a schematic finger cross section showing five veins (blue dots) rotated from -30° (left) to +30° (right) in 10° steps. The projection (bottom row) of the vein pattern is different depending on the rotation angle according to a non-linear transformation (originally published in [12]).

ive. For other perspectives, the resulting shape is different. Therefore, the estimation of the fingers' cross section shape was changed to a circle, resulting in a circular pattern normalization (CPN).

There are already capturing devices available, that are capable of acquiring multi-perspective finger vein images. Prommegger *et al*. [13] proposed a multi-perspective finger vein scanner that acquires a video of the vein structure all around the finger (360°). Veldhuis *et al*. [15] presented a capture device, that acquires images from three perspectives.

4. Perspective Cumulative Finger Vein Templates

As for MPE, also PCT requires the enrolment of finger vein images from multiple perspectives. Again, the rotation angles of the captured samples are spread linearly over the desired acquisition range and are normalized using CPN. Next, the vein pattern is extracted and the single templates are combined to one large cumulative template as following: (1) To suppress unwanted artefacts on the finger edges, some pixels are cut off from both sides. (2) The vein templates are combined together where their overlap reaches the highest correlation. The correlation is calculated as described in [9]. (3) For the first and the last image, the cut-off border is added again after all perspectives have been combined with each other.

During recognition, just as with existing systems, only one perspective is captured and compared to the generated PCT. This comparison is done using a correlation measure, calculated between the PCT and in x- and y-direction shifted and rotated versions of the probe image as described in [9]. The shift is executed over the entire height, which corresponds to the desired angular acquisition range, of the PCT.

During extraction of the vein structure, other details, e.g. skin folds, wrinkles, hair or other texture, are recognized. These distortions can be seen as noise in the vein pattern of the feature image which impede the PCT generation. In order to obtain satisfactory PCTs, these distortions must be reduced to a minimum. Therefore, the level of detail during feature extraction (compared to the level of detail used for other methods) is reduced by smoothing the input image.

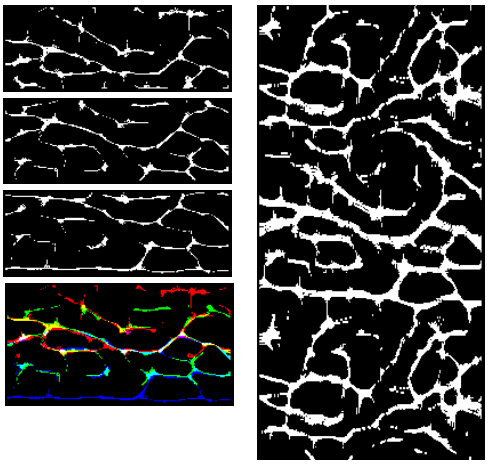

Figure 3. Example of an PCT. Left: single perspectives (rotation angle 30°) and the combined image of the three samples. Right: a PCT on the range of 360°.

Figure 3 shows such a PCT. On the left side there are three samples of finger vein templates with a rotation distance of 30°. The forth row is the combined image of the three samples. The red colour corresponds to the vein pattern of the first image, green to the 2nd one and blue to the third one, respectively. The right side shows the PCT of a finger in the full range of 360° generated with images acquired in a rotational distance of 15°.

Advantages of PCT compared to MBE are the reduced template size and a potential for a lower comparison runtime. The runtime improvement can be achieved by less horizontal shifts applied during the execution of the Miura matcher and the omission of the fusion step.

For a ROI of height h, which corresponds to the estim-

ated diameter of the finger, and length l, n enrolled templates (normalized with CPN) have a total height of

$$h_{MPE} = n \cdot \frac{h \cdot \pi}{2} \tag{1}$$

The PCT height for an angular range of φ is the arc length of φ plus the non-overlapping border of the first and last perspective

$$h_{PCT} = \left(\frac{\varphi}{360} + 2 \cdot \frac{\varphi}{n \cdot 360}\right) \cdot h \cdot \pi = \frac{n+2}{n} \cdot \frac{\varphi}{360} \cdot h \cdot \pi \tag{2}$$

For an enrolment of the whole finger ($\varphi = 360°$) with an angular distance of 30° between the acquired perspectives ($n = 12$), the template size is reduced by factor 5.

The number of horizontal shifts during comparison is related to the size of the templates and the configured shift of the Miura matcher. The shifts for MPE are

$$S_{MPE} = n \cdot (2 \cdot h_{shift} + 1) \tag{3}$$

where h_{shift} is the number of pixels shifted up and down during a comparison. The experiments performed in section 6 showed that a good estimation for h_{shift} is

$$h_{shift} = 2 \cdot \frac{\varphi}{n \cdot 360} \cdot h \tag{4}$$

For PCT, the probe template is shifted over the arc length φ.

$$S_{PCT} = \frac{\varphi}{360} \cdot h \cdot \pi \tag{5}$$

For the above scenario (360°, 12 perspectives), that leads to an reduction of the horizontal shifts by 30%.

5. Performance Validation Data Set

In order to be able to test the robustness of a recognition scheme against longitudinal finger rotation, data sets that depict realistic scenarios regarding finger rotation are needed. Such data sets must satisfy the following characteristics: (1) The data set needs to provide finger vein images from perspectives spread over the desired range. (2) The distribution of the rotation angles must follow the characteristics of the desired scenario. (3) It needs to contain enough longitudinal rotation in order that a rotation compensation is useful. (4) Ideally, also the rotation angles of the different samples are known.

Currently, there exists no publicly available data set that fulfills these properties. Therefore, two new data sets are generated from the publicly available subset (±45° around the palmar view) of the PLUSVein-FR. The first data set, PLUSVein-FR-ED, contains vein images whose rotation angles are equally distributed over the entire range of ±45°. It corresponds to the unconstrained placement of the finger in a contact-less acquisition system. The rotation angles of the second data set, PLUSVein-FR-ND, are normally distributed. This data set models a realistic real world scenario

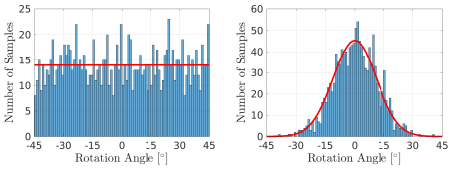

Figure 4. Distribution of rotation angles in the subsets. Left: PLUSVein-FR-ED, right: PLUSVein-FR-ND.

of a classical unsupervised single perspective acquisition system. Prommegger *et al*. estimated the rotation angles of different finger vein data sets in [14]. The SDUMLA-HMT [17] exhibited the highest degree of finger rotation with rotation angles up to 45° ($\sigma = 10.6°$). This standard deviation was used for the generation of the PLUSVein-FR-ND. The distributions of the rotation angles of the two subsets are depicted in Fig. 4. Both data sets are available for download on http://wavelab.at/sources/Prommegger19d.

6. Experiments

In the first part of the experiments, the performance of the proposed methods, MPE and PCT, all around the finger (360°) is analysed using perspectives of the PLUSVein-FR data set in steps of 5°, leading to 73 different perspectives (0° and 360° are acquired separately). Every perspective is considered as a separate data set. The template generation is done in the feature space utilizing MC features [10]. To determine the number of perspectives needed during enrolment, different rotational distances between the used perspective are tested (15°, 30° and 45°). Furthermore, to verify the effectiveness of the proposed methods, in the second part of the experiments both approaches are applied on the two introduced data sets, PLUSVein-FR-ED and PLUSVein-FR-ND, and compared to other finger recognition schemes that are tolerant against longitudinal finger rotation. The necessary enrolment samples are taken from the publicly available ±45° subset of the PLUSVein-FR.

6.1. Recognition Tool Chain

The finger vein recognition tool-chain consists of the following components: (1) For *finger region detection* and *finger alignment* an implementation that is based on [6] is used. (2) The *ROI extraction* differs from [6]: instad of cutting out a defined rectangle within the finger, similar to [2], a normalization of the finger to a fixed width is applied. (3) To improve the visibility of the vein pattern *Circular Gabor Filter* (CGF) [18] and simple *CLAHE* (local histogram equalisation) [19] are used during *pre-processing*. (4) As *feature extraction* method the well-established vein-pattern based *Maximum Curvature* method [10] is employed. (5) The *comparison* of the binary feature images is done us-

ing a correlation measure, calculated between the input images and in x- and y-direction shifted and rotated versions of the reference image as described in [9]. An implementation of the recognition tool-chain is available for download on http://wavelab.at/sources/Prommegger19d.

6.2. Experimental Protocol

For the experiments, the data sets are split into two subsets, one for enrolment and one for authentication. The enrolment subset contains two samples, the one for authentication three. To quantify the performance, the EER, the FMR100 (the lowest FNMR for FMR $\leq 1\%$), the FMR1000 (the lowest FNMR for FMR $\leq 0{,}1\%$) as well as the ZeroFMR (the lowest FNMR for FMR = 0%) are used. For the evaluation, the experiments follow the test protocol of the FVC2004 [7]: For calculating the genuine scores, all possible genuine comparisons are performed, which are $63 \cdot 4 \cdot 3 \cdot 2 = 1512$ matches. For calculating the impostor scores, only the first image of a finger is compared against the first image of all other fingers, resulting in $(63 \cdot 4) \cdot (63 \cdot 4 - 1) = 63252$ matches, so together 64764 matches in total.

As a reference for the quantification of MPE and PCT, the intra-perspective performance of all 73 perspectives, without applying any rotation compensation methods and by applying CPN, is evaluated. For this calculations every perspective is considered as its own data set, which implies, that every perspective is its own independent classical single perspective recognition system, where enrolment and probe image are acquired from the same perspective. Although the results are presented together, they are completely independent from each other. Rotational differences between the enrolment and probe sample would be subject to the same degradations as presented in [11]. Therefore, no rotational invariance can be concluded from the presentation of the intra-perspective results. As MPE and PCT aim to generate rotation invariant recognition results for a single finger vein image acquired from any perspective during authentication, results close to or even better than the intra-perspective results without rotation correction can be considered as good performance.

To quantify the decrease in performance of a method, the relative performance degradation (RPD), which is calculated as stated in equation (6), is used:

$$RPD = \frac{EER_x - EER_{ref}}{EER_{ref}}. \tag{6}$$

EER_{ref} is the EER of the reference data set and EER_x the EER of the evaluated data set. A RPD of 0 means no change in performance, a RPD of 1 corresponds to an EER increase to its doubled value. For a negative RPD, the performance increased. For the evaluation of the performance increase due to rotation correction, the relative performance increase

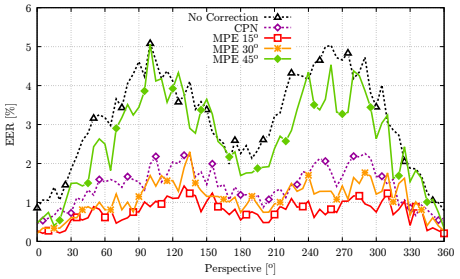

Figure 5. Recognition performance (EER): in-perspective vs MPE comparisons

(RPI) as in equation (7) is calculated:

$$RPI = \frac{EER_{ref} - EER_x}{EER_x}. \tag{7}$$

Again, EER_{ref} is the EER of the reference data set and EER_x the EER of the evaluated data set. A RPI of 0 means no change in the performance, a RPI of 1 corresponds to a drop in the EER to half of its value. For a negative RPI, the performance decreased. All values are given in percentage terms, e.g. 2.35 means 2.35%.

6.3. Results

6.3.1 Multi-Perspective Enrolment

For MPE, three different enrolment scenarios with different distances between the acquired samples are evaluated (15° → 24 perspectives, 30° → 12 and 45° → 8). Each of the 73 perspectives provided by PLUSVein-FR is compared against all enrolled samples. To get the final score, a simple maximum score level fusion is applied. The trend of the resulting EERs are depicted in Figure 5. Additionally to MPE, also the intra perspective performance results for applying no correction and CPN are visualized. The performance of both methods show the same trend, just at different EER levels: The best performance results are obtained in the palmar (0°) region followed by the dorsal (180°) region. The perspectives inbetween show inferior results, achieving the worst results around 90° and 270°. CPN outperforms no correction over the whole range in average by a factor 2, which corresponds to an RPI of 100%. As expected, the results of the MPE scenarios depend directly on the number of enrolment perspectives: the less the cameras are rotated away from each other, the better the resulting recognition accuracy is. MPE 15° achieves the overall best results. It's EER values are between 0.2 and 1.4% for all perspectives all around the finger, which corresponds to RPIs between 25% and 250%, followed by MPE 30° and MPE 45°. MPE 15° and MPE 30° even outperform the intra per-

Perspective	Method	EER (CI)	FMR100	FMR1000	ZeroFMR	RPD	RPI
0°	No Correction	0.87 (± 0.23)	0.86	1.39	3.71	-	-
	CPN	0.46 (± 0.17)	0.46	0.53	1.19	-	86.8
	MPE 15°	0.27 (± 0.13)	0.28	0.28	0.48	-	215.9
	MPE 30°	0.20 (± 0.11)	0.20	0.27	0.68	-	324.7
	MPE 45°	0.47 (± 0.17)	0.47	0.68	1.56	-	82.9
	PCT 15°	4.25 (± 0.50)	7.08	12.65	35.83	391.1	-
	PCT 30°	4.76 (± 0.53)	7.80	14.71	35.93	449.1	-
	PCT 45°	6.51 (± 0.61)	10.69	17.52	31.19	651.9	-
60°	No Correction	3.18 (± 0.43)	4.70	9.34	30.13	-	-
	CPN	1.53 (± 0.30)	1.66	2.98	7.68	-	108.4
	MPE 15°	0.62 (± 0.20)	0.62	1.24	1.99	-	415.2
	MPE 30°	0.81 (± 0.22)	0.81	1.69	3.99	-	291.6
	MPE 45°	2.50 (± 0.39)	3.11	5.95	13.31	-	27.2
	PCT 15°	5.84 (± 0.58)	11.68	20.54	35.85	83.7	-
	PCT 30°	5.28 (± 0.55)	9.34	16.72	32.97	66.2	-
	PCT 45°	8.11 (± 0.67)	16.28	26.62	53.58	155.2	-
120°	No Correction	4.11 (± 0.49)	5.97	10.01	17.57	-	-
	CPN	2.04 (± 0.35)	2.59	4.18	16.05	-	101.8
	MPE 15°	1.11 (± 0.26)	1.31	2.13	4.61	-	272.3
	MPE 30°	1.56 (± 0.31)	1.63	2.58	12.81	-	163.7
	MPE 45°	3.92 (± 0.48)	5.07	8.66	24.22	-	4.9
	PCT 15°	7.08 (± 0.64)	13.34	25.38	49.38	72.1	-
	PCT 30°	8.34 (± 0.68)	15.32	25.90	44.81	102.8	-
	PCT 45°	11.50 (± 0.79)	23.75	35.86	61.43	179.6	-
180°	No Correction	2.26 (± 0.36)	3.06	5.58	9.30	-	-
	CPN	1.19 (± 0.27)	1.20	2.26	5.25	-	89.1
	MPE 15°	0.55 (± 0.18)	0.48	1.31	3.58	-	310.4
	MPE 30°	0.74 (± 0.21)	0.68	1.63	3.32	-	203.2
	MPE 45°	1.69 (± 0.32)	1.96	3.45	6.90	-	33.6
	PCT 15°	3.37 (± 0.45)	4.40	9.22	15.61	49.1	-
	PCT 30°	4.34 (± 0.50)	5.83	10.17	21.02	92.2	-
	PCT 45°	4.86 (± 0.53)	7.31	11.43	22.60	115.0	-

Table 1. Performance results for evaluation in-perspectiv analysis, MPE and PCT in steps of 45°. RPD and RPI are calculated with respect to *No Correction*

spective CPN results. The performance of MPE 45° is just below the inter perspective comparisons without any correction. Table 1 holds the performance results for selected perspectives. All performance results can be downloaded at http://wavelab.at/sources/Prommegger19d.

6.3.2 Perspective Cumulative Finger Vein Templates

As for MPE, also for PCT three different enrolment scenarios with rotation distances of 15°, 30° and 45° between the acquired perspectives are evaluated. Again, all 73 perspectives are compared against the generated PCT. The trend of the resulting EERs are visualized inf Figure 6. All three methods perform worse than the intra perspective comparisons without any rotation compensation. The course of the PCT curves is relatively even. This also applies to those perspectives for which no enrolment samples have been acquired. Applying PCT 15° results in a RPD between 50% and 400%, PCT 30° between 60% and 450% and PCT 45° between 100% and 650%, respectively. The prominent jump at 180° is due to the generation of the template. It was generated from -180° to +180°. As a result of this, the template contains more information from this perspective as also the border, which was cut off during the template generation, is added to the PCT. The overall inferior results can be explained by the fact, that, as described in section 4, the level of detail had to be reduced in order to achieve satisfactory results when combining the single perspective templates to the cumulative template. Again, table 1 holds the results for selected perspectives.

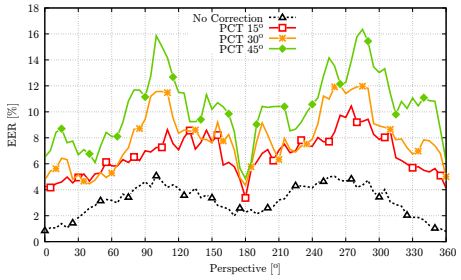

Figure 6. Recognition performance (EER): in-perspective vs PCT comparisons

6.3.3 Performance Validation

For the validation of the performance of the proposed methods, they are compared to well known recognition schemes, that are tolerant against longitudinal finger rotation, namely a rotation compensation using the information of the rotation angle provided by the data set (known angle method) [11], EPN [2], CPN and a method that compensates the rotational deformations without the knowledge of the actual rotation angle by applying a rotation correction in both directions using a pre-defined angle combined with score level fusion (fixed angle correction) [11]. Additionally, the performance of the unmodified data set is stated as a reference. The data sets used for validation are the data sets described in section 5 (PLUSVein-FR-ED and PLUSVein-FR-ND). The validation includes four different MPE scenarios: a two camera version including enrolment cameras positioned $\pm 20°$ from the palmar view (0°), 3 cameras ($\pm 30°$ and 0°), a 4 camera setting ($\pm 45°$ in steps of 30°) and a 7 camera setting ($\pm 45°$ in steps of 15°). The combined templates are again generated for camera distances of 15°, 30° and 45°. The vein images necessary for the MPE scenarios and for the generation of the PCTs are taken from the publicly available *PLUSVein-FR $\pm 45°$ sub set*.

Note that all rotation compensation schemes but MPE and PCT, only acquire a single perspective for enrolment and authentication. As a result of this, they are only tolerant against longitudinal finger rotation to a certain extent ($< \pm 30°$, [11]). MPE and PCT acquire multiple perspectives during enrolment and use this information for authentication against a single perspective. The comparison carried out in this section analyses the performance only in a limited range ($\pm 45°$) in which also single perspective enrolment methods can show a reasonable performance. As shown in the experiments, MPE and PCT are invariant against longitudinal finger rotation all around the finger. Nevertheless, these experiments give a good indication of the strengths (MPE) and weaknesses (PCT) of the proposed approaches.

The results for both data sets are listed in table 2. As mentioned in section 5, the PLUSVein-FR-ED contains finger vein images with rotation angles that are equally distributed in the range of $\pm 45°$. Therefore, the rotation distances between two samples of the same finger might be high. The maximum rotation angle of two samples of the same finger is 89°. This fact is also reflected in the recognition results of the different recognition schemes. Applying only horizontal and vertical shifts (Miura matcher [9]) cannot compensate this rotation. As a result of this, the resulting EER of 21.63% is high. Applying different schemes to increase the robustness against longitudinal finger rotation improves the Performance. EPN improves the performance to an EER of 15.87%, CPN to 15.34% and the fixed angle approach to 5.24%, respectively. As the data set also provides the rotation angle of the samples, it is possible to apply an exact rotation compensation, which improves the EER to 5.44%. The results of the MPE scenarios and the PCT setings are superior even to the exact rotation compensation. This is reasonable: due to the enrolment process, where more than one perspective is aquired for MBE and PCT, they hold more information of the vein pattern of the finger than a single perspective enrolment. Additionally, rotating the finger vein samples into their correct position using the provided rotation angle results in areas of the ROI, that contain no vein information (areas, where no vein information is present are filled with the average grey level of the image). Higher rotation angles result in larger ROI regions without vein information. In case of big distances in the rotation angles, this has a negative effect on the score of the Miura matcher. Fig. 7 shows two samples with a large rotational difference. The left side is rotated 45° to the left, the right one 45° to the right. The unmodified ROI images in the top row show a big difference between the pattern of both images. In the bottom row, which depicts the rotation corrected versions of the images, the vein structure is more similar. Both images hold quite a large region without any vein information. As the same region in the other sample contains vein information, the comparison score is reduced. When applying MPE or comparing to PCT, the samples are not rotated and this effect does not occur. The best results for MPE is achieved in the 7 camera scenario with an EER of 0.33%. The best PCT result with an EER of 3.00% is achieved when the rotational difference between the enrolment perspectives is 15°. This corresponds to an RPI of 6379% for MPE and 620% for PCT compared to the performance on the original data set.

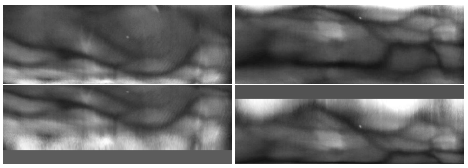

Figure 7. Finger samples exhibiting a large rotational distance (PLUSVein-FR: subjectId 50, fingerId 4, sampleNo 1, rotation angle $\pm 45°$). Top: acquired image, bottom: rotation corrected images.

The second data set, PLUSVein-FR-ND, consists of finger vein images which rotation angles are normally distributed over the range of $\pm 45°$ and should correspond to a realistic scenario. The rotation contained is a lot less than for PLUSVein-FR-ED. The EER for the original data set is 3.39%. EPN improves the EER to 1.72%, CPN to 1.52%, the fixed angle approach to 0.66% and the fixed angle correction to 1.13%, respectively. The different MPE scenarios again improve the performance. The best MPE res-

Data Set	Method	EER (CI)	FMR100	FMR1000	ZeroFMR	RPD	RPI
PLUSVein-FR-ED	No Correction	21.63 (± 1.01)	38.69	46.18	58.06	-	-
	CPN	15.34 (± 0.88)	23.89	28.73	40.88	-	41.0
	EPN	15.87 (± 0.89)	25.61	31.39	42.60	-	36.3
	Fixed Angle ($\varphi = 20°$)	5.24 (± 0.30)	7.00	8.85	12.97	-	312.5
	Known Angle	5.44 (± 0.55)	9.49	14.66	22.63	-	297.6
	MPE 2 Cameras	1.66 (± 0.31)	1.86	2.86	5.92	-	1202.8
	MPE 3 Cameras	1.13 (± 0.26)	1.13	1.60	3.13	-	1807.1
	MPE 4 Cameras	0.60 (± 0.19)	0.53	1.00	3.20	-	3513.8
	MPE 7 Cameras	0.33 (± 0.14)	0.20	0.87	2.07	-	6379.3
	PCT 15°	3.00 (± 0.42)	4.21	7.48	21.23	-	620.3
	PCT 30°	3.53 (± 0.45)	4.53	7.26	16.39	-	512.2
	PCT 45°	3.91 (± 0.48)	6.12	10.70	24.87	-	452.9
PLUSVein-FR-ND	No Correction	3.39 (± 0.44)	5.31	7.49	16.58	-	-
	CPN	1.52 (± 0.30)	1.72	2.32	5.37	-	122.3
	EPN	1.72 (± 0.32)	1.86	2.59	5.70	-	96.4
	Fixed Angle ($\varphi = 20°$)	0.66 (± 0.11)	0.60	1.05	1.48	-	412.4
	Known Angle	1.13 (± 0.26)	1.19	2.45	3.78	-	200.4
	MPE 2 Cameras	0.80 (± 0.22)	0.80	1.26	2.86	-	324.0
	MPE 3 Cameras	0.53 (± 0.18)	0.40	0.73	1.20	-	534.1
	MPE 4 Cameras	0.67 (± 0.20)	0.60	0.93	1.87	-	407.3
	MPE 7 Cameras	0.34 (± 0.14)	0.20	0.53	1.00	-	909.9
	PCT 15°	2.20 (± 0.36)	2.74	4.61	13.03	-	53.7
	PCT 30°	2.72 (± 0.40)	3.54	4.60	12.14	-	24.7
	PCT 45°	2.80 (± 0.40)	3.79	6.59	18.58	-	21.0

Table 2. Comparison of evaluated rotation compensation schemes.

ult is achieved for the 7 camera scenario hitting an EER of 0.34% which corresponds to an RPI of 910%. The PCT approach improves the recognition performance compared to the original data set as well, but not to the same extent as the other methods. The best PCT result is achieved with an EER of 2.20% for a rotational distance of 15° between the perspectives used for the PCT generation. Reasons for the lesser improvement compared to the other methods are: (1) According to [11], the other methods can handle small rotation better than larger rotations whereas PCT keeps the recognition performance quite stable over the whole range under investigation. (2) The single perspective templates used for the PCT generation contain less details than the templates used for the other approaches.

7. Conclusion

In this article, we proposed two novel methods for rotation invariant finger vein recognition. The first method, multi perspective enrolment, utilizes multiple finger vein images acquired during enrolment and compares, just as for commonly used finger vein recognition systems, a single perspective during authentication. The second method, perspective cumulative finger vein templates, combine multiple finger vein images from different perspectives into one larger template that holds the vein information over the whole range of interest. Additionally, we introduced two publicly available data sets, PLUSVein-FR-ED and PLUSVein-FR-ND, which were especially designed for the analysis of robustness of finger vein recognition systems against longitudinal finger rotation.

Both methods increase the recognition performance compared to the original data set without applying any rotation correction or compensation method. MPE achieves superior results with respect to all other rotation tolerant schemes. If enough cameras are used during enrolment, negative effects of longitudinal finger rotation on the recognition performance can be inhibited. PCT still has some issues, mainly related to the generation of the template. In order to achieve satisfactory results for the template generation, the degree of detail of the vein pattern had to be reduced. This inevitably leads to worse recognition rates. For both methods, the improvement of the recognition performance is achieved by increasing the effort (acquiring additional perspectives, template generation) during enrolment.

In our future work we will apply the PCT method not only in the feature space, but also in the image space. This would enable the possibility to use the proposed method not only on vein pattern based methods, but also on more sophisticated recognition systems as ASAVE [16] and DTFPM [8]. Also it might be possible to increase the level of detail in order to achieve better results. Additionally, we plan to further develop MPE in order that the number of required perspectives can be reduced. We also plan to evaluate the MPE approach for other recognition schemes than MC.

Acknowledgements

This work was supported in part by the European Union's Horizon 2020 Research and Innovation Program under Grant 700259, and in part by the FFG KIRAS Project AUTFingerATM under Grant 864785.

References

[1] Q. Chen, L. Yang, G. Yang, and Y. Yin. Geometric shape analysis based finger vein deformation detection and correction. *Neurocomputing*, 2018.

[2] B. Huang, Y. Dai, R. Li, D. Tang, and W. Li. Finger-vein authentication based on wide line detector and pattern normalization. In *Pattern Recognition (ICPR), 2010 20th International Conference on*, pages 1269–1272. IEEE, 2010.

[3] C. Kauba, B. Prommegger, and A. Uhl. The two sides of the finger - dorsal or palmar - which one is better in finger-vein recognition? In *Proceedings of the International Conference of the Biometrics Special Interest Group (BIOSIG'18)*, Darmstadt, Germany, 2018.

[4] A. Kumar and Y. Zhou. Human identification using finger images. *Image Processing, IEEE Transactions on*, 21(4):2228–2244, 2012.

[5] E. C. Lee, H. C. Lee, and K. R. Park. Finger vein recognition using minutia-based alignment and local binary pattern-based feature extraction. *International Journal of Imaging Systems and Technology*, 19(3):179–186, 2009.

[6] Y. Lu, S. J. Xie, S. Yoon, J. Yang, and D. S. Park. Robust finger vein roi localization based on flexible segmentation. *Sensors*, 13(11):14339–14366, 2013.

[7] D. Maio, D. Maltoni, R. Cappelli, J. L. Wayman, and A. K. Jain. FVC2004: Third Fingerprint Verification Competition. In *ICBA*, volume 3072 of *LNCS*, pages 1–7. Springer Verlag, 2004.

[8] Y. Matsuda, N. Miura, A. Nagasaka, H. Kiyomiu, and T. Miyatake. Finger-vein authentication based on deformation-tolerant feature-point matching. *Machine Vision and Applications*, 27(2):237–250, 2016.

[9] N. Miura, A. Nagasaka, and T. Miyatake. Feature extraction of finger-vein patterns based on repeated line tracking and its application to personal identification. *Machine Vision and Applications*, 15(4):194–203, 2004.

[10] N. Miura, A. Nagasaka, and T. Miyatake. Extraction of finger-vein patterns using maximum curvature points in image profiles. *IEICE transactions on information and systems*, 90(8):1185–1194, 2007.

[11] B. Prommegger, C. Kauba, M. Linortner, and A. Uhl. Longitudinal finger rotation - deformation detection and correction. *IEEE Transactions on Biometrics, Behavior, and Identity Science*, pages 1–17, 2019.

[12] B. Prommegger, C. Kauba, and A. Uhl. Longitudinal finger rotation - problems and effects in finger-vein recognition. In *Proceedings of the International Conference of the Biometrics Special Interest Group (BIOSIG'18)*, Darmstadt, Germany, 2018.

[13] B. Prommegger, C. Kauba, and A. Uhl. Multi-perspective finger-vein biometrics. In *Proceedings of the IEEE 9th International Conference on Biometrics: Theory, Applications, and Systems (BTAS2018)*, Los Angeles, California, USA, 2018.

[14] B. Prommegger, C. Kauba, and A. Uhl. On the extent of longitudinal finger rotation in publicly available finger vein data sets. In *Proceedings of the 12th IAPR/IEEE International Conference on Biometrics (ICB'19)*, pages 1–8, Crete, Greece, 2019.

[15] R. Veldhuis, L. Spreeuwers, B. Ton, and S. Rozendal. A high quality finger vein dataset collected using a custom designed capture device. In A. Uhl, C. Busch, S. Marcel, and R. Veldhuis, editors, *Handbook of Vascular Biometrics*, chapter 5, page 13 pages. Springer Science+Business Media, Boston, MA, USA, 2019.

[16] L. Yang, G. Yang, Y. Yin, and X. Xi. Finger vein recognition with anatomy structure analysis. *IEEE Transactions on Circuits and Systems for Video Technology*, pages 1–1, 2017.

[17] Y. Yin, L. Liu, and X. Sun. Sdumla-hmt: a multimodal biometric database. *Biometric Recognition*, pages 260–268, 2011.

[18] J. Zhang and J. Yang. Finger-vein image enhancement based on combination of gray-level grouping and circular gabor filter. In *Information Engineering and Computer Science, 2009. ICIECS 2009. International Conference on*, pages 1–4. IEEE, 2009.

[19] K. Zuiderveld. Contrast limited adaptive histogram equalization. In P. S. Heckbert, editor, *Graphics Gems IV*, pages 474–485. Morgan Kaufmann, 1994.

Advanced Multi-Perspective Enrolment in Finger Vein Recognition

Bernhard Prommegger and Andreas Uhl
University of Salzburg
Jakob-Haringer-Str. 2, 5020 Salzburg, AUSTRIA
Email: {bprommeg, uhl}@cs.sbg.ac.at

***Abstract*—Finger vein recognition deals with the recognition of subjects based on their venous pattern within the fingers. It has been shown that its recognition accuracy heavily depends on a good alignment of the acquired samples. There are several approaches that try to reduce the impact of finger misplacement. However, none of these approaches is able to prevent all possible types of finger misplacements. As finger vein scanners are evolving towards contact-less acquisition, alignment problems, especially due to longitudinal finger rotation, are becoming even more important. Along with rotation detection and correction, capturing the vein pattern from multiple perspectives, as e.g. in multiple-perspective enrolment (MPE, [1]), is a way to tackle the problem of longitudinal finger rotation. Involving multiple cameras increases cost and complexity of the capturing devices, and therefore their number should be kept to a minimum. Perspective multiplication for MPE (PM-MPE, [2]) successfully reduces the number of cameras needed during enrolment while keeping the recognition rates at a high level. So far, (PM-)MPE has only been applied using Maximum curvature features (MC, [3]). This work analyses further approaches to improve the their recognition rates and investigates the applicability of (PM-)MPE to recognition schemes using features other than MC.**

***Index Terms*—Finger vein recognition, longitudinal finger rotation, rotation invariant recognition system**

I. Introduction

Vascular pattern based biometric systems, commonly denoted as vein biometrics, offer several advantages over other well-established biometric recognition systems. In particular, hand and finger vein systems have become a serious alternative to fingerprint based ones for several applications. Vein based systems use the structure of the blood vessels inside the human body, which becomes visible under near-infrared (NIR) light. As the vein structure is located inside the human body, it is resistant to abrasion and external influences on the skin. Furthermore, a lifeness detection to detect presentation attacks can be performed easily [4].

The performance of finger vein recognition systems suffers from different internal and external factors. Internal factors include the design and configuration of the sensor itself, especially the NIR light source and the camera module. External factors include environmental conditions (e.g. temperature and humidity) and deformations due to misplacement of the finger, typically including shifts, tilt, bending and longitudinal rotation. Performance degradations caused by various types of finger misplacement are not new and have been addressed in several publications. The need for a robust finger vein image normalisation including rotational alignment has already been mentioned by Kumar and Zhou in 2012 [4]. Chen *et al*. [5] state that deformation correction can be done either during pre-processing, feature extraction or comparison. Moreover, the physical design of the sensor, e.g. [6], [7], can help to avoid misplacements of the finger. In [8] the authors showed that longitudinal finger rotation has a severe influence on the recognition performance of a finger vein recognition system. There are several approaches that try to reduce the influence of these issues in traditional single perspective systems during the processing of the vein patterns, e.g. [4], [5], [9]–[13]. Other systems try to utilize multi-camera capturing devices to overcome the problem of longitudinal finger rotation. Bunda [14] and Sonna Momo *et al*. [15] propose multi-perspective recognition systems using capturing devices that acquire the vascular template from three different perspectives at the same time. Kang *et al*. [16] proposed a finger vein recognition system in the 3D space. Prommegger and Uhl [1] introduced two methods that make finger vein recognition fully invariant against longitudinal rotation. Both methods acquire multiple perspectives during enrolment, while only one perspective is captured during recognition. The first approach, multi-perspective enrolment (MPE), compares the probe image to all acquired enrolment perspectives, while the second approach, perspective cumulative finger vein templates, generates a single template that holds the vein pattern all around the finger. In [2] the number of cameras needed during enrolment for MPE has successfully been reduced by introducing pseudo perspectives.

This article is an extension to the work presented in [1] and [2]. While in [1] and [2] only one recognition scheme, *Maximum curvature* (MC, [3]), was applied, this work analyses the applicability of (PM-)MPE to recognition schemes using features other than MC. The schemes under investigation are the *Wide Line Detector* (WLD, [9]), *Finger Vein Recognition With Anatomy Structure Analysis* (ASAVE, [13]) and a *SIFT*-based recognition scheme (SIFT, [17]). Furthermore, two additional adoptions to increase the performance of MPE and PM-MPE are analysed. The first approach strives to improve the performance of MPE by changing the position of the enrolment cameras, while the second method adopts PM-MPE by adding extra pseudo perspectives between two enrolment cameras. All experiments are carried out using the *PLUSVein*

978-1-7281-6232-4/20/$31.00 ©2020 IEEE

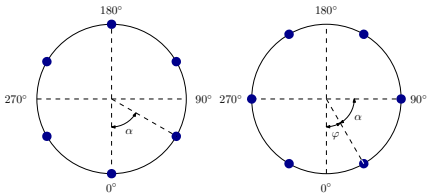

Fig. 1. Rotational shift of enrolment cameras for MPE: MPE as proposed in [1] (left) always includes the palmar view (0°), whereas for the proposed method (right) the start position is shifted by φ.

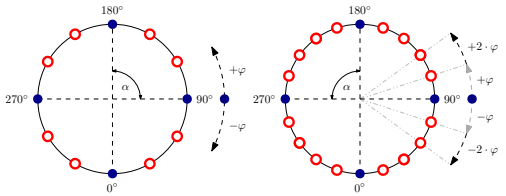

Fig. 2. Camera positioning for PM-MPE for a rotational distance of 90° between two adjacent enrolment perspectives. The filled blue dots are cameras, the red circles represent pseudo perspectives. The left image (originally published in [2]) shows the position of the pseudo perspectives as proposed in [2], the right side visualizes the principle of adding additional pseudo perspectives.

finger rotation data set (PLUSVein-FR) [18]. This article focuses on further analyses on and limitation of (PM-)MPE. Comparisons to methods that represent the state of the art in rotation invariant finger vein recognition have been omitted as such an analysis has already been carried out in the original publications [1], [2].

The reminder of this paper is organized as follows: In section II perspective shift for (PM-)MPE is described. Section III holds some details on PM-MPE and section IV the proposed approach to introduce additional pseudo perspectives. The experimental set-up together with its results are described in Section V. Section VI concludes the paper along with an outlook on future work.

II. Perspective Shifts for Multi-Perspective Enrolment

The positioning of the enrolment cameras around the finger can be an influential factor for the recognition performance of the system. Two aspects need to be considered: (1) the performance of the different perspectives itself and (2) the rotational distance of the probe sample to the nearest enrolment perspective. For (1) it has been shown that finger vein recognition systems perform best around the palmar and dorsal view and worst around 90° and 270° [18]. For (2) it has been shown in [12] that state of the art recognition systems cannot compensate rotational distances exceeding 30°.

MPE and PM-MPE, as proposed in [1] and [2], start the positioning of the enrolment cameras always at the most commonly used palmar perspective. For some configurations, i.e. MPE 60°, this leads to the simultaneous occurrence of (1) inferior performing perspectives and (2) the maximum distance of the probe sample to the acquired enrolment perspectives. By rotating the acquired enrolment perspectives with an rotation angle of φ, the two negative impact factors should be separated. Fig. 1 visualizes the idea for MPE 60°. The right image shows the positioning of the enrolment cameras for MPE as proposed in [1]: They are linearly spaced around the finger starting at the palmar view (0°) with a rotational distance between two adjacent cameras of $\alpha = 60°$. The perspectives acquired during enrolment are: 0°, 60°, 120°, 180°, 240° and 300°. The maximum distance of the recognition perspective and the closest enrolment perspective is reached exactly in-between two enrolment perspectives. As a consequence of this positioning, for the worst performing perspectives (90° and 270°, [18]), the distance to the nearest enrolment camera reaches its maximum of 30°. In the left image the enrolment cameras are shifted by an angle of $\varphi = 30°$. Due to this shift, there are enrolment cameras at 90° and 270°, and hence, the negative impact factors do not occur simultaneously any more.

III. Perspective Multiplication for Multi-Perspective Enrolment

PM-MPE, as proposed in [2], combines MPE and the fixed angle rotation compensation method of [12] to reduce the number of perspectives needed during enrolment. At enrolment n perspectives with a rotational distance of α are acquired. PM-MPE adds two pseudo perspectives between two adjacent cameras by rotating every perspective with an rotational angle of $\pm\varphi = {}^{\alpha}/_{3}$ in both directions. For authentication, just as for traditional single-perspective finger vein recognition schemes, only a single perspective is acquired and compared to all enrolled perspectives and the generated pseudo perspectives. This leads to $3{*}n$ comparisons for each authentication attempt. The left image of Fig. 2 shows the positions of the enrolment cameras and pseudo perspectives for $\alpha = 90°$ between two adjacent enrolment perspectives. The solid blue dots represent perspectives actually acquired during enrolment. As for MPE, they are spread linearly around the finger at 0°, 90°, 180° and 270°. The remaining perspectives (red circles) are generated by rotating the acquired finger vein images by a rotation angle of $\varphi = {}^{90°}/_{3} = 30°$ in both directions. It was shown in [2] that by applying PM-MPE, the distance of the enrolment perspectives can be increased while keeping the recognition performance at a high level.

IV. Generation of Additional Pseudo Perspectives for PM-MPE

The improvement in recognition performance of PM-MPE compared to MPE is based on the reduction of the horizontal shift executed during comparison. Deviating from PM-MPE, the approach proposed here, PMx-MPE, adds more than two pseudo perspectives between two enrolment perspectives. Each perspective is rotated m times with multiples of φ in both directions, where $\varphi = {}^{\alpha}/_{(2*m+1)}$. As a result of the additional pseudo perspectives, the rotational distance between the perspectives used for recognition is lower than for PM-MPE.

Enrolment Perspectives		Distance between adjacent perspectives				# of comparisons				Max distance recognition ↔ enrolment			
		MPE	PM-MPE	PM2-MPE	PM3-MPE	MPE	PM-MPE	PM2-MPE	PM3-MPE	MPE	PM-MPE	PM2-MPE	PM3-MPE
n	α	α	$\varphi = \alpha/3$	$\varphi = \alpha/5$	$\varphi = \alpha/7$	n	$3 \cdot n$	$5 \cdot n$	$7 \cdot n$	$\alpha/2$	$\varphi/2$	$\varphi/2$	$\varphi/2$
24	15°	15°	-	-	-	24	-	-	-	7.5°	-	-	-
12	30°	30°	10°	-	-	12	36	-	-	15°	5°	-	-
8	45°	45°	15°	9°	-	8	24	40	-	22.5°	7.5°	4.5°	-
6	60°	60°	20°	12°	8.6°	6	18	30	42	30°	10°	6°	4.3°

TABLE I

DISTANCE BETWEEN ADJACENT (PSEUDO) PERSPECTIVES, NUMBER OF COMPARISONS NEEDED DURING RECOGNITION AND MAXIMUM DISTANCE OF THE PROBE SAMPLE TO THE NEAREST (PSEUDO) PERSPECTIVE FOR MPE, PM-MPE, PM2-MPE AND PM3-MPE.

Therefore, the horizontal shifts during comparison can be reduced. According to the results of [19], this should lead to a better separation of genuine and impostor scores, which in turn results in a better recognition performance. The right side of Fig. 2 shows the principle for $\alpha = 90°$ and $m = 2$, which results in $2*m = 4$ pseudo perspectives between two adjacent enrolment perspectives. Each acquired perspective is rotated by $\pm\varphi$ and $\pm 2 * \varphi$. The distance between two perspectives is $\varphi = {}^{90°}/_{5} = 18°$ instead of 30° as for PM-MPE in [2].

A drawback of the additional pseudo perspectives is that the number of comparisons during recognition increases. Instead of $3 * n$ comparisons as for PM-MPE, the additional perspectives results in $(2 * m + 1) * n$ comparisons. The experiments in the section V-D should show if adding more pseudo perspectives improves the recognition rates and if so, if this improvement justifies the added computational cost for generating the additional pseudo perspectives during enrolment and comparisons during recognition. Table I contains detailed information about various settings (different numbers of enrolment cameras) of MPE and the PM-MPE. This includes the number of perspectives involved, the distance between the cameras, the maximum rotational distance between a probe sample with an arbitrary rotational position of the finger and the closest enrolment perspective and the number of comparisons needed for one recognition attempt.

V. EXPERIMENTS

The experiments are split into two parts: In the first part, the influence of perspective shifts, as explained in section II, is evaluated. The second part analyses the impact of the number of generated pseudo perspectives between two adjacent enrolment perspectives which is described in section IV.

A. Recognition Tool Chain

The finger vein recognition tool-chain consists of the following components: (1) For *finger region detection* and *finger alignment* an implementation that is based on [20] is used. (2) The *ROI extraction* differs from [20]: instead of cutting out a defined rectangle within the finger, similar to [9], a normalization of the finger to a fixed width is applied. (3) To improve the visibility of the vein pattern *High Frequency Emphasis Filtering* (HFE) [21], *Circular Gabor Filter* (CGF) [22] and simple *CLAHE* (local histogram equalisation) [23] are used during *pre-processing*. (4a) For the simple vein pattern based feature methods, MC and WLD, the binary feature images are compared using a correlation measure, calculated between the input images and in x- and y-direction shifted and rotated versions of the reference image as described in [24]. (4b) The more sophisticated vein pattern based method, ASAVE, applies feature extraction and comparison as proposed in [13], and (4c) the SIFT based approach as described in [17], respectively. An implementation of the recognition tool-chain together with the used configurations and results are available for download on http://www.wavelab.at/sources/Prommegger20a.

B. Experimental Protocol

For the experiments, the data set is split into tow subsets, one for enrolment and one for authentication. The enrolment subset contains two samples, the subset for authentication three samples. To quantify the performance, the EER, the FMR100 (the lowest FNMR for FMR $\leq 1\%$), the FMR1000 (the lowest FNMR for FMR $\leq 0{,}1\%$) as well as the ZeroFMR (the lowest FNMR for FMR = 0%) are used. For the evaluation, the experiments follow the test protocol of the FVC2004 [25].

Due to the high number of results generated during the experiments, only the EER values are visualized in the article. The detailed individual results for all performance descriptors for all perspectives and recognition schemes can be downloaded on http://www.wavelab.at/sources/Prommegger20a.

C. Baseline Results

In order to have a reference for the quantification of MPE and PM-MPE results, the intra-perspective performance (IPP) of all 73 perspectives, without applying any rotation compensation methods and by applying CPN [1], is evaluated. For this calculations every perspective is considered as its own data set, which implies, that every perspective is its own independent classical single perspective recognition system where enrolment and probe image are acquired from the same perspective. As a result of this, rotational differences between the samples due to finger misplacement, i.e. longitudinal finger rotation, are subject to the same degradations as presented in [8]. Although the results of the different perspectives are presented together, they are completely independent from each other. Therefore, no rotational invariance can be concluded from the presentation of the intra-perspective results. As MPE and PM-MPE aim to generate rotation invariant recognition results for a single finger vein image acquired from any perspective during recognition, results close to or even better than the intra-perspective results without rotation correction can be considered as good performance.

D. Perspective Shifts for Multi-Perspective Enrolment

The idea behind perspective shifts for MPE is to mitigate the prominent performance drops at 90° and 270° for MPE 60° and PM-MPE 60° by separating the two negative impact factors: (1) largest rotational distance to the perspective acquired

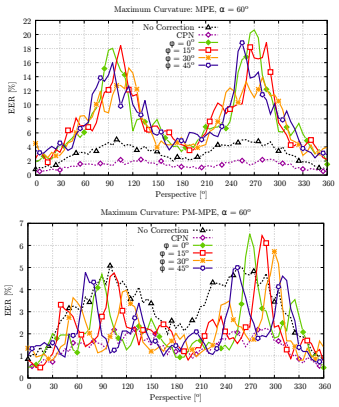

Fig. 3. Performance results (EER) for MPE (top) and PM-MPE (bottom) applying rotational shifts to the enrolment perspectives.

during enrolment and (2) inferior performing perspectives. This separation is achieved by rotating the enrolment cameras by an angle of φ (see Fig. 1). The experiments are carried out for MPE 60° and PM-MPE 60° using four different φ, namely 0° (no shift), 15°, 30° and 45°. With a shift of $\varphi = 30°$ there are enrolment cameras at 90° and 270°. This results in a separation of the two negative factors.

Fig. 3 depicts the results for MPE 60° and PM-MPE 60°. The shift of the enrolment cameras only leads to a shift of performance drop by the same angle φ, which is particularly evident in the PM-MPE plot (bottom). This indicates that the influence of the distance to the enrolment perspective is greater than that of the inferior perspectives. Prommegger *et al.* showed in [18] that MC cannot compensate longitudinal finger rotation $> 30°$. Considering these results, one can conclude that for MC a rotational distance of $\alpha > 60°$ between enrolment perspectives is not useful.

E. Pseudo-Perspectives in Perspective Multiplication for Multi-Perspective Enrolment

The experiments in this part serve two goals: They analyse (1) the impact of the number of generated pseudo perspectives between two adjacent enrolment perspectives and (2) the applicability of (PM-)MPE to recognition schemes using other features than MC. The schemes used are two simple vein pattern based ones using the well known MC and WLD features and a more sophisticated one, namely ASAVE. In addition, a keypoint based scheme (SIFT) is analysed. The rotational distance between two adjacent enrolment perspectives is $\alpha = 45°$ and 60°. The number of inserted pseudo perspectives between two cameras are 0 (MPE, [1]), 2 (PM-MPE, [2]), 4 (PM2-MPE) and 6 (PM3-MPE, only for $\alpha = 60°$). The latter two have not been applied before.

Fig. 4 shows the performance results (EER) of the vein pattern based methods (note the different scaling of the plots). The simple vein pattern based methods, MC (left column) and WLD (middle), behave similar: For $\alpha = 45°$ (top row), the EERs for MPE follow pretty much the intra-perspective results. They achieve the best results in the palmar region (around 0°) and the dorsal region (around 180°). The EERs inbetween are inferior, hitting its highest values around 90° and 270°. Introducing two pseudo perspectives (PM-MPE) noticeable improves the performance. The perspectives furthest away from the enrolment perspectives exhibit a noticeable performance degradation. These drops in the recognition performance are more prominent for MC and are visible as spikes in the EER curve at e.g. 67.5° and 292.5°. Generating four pseudo perspectives between two adjacent enrolment cameras still improves the performance, but not to the same degree as from MPE to PM-MPE. For $\alpha = 60°$ (bottom row), the performance of MPE delivers worse results than the intra-perspective results. Especially striking is the prominent performance degradation at 90° and 270°. Again, introducing pseudo perspectives improves the recognition results. Similar to MPE 45°, also MPE 60° shows drops in the performance for the perspectives with the maximum distance to the enrolment cameras. PM-MPE outperforms the intra-perspective results except for some regions with a large distance to the enrolment cameras, e.g. for MC at 270° and WLD around 300°. In turn with the results for PM2-MPE 45°, also PM2-MPE 60° shows a slight improvement compared to PM-MPE 60°. Introducing even more pseudo perspectives (PM3-MPE 60°) does not further improve the recognition performance.

When using MPE 45° in combination with ASAVE (left column), the performance is again similar to the intra-perspective results. Introducing pseudo perspectives still improves the results, but not to the same extend as for MC and WLD. The lower performance increase is reasonable as ASAVE has an integrated image alignment based on the vein backbone of the finger vein images. The creation of pseudo perspectives is in principle only an (albeit inaccurate) attempt to better align the images. Since ASAVE has already integrated such an alignment, the potential for improvement is lower. For more information on ASAVE, the interested reader is referred to the original article [13]. At a rotational distance of $\alpha = 60°$ similar results are given, although with slightly higher EERs. For ASAVE also the trend of the intra-perspective comparisons is interesting. Contrary to all other recognition schemes under investigation, the best results are achieved around 45° and 315°

The last studied recognition scheme is a keypoint based system using SIFT descriptors as features. SIFT is, to some degree, invariant against certain variations in the image, e.g. changes in the illumination, and some transformations, e.g. translation, rotation or scaling. Therefore, the introduction of pseudo perspectives should not have an positive effect on the recognition performance of the system. Fig. 5 depicts the trend of SIFT's EER. The achieved EERs for MPE are higher than for the intra-perspective comparisons. For both, $\alpha = 45°$ and 60°, the spikes between the enrolment perspectives are apparent. This is in line with the results of [12] where the authors showed that applying SIFT together with elliptic pattern normalization, which is similar to the used CPN, shows

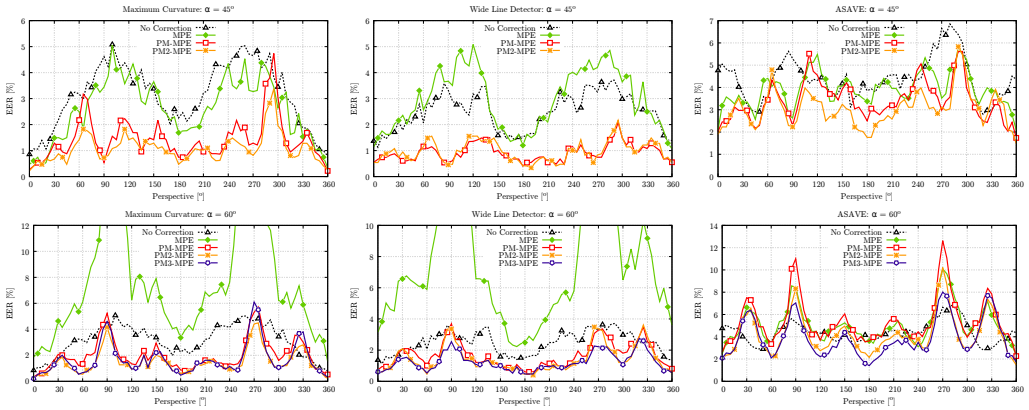

Fig. 4. Performance results (EER) for MC (left), WLD (middle) and ASAVE (right) using different rotational distances between adjacent enrolment perspectives: $\alpha = 45°$ (top), $\alpha = 60°$ (bottom).

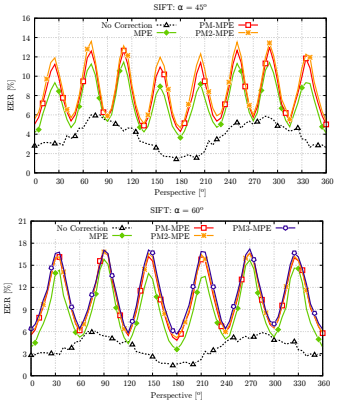

Fig. 5. Performance results (EER) for SIFT applying MPE, PM-MPE, PM2-MPE and PM3-MPE for $\alpha = 45°$ and 60°.

a higher performance degradation compared to simple vein pattern based systems. It delivers only good recognition rates for rotational distances $< \pm 15°$. The maximum distance for $\alpha = 45°$ and 60° is 22.5° and 30°, respectively. This implies that in areas exceeding this 15°, the rotation can no longer be compensated. As expected, the introduction of additional pseudo perspectives does not improve the recognition rates, in contrary, they got slightly worse.

VI. Conclusion

The analysis of the different recognition schemes in section V-D showed that simple vein pattern based systems benefit most from the insertion of pseudo perspectives. For schemes that have already some kind of image alignment included, the benefit of adding additional perspectives is lower. As already shown in [2], MC benefits from introducing two pseudo perspectives (PM-MPE) between two neighbouring enrolment cameras. Using four additional perspectives (PM2-MPE), results into another slight improvement. Adding more perspectives (PM3-MPE) does not further improve the performance. WLD, the second simple vein pattern based algorithm, shows the same behaviour but with better results for methods using perspective multiplication. For ASAVE, a more sophisticated vein pattern based method, applying MPE also results in rotation invariant recognition results. As ASAVE pre-aligns the images using their vein backbone, introducing pseudo perspectives has not the same impact as for the simple methods MC and WLD.

The last method examined, a SIFT-based approach, does not seem to be suitable for (PM)-MPE. The achieved recognition rates are noticeable worse than those of the intra-perspective comparisons. Furthermore, this approach is more sensitive to longitudinal rotation than vein pattern based methods.

For the analysis of perspective shifts, we changed the camera positions from 0° (original setting from [1] and [2]) to 45° in steps of 15°. The experiments showed that a shift of the enrolment perspectives did not result in an improvement of the recognition performance in regions with a high rotational distance to the enrolment cameras. The performance drop is only shifted with the same angle as the enrolment cameras were rotated. This indicates that the influence of an inferior intra-perspective performance is less than the impact of a large rotational distance to the enrolment cameras. This holds true for both, MPE and PM-MPE. Considering these results along with those of [12], rotational distances of $\alpha > 60°$ between the enrolment perspectives are not useful.

For the analysis of introducing additional pseudo perspectives for PM-MPE, we inserted different numbers of pseudo perspectives between adjacent enrolment cameras. The experiments showed that simple vein pattern based systems benefit most from the insertion of pseudo perspectives. For

schemes that have already some kind of image alignment included, the benefit of adding additional perspectives is lower. MC and WLD benefit from introducing two pseudo perspectives (PM-MPE) between two neighboring enrolment cameras. Using four additional perspectives (PM2-MPE) results into another slight improvement. Adding more perspectives (PM3-MPE) does not further improve the performance. ASAVE, a more sophisticated vein pattern based system, still benefits from the use of PM-MPE, the impact of the introduction of additional perspectives is limited. The SIFT-based recognition system does not benefit from the introduction of pseudo perspectives at all.

Adding pseudo perspectives during enrolment introduces computational cost for their generation during enrolment and the additional comparisons for every recognition attempt. With standard applications, enrolment is carried out once while recognition is executed numerous times. Therefore, the additional costs during registration are not so decisive, especially not if it reduces the number of acquired perspectives and thus the cost and complexity of the capturing device. This applies e.g. for PM-MPE 60°: compared to MPE 45° one can save two cameras while achieving similar recognition rates. Compared to MPE the number of comparisons for a recognition attempt are trippled for PM-MPE, quintupled for PM2-MPE and increased by seven times for PM3-MPE. The performance gain for PM-MPE justified this extra effort. When looking at the results of PM2-MPE and PM3-MPE, the extra effort is not justifiable.

In our future work, we aim to further improve the invariance of finger vein recognition with respect to longitudinal finger rotation. We will experiment with different camera settings, e.g. multi perspective enrolment combined with multi perspective authentication. Furthermore, we will try to improve the results for perspective cumulative finger vein templates as proposed in [1].

Acknowledgements

This project was partly funded the FFG KIRAS project AUTFingerATM under grant No. 864785 and the FWF project "Advanced Methods and Applications for Fingervein Recognition" under grant No. P 32201-NBL.

References

[1] B. Prommegger and A. Uhl, "Rotation invariant finger vein recognition," in *Proceedings of the IEEE 10th International Conference on Biometrics: Theory, Applications, and Systems (BTAS2019)*, Tampa, Florida, USA, 2019.

[2] ——, "Perspective multiplication for multi-perspective enrolment in finger vein recognition," in *Proceedings of the 18th International Conference of the Biometrics Special Interest Group (BIOSIG'19)*, Darmstadt, Germany, 2019.

[3] N. Miura, A. Nagasaka, and T. Miyatake, "Extraction of finger-vein patterns using maximum curvature points in image profiles," *IEICE transactions on information and systems*, vol. 90, no. 8, pp. 1185–1194, 2007.

[4] A. Kumar and Y. Zhou, "Human identification using finger images," *Image Processing, IEEE Transactions on*, vol. 21, no. 4, pp. 2228–2244, 2012.

[5] Q. Chen, L. Yang, G. Yang, and Y. Yin, "Geometric shape analysis based finger vein deformation detection and correction," *Neurocomputing*, 2018.

[6] N. Miura, T. Miyatake, A. Nagasaka, and H. Kiyomizu, "Finger vein authentication device," 7 2014, uS Patent 8,855,376.

[7] C. Kauba, B. Prommegger, and A. Uhl, "The two sides of the finger - an evaluation on the recognition performance of dorsal vs. palmar finger-veins," in *Proceedings of the International Conference of the Biometrics Special Interest Group (BIOSIG'18)*, Darmstadt, Germany, 2018.

[8] B. Prommegger, C. Kauba, and A. Uhl, "Longitudinal finger rotation - problems and effects in finger-vein recognition," in *Proceedings of the International Conference of the Biometrics Special Interest Group (BIOSIG'18)*, Darmstadt, Germany, 2018.

[9] B. Huang, Y. Dai, R. Li, D. Tang, and W. Li, "Finger-vein authentication based on wide line detector and pattern normalization," in *Pattern Recognition (ICPR), 2010 20th International Conference on*. IEEE, 2010, pp. 1269–1272.

[10] E. C. Lee, H. C. Lee, and K. R. Park, "Finger vein recognition using minutia-based alignment and local binary pattern-based feature extraction," *International Journal of Imaging Systems and Technology*, vol. 19, no. 3, pp. 179–186, 2009.

[11] Y. Matsuda, N. Miura, A. Nagasaka, H. Kiyomiu, and T. Miyatake, "Finger-vein authentication based on deformation-tolerant feature-point matching," *Machine Vision and Applications*, vol. 27, no. 2, pp. 237–250, 2016.

[12] B. Prommegger, C. Kauba, M. Linortner, and A. Uhl, "Longitudinal finger rotation - deformation detection and correction," *IEEE Transactions on Biometrics, Behavior, and Identity Science*, vol. 1, no. 2, pp. 123–138, 2019.

[13] L. Yang, G. Yang, Y. Yin, and X. Xi, "Finger vein recognition with anatomy structure analysis," *IEEE Transactions on Circuits and Systems for Video Technology*, pp. 1–1, 2017.

[14] S. Bunda, "3D point cloud reconstruction based on the finger vascular pattern," B.S. thesis, University of Twente, 2018. [Online]. Available: https://essay.utwente.nl/75284/1/3d-finger-vein-final-Sebastian-Bunda.pdf

[15] L. Sonna Momo, L. Cerqueira Torres, S. Marcel, A. Anjos, M. Liebling, A. Shajkofci, S. Amoos, A. Woeffray, A. Sierro, P. Roduit, P. Ferez, and L. Bonvin, "Method and device for biometric vascular recognition and/or identification," WIPO (PCT) Patent WO/2019/150 254, 08 08, 2019.

[16] W. Kang, H. Liu, W. Luo, and F. Deng, "Study of a full-view 3D finger vein verification technique," *IEEE Transactions on Information Forensics and Security*, pp. 1–1, 2019.

[17] C. Kauba, J. Reissig, and A. Uhl, "Pre-processing cascades and fusion in finger vein recognition," in *Proceedings of the International Conference of the Biometrics Special Interest Group (BIOSIG'14)*, Darmstadt, Germany, sep 2014.

[18] B. Prommegger, C. Kauba, and A. Uhl, "Multi-perspective finger-vein biometrics," in *Proceedings of the IEEE 9th International Conference on Biometrics: Theory, Applications, and Systems (BTAS2018)*, Los Angeles, California, USA, 2018.

[19] ——, "On the extent of longitudinal finger rotation in publicly available finger vein data sets," in *Proceedings of the 12th IAPR/IEEE International Conference on Biometrics (ICB'19)*, Crete, Greece, 2019, pp. 1–8.

[20] Y. Lu, S. J. Xie, S. Yoon, J. Yang, and D. S. Park, "Robust finger vein roi localization based on flexible segmentation," *Sensors*, vol. 13, no. 11, pp. 14 339–14 366, 2013.

[21] J. Zhao, H. Tian, W. Xu, and X. Li, "A new approach to hand vein image enhancement," in *Intelligent Computation Technology and Automation, 2009. ICICTA'09. Second International Conference on*, vol. 1. IEEE, 2009, pp. 499–501.

[22] J. Zhang and J. Yang, "Finger-vein image enhancement based on combination of gray-level grouping and circular gabor filter," in *Information Engineering and Computer Science, 2009. ICIECS 2009. International Conference on*. IEEE, 2009, pp. 1–4.

[23] K. Zuiderveld, "Contrast limited adaptive histogram equalization," in *Graphics Gems IV*, P. S. Heckbert, Ed. Morgan Kaufmann, 1994, pp. 474–485.

[24] N. Miura, A. Nagasaka, and T. Miyatake, "Feature extraction of finger-vein patterns based on repeated line tracking and its application to personal identification," *Machine Vision and Applications*, vol. 15, no. 4, pp. 194–203, 2004.

[25] D. Maio, D. Maltoni, R. Cappelli, J. L. Wayman, and A. K. Jain, "FVC2004: Third Fingerprint Verification Competition," in *ICBA*, ser. LNCS, vol. 3072. Springer Verlag, 2004, pp. 1–7.

Rotation Detection in Finger Vein Biometrics using CNNs

Bernhard Prommegger* and Georg Wimmer* and Andreas Uhl
Department of Computer Sciences
University of Salzburg
Salzburg, Austria
Email: {bprommeg, gwimmer, uhl}@cs.sbg.ac.at
*: These authors contributed equally

***Abstract*—Finger vein recognition deals with the identification of subjects based on their venous pattern within the fingers. The recognition accuracy of finger vein recognition systems suffers from different internal and external factors. One of the major problems are misplacements of the finger during acquisition. In particular longitudinal finger rotation poses a severe problem for such recognition systems. The detection and correction of such rotations is a difficult task as typically finger vein scanners acquire only a single image from the vein pattern. Therefore, important information such as the shape of the finger or the depth of the veins within the finger, which are needed for the rotation detection, are not available. This work presents a CNN based rotation detector that is capable of estimating the rotational difference between vein images of the same finger without providing any additional information. The experiments executed not only show that the method delivers highly accurate results, but it also generalizes so that the trained CNN can also be applied on data sets which have not been included during the training of the CNN. Correcting the rotation difference between images using the CNN's rotation prediction leads to EER improvements between 50-260% for a well-established vein-pattern based method (*Maximum Curvature*) on four public finger vein databases.**

I. Introduction

Vascular pattern based biometric systems, commonly denoted as vein biometrics, offer several advantages over other well-established biometric recognition systems. In particular, hand and finger vein systems have become a serious alternative to fingerprint based ones for several applications. Vein based systems use the structure of the blood vessels inside the human body, which becomes visible under near-infrared (NIR) light. As the vein structure is located inside the human body, it is resistant to abrasion and external influences on the skin. Furthermore, due to the blood flow exhibited in NIR finger vein videos, liveness detection techniques can be applied to prevent presentation attacks [2], [25].

The performance of finger vein recognition systems suffers from different internal and external factors. Internal factors include the design and configuration of the sensor itself, especially the NIR light source and the camera module. External factors include environmental conditions (e.g. temperature and humidity) and deformations due to misplacement of the finger, typically including shifts, tilt, bending and longitudinal rotation.

This project was partly funded from the FFG KIRAS project AUTFingerATM under grant No. 864785 and the FWF project "Advanced Methods and Applications for Fingervein Recognition" under grant No. P 32201-NBL.

Performance degradations caused by various types of finger misplacement are not new and have been addressed in several publications. Kumar and Zhou [12] addressed the need for robust finger vein image normalization, including rotational alignment, already in 2012. Chen *et al.* [4] stated that deformations caused by a misplacement of the finger can be corrected either during pre-processing, feature extraction or comparison. Moreover, the design of the finger vein sensor helps to avoid or reduce misplacements of the finger as well. In [20] the authors showed, that longitudinal finger rotation has a severe influence on the recognition performance of finger vein recognition systems. There are several approaches that try to handle these issues during the processing of the vein images. These approaches can be grouped into two different categories: (1) approaches that use classical single perspective capturing devices, e.g. [4], [5], [9], [13], [16], [19], [31] and (2) methods that acquire multiple perspectives either during enrolment [23], [24], or for both, enrolment and recognition, [3], [10], [28]. However, none of theses approaches quantify the extent (i.e. the rotation angle) of the misplacements on which the deformation is based on. Prommegger *et al.* estimated the rotation angles in four publicly available data sets in [22]. For the rotation estimation between two finger vein samples, one sample is rotated 90 times in the range of $\pm 45°$ in steps of $1°$. The other sample is compared to the first sample and its 90 rotated versions, so 91 comparisons in total. The rotation angle is taken from the comparison at which the highest correlation (the highest score) is achieved. However, such a time-intensive empirical approach can only be used to analyse existing data sets, but is not suitable for real world applications. Therefore, a system that is able to determine the rotation angle between two vein images in real time would be desirable. This article proposes a CNN based rotation detector that is capable of doing so.

CNNs have already been used for rotation estimation in several biometric applications. In [26] a siames network based approach was used to estimate the rotation of finger prints. In [6], CNNs were applied to detect hands and estimate their rotation and in [8], CNNs were applied to estimate head pose

angles for face-related applications like face recognition. Up to now, there is no CNN-based prior work that tries to estimate the rotation of finger vein images.

The main contribution of this work is the proposal of a CNN-based rotation detector that estimates the difference in longitudinal rotation between vein images of the same finger. The experimental results show that the CNN is not only capable of estimating the rotation for the data set it is trained on, but can also be used for data sets not included during training. The CNN has been trained using data provided by the *PROTECT Multimodal Dataset* (PMMDB) [27] and evaluated on the *PLUSVein Finger Rotation Dataset* (PLUSVein-FR) [21]. To verify the generalisability of the proposed model, it is also applied on four often used publicly available data sets, namely SDUMLA-HMT [32], FV-USM [1], UTFVP [29] and PLUSVein-FV3 [11]).

The reminder of this paper is organized as follows: Longitudinal finger rotation and the problems it causes for finger vein recognition systems are described in more detail in section II. Sections III hold all details on the used CNN model and its training, section IV describes the region of interest detection and section V explains the rotation correction of finger vein images. The experimental setup together with its results are described in section VI. Section VII concludes the paper.

II. Longitudinal Finger Rotation in Finger Vein Recognition

Typically, finger vein scanners are designed to acquire a single finger at a time. Different types of finger misplacement can easily occur with these scanners. The different types of finger misplacement includes planar shifts and rotations, a change of the distance to the camera (scaling), finger bending, finger tilt (finger tip and root are not in the same plane) and longitudinal finger rotation. As described in [20], the influence of some of these problematic misplacements can be reduced or even prevented completely either during acquisition by adding support structures for finger positioning or a correction during pre-processing, feature extraction or comparison. Almost all currently available sensors use such support structures, but most of them still do not prevent longitudinal finger rotation. Thus, longitudinal finger rotation poses a severe problem to finger vein recognition systems.

The vein structure captured in finger vein images is a projection of the blood vessel structure in the 3D space onto a 2D plane. If the finger is rotated along its longitudinal axis, the vein pattern is deformed according to a non-linear transformation. Figure 1 shows the effect of longitudinal finger rotation on the vein pattern. The finger cross section (top row) is rotated from -30° to +30°. As a result of the rotation the projected pattern of the veins (bottom row) changes as well. Depending on the relative position of the veins to each other and the rotation angle, some of the captured veins might even merge into a single one. The vein structures of -30° (left), 0° (middle) and 30° (right) are completely different. Widely used vein recognition schemes can handle such deformations only to a certain extent [20]. If the deformations caused by the longitudinal rotation are corrected, the negative effect can be reduced but not completely prevented [19].

III. Rotation Detection using CNNs

The idea of the CNN-based rotation detector is to have pairs of different rotated but otherwise identical images as inputs for a CNN, so that it can learn to estimate the rotation difference. Typically, CNN inputs in image processing tasks are either 3-channel images (images in RGB or other color spaces) or one channel images (grayscale images). The proposed approach follows a different strategy: It uses a 2-channel input, where both channels contain grayscale finger vein images, with the image of the second channel being a rotated version of the image of the first channel (see figure 2). A somehow similar approach was already applied in [7], where two finger vein images where merged to a 2-channel image which was used as CNN input. However, in [7], the CNN was directly used for identification (using the cross entropy loss) whereas the proposed approach estimates the rotational difference between the two images.

In order to learn the rotation difference $\varphi_{I_i,I_i^{rotated}}$ between a pair of differently rotated images, I_i and $I_i^{rotated}$, the mean squared error (MSE) loss function, which is defined in Eq. (1), is applied.

$$L = \frac{1}{N}\sum_{i=1}^{N}(\varphi_i - \hat{\varphi}_i)^2 \tag{1}$$

φ_i is the actual rotational distance between a pair of training images, $\hat{\varphi}_i$ is the CNN's prediction of the rotation angle of the considered image pair and N is the batch size.

Figure 2 visualizes the CNN training process.

As CNN, the ResNeXt [30] architecture (ResNeXt-101), a highly modularized and deep network architecture for image classification, is used. The CNN weights are initialized from a model that was already trained on the ImageNet database[1]. The pre-trained model was trained on 3-channel RGB images, whereas the proposed model requires two channel input images. The problem is solved by replacing the original 3-channel filter kernels of the first convolutional layer with 2-channel filter kernels, whereas both channels of the new filter kernel are grayscale versions of the original 3-channel filter kernel. Furthermore, instead of the originally 1000-dimensional output from the ImageNet database, a one-dimensional CNN output (the predicted rotation difference) is required. Therefore, the last fully connected layer is resized from 1000*2048 to 1*2048 using randomly initialized weights.

IV. Region of Interest Detection

The *region of interest* (ROI), which serves as input for the CNN as well as the recognition tool-chain in section VI-C2, is extracted as following: First, an edge detection algorithm is used to detect the finger outlines. The area between the two finger lines is accounted as finger region. Next, a straight line is fitted between the two finger lines. This line represents

[1] http://www.image-net.org/

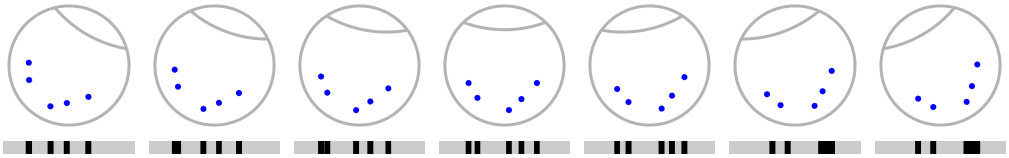

Fig. 1. Longitudinal finger rotation principle: a schematic finger cross section showing five veins (blue dots) rotated from -30° (left) to +30° (right) in 10° steps. The projection of the vein pattern (bottom row) is different depending on the rotation angle according to a non-linear transformation (originally published in [20]).

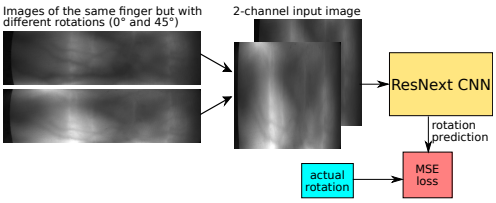

Fig. 2. Scheme of CNN training for rotation estimation

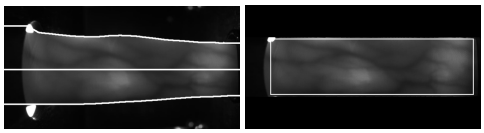

Fig. 3. ROI extraction - left: finger line detection. The straight line in the middle represents the center of the finger at which it is horizontally aligned. The top and bottom lines are the detected finger outlines which separate the finger from the background. The region between the lines is regarded as finger region. Right: the finger region is transformed to a fixed height. Afterwards the ROI, visualized as white square, of a fixed size is cut out.

the center of the finger. Based on this center line, the finger is aligned (rotated and vertically shifted) such that it is in a horizontal position and the center line of the finger is in the middle of the image. The area outside of the finger lines is masked out (pixels set to black). Afterwards, the finger region is transformed to a fixed height. In the last step, the finger ROI is cut out. Fig. 3 visualizes this process. The left image shows the finger with the center and finger outlines, the right image shows the final ROI after its transformation to a fixed height.

V. Rotation Correction of Finger Vein Images

For the generation of rotated vein images, not only the position of the veins in the 2D image, but also the shape of the finger and the depth of the veins within the finger have to be known. As the last two informations are not available in general, both need to be estimated. In this work, it is assumed that the cross section of a finger approximately resembles a circle (as e.g. Matsuda *et al*. did in [16]) and that the captured veins are close to the finger surface (cf. Huang *et al*. [9]).

The rotation of the veins by an angle of φ_{rotate} is calculated by applying a rotation matrix given in Eq. (2).

$$\begin{bmatrix} x_r \\ y_r \end{bmatrix} = \begin{bmatrix} cos(-\varphi_{rotate}) & -sin(-\varphi_{rotate}) \\ sin(-\varphi_{rotate}) & cos(-\varphi_{rotate}) \end{bmatrix} * \begin{bmatrix} x \\ y \end{bmatrix} \quad (2)$$

x and y are the coordinates of the vein pixel in the acquired image, x_r and y_r the ones in the rotated image. x is the position of the pixel in the vein pattern, y is calculated by

$$y = \sqrt{r^2 - x^2} \quad (3)$$

where r is the approximated radius of the finger, which corresponds to half of the height of the vein image. The part of the rotated ROI image that contains no information (due to the transform) is filled with the average gray level of the image. For more details, the interested reader is referred to [22].

VI. Experiments

The aim of the experiments is to show that a CNN can be trained to estimate the longitudinal rotation between two finger vein samples of the same finger using the approach presented ins section III. The rotational range, for which the CNN should be capable of estimating the longitudinal finger rotation, was determined based on the results of [19]. There, Prommegger *et al*. showed that a rotation correction gives very good results in the range of $\pm 30°$. However, a correction for rotation angles of more than 45° no longer makes sense as the recognition rates drop rapidly. Therefore, this work analyses the rotation estimation in the range of $\pm 45°$. Although, the range of particular interest is that between $\pm 30°$.

The training of the CNN model is done using data from the PMMDB data set. The range Θ, from which the training samples are taken is varied from $\pm 45°$ to $\pm 60°$ in steps of 5°. The evaluations are carried out on the PLUSVein-FR. To prove the generalizability of the model, it is also applied on four publicly available data sets, SDUMLA-HMT, FV-USM, UTFVP and PLUSVein-FV3, which have not been included during training. The rotation angles of these four data sets have also been evaluated in [22] and therefore, a direct comparison of the results from this work and [22] is possible.

A. Data Sets

The PLUSVein-FR provides vein images of perspectives all around the finger (360°) in steps of 1°. It was acquired for 63 different subjects, 4 fingers per subject, which sums up to

a total of 252 unique fingers. For each finger, five samples were acquired. Each one of the five samples consists of 361 images (one per perspective, 0° and 360° have been acquired separately). This results in $252 \cdot 5 = 1.260$ finger vein images per perspective. This work uses the publicly available subset *±45° Around the Palmar View* [19], which contains all images acquired for the 92 perspectives perspectives between -45° and +45°, resulting in a total of $92 \times 1.260 = 115.920$ vein images.

The PMMDB finger vein database was acquired in two data acquisition events with one year between the two sessions. In this work only data acquired during the second session using the same capturing device as for the PLUSVein-FR is used. From the 33 acquired subjects, only 29 are used in this work (4 subjects are part of both, PMMDB and PLUSVein-FR, and therefore were removed from PMMDB). This sums up to a total of 116 unique fingers (4 fingers per subject). As the two data sets were acquired using the same capturing device and the same acquisition protocol, they are very similar.

To show the generalizability of the presented rotation detector, it was used to evaluate the rotation angles in four publicly available finger vein data sets: SDUMLA-HMT, FV-USM, UTFVP and PLUSVein-FV3 (only the dorsal images acquired by the laser version of the sensor). The data sets itself do not provide any information on the longitudinal rotation of the samples. In [22], their rotation angles have been estimated. According to these estimates, PLUSVein-FV3 shows the lowest degree of longitudinal finger rotation, followed by UTFVP and FV-USM, while SDUMLA-HMT exhibits the highest amount.

B. Rotation Detection using CNNs

This Section describes the experimental setup for CNN training and evaluation and presents the CNN results.

1) Experimental Setup for CNN Training: CNN training is performed on pairs of images from the PMMDB database. For each image of the PMMDB database in the relevant range of $\pm\Theta$, a randomly chosen image of the same subject and sample but from a different perspective is selected as the second image of the input image pair (remember, for the PMMDB vein images are acquired all around the finger in steps of 1° $\Rightarrow$ one sample consists of 361 vein images from 361 different perspectives, where 0° and 360° are acquired separately). For these pairs of images, the exact rotational difference is known. Theoretically, 0° and 360° should be the same but practically there can occur small differences because of accumulated errors across the 360° rotation or small pose changes of the finger during data acquisition. Hence, to avoid any training errors, the pairs of images for CNN training are always selected either from the positive $[0°, \Theta]$ or negative range $[-\Theta, 360°]$, but no combinations across both rotational ranges.

The CNNs are trained for 60 epochs using a batch size of 8. Training starts with a learning rate of 0.0001 and is subsequently reduced by multiplying it with factor 0.3 after 20, 30, 40 and 50 epochs of CNN training. In every epoch, each of the 77.704 images of the PMMDB database is used once as first image of an image pair, the second image is randomly chosen from the same range as the first one. First, the 2-channel input image (the image pair) is resized to size 224×254. Data augmentation is applied by randomly cropping image patches of size 224×224 (the required input size for the CNN) from the resized image independently for each of the two channels. In that way the CNN's robustness to horizontal shifts (resulting from finger misplacements) is increased. This is important since there are no shifts between finger images of the same sample, whereas for evaluation, image pairs are built of images from different samples and so shifts do occur (also in practical application, the acquired images are subject to such misplacements). For evaluation, data augmentation is skipped and patches of size 224×224 are directly cropped from the center of the resized 224×254 images.

2) Evaluation Protocol: For evaluation, the trained CNN is applied on the subset *±45° around the palmar view* of the PLUSVein-FR data set. As already mentioned, PLUSVein-FR and PMMDB have been acquired using the same sensor and acquisition protocol. The only difference are the acquired subjects.

The rotation angles are always evaluated with respect to the palmar perspective (0° or 360°) of the first sample of each finger (denoted as reference image). Just as for the training setup, depending on the rotation angle α of the probe image, the rotation detection is made against the reference image at 0° ($\alpha >= 0°$) or 360° ($\alpha < 0°$), respectively. To achieve a more robust result, similar to [22], the rotation angle $\Phi_{i(\alpha)}$ is calculated as the average of $\hat{\varphi}_{i(\alpha),\text{ref}}$ (the predicted angle of the i^{th} sample at α against the reference image) and $\hat{\varphi}_{\text{ref},i(\alpha)}$ (the predicted angle of the reference image against the i^{th} sample at α):

$$\Phi_{i(\alpha)} = \text{avg}\left(\hat{\varphi}_{i(\alpha),\text{ref}}, -\hat{\varphi}_{\text{ref},i(\alpha)}\right) \tag{4}$$

As the CNN is trained on the range of $\pm\Theta$, it is not capable of estimating rotation angles outside of this range. Prediction results that exceed Θ are rejected and the resulting rotation angle $\Phi_{i(\alpha)}$ is taken from the remaining prediction. If both estimates, $\hat{\varphi}_{i(\alpha),\text{ref}}$ and $\hat{\varphi}_{\text{ref},i(\alpha)}$, are rejected, the rotation angle is set to 0°.

In order to correct any rotational misalignments between two samples of the same finger, the rotational distance of the i^{th} sample at the palmar view to the palmar view of the first sample ($\Phi_{i(palmar)}$) is subtracted from $\Phi_{i(\alpha)}$. The predicted rotation angle $\hat{\alpha}$ is thus determined as follows:

$$\hat{\alpha} = \Phi_{i(\alpha)} - \Phi_{i(palmar)} \tag{5}$$

3) Results: Figure 4 shows the result for all four training ranges Θ. The red solid line represents the median, the blue dashed lines mark the limits of the 90% quantile. The thinner dash-dotted lines serve as ledger lines for the ideal rotation prediction (prediction error = 0°) and ±15° (this is the range in which, according to [19], commonly used recognition deliver good recognition rates even without any rotation correction or compensation). For all four training ranges Θ, up to a rotation angle of ±30°, the median of the predictions is quite close to the ideal prediction. Outside of this range, the prediction

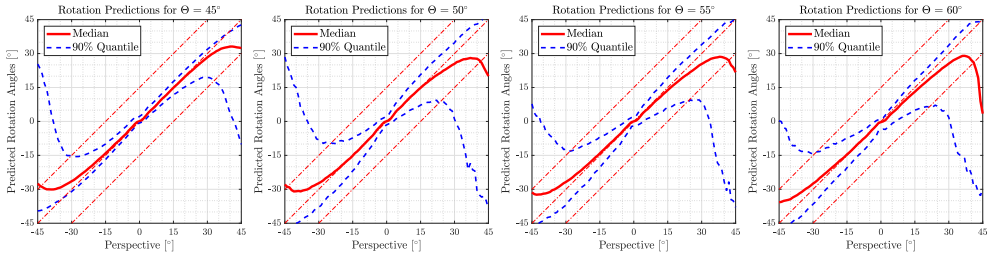

Fig. 4. Results of rotation detection on PLUSVein-FR (median and 90% quantile) for different training ranges Θ. From left to right: ±45°, ±50°, ±55°and ±60°

error increases. In general, the proposed CNN-model tends to underestimate the rotation angle. This can be seen in the plots by the fact, that the median is below the ideal estimate for rotation angles >0° and above for angles <0°, respectively. For $\Theta = 45°$, the estimation error stays below 15° on the examined range. With increasing training range, the prediction error for larger rotation angles increase. This is especially obvious for rotations $> +35°$ for $\Theta = 60°$.

The 90% quantile visualizes the accuracy of the determined rotation angles. For $\Theta = 45°$, up to $\pm 30°$, the limits of the quantile are close to the median. In this area it also remains within the $\pm 15°$ range. For rotation angles that exceed 30°, the deviations of the prediction increase. This widens the 90% quantile. Increasing the angular range Θ, from which the training data is taken, does not improve the predictions. In contrary, the estimates differ more from their actual value.

C. Application on Public Finger Vein Data Sets

Both data sets used in section VI-B, PMMDB and PLUSVein-FR, have been acquired using the same capturing device following the same acquisition protocol. Therefore, the data sets (with exception of the acquired subjects) are very similar. To show that the trained model is not limited to a specific data set or sensor, it is also applied on four publicly available data sets, namely SDUMLA-HMT, FV-USM, UTFVP and PLUSVein-FV3, that were acquired using different capturing devices and acquisition protocols. Experiments are conducted to show the positive effect of rotation correction on the EERs for the four public datasets. The performance results are evaluated using the best performing model of section VI-B ($\Theta = 45°$).

1) Evaluation Protocol: As in [22], the data sets are corrected on the basis of the estimated rotation angles. As a result, all images of a finger should be aligned with each other with respect to their longitudinal rotation. The results are compared to those of the original data set (ORI) and the results achieved in [22]. For the experiments two corrected data sets are generated: In the first version (ROT), all samples are corrected with respect to the first sample of each finger, in the second one (ROT Mean), all samples of a finger are corrected with respect to the calculated mean rotation angle of this finger. In real world applications, the rotation correction differs from the two approaches mentioned above (ROT, ROT Mean). There, it is not clear if the enrolment and probe sample are actually from the same finger/subject. As a result of this, the rotation estimation and correction needs to be executed prior to every comparison (regardless of whether it is a genuine or impostor comparison).

TABLE I
NUMBER OF COMPARISONS FOR EACH DATA SET

Name	Genuine	Impostor	Total
SDUMLA-HMT	9540	200340	209880
UTFVP	2160	63720	65880
FV-USM	32472	120048	152520
PLUSVein-FV3	3600	63720	67320

To quantify the performance of the data sets, the EER is used. The experiments follow the test protocol of the FVC2004 [15]: For calculating the genuine scores, all possible genuine comparisons are performed. For calculating the impostor scores, only the first sample of a finger is compared against the first sample of all other fingers. The resulting numbers of comparisons for all data sets are listed in table I. To quantify the change of the performance, the relative performance increase (RPI) as stated in Eq. (6) is used.

$$RPI = \frac{EER_{ref} - EER_x}{EER_x} \tag{6}$$

EER_{ref} is the EER of the reference data set and EER_x the EER of the evaluated data set.

2) Recognition Tool-Chain: The finger vein recognition tool-chain consists of the following components:

1) The ROIs are extracted as described in section IV
2) The rotation angle between two vein images is estimated using the CNN rotation estimator in section VI-B (training range $\Theta = 45°$)
3) Rotated versions of the input images are generated as described in section V
4) To improve the visibility of the vein pattern *High Frequency Emphasis Filtering* (HFE) [34], *Circular Gabor Filter* (CGF) [33] and simple *CLAHE* (local histogram equalisation) [35] are used as *pre-processing* steps.

TABLE II
RECOGNITION PERFORMANCE OF THE EVALUATED DATA SETS AND ITS CORRECTED VERSIONS: ORI = ORIGINAL DATA SET, ROT = ROTATION CORRECTED TO 1ST IMAGE, ROT MEAN = ROTATION CORRECTED TO MEAN OF FINGER. BEST ACHIEVED EER AND RPI VALUES ARE HIGHLIGHTED IN BOLD.

Data Set	Correction	Method	Performance Indicators EER [%]	RPI [%]
SDUMLA-HMT	ORI	-	4.73	-
	ROT	proposed	1.30	263.40
		ICB'19 [22]	**1.07**	**341.59**
	ROT Mean	proposed	1.37	244.77
		ICB'19 [22]	1.14	315.85
FV-USM	ORI	-	1.23	-
	ROT	proposed	**0.52**	**137.03**
		ICB'19 [22]	0.56	120.06
	ROT Mean	proposed	0.76	61.89
		ICB'19 [22]	0.77	59.38
UTFVP	ORI	-	0.42	-
	ROT	proposed	0.18	125.47
		ICB'19 [22]	0.19	124.53
	ROT Mean	proposed	0.19	115.54
		ICB'19 [22]	**0.09**	**349.06**
PLUSVein-FV3	ORI	-	0.08	-
	ROT	proposed	**0.05**	**61.23**
		ICB'19 [22]	0.06	50.00
	ROT Mean	proposed	0.06	52.12
		ICB'19 [22]	0.08	0.94

5) As *feature extraction* method, the well-established vein-pattern based *Maximum Curvature* method (MC) [18] is employed.
6) The *comparison* of the binary feature images is done using a correlation measure, calculated between the input images and in x- and y-direction shifted versions of the reference image as described in [17].

3) Results: Table II holds the performance results of the proposed method as well as for the unmodified data set (ORI) and the results achieved in [22] for all four data sets. Both corrected data sets outperform the original data set in all four cases. For all data sets, the correction with respect to the first sample achieves slightly better results. The highest performance increase is achieved for SDUMLA-HMT. There the EER dropped from 4.73% (ORI) to 1.3% (ROT), which corresponds to a RPI of 263%. For the three other data sets the performance increased as well, but not to the same extent. For FV-USM the performance increased by 137%, for UTFVP by 125% and for PLUSVein-FV3 by 61%, respectively. These results essentially correspond with those achieved in [22]. SDUMLA-HMT shows the biggest performance differences. Such a result was to be expected since (according to [22]) this data set contains the largest rotation angles, including rotations up to 45°. According to the results of section VI-B3, the accuracy of the predicted rotations decreases noticeable for rotations above $\pm 30°$.

TABLE III
MEAN AND STANDARD DEVIATION OVER THE ABSOLUTE VALUED DIFFERENCES OF THE PREDICTED ROTATION ANGLES OF THE PROPOSED SYSTEM TO THE RESULTS IN [22]

Name	Mean	Standard Deviation
SDUMLA-HMT	3.07°	3.87°
UTFVP	2.18°	2.04°
FV-USM	1.78°	2.00°
PLUSVein-FV3	1.32°	1.35°

The main advantage of the proposed rotation detector is its applicability in real world finger vein recognition systems. The detection of one rotation angle requires only a single forward pass of the proposed CNN which takes in average 15ms (GPU: GeForce GTX Titan X). The approach in [22] needs 91 comparisons (2.621ms per comparison or 238ms in total) if all 91 rotated versions of each image are already available in storage.

Table III shows the mean and the standard deviation for the difference between the predictions of the proposed approach and the estimated rotation angles of [22]. The mean deviation is below 3.1° for all four databases, the standard deviation is never higher than 4°. The low differences between the rotation angles of both independent approaches imply that the predicted angles should be fairly accurate estimates. Therefore, also the majority of the errors in the prediction will be below $\pm 15°$, which, according to [19], can be compensated by commonly used finger vein recognition systems.

VII. CONCLUSIONS

In this article, a CNN-based rotation detector for finger vein biometrics was presented. The detector accurately estimates the longitudinal rotation between two finger vein images of the same finger and is not limited on the data sets it was trained on. The prediction of one rotation angle is very fast (one estimation takes approximately 15ms on a GPU system). This makes the proposed detector the first system that can be practically applied in finger vein recognition systems.

The first part of the experiments analysed the accuracy of the estimated rotation angles. The results showed, that the rotation detector delivers accurate results in the range of particular interest ($\pm 30°$). For rotation angles $>30°$, the estimation error rises noticeable.

To show that the system is not limited to the data set it was trained on, it was applied on four publicly available finger vein data sets, that differ from the training data (different capturing devices and acquisition protocols). A rotation correction using the estimated rotation angles leads to distinct improvements in the EER on all four data sets between 50 and 260% compared to the performance without rotation correction. The only prerequisite to apply the proposed system is that the ROIs of the finger vein images are extracted in the same way as during the training of the CNN.

REFERENCES

[1] M. S. M. Asaari, S. A. Suandi, and B. A. Rosdi. Fusion of band limited phase only correlation and width centroid contour distance for finger

based biometrics. *Expert Systems with Applications*, 41(7):3367–3382, 2014.

[2] J. Y. Bok, K. H. Suh, and E. C. Lee. Detecting fake finger-vein data using remote photoplethysmography. *Electronics*, 8(9):1016, 2019.

[3] S. Bunda. 3D point cloud reconstruction based on the finger vascular pattern. B.S. thesis, University of Twente, 2018.

[4] Q. Chen, L. Yang, G. Yang, and Y. Yin. Geometric shape analysis based finger vein deformation detection and correction. *Neurocomputing*, 2018.

[5] Q. Chen, L. Yang, G. Yang, Y. Yin, and X. Meng. DFVR: Deformable finger vein recognition. In *2017 IEEE International Conference on Acoustics, Speech and Signal Processing (ICASSP)*, pages 1278–1282, March 2017.

[6] X. Deng, Y. Yuan, Y. Zhang, P. Tan, L. Chang, S. Yang, and H. Wang. Joint hand detection and rotation estimation by using CNN. *CoRR*, abs/1612.02742, 2016.

[7] Houjun Huang, S. Liu, H. Zheng, L. Ni, Yi Zhang, and W. Li. Deepvein: Novel finger vein verification methods based on deep convolutional neural networks. In *2017 IEEE International Conference on Identity, Security and Behavior Analysis (ISBA)*, pages 1–8, Feb 2017.

[8] H. Hsu, T. Wu, S. Wan, W. H. Wong, and C. Lee. Quatnet: Quaternion-based head pose estimation with multiregression loss. *IEEE Transactions on Multimedia*, 21(4):1035–1046, 2019.

[9] B. Huang, Y. Dai, R. Li, D. Tang, and W. Li. Finger-vein authentication based on wide line detector and pattern normalization. In *Pattern Recognition (ICPR), 2010 20th International Conference on*, pages 1269–1272. IEEE, 2010.

[10] W. Kang, H. Liu, W. Luo, and F. Deng. Study of a full-view 3D finger vein verification technique. *IEEE Transactions on Information Forensics and Security*, pages 1–1, 2019.

[11] C. Kauba, B. Prommegger, and A. Uhl. Focussing the beam - a new laser illumination based data set providing insights to finger-vein recognition. In *Proceedings of the IEEE 9th International Conference on Biometrics: Theory, Applications, and Systems (BTAS2018)*, pages 1–9, Los Angeles, California, USA, 2018.

[12] A. Kumar and Y. Zhou. Human identification using finger images. *Image Processing, IEEE Transactions on*, 21(4):2228–2244, 2012.

[13] E. C. Lee, H. C. Lee, and K. R. Park. Finger vein recognition using minutia-based alignment and local binary pattern-based feature extraction. *International Journal of Imaging Systems and Technology*, 19(3):179–186, 2009.

[14] Y. Lu, S. J. Xie, S. Yoon, J. Yang, and D. S. Park. Robust finger vein roi localization based on flexible segmentation. *Sensors*, 13(11):14339–14366, 2013.

[15] D. Maio, D. Maltoni, R. Cappelli, J. L. Wayman, and A. K. Jain. FVC2004: Third Fingerprint Verification Competition. In *ICBA*, volume 3072 of *LNCS*, pages 1–7. Springer Verlag, 2004.

[16] Y. Matsuda, N. Miura, A. Nagasaka, H. Kiyomiu, and T. Miyatake. Finger-vein authentication based on deformation-tolerant feature-point matching. *Machine Vision and Applications*, 27(2):237–250, 2016.

[17] N. Miura, A. Nagasaka, and T. Miyatake. Feature extraction of finger-vein patterns based on repeated line tracking and its application to personal identification. *Machine Vision and Applications*, 15(4):194–203, 2004.

[18] N. Miura, A. Nagasaka, and T. Miyatake. Extraction of finger-vein patterns using maximum curvature points in image profiles. *IEICE transactions on information and systems*, 90(8):1185–1194, 2007.

[19] B. Prommegger, C. Kauba, M. Linortner, and A. Uhl. Longitudinal finger rotation - deformation detection and correction. *IEEE Transactions on Biometrics, Behavior, and Identity Science*, 1(2):123–138, 2019.

[20] B. Prommegger, C. Kauba, and A. Uhl. Longitudinal finger rotation - problems and effects in finger-vein recognition. In *Proceedings of the International Conference of the Biometrics Special Interest Group (BIOSIG'18)*, Darmstadt, Germany, 2018.

[21] B. Prommegger, C. Kauba, and A. Uhl. Multi-perspective finger-vein biometrics. In *Proceedings of the IEEE 9th International Conference on Biometrics: Theory, Applications, and Systems (BTAS2018)*, Los Angeles, California, USA, 2018.

[22] B. Prommegger, C. Kauba, and A. Uhl. On the extent of longitudinal finger rotation in publicly available finger vein data sets. In *Proceedings of the 12th IAPR/IEEE International Conference on Biometrics (ICB'19)*, pages 1–8, Crete, Greece, 2019.

[23] B. Prommegger and A. Uhl. Perspective multiplication for multi-perspective enrolment in finger vein recognition. In *Proceedings of the 18th International Conference of the Biometrics Special Interest Group (BIOSIG'19)*, Darmstadt, Germany, 2019.

[24] B. Prommegger and A. Uhl. Rotation invariant finger vein recognition. In *Proceedings of the IEEE 10th International Conference on Biometrics: Theory, Applications, and Systems (BTAS2019)*, Tampa, Florida, USA, 2019.

[25] R. Raghavendra and C. Busch. Exploring dorsal finger vein pattern for robust person recognition. In *2015 International Conference on Biometrics (ICB)*, pages 341–348, May 2015.

[26] P. Schuch, J. M. May, and C. Busch. Unsupervised learning of fingerprint rotations. In *2018 International Conference of the Biometrics Special Interest Group (BIOSIG)*, pages 1–6, 2018.

[27] A. F. Sequeira, J. Ferryman, L. Chen, C. Galdi, J.-L. Dugelay, V. Chiesa, A. Uhl, B. Prommegger, C. Kauba, S. Kirchgasser, A. Grudzien, M. Kowalski, L. Szklarski, P. Maik, and P. Gmitrowicz. Protect multimodal db: a multimodal biometrics dataset envisaging border control. In *Proceedings of the International Conference of the Biometrics Special Interest Group (BIOSIG'18)*, pages 1–8, Darmstadt, Germany, 2018.

[28] L. Sonna Momo, L. Cerqueira Torres, S. Marcel, A. Anjos, M. Liebling, A. Shajkofci, S. Amoos, A. Woeffray, A. Sierro, P. Roduit, P. Ferez, and L. Bonvin. Method and Device for Biometric Vascular Recognition and/or Identification, WIPO (PCT) Patent WO/2019/150254, 08 2019.

[29] B. Ton and R. Veldhuis. A high quality finger vascular pattern dataset collected using a custom designed capturing device. In *International Conference on Biometrics, ICB 2013*. IEEE, 2013.

[30] S. Xie, R. B. Girshick, P. Dollár, Z. Tu, and K. He. Aggregated residual transformations for deep neural networks. *CoRR*, abs/1611.05431, 2016.

[31] L. Yang, G. Yang, Y. Yin, and X. Xi. Finger vein recognition with anatomy structure analysis. *IEEE Transactions on Circuits and Systems for Video Technology*, pages 1–1, 2017.

[32] Y. Yin, L. Liu, and X. Sun. Sdumla-hmt: a multimodal biometric database. *Biometric Recognition*, pages 260–268, 2011.

[33] J. Zhang and J. Yang. Finger-vein image enhancement based on combination of gray-level grouping and circular gabor filter. In *Information Engineering and Computer Science, 2009. ICIECS 2009. International Conference on*, pages 1–4. IEEE, 2009.

[34] J. Zhao, H. Tian, W. Xu, and X. Li. A new approach to hand vein image enhancement. In *Intelligent Computation Technology and Automation, 2009. ICICTA'09. Second International Conference on*, volume 1, pages 499–501. IEEE, 2009.

[35] K. Zuiderveld. Contrast limited adaptive histogram equalization. In P. S. Heckbert, editor, *Graphics Gems IV*, pages 474–485. Morgan Kaufmann, 1994.

A. Brömme, C. Busch, A. Dantcheva, C. Rathgeb and A. Uhl (Eds.): BIOSIG 2018,
Lecture Notes in Informatics (LNI), Gesellschaft für Informatik, Bonn 2018 1

The Two Sides of the Finger - An Evaluation on the Recognition Performance of Dorsal vs. Palmar Finger-Veins

Christof Kauba[1], Bernhard Prommegger[1], Andreas Uhl[1]

Abstract: Vascular pattern (vein) based biometrics, especially finger- and hand-vein recognition gain more and more attention. In finger-vein recognition, the images are usually captured from the palmar (bottom) side of the finger. Dorsal (top) side finger vein recognition has not got much attention so far. In this paper we establish a new, publicly available, two-sided (dorsal and palmar) finger-vein data set. The data set is captured using two custom designed finger vein scanners, one based on near-infrared LED illumination, the other one on near-infrared laser modules. A recognition performance comparison between the single subsets (palmar and dorsal) as well as cross-subset (palmar vs. dorsal) comparison is conducted using several well-established finger-vein recognition schemes. The experimental results confirm that the palmar side achieves the overall best recognition performance but in general the dorsal side works better due to inherent finger texture information.

Keywords: Finger Vein Recognition, Palmar-Dorsal Data Set, Performance Evaluation, Finger Texture Analysis, Finger Vein Scanner Device

1 Introduction

Vein or to be more precise vascular pattern based recognition is an emerging new biometric as it might help to overcome some of the problems existing biometric recognition systems suffer from. Vein based systems rely on the structure of the vascular pattern formed by the blood vessels inside the human body tissue, which becomes visible in near-infrared (NIR) light only. Vein based biometrics are insensitive to abrasion and skin surface conditions. Moreover, a liveness detection can be performed easily [KZ12]. Especially hand- and finger-vein based systems are introduced in commercial systems too. In finger-vein recognition it is common to use the palmar (bottom) side of the finger. The dorsal (top) side of the finger has only got little attention so far. Moreover, it is not clear if the palmar or the dorsal side yields a better recognition performance.

The main contribution of this paper is a new two-side finger-vein data set, comprising dorsal as well as palmar finger-vein images captured from the same subjects. Our data set provides high resolution palmar and dorsal finger-vein images of 360 individual fingers. It contains 4 subsets: one palmar and one dorsal one captured utilising our NIR LED and our NIR laser module based scanner, respectively. Based on these data sets a recognition performance evaluation of both, the palmar and dorsal subsets is conducted in order to answer the question: which side is better in terms of recognition performance - palmar or dorsal? In addition, a cross-comparison experiment between the palmar and dorsal view was done

[1] Department of Computer Sciences, University of Salzburg, AUSTRIA, {ckauba, bprommeg, uhl}@cs.sbg.ac.at

to confirm that the vein patters differ and a cross-comparison is not possible. Moreover, a finger texture analysis is conducted in order to quantify the amount of information which is extracted unintentionally from the skin surface texture instead of the vein patterns.

The rest of this paper is organised as follows: Section 2 gives an overview on publicly available finger-vein data sets and related work on dorsal finger-veins, followed by a description of our new two-side, dorsal and palmar, finger vein data set as well as the scanner device. Section 3 outlines the experimental set-up, including the recognition tool-chain as well as the evaluation protocol and presents the performance evaluation results together with a results discussion. Section 4 concludes this paper.

2 Finger-Vein Data Sets

Tab. 1 gives an overview on the 8 publicly available finger vein data sets we found so far. Only one of these data sets includes images that are captured from the dorsal side of the finger, which is the PROTECT Multimodal Database [UoR17]. All the other data sets are captured from the palmar side of the finger. There is some research on dorsal finger-veins, e.g. the work of Raghavendra and Busch [RB15] but their data set has never been published. Heenaye and Khan [HK12] established a dorsal and palmar hand-vein data set and did a score level fusion to improve the overall recognition results. However, they did no direct comparison of the individual performances of palmar and dorsal images. Due to the fact that the vein geometry and properties are different for hand- and finger-veins (finger-veins are smaller and more dense compared to hand-veins), recognition performance results for finger-veins cannot be inferred from hand-veins. To the best of our knowledge there is no work on the direct comparison of palmar and dorsal finger-vein images. Hence, it is not obvious if the palmar or the dorsal side achieves a better recognition performance.

name	subjects	fingers	images	dors/palm	sess.	resolution
UTFVP [TV13]	60	6	1440	palmar	2	672×380
SDUMLA-HMT [YLS11]	106	6	3816	palmar	1	320×240
FV-USM [ASR14]	123	4	5940	palmar	2	640×480
VERA FingerVein [TVM14]	110	2	440	palmar	2	665×250
MMCBNU_6000 [Lu13]	100	6	6000	palmar	1	640×480
THU-FVFDT [YYL09]	610	2	6540	palmar	2	720×576
HKPU-FID [KZ12]	156	2	3132	palmar	2	512×256
PMMDB-FV [UoR17]	20	4	240	dorsal	1	1280×440

Tab. 1: Overview on publicly available finger-vein data sets. Note: only one contains dorsal images.

2.1 PLUSVein Dorsal-Palmar Finger-Vein Data Set

Our PLUSVein Dorsal-Palmar finger-vein data set was acquired with our two custom designed finger vein scanners, an NIR LED and a NIR laser module based version, which are depicted in Fig. 1. The scanners are designed to capture 3 fingers (index, middle and ring finger) at once. Both scanners are based on an NIR enhanced industrial camera equipped with a 9 mm lens in combination with an NIR pass-through filter. Its main light source is

a transillumination one consisting of 3 stripes (one underneath each finger) of NIR LEDs for the LED version or NIR laser modules for the laser version of the scanner, respectively. Each LED/laser module is brightness controlled individually and automatically based on a preset brightness value to achieve an optimal image contrast. An LED ring consisting of 8 850 nm LEDs, 8 950 nm LEDs and 8 daylight LEDs for capturing reflected light images is situated on top of the device and can be automatically brightness controlled too. To assist in positioning of the finger, the lower part contains a custom 3D printed finger support which also serves as a bracket for the 3 illumination stripes.

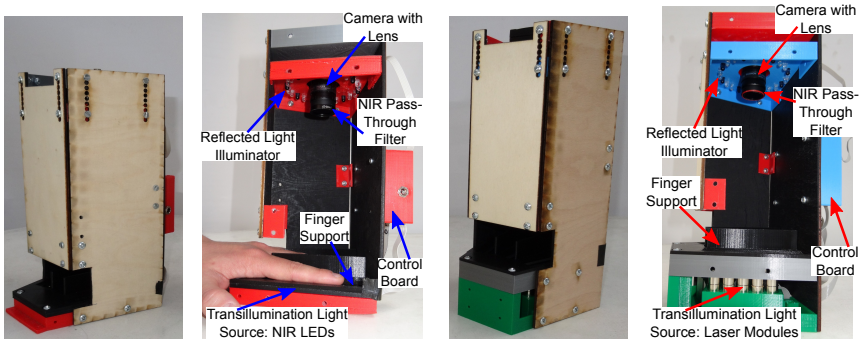

Fig. 1: Left: LED based finger-vein scanner, right: laser module based finger vein scanner

The finger-vein data set itself consists of 4 subsets: one dorsal and one palmar finger-vein subset captured using transillumination with the LED and the laser module based scanner, respectively. 60 subjects, 6 fingers (left and right index, middle and ring finger) and 5 images per finger in 1 session were captured for each of the four subsets. So each subset consists of the same 360 individual fingers but captured from a different view - palmar for the first two and dorsal for the second two. Each scanner captures 3 fingers at a time. Thus, each subset contains 600 raw finger-vein images. Some example images can be seen in Fig. 2. The images are then separated into 3 parts, corresponding to index, middle and ring finger, respectively. Hence, there are effectively 1800 images in each subset and 7200 images in total for the whole data set. The raw images have a resolution of 1280×1024 pixels and are stored in 8 bit greyscale png format. The finger separated images have a resolution of 420×1024 pixels and the visible area of the finger inside the images is about 200×750 pixels per finger. The data set is publicly available for research purposes and can be downloaded at: `http://www.wavelab.at/sources/PLUSVein-FV3/`.

3 Experiments

The finger-vein processing tool-chain consists of ROI (region of interest) extraction, pre-processing, feature extraction and comparison. At first the input image is split into 3 parts based on fixed coordinates, corresponding to index, middle and ring finger, respectively. From here on each image is processed individually. The ROI is extracted by first detecting the finger outline. Then the area outside the finger is masked out (pixels set to black). Afterwards, the finger is aligned (rotated and shifted) such that it is in upright position in

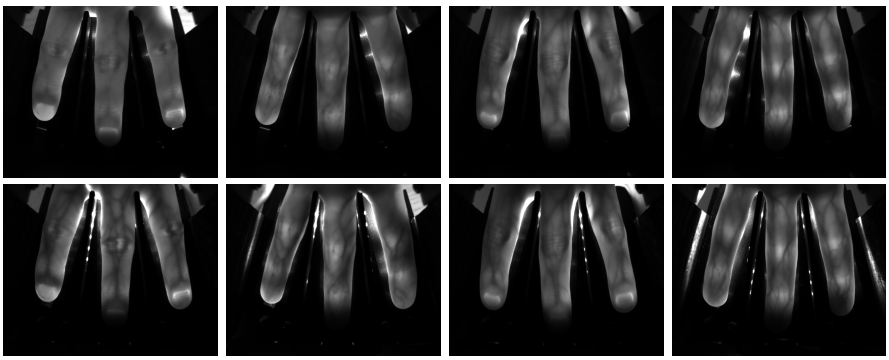

Fig. 2: Finger-vein example images captured by our three finger vein scanners, top: laser scanner, bottom: LED scanner, first and third column: dorsal, second and fourth column: palmar

the centre of the image based on a straight centre line which is fitted into the finger and a rectangular ROI is fit inside the finger area. The ROI images have a size of 192×736 pixels. To improve the visibility of the vein pattern we employ **High Frequency Emphasis Filtering** (HFE), **Circular Gabor Filter** (CGF) and simple **CLAHE** (local histogram equalisation) as preprocessing. We opted for three well-established binarisation type feature extraction methods as well as one **SIFT** key-point based method (SIFT) with additional key-point filtering. **Maximum Curvature** (MC) [MNM07], **Principal Curvature** (PC) [Ch09] and **Gabor Filter** (GF) [KZ12] aim to extract the vein pattern from the background resulting in a binary image, followed by a comparison of these binary images. Comparing the binary feature images is done using template matching as suggested by Miura et al. [MNM07]: The maximum correlation value, calculated between the input images and in x- and y-direction shifted and rotated versions of the reference image is used as comparison score. For more details on the preprocessing, feature extraction and comparison methods please refer to [KRU14].

The EER as well as the FMR1000 (the lowest $FNMR$ for $FMR \leq 0.1\%$) and the ZeroFMR (the lowest $FNMR$ for $FMR = 0\%$) are used to quantify the performance. All possible genuine comparisons are performed, which are $60 \cdot 6 \cdot \frac{5 \cdot 4}{2} = 3600$ comparisons, while for the impostor comparisons only the first image of each finger is compared against the first image of all other fingers, resulting in $\frac{60 \cdot 6 \cdot (60 \cdot 6 - 1)}{2} = 64620$ impostor comparisons and68220 comparisons in total. All result values are given in percentage terms, e.g. 2.78 means 2.78%. An implementation of the complete processing tool-chain as well as the scores and detailed results are available at: `http://www.wavelab.at/sources/Kauba18d/`.

3.1 Single Subset Results

Tab. 2 lists the recognition performance in terms of EER (the value in brackets is the 90% confidence interval), FMR1000 and ZeroFMR for both data sets, the LED and the laser

scanner one. The DET plots are depicted in Fig. 3. The same settings per recognition scheme have been used for both subsets: dorsal/palmar but different ones for laser and LED. For the LED palmar subset MC performed best, achieving an EER of 0.06%, followed by PC and SIFT while GF performed worst. For the dorsal subset the situation is different: This time SIFT performed best with an EER of 0.06%, followed by PC and MC while GF achieved the worst performance. All schemes perform slightly worse on the laser scanner data set, with MC achieving the best overall EER of 0.11% on the palmar sub set, except for GF on laser palmar which is superior to the LED palmar sub set. The table reveals that only MC performs better for palmar finger-vein images. PC, SIFT and GF perform better on the dorsal subset. Especially SIFT and GF perform much better on dorsal than palmar images. The FMR1000 and ZeroFMR results follow the same trend as the EER ones.

		Dorsal			Palmar		
		EER	FMR1000	ZeroFMR	EER	FMR1000	ZeroFMR
LED	MC	0.17 (±0.07)	0.19	0.22	**0.06** (±0.04)	**0.03**	**0.19**
	PC	0.11 (±0.06)	0.11	**0.11**	0.17 (±0.07)	0.19	0.64
	SIFT	**0.06** (±0.04)	**0.06**	0.28	0.64 (±0.13)	1.67	3.83
	GF	0.25 (±0.08)	0.28	0.75	1.42 (±0.2)	2.36	6.64
Laser	MC	0.2 (±0.07)	0.28	**0.64**	**0.11** (±0.06)	**0.11**	**0.33**
	PC	0.44 (±0.11)	0.53	1.14	0.48 (±0.11)	0.69	0.97
	SIFT	**0.13** (±0.06)	**0.17**	0.89	1.25 (±0.19)	3.0	6.44
	GF	0.64 (±0.14)	0.81	1.5	1.19 (±0.18)	2.17	3.92

Tab. 2: Recognition performance results, dorsal and palmar for both data sets (LED + laser), best results per side and scanner are highlighted **bold**

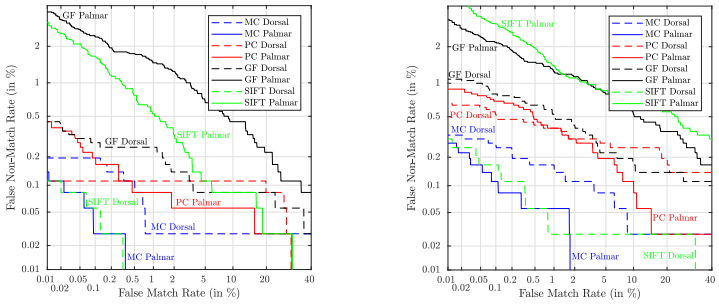

Fig. 3: DET plots: LED based scanner (left) and laser based scanner (right)

3.2 Dorsal-Palmar Cross-Comparison Results

By applying transillumination only the veins which are close to the finger skin become visible as discussed in [MNM04] and [Ko00]. As these surface vein patterns on the palmar and dorsal side of the finger differ [GG74], a cross comparison between palmar and dorsal images will not be possible. For the sake of completness we performed a cross comparison between the palmar and flipped dorsal (palmar images have been captured by turning the finger 180° around its axis) images. The results given in Tab. 3 confirm that that a cross-

comparison between dorsal and palmar images of the same fingers is not possible (EER around 50%, FMR1000 and ZeroFMR nearly 100%).

	LED				Laser			
	MC	PC	SIFT	GF	MC	PC	SIFT	GF
EER	47	50	47	49	49	50	46	48
FMR1000	99	99	99	99	99	99	99	99
ZeroFMR	99	99	100	100	100	100	100	100

Tab. 3: Cross-comparison (palmar vs. dorsal) results for both data sets (LED + laser). The values indicate that a comparison between dorsal and palmar is not possible

3.3 Finger Texture Analysis

Fig. 4 shows a comparison of the extracted features for MC and GF on palmar and dorsal LED scanner images, respectively. There is some finger surface texture visible in both, the palmar and dorsal images, but it is more pronounced in the dorsal ones. Especially GF does not only extract vein lines, but also the wrinkles and the finger texture. Also SIFT, as a general purpose key-point descriptor uses the additional information present due to the finger texture. On the other hand, MC tries to suppress the non-vein texture and therefore mainly relies on the vein lines. It shows less extracted features that actually belong to the finger texture instead of vein lines than GF. To quantify the amount of finger texture and wrinkle information present in the extracted vein features we rely on the three binarisation type feature extractors (MC, PC and GF) and perform an edge detection based analysis: Most finger vein lines are apparent as horizontal lines while the finger texture and wrinkles are usually apparent as vertical lines. Thus, vertical edges correspond to finger texture information whereas horizontal edges correspond to vein lines, respectively. We apply a Prewitt filter based edge detection to detect vertical and horizontal edges separately and quantify the amount of edge information: $e = \frac{p_e}{w \cdot h}$ where e is the amount of edge information in the image, p_e are the detected edge pixels and w, h is the image width and height, respectively. Afterwards, the ratio between vertical and total edges is used to predict the amount of finger texture information present in the images: $fti = \frac{e_v}{e_h}$, where e_v and e_h is the vertical and horizontal edge information, respectively. Higher values of fti correspond to a higher amount of finger texture information present. Tab. 4 shows these values for MC, PC and GF based on the LED scanner images (SIFT does not produce binary output images). For all 3 feature extraction schemes the finger texture information present in the dorsal feature images is higher than in the palmar ones (1.369 times for MC, 1.281 for PC and 1.752 for GF). This additional features originating from the finger texture help in discriminating between different fingers and thus increase the recognition performance. Consequently PC, GF and SIFT perform better for the dorsal images due to the additional finger texture information compared to the palmar images.

4 Conclusion

We established a new dorsal and palmar finger-vein data set, containing 7200 images from 360 different fingers, captured with two different custom designed scanners, an LED based one and a laser module based one. Based on this data set we did a direct comparison of

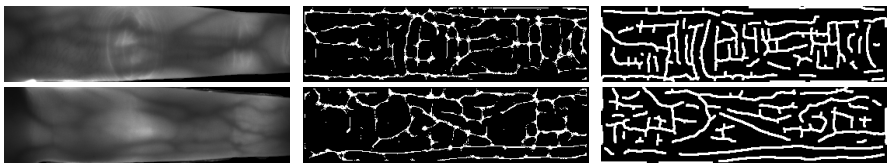

Fig. 4: Comparison between dorsal (top) and palmar (bottom) extracted features for MC (middle) and GF (right). The dorsal images show more finger texture (vertical lines) especially for GF compared to the palmar ones.

	Dorsal			Palmar			Dorsal/Palmar
	e_v	e_h	fti	e_v	e_h	fti	fti_D/fti_P
MC	0.0134	0.0203	0.6737	0.0104	0.0213	0.4918	1.369
PC	0.0139	0.0174	0.8013	0.0109	0.0176	0.6255	1.281
GF	0.0158	0.0189	0.8627	0.0138	0.0233	0.4571	1.752

Tab. 4: Finger texture information contained in the dorsal and palmar LED scanner images quantified in terms of horizontal and vertical edges. Higher values of fti correspond to more finger texture information present.

palmar and dorsal finger-vein images in terms of recognition performance using several well-established recognition schemes. The experimental results reveal that the overall best performance is achieved for palmar images. Although, in general the dorsal images perform better than the palmar ones, mainly due to the fact that not only the vein lines are extracted during feature extraction, but also the finger texture and wrinkles are considered. The dorsal images show more texture information than the palmar ones and consequently, most of the tested recognition schemes work better using the dorsal images. Moreover, our results confirmed that a cross-comparison between palmar and dorsal vein patterns is not possible.

Our future work will include tests with some more state-of-the-art finger-vein recognition schemes. Moreover, we are going to design a suitable preprocessing method to suppress the finger texture information and wrinkles in order to have the extracted features based on vein lines only and thus to make the results independent from the finger texture information. After all, vein recognition should only deal with vascular pattern information and not the skin surface texture one.

Acknowledgements

This project has received funding from the European Union's Horizon 2020 research and innovation program under grant agreement No. 700259.

References

[ASR14] Asaari, Mohd Shahrimie Mohd; Suandi, Shahrel A; Rosdi, Bakhtiar Affendi: Fusion of band limited phase only correlation and width centroid contour distance for finger based

biometrics. Expert Systems with Applications, 41(7):3367–3382, 2014.

[Ch09] Choi, Joon Hwan; Song, Wonseok; Kim, Taejeong; Lee, Seung-Rae; Kim, Hee Chan: Finger vein extraction using gradient normalization and principal curvature. Jgg. 7251, 2009.

[GG74] Gray, Henry; Goss, Charles Mayo: Anatomy of the human body. American Journal of Physical Medicine & Rehabilitation, 53(6):293, 1974.

[HK12] Heenaye, Maleika; Khan, Mamode: A Multimodal Hand Vein Biometric based on Score Level Fusion. Procedia Engineering, 41:897 – 903, 2012. International Symposium on Robotics and Intelligent Sensors 2012 (IRIS 2012).

[Ko00] Kono, Miyuki: A new method for the identification of individuals by using of vein pattern matching of a finger. In: Proc. Fifth Symposium on Pattern Measurement, Yamaguchi, Japan, 2000. S. 9–12, 2000.

[KRU14] Kauba, Christof; Reissig, Jakob; Uhl, Andreas: Pre-processing cascades and fusion in finger vein recognition. In: Proceedings of the International Conference of the Biometrics Special Interest Group (BIOSIG'14). Darmstadt, Germany, September 2014.

[KZ12] Kumar, Ajay; Zhou, Yingbo: Human identification using finger images. Image Processing, IEEE Transactions on, 21(4):2228–2244, 2012.

[Lu13] Lu, Yu; Xie, Shan Juan; Yoon, Sook; Wang, Zhihui; Park, Dong Sun: An available database for the research of finger vein recognition. In: Image and Signal Processing (CISP), 2013 6th International Congress on. Jgg. 1. IEEE, S. 410–415, 2013.

[MNM04] Miura, Naoto; Nagasaka, Akio; Miyatake, Takafumi: Feature extraction of finger-vein patterns based on repeated line tracking and its application to personal identification. Machine Vision and Applications, 15(4):194–203, 2004.

[MNM07] Miura, Naoto; Nagasaka, Akio; Miyatake, Takafumi: Extraction of finger-vein patterns using maximum curvature points in image profiles. IEICE transactions on information and systems, 90(8):1185–1194, 2007.

[RB15] Raghavendra, R.; Busch, C.: Exploring dorsal finger vein pattern for robust person recognition. In: 2015 International Conference on Biometrics (ICB). S. 341–348, May 2015.

[TV13] Ton, B.T.; Veldhuis, R.N.J.: A high quality finger vascular pattern dataset collected using a custom designed capturing device. In: International Conference on Biometrics, ICB 2013. IEEE, 2013.

[TVM14] Tome, Pedro; Vanoni, Matthias; Marcel, Sébastien: On the Vulnerability of Finger Vein Recognition to Spoofing. In: IEEE International Conference of the Biometrics Special Interest Group (BIOSIG). September 2014.

[UoR17] University of Reading: , PROTECT Multimodal DB Dataset, June 2017. Available by request at http://projectprotect.eu/dataset/.

[YLS11] Yin, Yilong; Liu, Lili; Sun, Xiwei: SDUMLA-HMT: a multimodal biometric database. Biometric Recognition, S. 260–268, 2011.

[YYL09] Yang, Wenming; Yu, Xiang; Liao, Qingmin: Personal authentication using finger vein pattern and finger-dorsa texture fusion. In: Proceedings of the 17th ACM international conference on Multimedia. ACM, S. 905–908, 2009.

A. Brömme, C. Busch, A. Dantcheva, C. Rathgeb and A. Uhl (Eds.): BIOSIG 2018,
Lecture Notes in Informatics (LNI), Gesellschaft für Informatik, Bonn 2018 1

Longitudinal Finger Rotation - Problems and Effects in Finger-Vein Recognition

Bernhard Prommegger[1], Christof Kauba[1] and Andreas Uhl[1]

Abstract: Finger-vein scanners or vein-based biometrics in general are becoming more and more popular. Commercial off-the-shelf finger-vein scanners usually capture only one finger from the palmar side using transillumination. Most scanners have a contact area and a finger-shaped support where the finger has to be placed onto in order to prevent misplacements of the finger including shifts, planar rotation and tilts. However, this is not able to prevent rotation of the finger along its longitudinal axis (also called non-planar finger rotation). This kind of finger rotation poses a severe problem in finger-vein recognition as the resulting vein image may represent entirely different patterns due to the perspective projection. We evaluated the robustness of several finger-vein recognition schemes against longitudinal finger rotation. Therefore, we established a finger-vein data set exhibiting longitudinal finger rotation in steps of 1° covering a range of ±90°. Our experimental results confirm that the performance of most of the simple recognition schemes rapidly decreases for more than 10° of rotation, while more advanced schemes are able to handle up to 30°.

Keywords: Longitudinal Finger Rotation, Finger-Vein Recognition, Multi-Perspective Finger-Vein Data Set, Performance Evaluation, Finger Vein Scanner Device

1 Introduction

Vascular pattern based biometrics, commonly denoted as vein biometrics, provide several advantages over other, well-established biometric recognition systems. Especially hand- and finger-vein based systems tend to replace fingerprint based ones in some application areas. Vein based systems rely on the structure of the vascular pattern formed by the blood vessels inside the human body tissue, which becomes visible in near-infrared (NIR) light only. This vessel structure is within the human body and thus vein based systems are insensitive to abrasion and skin surface conditions. Moreover, a liveness detection can be performed easily [KZ12].

However, finger-vein recognition systems are far from being perfect in terms of accuracy, reliability and usability. Their recognition performance may suffer from different internal and external factors which might lead to a lower performance. Internal factors include the configuration of the scanner itself, the illumination source and the NIR camera. Most of the internal and external factors impacting the finger-vein recognition performance can be ruled out by means of adding components to the scanner or tuning the scanner settings. External factors can be divided into environmental ones, including ambient light, dust or dirt on the sensor, high humidity, electromagnetic radiation, etc. and factors regarding the

[1] Department of Computer Sciences, University of Salzburg, AUSTRIA,
{bprommeg, ckauba, uhl}@cs.sbg.ac.at

presentation of the finger to the scanner device. The latter includes finger movement during acquisition and finger misplacement in general. Some of the environmental factors can be ruled out by using additional components for the vein scanner, e.g. the influence ambient light can be reduced by installing an NIR pass-through filter. However, especially tilt and rotation of the finger along its longitudinal axis (which are a form or finger misplacement) are hard to tackle. While the tilt can be avoided to a certain extent, as soon as there is only one finger to be captured, it is hard to avoid rotation of the finger along its longitudinal axis, especially for touchless finger-vein scanners, but not restricted to touchless operation. Hence, this is one of the main factors influencing the recognition performance of finger-vein systems in practical applications and it would be desirable if finger vein recognition schemes are able to tolerate such a rotation at least to a certain extent. To the best of our knowledge no systematic investigation of this particular problem has been performed so far. The analysis of these and other factors impacting the recognition performance of finger-vein recognition systems can be summarised as robustness analysis.

Some authors state that there is the problem of finger rotation along the longitudinal axis, which is also called out-plane finger rotation or non-planar rotation, while others claim that their recognition scheme is able to tolerate this up to a certain degree. Matsuda et al. [Ma16] claim that their recognition scheme is robust against this kind of finger misplacement. They did experiments and showed that their scheme is robust against these rotations up to $\pm 30°$, but their test data set, which is not publicly available, only consisted of vein images captured from 5 different people. Chen et al. [Ch18] proposed an approach to correct different types of finger deformations based on a finger geometric analysis. Their work includes finger rotation along the longitudinal axis as well (they call it type 3 deformation). They showed that by a non-linear correction of the finger rotation the recognition performance can be improved. However, they only estimate the amount of deformation, i.e. the rotation angle, while there is no ground-truth information of the actual rotation angle available.

The main contribution of our work is a systematic robustness evaluation of several finger vein recognition schemes against the finger's longitudinal rotation. In order to investigate the impact of longitudinal finger rotation a suitable data set is needed. Unfortunately, there is no such data set available, mainly because a specifically designed finger-vein scanner device is mandatory to acquire one. Thus, we established a finger rotation data set, exhibiting transillumination finger-vein images captured in different rotation angles in $1°$ steps in a range of $\pm 90°$ starting from the palmar view. This data set was captured using our custom designed, multi-perspective finger-vein scanner device and will be made publicly available in the future. Our experimental results show that longitudinal finger rotation poses a severe problem for most finger-vein recognition schemes.

The rest of this paper is organised as follows: Section 2 illustrates the problem of the finger's longitudinal rotation in detail. Section 3 presents our multi-perspective finger-vein scanner device and the finger rotation data set. Section 4 describes the experimental set-up and presents the performance evaluation results together with a results discussion. Section 5 concludes this paper along with an outlook on future work.

2 The Longitudinal Finger Rotation Problem

Usually, finger-vein scanners are designed to capture only one finger at a time. For these scanners, finger misplacements are a severe problem. There are different types of misplacement: shifts of the finger in x- and y-direction (planar shifts), shifts of the finger in z-direction, in-plane (planar) rotation of the finger, tilts of the finger and rotation around the finger's longitudinal axis. The planar shifts as well as the planar rotations can be reduced by guiding walls alongside the finger, end tips or a finger-shaped support. Shifts of the finger in z-direction are usually not a problem if the sensor has a surface where the finger has to be placed onto. Remaining planar shifts and rotations can be compensated in software by aligning the images based on the finger outline. Tilts of the finger can be avoided by using capacitive or pressure-sensitive sensors on the scanner surface which detect if the finger is placed correctly. However, rotations around the finger's longitudinal axis cannot be detected reliably by most available commercial available sensors. This problem could be avoided if the sensors would not only acquire one finger, but require the subject to place the full hand or at least more than one finger, as proposed by Kauba et al. in [KPU18], on the sensor. Fig. 1 shows an example of the longitudinal finger rotation, also called non-planar rotation or out-plane rotation by some authors, using an off-the-shelf commercial finger vein scanner. In a supervised acquisition scenario, the supervisor can tell the user to place his finger correctly. However, if the acquisition is not supervised, such longitudinal rotations of the finger impose a severe problem. This problem gets worse if the scanner is designed to operate in a contact-less way and does not have a contact surface.

Fig. 1: Finger rotation example using a commercial scanner (rotation counter-clockwise)

The captured image is a projection of the finger situated in a 3D space onto a 2D plane. This principle is depicted in Fig. 2. If the finger is rotated around its longitudinal axis, the vein patterns look different due to the change in the perspective or the projection, respectively. This projective transformation cannot be reverted using translation or rotation on the images, but can be compensated to some degree if either the rotation angle is known or can be estimated. Estimating the rotation from a single image can be a challenging task. If the angle of rotation increases, some vein lines might merge due to the perspective projection. In this case, there is no way to revert the effects caused by the longitudinal finger rotation. Thus, it would be desirable if the recognition scheme is robust against longitudinal finger rotation, at least to a certain extent. To the best of our knowledge, until now the robustness against finger rotation has not been systematically evaluated.

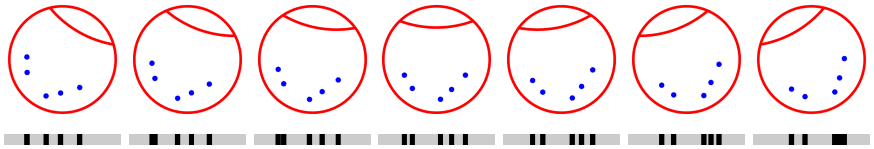

Fig. 2: Finger longitudinal axis rotation principle: a schematic finger cross section showing five veins (blue dots) rotated from $-30°$ (left) to $+30°$ (right) in $10°$ steps. The projection (bottom row) of the vein pattern is different according to the rotation angle following a non-linear transformation

3 PLUSVein-Finger Rotation Data Set

The finger rotation data set has been acquired using our custom designed multi-perspective finger vein scanner, shown in Fig. 3 right. The image sensor is an NIR enhanced industrial camera (IDS Imaging UI-1240ML-NIR), equipped with a 9 mm wide-angle-lens (Fujion HF9HA-1b) and a NIR long-pass filter (Midopt LP780). Five 808 nm NIR laser modules form the light source, positioned on the opposite side of the camera (transillumination), including an integrated automatic brightness control to achieve an optimal image contrast. To capture different perspectives or rotation angles, the camera and the illuminator rotate around the finger which is placed at the axis of rotation. This rotation principle is depicted in Fig. 3 left. The finger is stabilised with the help of a finger-tip shaped hole on the finger end and a height-adjustable finger trunk plate on the finger trunk. All parts except the camera, lens, filter and the laser modules were designed and manufactured by ourselves.

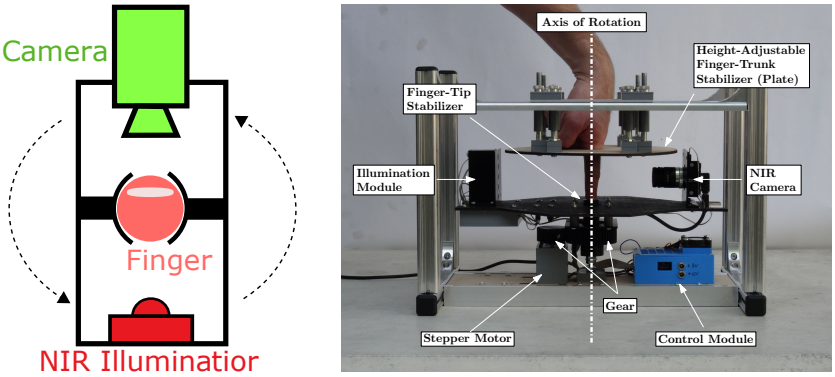

Fig. 3: Left: Principle of the multi-perspective finger vein scanner, right: the scanner itself (originally published in [PKU18], © 2018 IEEE)

The data set itself contains a total of 252 unique fingers from 63 different subjects, four fingers (right and left index and middle finger, respectively) per subject. Video sequences with a rotation speed adjusted to the frame rate were captured such that frames in $1°$ steps can be extracted in a range of $\pm 90°$ starting from the palmar view, by rotating the scanner around the finger's longitudinal axis. This leads to the same output images as if the finger would rotate itself. The capture process was repeated 5 times per finger. For each degree

of rotation there are 1260 images, resulting in 228060 images in total. Fig. 4 shows some example images in 10° steps and the corresponding extracted finger veins using Maximum Curvature [MNM07]. It becomes clearly visible that the extracted vein patterns are distinct among the different views (note the highlighted areas in the bottom row of the figure). The gender distribution of the volunteers is balanced. Among the 63 subjects 36 of the subjects are male, the remaining 27 are female. The youngest subject was 18, the oldest one 79. The image resolution is 650×1280 pixels.

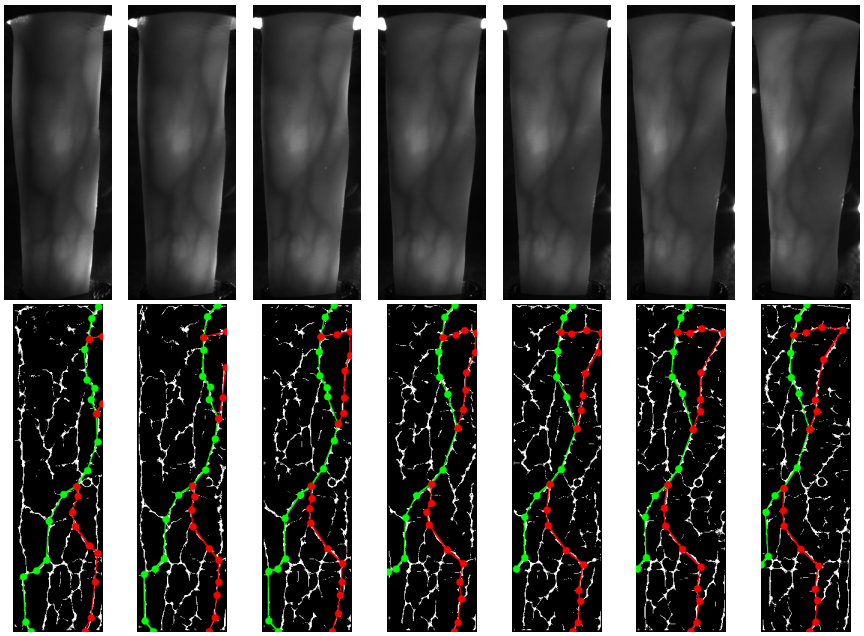

Fig. 4: Top: example images in 10° steps, from left to right: -30°, -20°, -10°, 0°, 10°, 20°, 30°, bottom: corresponding extracted MC features with two highlighted vein paths.

4 Experiments

Recognition Tool-chain: Fig. 5 shows the components of a biometric recognition system: The biometric trait is captured by a biometric sensor and afterwards processed in the recognition tool-chain which consists of preprocessing (ROI (region of interest) extraction and image enhancement), feature extraction and comparison. The input of our tool-chain are the videos captured by our mulit-perspecitve finger vein scanner. At first the frames corresponding to 1° steps are extracted from the video sequences. Afterwards each image is processed individually: the ROI is extracted and the the finger outline detected by the help of an edge detection algorithms. Then a straight centre line is fitted into the finger. Based on this centre line, the finger is aligned (rotated and shifted) such that it is in horizontal position in the middle of the image. The area outside the finger is masked out

(pixels set to black) and a rectangular ROI is fit inside the finger area. The ROI images have a size of 300×1100 pixels. To improve the visibility of the vein pattern we use **High Frequency Emphasis Filtering** (HFE), **Circular Gabor Filter** (CGF) and simple **CLAHE** (local histogram equalisation) as preprocessing. We opted for three well-established binarisation type feature extraction methods as well as two key-point based method. **Maximum Curvature** (MC) [MNM07], **Principal Curvature** (PC) [Ch09] and **Gabor Filter** (GF) [KZ12] aim to extract the vein pattern from the background resulting in a binary image, followed by a comparison of these binary images. Comparing the binary feature images is done using a correlation measure, calculated between the input images and in x- and y-direction shifted and rotated versions of the reference image. In addition, two key-point based recognition schemes, a **SIFT** [KRU14] based technique with additional key-point filtering and **Deformation-Tolerant Feature-Point Matching** (DTFPM) proposed by Matsuda et al. [Ma16] are used. For more details on the preprocessing methods please refer to [KRU14].

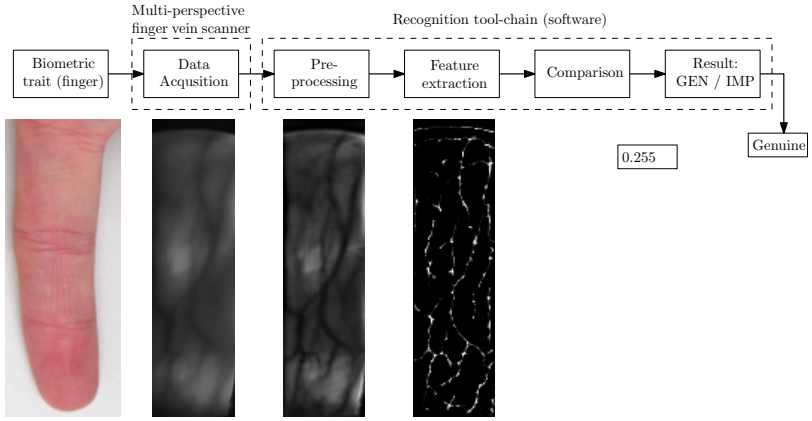

Fig. 5: Basic components of a biometric recognition system

Evaluation Protocol: To quantify the performance, the EER as well as the FMR1000 (the lowest FNMR for FMR $\leq 0.1\%$) and the ZeroFMR (the lowest FNMR for FMR $= 0\%$) are used. For calculating the genuine scores, all possible genuine comparisons are performed, which are $63 \cdot 4 \cdot 5 \cdot 5 = 6300$ comparisons. For calculating the impostor scores, only the first image of a finger is compared against the first image of all other fingers, resulting in $4 \cdot 63 \cdot 63 = 15876$ compares, so 22176 compares in total. An implementation of the complete processing tool-chain as well as the scores and detailed results are available at: `http://www.wavelab.at/sources/Prommegger18b/`.

Experimental Results: Table 1 lists the baseline performance results for the different finger-vein recognition schemes at the palmar view (0°). PC achieves the best recogniti-

on performance with an EER of 0.48%, followed by MC, DTFPM and SIFT while GF performs worst.

	PC	MC	DTFPM	SIFT	GF
EER [%]	0.48	0.59	1.15	1.53	3.14
FMR1000 [%]	0.79	0.83	2.54	4.88	5.40
ZeroFMR[%]	1.51	1.31	3.93	6.43	7.82

Tab. 1: Baseline performance results (palmar view, 0°) for the different recognition schemes

In order to quantify the robustness against longitudinal finger rotations, the images captured in the different angles from $-90°$ to $90°$ in $1°$ steps are compared against the palmar view (rotation of 0°). The trend of the absolute EER is shown in Fig. 6 left column. The relative performance degradation (RPD) $\left(\frac{EER_{rotated}-EER_{palmar}}{EER_{palmar}}\right)$ is depicted in the right column. The bottom row shows the area of $\pm 25°$ from the palmar view in more detail. Note that the RPD is calculated with respect to its baseline EER of each recognition scheme. As a result of this, the maximum RPD is limited by $RPD_{max} = \frac{EER_{max}-EER_{baseleine}}{EER_{baseline}}$ where EER_{max} is $\sim 50\%$.

MC (red line with triangular marker) and PC (green line with square marker) show a similar performance: up to a rotation angle of $\pm 10°$ the EER rises just above 1% which corresponds to a relative performance decrease about 100%. With increasing rotation angle, the recognition performance diminishes at a higher rate. At $\pm 10°$ the EER reaches 2%, between $\pm 20°$ and $\pm 25°$ the EER jumps above 10%. Around $\pm 30°$ the EER exceeds 30%, at $\pm 45°$ already 45%, i.e. recognition is no longer meaningful. DTFPM (brown line with star marker) has a higher baseline EER (1.15%) at the palmar view but its EER increases most gently, leading to the best robustness against finger rotation. At $\pm 10°$ the performance degradation is only 30% (EER: 1.53%). Starting from $\pm 17°$ DTFPM outperforms all other schemes. At $\pm 30°$ its EER is still below 7%. Matsuda et al. [Ma16] reported a baseline EER of 0.152% and a relative performance degradation of 230% (EER: 0.501%) at $\pm 30°$. However, neither their data set nor an implementation of their proposed approach is available. With our full re-implementation we are able to confirm their claimed robustness against finger rotation, but with a relative performance degradation of 500% instead of 230%. SIFT (blue line with diamond marker) is more robust against finger rotation than PC and MC, too. However, its baseline EER is higher than the one of DTFPM. GF (black line with cross marker) has the highest baseline EER (3.18%) and a similar relative performance degradation as MC and PC. Due to its high baseline EER, its RPD_{max} is lower than RPD_{max} for PC and MC. FMR1000 and ZeroFMR, visualized in Fig. 7, follow the same trend as the EER: first, the increase is relatively small and starts to rise sharply at $\pm 15°$. FMR1000 exhibits values close to 100 from $\pm 45°$ onwards for all algorithms evaluated, ZeroFMR already at $\pm 35°$. DTFPM shows the best results for both, FMR1000 and ZeroFMR. Consequently, a longitudinal finger rotation angle of $\pm 30°$ poses a severe problem for all evaluated schemes except DTFPM. A rotation angle of more than $\pm 45°$makes recognition nearly impossible.

To assist the reader in comparing the performance values at different rotation angles, Tab. 2 lists the EER per rotation angle from 0° - $\pm 45°$. The best EER for every rotation angle is

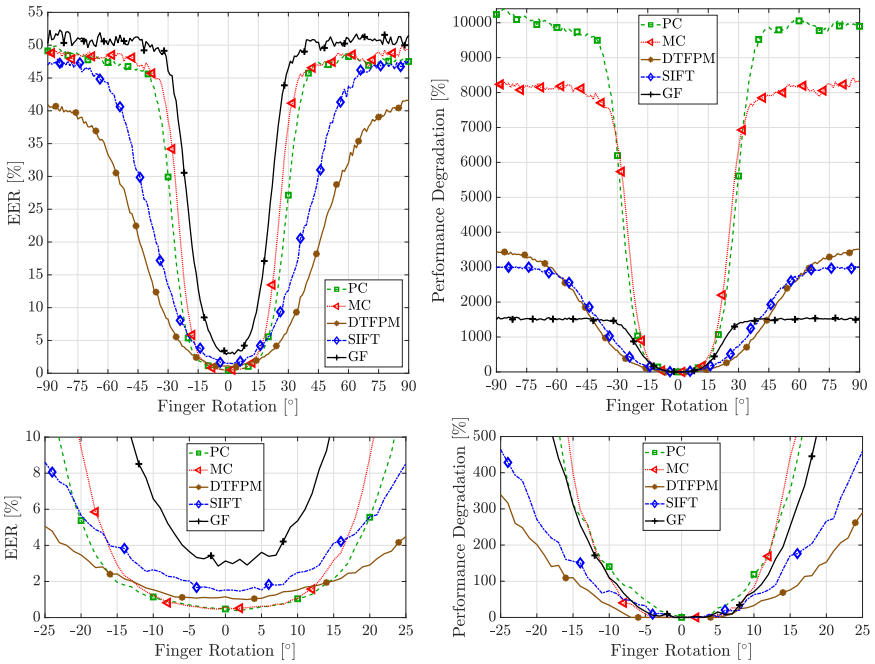

Fig. 6: Trend of performance indicators across the different rotation angles from −90° to 90° (0° corresponds to the palmar view), left: absolute EER values, right: relative change of EER in %. The bottom row shows a more detailed view from −25° to 25°.

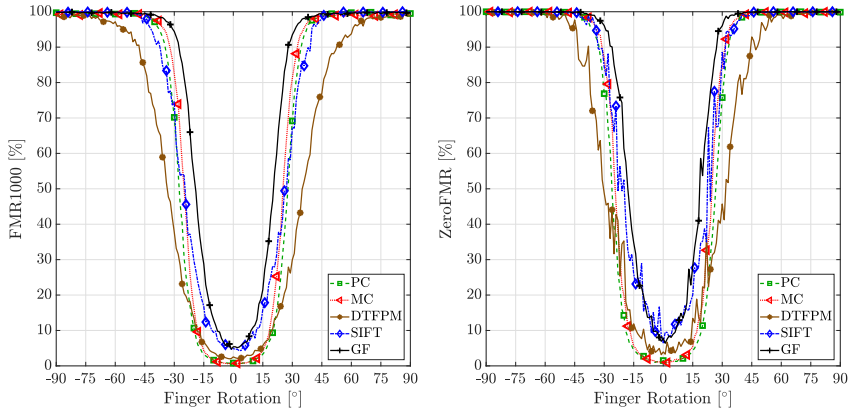

Fig. 7: Trend of performance indicators across the different rotation angles from −90° to 90° (0° corresponds to the palmar view), left: FMR1000, right ZeroFMR in %

highlighted **bold**. This table confirms that up to a certain rotation, the well established vein pattern based algorithms show the best performance. It can be seen that if the rotation exceeds a certain angle, key-point based algorithms, especially DTFPM, outperform traditional approaches.

	±0°	±5°	±10°	±15°	±20°	±25°	±30°	±45°
PC	**0.48**	**0.60**	**1.04**	**1.96**	5.38	13.43	27.14	46.50
MC	0.59	0.62	1.07	2.92	8.88	22.34	37.91	46.82
DTFPM	1.15	1.07	1.53	2.03	**2.91**	**4.49**	**6.97**	**19.26**
SIFT	1.53	1.53	2.49	3.90	5.59	8.53	12.61	30.15
GF	3.14	3.62	5.36	11.03	22.70	37.86	46.06	50.46

Tab. 2: EER at specific rotation angles [%]

Tab. 3 lists the relative performance degradation for the same rotation angles. With respect to RPD, DTFPM performs best followed by SIFT. Although GF shows the lowest RPD for ±45°, it has the worst recognition rate of all feature types, with an EER of ∼ 50%. The low RPD is due to the highest baseline result compared to the other feature types. The two tables (Tab. 2 and Tab. 3) clearly show that the evaluated key-point based algorithms are more tolerant against finger rotation than the vein pattern based ones. The key-point based algorithms match relevant key-points against each other instead of comparing binarised vein structures. If the detection and matching of theses points is insensitive to changes in the vein patterns due to longitudinal finger rotation, the results of a comparison in a biometric recognition system is less sensitive as well.

	±0°	±5°	±10°	±15°	±20°	±25°	±30°	±45°
PC	**0**%	26%	119%	312%	1031%	2727%	5610%	9684%
MC	**0**%	7%	83%	399%	1416%	3715%	6373%	7894%
DTFPM	**0**%	**0**%	**33**%	**76**%	**153**%	**290**%	**505**%	1573%
SIFT	**0**%	**0**%	63%	155%	266%	459%	726%	1876%
GF	**0**%	15%	71%	252%	624%	1107%	1369%	**1509**%

Tab. 3: Relative performance degradation at specific rotation angles [%]

Tab. 4 is the inverse of Tab. 3 and shows rotation angle at which a certain performance drop is hit. While vein pattern based algorithms (MC, PC, GF) reach 100 performance decrease around ±10°, key-point based systems tolerate higher rotation angles, e.g. DTFPM reaches a RPD of 100% at 14°. The further the finger is rotated, the more pronounced this trend becomes: the relative performance decrease of SIFT and especially DTFPM is lower than the one of PC, MC and GF. DTFPM exceeds a RPD of 500% at 28° whereas for PC, MC and GF this performance decrease is already achieved just above ±15°.

5 Conclusion

We investigated the problem of finger rotation around its longitudinal axis, also called non-planar or out-plane rotation of the finger in the scope of finger-vein recognition. This kind of finger misplacement poses a severe problem for practical applications of finger-

	10%	25%	50%	100%	200%	300%	400%	500%
PC	±1°	±3°	±5°	±8°	±12°	±13°	±15°	±16°
MC	±5°	±6°	±8°	±9°	±12°	±13°	±14°	±15°
DTFPM	±**7**°	±**8**°	±**11**°	±**14**°	±**19**°	±**23**°	±**26**°	±**28**°
SIFT	±4°	±4°	±8°	±12°	±16°	±20°	±23°	±25°
GF	±4°	±5°	±7°	±9°	±12°	±14°	±16°	±17°

Tab. 4: Rotation angle at which a certain relative performance degradation is hit

vein scanners, including most of the available off-the-shelf single finger commercial finger vein scanners, as this rotation cannot be prevented by means of the scanner hardware construction and is hard to be compensated afterwards by image preprocessing (assuming that the rotation angle is not known). We established a new finger rotation data set comprising finger-vein images captured in 1° steps of longitudinal rotation in a range of ±90° starting from the palmar view.

Our performance evaluation results confirm, that longitudinal finger rotation is a severe problem for the recognition performance of finger-vein systems. All recognition schemes are able to tolerate up to ±10° of rotation at a relative performance loss of less than 120%. The key-point based algorithms DTFPM and SIFT are more robust against finger rotation, but their baseline performance is worse compared to PC and MC. GF generally performs worst. However, for rotation angles more than 30°, which can occur in practical applications of finger-vein scanners, the recognition performance drops dramatically. This problem gets even worse for touchless finger-vein scanners with more degrees of freedom during image acquisition.

If only the planar finger-vein images are available, the ability of a recognition scheme to cope with longitudinal rotation of the finger is very limited due to the perspective mapping during imaging. One way to make finger-vein recognition more robust against finger rotation is by improving the scanner hardware, e.g by mounting an additional finger positioning support where the whole hand is placed on a kind of shelf such that the rotation of the finger can be restricted. Another option is using stereo or 3D camera systems, which is beneficial for touchless scanners anyway, in order to estimate the rotation angle of the finger and compensate for the rotation by applying a perspective transform. Another way is trying to estimate the rotation angle and compensate the rotation like Chen et al. [Ch18] proposed, which will be evaluated in our future work.

For our data set the exact longitudinal finger rotation is known. This information can be used to perform a systematic evaluation of the approach in [Ch18]. A further approach is to correct the perspective distortion by applying a non-linear transform using the known rotation angle. We will evaluate the recognition performance which can be retained at certain rotation angles for both approaches in order to determine the maximum possible rotation angle at which a reasonable recognition is still feasible.

Acknowledgements

This project has received funding from the European Union's Horizon 2020 research and innovation program under grant agreement No. 700259.

References

[Ch09] Choi, Joon Hwan; Song, Wonseok; Kim, Taejeong; Lee, Seung-Rae; Kim, Hee Chan: Finger vein extraction using gradient normalization and principal curvature. volume 7251, pp. 7251 – 7251 – 9, 2009.

[Ch18] Chen, Qing; Yang, Lu; Yang, Gongping; Yin, Yilong: Geometric shape analysis based finger vein deformation detection and correction. Neurocomputing, 2018.

[KPU18] Kauba, Christof; Prommegger, Bernhard; Uhl, Andreas: The Two Sides of the Finger - Dorsal or Palmar - Which One is Better in Finger-Vein Recognition? In: Proceedings of the International Conference of the Biometrics Special Interest Group (BIOSIG'18). Darmstadt, Germany, 2018.

[KRU14] Kauba, Christof; Reissig, Jakob; Uhl, Andreas: Pre-processing cascades and fusion in finger vein recognition. In: Proceedings of the International Conference of the Biometrics Special Interest Group (BIOSIG'14). Darmstadt, Germany, sep 2014.

[KZ12] Kumar, Ajay; Zhou, Yingbo: Human identification using finger images. Image Processing, IEEE Transactions on, 21(4):2228–2244, 2012.

[Ma16] Matsuda, Yusuke; Miura, Naoto; Nagasaka, Akio; Kiyomizu, Harumi; Miyatake, Takafumi: Finger-vein authentication based on deformation-tolerant feature-point matching. Machine Vision and Applications, 27(2):237–250, 2016.

[MNM07] Miura, Naoto; Nagasaka, Akio; Miyatake, Takafumi: Extraction of finger-vein patterns using maximum curvature points in image profiles. IEICE transactions on information and systems, 90(8):1185–1194, 2007.

[PKU18] Prommegger, Bernhard; Kauba, Christof; Uhl, Andreas: Multi-Perspective Finger-Vein Biometrics. In: Proceedings of the IEEE 9th International Conference on Biometrics: Theory, Applications, and Systems (BTAS2018). Los Angeles, California, USA, pp. 1–9, 2018.

A. Brömme, C. Busch, A. Dantcheva, C. Rathgeb and A. Uhl (Eds.): BIOSIG 2019,
Lecture Notes in Informatics (LNI), Gesellschaft für Informatik, Bonn 2019 1

Perspective Multiplication for Multi-Perspective Enrolment in Finger Vein Recognition

Bernhard Prommegger[1], Andreas Uhl[1]

Abstract: Finger vein recognition deals with the identification of subjects based on their venous pattern within the fingers. It has been shown that its recognition accuracy heavily depends on a good alignment of the acquired samples. There are several approaches that try to reduce the impact of finger misplacement. However, none of this approaches is able to prevent all possible types of finger misplacements. As finger vein scanners are evolving towards contact-less acquisition, alignment problems, especially due to longitudinal finger rotation, are becoming even more important. One way to tackle this problem is capturing the vein structure from different perspectives during enrolment, but cost and complexity of capturing devices increases with the number of involved cameras. In this article, a new method to reduce the number of cameras needed for multi-perspective enrolment is presented. The reduction is achieved by introducing additional pseudo perspectives in-between two adjacent cameras. The obtained perspectives are used for additional comparisons during authentication. This way, the complexity of the enrolment devices can be reduced while keeping the recognition performance at a high level.

Keywords: Finger Vein Recognition, Longitudinal Finger Rotation, Multi-Perspective Enrolment, Perspective Multiplication.

1 Introduction

Vascular pattern based biometric systems, commonly denoted as vein biometrics, offer several advantages over other well-established biometric recognition systems. In particular, hand and finger vein systems have become a serious alternative to fingerprint based ones for several applications. Vein based systems use the structure of the blood vessels inside the human body, which becomes visible under near-infrared (NIR) light. As the vein structure is located inside the human body, it is resistant to abrasion and external influences on the skin. Furthermore, a lifeness detection to detect presentation attacks can be performed easily [KZ12].

The performance of finger vein recognition systems suffers from different internal and external factors. Internal factors include the design and configuration of the sensor itself, especially the NIR light source and the camera module. External factors include environmental conditions (e.g. temperature and humidity) and deformations due to misplacement of the finger, typically including shifts, tilt, bending and longitudinal rotation. Several publications addressed that such finger misplacements cause degradations in the performance of recognition systems: The need for a robust finger vein image normalisation including rotational alignment has already been mentioned by Kumar and Zhou in

[1] Department of Computer Sciences, University of Salzburg, AUSTRIA, {bprommeg, uhl}@cs.sbg.ac.at

2012 [KZ12]. Chen *et al.* [Ch18] state that deformation correction can be done either during pre-processing, feature extraction or comparison. Moreover, the physical design of the sensor, e.g. as proposed by Kauba *et al.* [KPU18], can help to avoid misplacements of the finger. In [PKU18a] the authors showed, that longitudinal finger rotation has a severe influence on the recognition performance of a finger vein recognition system. There are several approaches that try to reduce the influence of these issues during the processing of the vein patterns, e.g. [Ch18, Hu10, KZ12, LLP09, Ma16, Pr19, Ya17]. Prommegger and Uhl [PU19] introduced two methods that make finger vein recognition invariant against longitudinal rotation. Both methods acquire multiple perspectives during enrolment, while actual authentication is done with traditional single-perspective acquisition. The first approach, multi-perspective enrolment (MPE), compares the probe image to all acquired enrolment perspectives, while the second approach, perspective cumulative finger vein templates, generates a single template that contains the vein pattern all around the finger. As finger vein systems evolve towards contact-less operation, problems resulting from finger misplacements, e.g. longitudinal rotation, will receive more attention in the future.

The main contribution of this work is the proposal of a method, perspective multiplication for multi-perspective enrolment (PM-MPE), to reduce the complexity and cost of the capturing device needed for multi-perspective enrolment for finger vein recognition. By combining MPE with the fixed angle method from [Pr19], the number of perspectives needed during enrolment of subjects is effectively reduced while the recognition performance is kept on a high level. The experiments are carried out using the *PLUSVein finger rotation data set* (PLUSVein-FR) [PKU18b]. To show the effectiveness of the proposed approach, its recognition results are compared to the results of original the MPE approach in [PU19].

The reminder of this paper is organized as follows: In section 2 the proposed method for reducing the perspectives acquired during enrolment is described. The experimental set-up together with its results are described in Section 3. Section 4 concludes the paper along with an outlook on future work.

2 Perspective Multiplication for Multi-Perspective Enrolment

MPE, as proposed in [PU19], requires the acquisition of multiple perspectives during enrolment. The angles of the different perspectives are linearly spaced over the desired acquisition range. For authentication, only a single perspective is acquired and compared to all enrolment samples together with a maximum rule score level fusion. If enough cameras are used during enrolment, negative effects of longitudinal finger rotation on the recognition performance can be inhibited. The invariance against longitudinal rotation is achieved by increasing the effort during enrolment (acquiring additional perspectives, feature extraction) and comparison (multi-perspective comparison). Additionally to the acquisition of multiple perspectives also circular pattern normalization (CPN, [PU19]), which essentially corresponds to a rolling of the finger assuming a circular finger shape, is applied.

It has been been shown that rotation compensation can effectively improve the recognition performance, e.g. [Ch18, Hu10, LLP09, Ma16, Pr19, Ya17]. Prommegger *et al.* [Pr19] pro-

posed an approach that rotates the enrolled image by an pre-defined angle and compare the probe sample against all three versions: the original and the two rotated ones. This method improves the range, in which well performing vein pattern based recognition schemes achieve reasonable recognition results, from approximately $\pm 15°$ to nearly $\pm 30°$. Perspective multiplication for multi-perspective enrolment (PM-MPE), which is introduced in this paper, uses this knowledge to reduce the number of perspectives needed for MPE. During enrolment n perspectives with a rotational distance of α are acquired. PM-MPE adds two pseudo perspectives between two adjacent cameras by rotating every perspective with an rotational angle of $\pm\varphi = 1/3\alpha$ in both directions, where α is the rotational distance between two cameras. For authentication, as for traditional single-perspective finger vein recognition schemes, only a single perspective is acquired and compared to all enrolled perspectives and the generated pseudo perspectives. This leads to $3 * n$ comparisons for each authentication attempt. Fig. 1 shows this principle for a distance of 30° between two perspectives. On the left side, the MPE approach is visualized. It needs 12 cameras linearly spaced over the whole circle. On the right side the PM-MPE setup is visualized. It needs only four cameras (solid blue dots) positioned at 0°, 90°, 180° and 270°. The remaining perspectives (red circles) are generated by rotating the acquired finger vein images by a rotation angle of $\varphi = 30°$ in both directions.

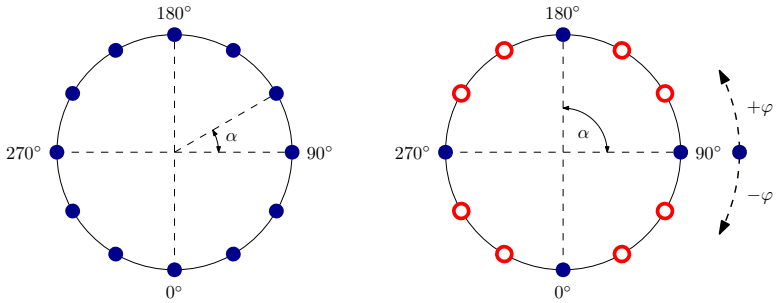

Fig. 1: Camera positioning for MPE (left) and PM-MPE (right) for a rotational distance of 30° between the perspectives. The filled blue dots are cameras, the red circles represent rotated perspectives.

MPE and PM-MPE are evaluated using vein pattern based features in combination with a correlation based comparison where the score is calculated between the input images and in horizontal and vertical direction shifted and rotated versions of the reference image as described in [MNM04]. The number of pixels shifted up and down (vertical shift) during the comparison depends on the angular range acquired during enrolment Θ (when enrolling the whole finger $\Theta = 360°$), the number n of cameras involved and the height h of the extracted ROIs after applying CPN. According to [PU19], a good estimation for the this shift for MPE is

$$S_{\text{MPE}} = 2 \cdot \frac{\Theta}{n \cdot 360} \cdot h \tag{1}$$

The experiments performed in section 3 showed that by introducing pseudo perspectives, the vertical shift during comparison can be reduced by 50% to

$$S_{\text{PM-MPE}} = \frac{\Theta}{n \cdot 360} \cdot h \tag{2}$$

As indicated in [PKU19], a reduction of the shifts during comparison leads to lower scores in general, whereby the reduction of the impostor scores is higher than the one for genuine comparisons. This leads to a better separation of genuine and impostor scores, which in turn results in a better recognition rate.

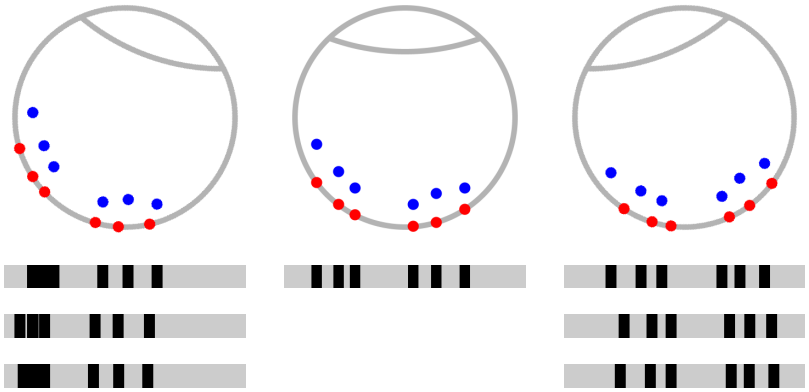

Fig. 2: Principle of pseudo perspective generation. Middle: cross section of a finger acquired during enrolment (top row). The blue points depict the veins inside the finger, the red points the veins projected on the skin surface of the finger. The bar below is the projected vein pattern. Left and right column: pseudo perspectives generated from the enrolment perspective. Top row: rotated versions of the finger ($\varphi = \pm 20°$). Vein patterns: projection generated from the blue veins (top) and the red ones (middle), respectively. The bottom pattern is a shifted version of the blue vein pattern.

As mentioned above, the pseudo perspectives are generated by rotating the enrolment images by a defined angle of $\pm\varphi$. For an accurate rotation of the vein pattern, the position of the veins in the 2D image as well as the shape of the finger and the depth of the veins within the finger has to be known. As this information is not available in general, both need to be estimated. In this work it is assumed that a finger's cross section is approximately a circle (like Matsuda et al. assumed in [Ma16]) and that the imaged veins are located near to the skin surface [Hu10] and therefore can be assumed to be located on the skin surface. Fig. 2 depicts the principle of the generation of the additional perspectives for $\varphi = 20°$. The image in the middle shows a schematic cross section of the finger in its position during enrolment. The blue dots represent the veins within the finger. The bar below is a projection of the vein pattern onto a 2D plain (representing the acquired vein pattern), where the black areas correspond to the veins. Before rotating the image for the perspective generation, the vein pattern is projected back onto the skin of the finger. The resulting vein position are visualized as red dots in the cross section. The left and right columns represent the generated pseudo perspectives, rotated by φ once to the left and once to the right. Since the projected veins (red dots) are located on the surface of the skin,

their position slightly deviates from that of the real veins (blue dots) in their true position after the rotation. As a result, also the vein patterns are slightly different. This deviation is illustrated by means of the vein patterns under the cross-section: the first pattern is the projection of the veins in its real position (blue dots), the second row the one of the rotated veins (red dots), respectively. The visually most noticeable difference between the two patterns is the horizontal shift. If they are aligned according to the highest correlation between them (as it is done with the Miura Matcher [MNM04] and visualized in the bottom row), the result is a high match. Please note that, although this explanation is done using vein patterns (feature space), the generation of the pseudo perspectives for PM-MPE is executed in the image space.

For the calculation of the pseudo perspectives, the position of a pixel within the ROI extracted from the enrolment image is defined by its x-coordinate x_{enrol} and the corresponding y-coordinate y_{enrol}, which is calculated by (3)

$$y_{enrol} = \sqrt{r^2 - x_{enrol}^2} \tag{3}$$

where r is the approximated radius of the finger. r is half the finger width, which corresponds to half of the height of the extracted finger ROI. The rotation for the pseudo perspective is calculated by applying the rotation matrix given in (4).

$$\begin{bmatrix} x_{pseudo} \\ y_{pseudo} \end{bmatrix} = \begin{bmatrix} cos(-\varphi) & -sin(-\varphi) \\ sin(-\varphi) & cos(-\varphi) \end{bmatrix} * \begin{bmatrix} x_{enrol} \\ y_{enrol} \end{bmatrix} \tag{4}$$

x_{pseudo} and y_{pseudo} are the coordinates of the vein pixel in the pseudo perspective and φ is the rotation angle. The actual image for the pseudo perspective is calculated from the grey values at x_{pseudo} using linear interpolation. Fig. 3 shows the ROIs (top row) and extracted MC features (bottom row) of an enrolled image (middle column) and its generated pseudo perspectives (left and right column). The pseudo perspectives are rotated versions of the enrolled image. The part of the pseudo perspectives that contain no information (due to the transform) is filled wit the average grey level of the image.

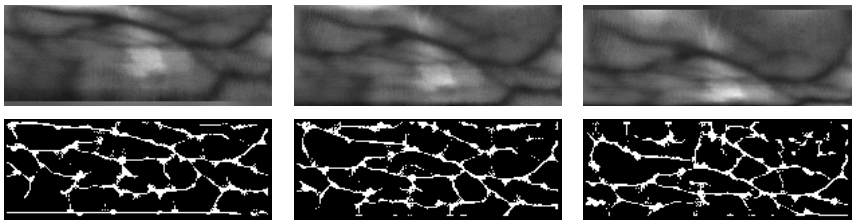

Fig. 3: ROI (top row) and extracted MC features (bottom row) of sample images of the PLUSVein-FR. Middle: enrolment image, left and right: generated pseudo perspectives for $\varphi = \pm 20°$.

3 Experiments

In this section the results of the experiments carried out to evaluate the performance of the proposed PM-MPE approach are described. The method is analysed for different rotational distances between the acquired perspectives ($\alpha = 30°$, 45° and 60°). Its results are compared to the results for MPE without perspective multiplication.

Data Set: The data set in use is the *PLUSVein Finger Rotation Data Set* (PLUSVein-FR). It has been acquired using a custom designed multi-perspective finger vein scanner that acquires finger vein images all around the finger (360°) with a resolution of 1°. It contains finger images captured from 63 different subjects, 4 fingers per subject, which sums up to a total of 252 unique fingers. Each finger is acquired 5 times. This results in 1.260 images per perspective. In this paper a subset containing perspectives in steps of 5°, resulting in 73 different perspectives (0° and 360° are acquired separately), is used. For more details on the data set the interested reader is referred to the authors previous publications [PKU18b, PKU18a].

Recognition Tool Chain: The finger vein recognition tool-chain consists of the following components: (1) For *finger region detection* and *finger alignment* an implementation that is based on [Lu13] is used. (2) The *ROI extraction* differs from [Lu13]: Instead of cutting out a defined rectangle within the finger, similar to [Hu10], a normalization of the finger to a fixed width is applied. (3) To improve the visibility of the vein pattern *Circular Gabor Filter* (CGF) [ZY09] and simple *CLAHE* (local histogram equalisation) [Zu94] are used during *pre-processing*. (4) As *feature extraction* method the well-established vein-pattern based *Maximum Curvature* (MC) method [MNM07] is employed. (5) The *comparison* of the binary feature images is done using a correlation measure, calculated between the input images and in x- and y-direction shifted and rotated versions of the reference image as described in [MNM04]. An implementation of the recognition tool-chain together with the used configurations and results are available for download on `http://wavelab.at/sources/Prommegger19e`.

Experimental Protocol: For the experiments, the data set is split into tow subsets, one for enrolment and one for authentication. The enrolment subset contains two samples, the subset for authentication three samples. To quantify the performance, the EER, the FMR100 (the lowest FNMR for FMR $\leq 1\%$), the FMR1000 (the lowest FNMR for FMR $\leq 0{,}1\%$) as well as the ZeroFMR (the lowest FNMR for FMR = 0%) are used. For the evaluation, the experiments follow the test protocol of the FVC2004 [Ma04]: For calculating the genuine scores, all possible genuine comparisons are performed, which are $63 \cdot 4 \cdot 3 \cdot 2 = 1512$ matches. For calculating the impostor scores, only the first image of a finger is compared against the first image of all other fingers, resulting in $(63 \cdot 4) \cdot (63 \cdot 4 - 1) = 63252$ matches, so together 64764 matches in total.

In order to have a reference for the quantification of MPE and PM-MPE results, the intra-perspective performance (IPP) of all 73 perspectives, without applying any rotation compensation methods and by applying CPN [PU19], is evaluated. For this calculations every perspective is considered as its own data set, which implies, that every perspective is its own independent classical single perspective recognition system where enrolment and probe image are acquired from the same perspective. As a result of this, rotational differences between the samples due to finger misplacement, i.e. longitudinal finger rotation, are subject to the same degradations as presented in [PKU18a]. Although the results of the different perspectives are presented together, they are completely independent from each other. Therefore, no rotational invariance can be concluded from the presentation of the intra-perspective results. As MPE and PM-MPE aim to generate rotation invariant recognition results for a single finger vein image acquired from any perspective during authentication, results close to or even better than the intra-perspective results without rotation correction can be considered as good performance.

Results: The left plot of Fig. 4 depicts the trend of the EER for MPE with rotational distances of $\alpha = 15°$, $30°$, $45°$ and $60°$ and the intra-perspective performance results for applying no correction and CPN are visualized. Here MPE α means that the cameras for enrolment are positioned linearly spaced all around the finger (360°) with a rotational distance of α between two adjacent perspectives. For MPE 15° this results in $^{360}/_{15} = 24$ cameras, for MPE 30° in $^{360}/_{30} = 12$ cameras and so on. The best results for intra-perspective comparisons without rotation correction or applying CPN are obtained in the palmar region (0°) followed by the dorsal region (180°). The perspectives in-between show inferior results, achieving the worst results around 90° and 270°. CPN outperforms the results of no correction over the whole range in average by a factor of 2. MPE 15° and 30° clearly outperform the intra-perspective comparisons without rotation correction. This is reasonable since the PLUSVein-FR data set is, as all finger vein data sets, also subject to finger misplacements, e.g. longitudinal finger rotation, during its acquisition. By applying rotation correction or compensation methods, e.g. CPN, the negative effect on the recognition performance can be reduced. The results for MPE 45° are essentially the same as those of the intra-perspective comparisons without any rotation correction. MPE 60° delivers the worst results. Especially striking is the prominent performance degradation at 90° and 270°. There are two reasons for the bad performance in this regions: (1) As it can be seen from the intra-perspective evaluations, the performance in this region is generally inferior and (2) the distance to the acquired enrolment perspectives reaches its maximum. For MPE 60°, finger vein images are acquired at 0°, 60°, 120°, 180°, 240° and 300°. For 90° and 270° this results in a rotational distance of 30° to the closest enrolment perspective. In [Pr19], the authors showed, that EPN, which is similar to the used CPN, cannot compensate such a high rotation. The simultaneous occurrence of both reasons explain the large performance drop to EERs of up to 20%.

The right plot of Fig. 4 shows the results for PM-MPE with rotational distances of $\alpha = 30°$, $45°$ and $60°$ and the intra-perspective performance results applying no correction and CPN (note the different scaling compared to the MPE plot). α in PM-MPE α is again the rotational distance between two adjacent enrolment cameras. As described in section 2,

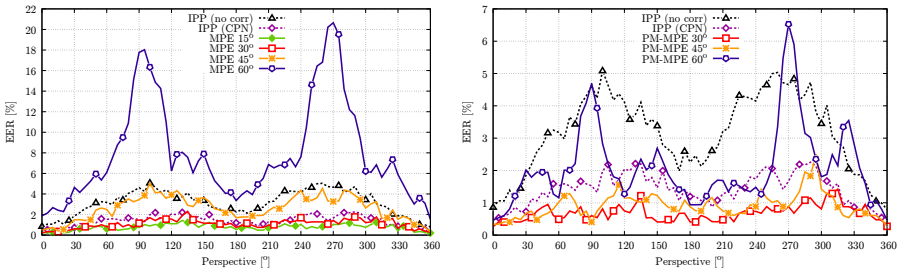

Fig. 4: Performance Results (EER) for MPE (left) and PM-MPE (right).

for PM-MPE the number of perspectives is tripled by generating pseudo perspectives of the acquired enrolment perspectives by rotating them with $\pm\varphi = {}^1\!/_3\alpha$. PM-MPE 30° and PM-MPE 45° outperform the intra-perspective results showing a quite stable performance over the whole range from 0° to 360° with EERs below 2%. PM-MPE 60° exhibits the worst performance of the PM-MPE settings. The shape of the line shows that the performance for the perspectives degrades with the distance to the enrolment perspectives. This leads to a performance degradation around the perspectives that are farthest away from the enrolment perspectives, namely 30°, 90°, 150°, 210°, 270° and 330°. As for MPE 60°, the highest EER values are obtained around 90° and 270°. Except for the regions around 270° and 330°, PM-MPE 60° still outperforms the intra-perspective performance without correction.

Fig. 5 shows the trend of FMR100 and FMR1000 for both MPE and PM-MPE. FMR100 and FMR1000 follow the same trend as the EER in Fig. 4, just at a higher level.

For the comparison of the performance of MPE vs PM-MPE, the results of the two methods are shown side by side in Fig. 6. Each of the three subplots depicts the results for one rotational distance of the enrolment perspectives ($\alpha = 30°, 45°$ and 60°). They contain lines for MPE α, PM-MPE α and MPE (α-15°). Additionally, the results of the intra-perspective analysis without rotation correction and for applying CPN are added as references. One can see, that PM-MPE noticeable improves the robustness against longitudinal finger rotation. Multiplying the acquired enrolment perspectives always leads to an increase of the recognition performance compared to pure MPE with the same α. The experiments showed, that PM-MPE α even achieves recognition rates that are comparable to the ones of MPE with a 15° smaller α.

4 Conclusion

In this article, we introduced a method that effectively reduces the number of perspectives needed to be acquired during enrolment for MPE. The reduction is achieved by generating pseudo perspectives from the enrolled perspectives, captured in a rotational distance of

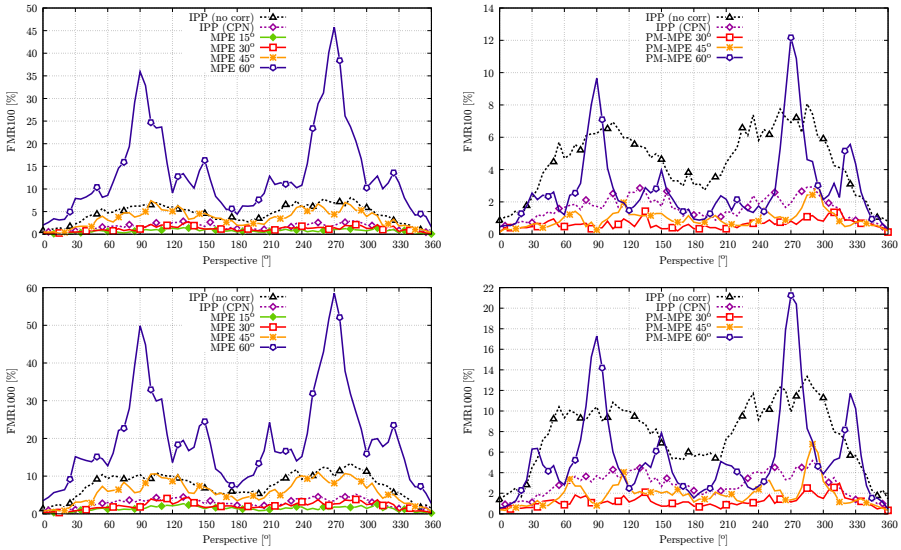

Fig. 5: Performance Results MPE (left) and PM-MPE (right): FMR100 (top) and FMR1000 (bottom).

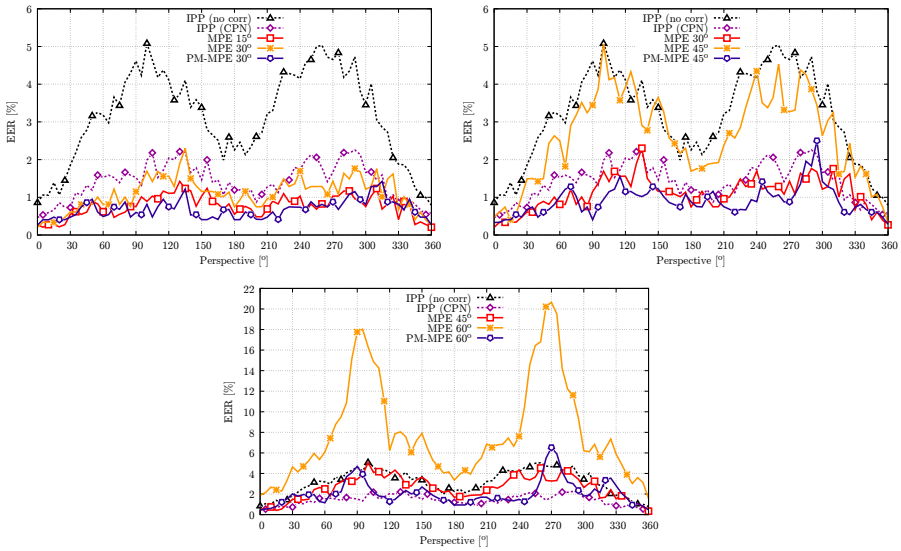

Fig. 6: Performance Results (EER) of MPE vs PM-MPE for a rotational distance of 30° (top-left), 45° (top-right) and 60° (bottom).

α, by rotating them with an angle of $\pm\varphi = 1/3\alpha$. The obtained perspectives are used for additional comparisons during authentication.

The results showed that by applying PM-MPE, the rotational distance α between two enrolment perspectives can be increased by 15° while still getting comparable results. From MPE 15° to PM-MPE 30° this halves the number of cameras from 24 to 12, for 30° from 12 to 8 (reduction of ⅓) and for 45° from 8 to 6 (reduction of ¼), respectively. A rotational distance of $\alpha > 60°$ is neither useful for MPE, nor PM-MPE as currently available finger vein recognition systems are not able to compensate such high rotations. Reducing the number of perspectives acquired during enrolment reduces the cost and complexity of enrolment devices. Using PM-MPE on a limited range of e.g. ±90°, would lead to enrolment devices with 3-4 cameras. Veldhuis *et al.* already presented a device that is capable of simultaneously acquiring 3 perspectives in [Ve19].

In our future work, we aim to further improve the performance (PM-)MPE and reduce the number of perspectives acquired during enrolment. Possible enhancements are a different positioning of the enrolment cameras (e.g. non-linear) or the generation of more than 2 pseudo perspectives between two adjacent enrolment perspectives. We also plan to evaluate MPE and PM-MPE for other recognition schemes than MC.

Acknowledgements

This work was supported in part by the European Union's Horizon 2020 Research and Innovation Program under Grant 700259, and in part by the FFG KIRAS Project AUTFingerATM under Grant 864785.

References

[Ch18] Chen, Qing; Yang, Lu; Yang, Gongping; Yin, Yilong: Geometric shape analysis based finger vein deformation detection and correction. Neurocomputing, 2018.

[Hu10] Huang, Beining; Dai, Yanggang; Li, Rongfeng; Tang, Darun; Li, Wenxin: Finger-vein authentication based on wide line detector and pattern normalization. In: Pattern Recognition (ICPR), 2010 20th International Conference on. IEEE, pp. 1269–1272, 2010.

[KPU18] Kauba, Christof; Prommegger, Bernhard; Uhl, Andreas: The Two Sides of the Finger - An Evaluation on the Recognition Performance of Dorsal vs. Palmar Finger-Veins. In: Proceedings of the International Conference of the Biometrics Special Interest Group (BIOSIG'18). Darmstadt, Germany, 2018.

[KZ12] Kumar, Ajay; Zhou, Yingbo: Human identification using finger images. Image Processing, IEEE Transactions on, 21(4):2228–2244, 2012.

[LLP09] Lee, Eui Chul; Lee, Hyeon Chang; Park, Kang Ryoung: Finger vein recognition using minutia-based alignment and local binary pattern-based feature extraction. International Journal of Imaging Systems and Technology, 19(3):179–186, 2009.

[Lu13] Lu, Yu; Xie, Shan Juan; Yoon, Sook; Yang, Jucheng; Park, Dong Sun: Robust finger vein ROI localization based on flexible segmentation. Sensors, 13(11):14339–14366, 2013.

[Ma04] Maio, Dario; Maltoni, Davide; Cappelli, Raffaele; Wayman, James L.; Jain, Anil K.: FVC2004: Third Fingerprint Verification Competition. In: ICBA. volume 3072 of LNCS. Springer Verlag, pp. 1–7, 2004.

[Ma16] Matsuda, Yusuke; Miura, Naoto; Nagasaka, Akio; Kiyomiu, Harumi; Miyatake, Takafumi: Finger-vein authentication based on deformation-tolerant feature-point matching. Machine Vision and Applications, 27(2):237–250, 2016.

[MNM04] Miura, Naoto; Nagasaka, Akio; Miyatake, Takafumi: Feature extraction of finger-vein patterns based on repeated line tracking and its application to personal identification. Machine Vision and Applications, 15(4):194–203, 2004.

[MNM07] Miura, Naoto; Nagasaka, Akio; Miyatake, Takafumi: Extraction of finger-vein patterns using maximum curvature points in image profiles. IEICE transactions on information and systems, 90(8):1185–1194, 2007.

[PKU18a] Prommegger, Bernhard; Kauba, Christof; Uhl, Andreas: Longitudinal Finger Rotation - Problems and Effects in Finger-Vein Recognition. In: Proceedings of the International Conference of the Biometrics Special Interest Group (BIOSIG'18). Darmstadt, Germany, 2018.

[PKU18b] Prommegger, Bernhard; Kauba, Christof; Uhl, Andreas: Multi-Perspective Finger-Vein Biometrics. In: Proceedings of the IEEE 9th International Conference on Biometrics: Theory, Applications, and Systems (BTAS2018). Los Angeles, California, USA, 2018.

[PKU19] Prommegger, Bernhard; Kauba, Christof; Uhl, Andreas: On the Extent of Longitudinal Finger Rotation in Publicly Available Finger Vein Data Sets. In: Proceedings of the 12th IAPR/IEEE International Conference on Biometrics (ICB'19). Crete, Greece, pp. 1–8, 2019.

[Pr19] Prommegger, Bernhard; Kauba, Christof; Linortner, Michael; Uhl, Andreas: Longitudinal Finger Rotation - Deformation Detection and Correction. IEEE Transactions on Biometrics, Behavior, and Identity Science, 1(2):123–138, 2019.

[PU19] Prommegger, Bernhard; Uhl, Andreas: Rotation Invariant Finger Vein Recognition. In: Proceedings of the IEEE 10th International Conference on Biometrics: Theory, Applications, and Systems (BTAS2019). Tampa, Florida, USA, 2019.

[Ve19] Veldhuis, Raymond; Spreeuwers, Luuk; Ton, Bram; Rozendal, Sjoerd: A high quality finger vein dataset collected using a custom designed capture device. In (Uhl, Andreas; Busch, Christoph; Marcel, Sebastien; Veldhuis, Raymond, eds): Handbook of Vascular Biometrics, chapter 5, p. 13 pages. Springer Science+Business Media, Boston, MA, USA, 2019.

[Ya17] Yang, Lu; Yang, Gongping; Yin, Yilong; Xi, Xiaoming: Finger Vein Recognition with Anatomy Structure Analysis. IEEE Transactions on Circuits and Systems for Video Technology, pp. 1–1, 2017.

[Zu94] Zuiderveld, K.: Contrast Limited Adaptive Histogram Equalization. In (Heckbert, Paul S., ed.): Graphics Gems IV, pp. 474–485. Morgan Kaufmann, 1994.

[ZY09] Zhang, Jing; Yang, Jinfeng: Finger-vein image enhancement based on combination of gray-level grouping and circular Gabor filter. In: Information Engineering and Computer Science, 2009. ICIECS 2009. International Conference on. IEEE, pp. 1–4, 2009.

sensors

MDPI

Article

Combined Fully Contactless Finger and Hand Vein Capturing Device with a Corresponding dataset

Christof Kauba *, Bernhard Prommegger and Andreas Uhl

Department of Computer Sciences, University of Salzburg, Jakob-Haringer-Str. 2, 5020 Salzburg, Austria; bprommeg@cs.sbg.ac.at (B.P.) uhl@cs.sbg.ac.at (A.U.)

* Correspondence: ckauba@cs.sbg.ac.at; Tel.: +43-662-8044-6334

Received: 15 October 2019; Accepted: 13 November 2019; Published: date

check for updates

Abstract: Vascular pattern based biometric recognition is gaining more and more attention, with a trend towards contactless acquisition. An important requirement for conducting research in vascular pattern recognition are available datasets. These datasets can be established using a suitable biometric capturing device. A sophisticated capturing device design is important for good image quality and, furthermore, at a decent recognition rate. We propose a novel contactless capturing device design, including technical details of its individual parts. Our capturing device is suitable for finger and hand vein image acquisition and is able to acquire palmar finger vein images using light transmission as well as palmar hand vein images using reflected light. An experimental evaluation using several well-established vein recognition schemes on a dataset acquired with the proposed capturing device confirms its good image quality and competitive recognition performance. This challenging dataset, which is one of the first publicly available contactless finger and hand vein datasets, is published as well.

Keywords: finger vein recognition; hand vein recognition; contact-less acquisition device; public vascular pattern dataset; biometric recognition performance evaluation

1. Introduction

Biometric authentication is gaining more and more attention and replaces traditional authentication methods like passwords, signatures and tokens. It offers higher security and increased user convenience compared to traditional methods. Biometric authentication techniques are based on so-called biometric traits, which are behavioural or physiological characteristics of a person. These biometric traits are unique to every person. The most commonly used biometric traits include fingerprints, face and iris. Recently, vascular pattern based biometrics, especially hand and finger based vascular patterns (usually denoted as hand and finger vein recognition) have become more popular as well. Since the first commercial contactless palm vein acquisition device from Fujitsu [1] became available in 2003, vascular pattern based biometrics have been employed in several application areas, especially in the banking area [2,3]. Vascular pattern based biometrics have several advantages over, for example, fingerprints [4]. This biometric trait is based on the patterns formed by the blood vessels, located underneath the skin, that is, it is an internal biometric trait. While fingerprints are susceptible to dirt and moisture on the skin, skin damage and abrasion, the vascular patterns are assumed to be insensitive to these skin conditions. Furthermore, vascular pattern based biometrics are more resistant to presentation attacks and forgery than are fingerprints and face [4] as the blood vessels are located beneath the skin and are only visible in near-infrared light.

1.1. Acquisition Principle and Capturing Devices

To render the patterns formed by the blood vessels visible, special acquisition devices are necessary. These devices are usually denoted as biometric scanners or sensors. The haemoglobin contained in the blood, which is flowing through the veins and arteries, has a higher light absorption coefficient in the near-infrared (NIR) wavelength spectrum (between 700 and 950 nm) than the surrounding tissue. Hence, the vascular pattern can be rendered visible by applying an NIR light source and capturing images using an NIR sensitive camera, which resembles the main parts of a finger or hand vein scanner. There are two distinct configurations depending on the relative positioning of the light source and the camera—light transmission and reflected light (see Figure 1 for an illustration). In the reflected light set-up, the camera and the light source are positioned on the same side of the finger/hand, whereas in the light transmission set-up, both are positioned on opposite sides of the finger/hand. A further distinction can be made regarding the side of the finger/hand which is captured—palmar or dorsal. Palmar refers to the bottom side of the finger/hand, while dorsal images are captured from the top side.

In both finger and hand vein recognition, usually the palmar side is utilised. While reflected light is the preferred set-up in hand vein recognition, finger vein scanners mainly capture the images using light transmission or light dispersion [5,6]. These days there are several commercial off-the-shelf (COTS) solutions for hand as well as finger vein recognition available for a wide range of application scenarios, from securing a personal computer over additional authentication at an automated teller machine (ATM) to high security access control systems at industry buildings. However, most of the COTS solutions have one major drawback for academia and research—the COTS scanners do not output the raw vein images. Instead, they only provide a template, encoded in a proprietary format which is defined by the manufacturer. These templates can only be used with the software provided by the manufacturer, hence limiting the use of those devices in research. Thus, research institutions began to construct their own, custom capturing devices for finger and hand vein images.

The main contribution of this work is the design of such a capturing device. We propose a fully contactless, combined finger and hand vein capturing device and the publication of a vascular pattern dataset, acquired with this device. Contactless acquisition devices have several advantages over touch based ones. The main advantage is that contactless devices achieve a higher user acceptability, mainly due to hygienic reasons and easier handling of the devices. Moreover, contactless acquisition preserves the vascular patterns from distortions [4]. On the other hand, contactless acquisition introduces some challenges as well—due to the higher degree of freedom in terms of finger/hand movement, the physical device design as well as the processing of the vascular pattern images has to account for different types of distortions/artefacts resulting from the image acquisition, including longitudinal finger rotation [7], finger bending and tilts as well as all kinds of translations and rotations of the fingers/hand. Besides these types of misplacements, one of the main challenges is to provide a uniform illumination within the whole range of the allowed relative position of the finger/hand to the capturing device. In the following we give an overview of related work on finger as well as hand vein capturing devices.

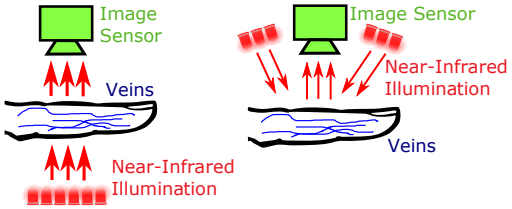

Figure 1. Light source and image sensor positioning, left: light transmission, right: reflected light.

1.2. Related Work

As the proposed capturing device design is a contactless one, we focus on contactless finger and hand vein capturing devices. While contactless acquisition has become common practice in hand vein recognition, the majority of the capturing devices in finger vein recognition are still contact based.

Almost all of the widely employed COTS finger vein capturing devices are contact based ones, capturing the finger from the palmar view using light transmission or light dispersion. The two major companies providing finger vein authentication solutions are Hitachi Ltd. (Tokyo, Japan) and Mofiria Ltd (Tokio, Japan). The most commonly used devices include the Hitachi H-1 USB finger vein scanner [8] and the Mofiria FVA-U3SX [5] as well as the Mofiria FVA-U4ST [6]. As those are commercial products, not many details about their design have been disclosed, except the recognition performance according to the manufacturers' data sheets. Due to the challenges and problems with contactless acquisition, there are only a few contactless finger vein capturing devices proposed in research. One of these devices is a mobile finger vein scanner for Android proposed by Sierro et al. [9]. Their prototype device captures contactless palmar finger vein images using reflected light. The illumination source consists of 12,850 nm LEDs, organised in 3 groups of 4 LEDs each (wide angle VSMG3700 and SFH4059 LEDs), providing global as well as optimised homogeneous illumination compensation. The power of each LED group can be adjusted using the Android software. The camera is a low-cost OV7670 colour one, using a CMOS sensor and a wide angle 2.1 mm lens with a maximum resolution of 640 × 480 pixel. They used an additional NIR pass-through filter with a cut-off wavelength of 740 nm. Another contactless finger vein capturing device was proposed by Kim et al. [10]. This device is based on NIR lasers and uses light transmission. The NIR lasers are manufactured by Lasiris Laser in StokerYale, Canada. A laser line generator lens (E43-475 from Edmund optics in Singapore) with a fixed pan angle is added in order to generate a line laser from the spot laser and should enable a uniform illumination along the finger. The image sensor is a GF 038B NIR CCD (charge coupled device) Camera from ALLIED Vision Technologies, Germany, which is equipped with an additional IR-pass filter. No further details about this device are available, the authors do not even include an image showing their capturing device in the paper. Another contactless device is proposed by Raghavendra et al. [11]. Their low-cost capturing device is able to acquire palmar finger vein images using light transmission as well as fingerprint images in a contactless manner and consists of a NIR light source, a physical structure to achieve a sufficient light intensity, a visible light source and a camera including a lens. The NIR light source is composed of 40 TSDD5210 NIR LEDs with a peak wavelength of 870 nm. The physical structure to achieve a sufficient illumination is wrapped with aluminium foil. The camera is a DMK 22BUC03 monochrome CMOS camera equipped with a T3Z0312CS 8 mm lens. The maximum resolution is 744 × 480 pixel. Even though the device is a contactless one, the images of the capturing device in the paper reveal that the range of motion for the finger is quite limited in every direction (x, y and z) due to the small opening of the device where the finger has to be placed in. None of the above mentioned capturing devices uses a special NIR enhanced camera. Thus, the resulting image quality in combination with an NIR light source is limited. A more recent device was proposed by Matsuda et al. [12]. It is a contactless walk-through style device which allows to capture multiple fingers at once in real time. It consists of an NIR camera and a depth camera, arranged below the finger placing part and an adaptive, multi-light source arranged vertically on the side of the finger placing part. No further technical details about this device are available but there is an official website from Hitachi [13] showing some images of the sensor prototype.

In the early stage of hand vein recognition, most capturing devices used almost closed box devices having a glass plate and some kind of pegs to force the hand to be placed in a defined position [14,15]. The users found this way of providing their biometric inconvenient and thus, the capturing devices developed from semi contactless ones (e.g., only using some hand attachment or guide [16,17] or a glass plate only [18]) to fully contactless ones. The following review of contactless hand vein capturing devices is not exhaustive but shall provide an overview over the major types of different device designs. The most well-known COTS hand vein authentication system is Fujitsu's PalmSecure™ [19]

one. Their capturing device [20] is contactless and small sized: 35 × 35 × 27 mm. There are many non-commercial devices which have been proposed in several research papers as well, for example, the capturing device originally used to acquire the CASIA Multi-Spectral Palmprint Image Database V1.0 [21]. This device captures palmar hand images using six different wavelengths. It is a box with an opening in the front where the data subject has to put the hand inside. The CCD camera is located at the bottom of the device and the LEDs in different wavelength spectra are located around the camera. Sierro et al. [9] also proposed two contactless palm vein capturing device prototypes. Both are using the reflected light set-up and are equipped with ultrasonic sensors to measure the distance between the camera and the hand. The first prototype uses 20,940 nm LEDs (TSAL6400) as a light source and a Sony ICX618 CCD camera in combination with a 920 nm long-pass filter. The second prototype is able to capture multi-spectral images and uses an additional PTFE (Teflon) sheet to achieve a more uniform illumination. Michael et al. [22] proposed a low-cost contactless capturing device. It has one NIR and one visible light camera to capture both, palm vein and palm print images. The NIR camera has a NIR pass-through filter with a cut-off wavelength of 900 nm. The light source consists of 3 rows of 8 NIR LEDs and 3 yellowish light bulbs to capture the palm prints. The light source is covered by a diffusor paper. Zhang et al. [23] presented an approach to match hand veins using 3D point cloud matching. They use a binocular stereoscopic vision device as contactless capturing device. The hand is place above an NIR light source, consisting of 850 nm LEDs. Dorsal hand vein and knuckle shape images are captured by two NIR sensitive CCD cameras in a stereoscopic set-up, both having an additional NIR pass-through filter. Fletcher et al. [24] developed a mobile hand vein biometric system for health patient identification. They proposed two capturing devices; the first one uses an android smart phone in combination with a rechargeable 850 nm LED light source. The second one employs a low-cost webcam (Gearhead WC1100BLU USB) with integrated 940 nm LEDs and an optical filter, which is powered and controlled by an Android tablet. Both acquire contactless palmar hand vein images. Debiasi et al. [25] presented an illumination add-on for mobile hand vein image acquisition. This device can be used in combination with a modified smart phone (NIR blocking filter removed) to acquire contactless hand vein images from the palmar as well as the dorsal side. They also published a dataset containing palmar and dorsal hand vein images in the scope of the PROTECT Multimodal Biometric Database [26].

While most of the above mentioned capturing device designs are based on low-cost modified cameras, our design is based on a special NIR-enhanced industrial camera in combination with an optimal lens and an additional NIR pass-through filter to reduce image distortions and achieve the best possible image quality. Furthermore, in contrast to other existing designs we employ NIR laser modules instead of LEDs which enable a higher range of finger movement without impacting the image quality. Our capturing device is the first of its kind, able to use light transmission as well as reflected light. Moreover, it is the first combined capturing device, able to acquire finger as well as hand vein images. Finally, we do not only present a new capturing device design including all its technical details, but we also publish a corresponding dataset together with image quality and baseline recognition performance evaluation results on that dataset, which makes this work particularly valuable in the field of finger and hand vein recognition.

1.3. Main Contributions

The main contributions of this paper are:

- Design of a novel fully contactless combined finger and hand vein capturing device featuring laser modules instead of NIR LEDs, a special NIR enhanced industrial camera with an additional NIR pass-through filter to achieve the best possible image quality, an optimal lens and distance between the finger/hand and the camera to allow for minimal image distortions as well as an automated illumination control to provide a uniform illumination throughout the finger/hand surface and to arrive at the best possible contrast and image quality.

- Publication of all major technical details of the capturing device design—in this work we describe all the major components of the proposed capturing device design. Further technical details are available on request, which makes it easy to reproduce our design.
- Public finger and hand vein image database established with the proposed capturing device—together with this paper we publish the finger and hand vein datasets acquired with the proposed capturing device. These datasets are publicly available free of charge for research purposes and the finger vein one is the first publicly available contactless finger vein recognition dataset. Due to the nature of contactless acquisition, these datasets are challenging in terms of the different types of the finger/hand misplacements they include.
- Evaluation of the acquired database in terms of image quality and biometric recognition performance—the images acquired with our sensor are evaluated using several image quality assessment schemes. Furthermore, some well-established vein recognition methods implemented in our already open source vein recognition framework are utilised to evaluate the finger and hand vein datasets. This ensures full reproducibility of our published results. The achieved recognition performance during our evaluation is competitive with other state-of-the-art finger and hand vein acquisition devices, validate the advantages of our proposed capturing device design and prove the good image quality and recognition performance of our capturing device.

The remainder of this paper is organised as follows: Section 2 explains our proposed contactless finger and hand vein capturing device design, introduces the dataset acquired with the help of the proposed capturing device and it explains the experimental set-up, including the utilised recognition tool-chain, the evaluation protocol and the processing of the captured vein images. Section 3 lists the evaluation results of both, the acquired finger and hand vein dataset in terms of image quality and recognition accuracy, as well as the recognition accuracy of the considered fusion combinations. A discussion of the evaluation results, including a comparison with recognition performance results achieved by other capturing devices is provided in Section 4. Section 5 concludes this paper and gives an outlook on future work.

2. Materials and Methods

As mentioned in the introduction, a typical finger or hand vein capturing device consists of an NIR sensitive camera and some kind of NIR light source. In the following, the general design of our proposed contactless finger and hand vein capturing device as well as all the individual parts, including technical details and the design decisions are given. Afterwards, the acquired dataset and the utilised biometric recognition tool-chain are described.

2.1. Contactless Finger and Hand Vein Acquisition Device

Figure 2 shows our contactless finger and hand vein capturing device with all its individual parts annotated. It consists of an NIR enhanced camera together with a suitable lens and an additional NIR pass-through filter, two NIR illuminators, one laser module based for light transmission as well as one NIR LED based for reflected light, an illumination control board, a touchscreen display to assist the user during the acquisition process and its metal frame together with the wooden housing parts. All its parts are either standard parts which can be easily bought at a local hardware store or custom designed parts which are either laser cut plywood or 3D printed plastic parts and can easily be reproduced as well. The 3D models and technical drawings of those parts are provided on request. The following list summarises the main advantages and differences of our proposed design over the existing ones presented in Section 1.2.

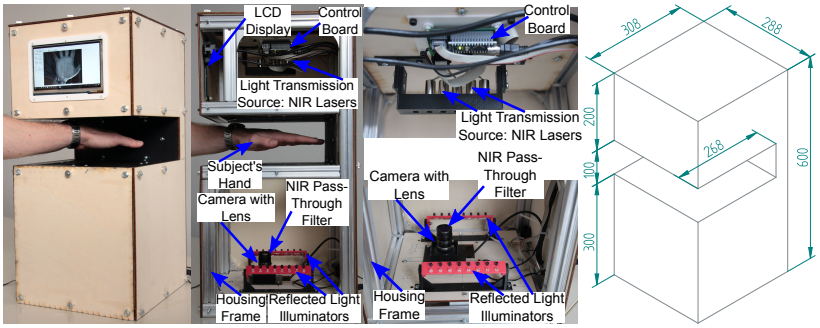

Figure 2. Contactless finger and hand vein capturing device, from left to right: device in use during acquisition, side view with annotated parts, top side view and bottom side detail view, housing including dimensions.

- Reflected light as well as light transmission—it is the first acquisition device of its kind, able to acquire reflected light as well as light transmission images. This extends the range of possible uses of this capturing device and speeds up the acquisition process if both types of illumination set-ups shall be investigated.
- Suitable for finger as well as hand vein images—it is possible to acquire palmar finger as well as hand vein images with the same device. Again, this is the first capturing device able to acquire both using the same device. In the default configuration, finger vein images are captured using light transmission while hand vein images are captured using reflected light but this can be changed in the set-up so there is a high flexibility in terms of possible acquisition configurations.
- NIR laser modules for light transmission illumination—the application of NIR laser modules has not been that common in finger vein recognition so far. In a contactless acquisition set-up, laser modules exhibit several advantages over LEDs, especially if it comes to increased range of finger/hand movement as well as an optimal illumination and image contrast [27]. Hence, we decided to equip our capturing device with NIR laser modules.
- Illumination control board and automated brightness control algorithm—the integrated brightness control board handles the illumination intensity of both, the light transmission and the reflected light illuminators. Each of the laser modules in the light transmission illuminator can be brightness controlled separately and independent from the others. This illumination control in combination with our automated brightness control algorithm enables an optimal image contrast without having the operator do any manual settings.
- Special NIR enhanced industrial camera—our capturing device uses a special NIR enhanced industrial camera. In contrast to modified (NIR blocking filter removed) visible light cameras, those NIR enhanced camera have an increased quantum efficiency in the NIR spectrum. This leads to a higher image contrast and quality compared to cheap, modified visible light cameras.
- Optimal lens set-up and distance between camera and finger/hand—in contrast to many other, mainly smaller devices (in terms of physical size of the device), we decided to use a lens with a focal length of 9 mm. This allows for minimal image distortions all over the image area, especially at the image borders at the cost of an increased distance between the camera and the finger/hand. Hence, our capturing device is rather big compared to others.
- Easy to reproduce design—in contrast to most other proposed capturing devices, for which only very few details are available, we provide references to the data sheets and technical details of all of the capturing device's parts. Furthermore, we provide the 3D models and technical

drawings for the frame parts and the 3D printed parts on request. Hence, it is easy to reproduce our proposed capturing device design.

- Fast data acquisition—due to the automated brightness control and the automated acquisition process, sample data acquisition is fast. Capturing a hand vein image only takes less than a second and capturing a finger vein images takes between 2–4 s once the data subject placed their finger/hand.
- Ease of use during data acquisition—in contrast to other available vein capturing devices, for our proposed device the data subjects do not need to align their fingers/hands with some contact surface or pegs. This is one of the main advantages of our contactless design, making the data acquisition easier for the data subjects as well as for the operators. The automated illumination control algorithm and the intuitive graphical capturing software further contribute to a smooth and easy data acquisition process. Moreover, the integrated touchscreen display assists the data subjects by indicating which finger/hand to place at the sensor, how to place it and indicates potential misplacements.
- Biometric fusion can be employed to increase the recognition performance—our proposed capturing device acquires finger vein images as well as hand vein images using two different wavelengths of illumination. Hence, it is easily possible to increase the recognition performance by applying biometric fusion at sensor level with different fusion combinations. An evaluation of selected combinations is done in Section 3.3.

After this general overview of our capturing device we now describe its individual parts.

2.1.1. Camera, Lens and Filter

The camera is an IDS Imaging UI-ML3240-NIR [28] with a maximum resolution of 1280 × 1024 pixels and a maximum frame rate of 60 fps. It is based on the EV76C661ABT CMOS monochrome image sensor, having a colour depth of 8 bit, a maximum resolution of 1.31 Megapixels, with a pixel size of 5.3 µm and a sensor diagonal of 1/1.84 inches. The main advantage of this camera compared to modified webcams and other visible light cameras is that it is an NIR enhanced industrial camera, which is specifically designed to achieve a high quantum efficiency within the NIR spectrum. Due to its increased NIR sensitivity, an NIR enhanced camera achieves a higher image contrast in the NIR spectrum than a visible wavelength one, which is shown in Figure 3 left, depicting its quantum efficiency chart. The peak wavelengths of our NIR LEDs (850 nm + 950 nm) and NIR laser modules (808 nm) are within the increased sensitivity range of the image sensor.

The camera is equipped with a Fujifilm HF9HA-1B 9 mm fixed focal lens [29]. A lens with an increased focal length has less image distortions but requires a larger distance from the finger, thus increasing the overall size of the scanner. A shorter focal length reduces the minimum distance to the finger but increases the image distortions, especially at the image boundaries. Thus, we decided to use a 9 mm focal length as the best trade-off between the distance to the finger, that is, the overall scanner dimensions and the image distortions introduced due to the lens. A MIDOPT FIL LP780/27 [30] NIR pass-through filter is mounted on top of the lens to further suppress the negative influence of ambient light. The filter transmission chart is depicted in Figure 3 on the right.

2.1.2. Light Sources—Reflected Light and Light Transmission

The capturing device uses two different light sources—a light transmission and a reflected light one. The light transmission illuminator consists of 5 laser diodes [31] including an adjustable constant-current laser diode driver printed circuit board (PCB) [32] and a TO-18 housing with a focus adjustable lens [33] for each of the laser modules (the combination of laser diode + control PCB + housing is denoted as laser module or laser). The laser diodes have a peak wavelength of 808 nm and an optical output power of 300 mW. Each laser module can be brightness controlled separately. The main advantages of the laser modules over LEDs is their higher optical output power and their narrow

radiation half angle. This enables a higher degree of vertical finger movement without degrading the image quality [27].

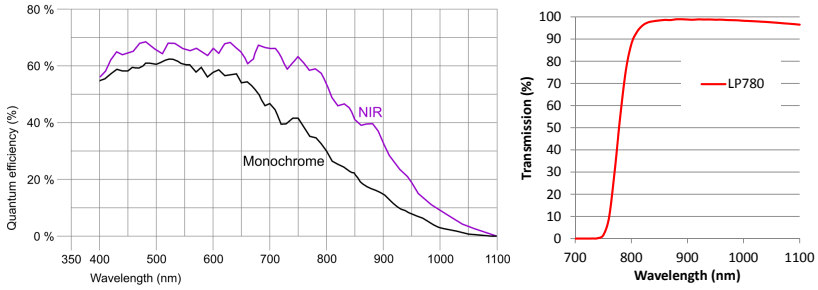

Figure 3. (**Left**) IDS UI-ML-3240-NIR quantum efficiency chart, (**right**) LP780 transmission chart.

The reflected light illuminator consists of 2 individual illuminators, one at each side of the camera (left and right). Each illuminator is composed of two rows of 8 LEDs each. The first row consists of 850 nm LEDs (Osram SFH 4550 [34] with a radiation half angle of ±3° and a max. radiant intensity of 700 mW/sr). The second row consists of 950 nm LEDs (Vishay Semiconductors CQY 99 [35] with a radiation half angle of ±22° and a maximum radiant intensity of 35 mW/sr). These two types of LEDs have peak wavelengths that are within the recommended spectrum for vascular pattern recognition. Each row can be brightness controlled as well, however only the whole row instead of each individual LED can be set to a certain brightness level. The emission spectra of the 850nm LEDs and the NIR laser modules can be seen in Figure 4, left and right, respectively.

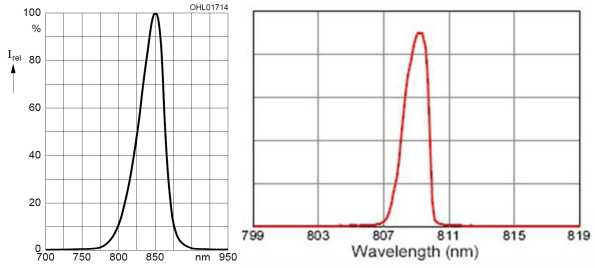

Figure 4. Emission spectrum of the 850nm near infrared (NIR) LEDs (**left**) and the NIR laser modules (**right**), taken from the data sheet [34].

2.1.3. Illumination Control Board and Brightness Control Algorithm

The schematic structure of the control board is depicted in Figure 5. The two main components of the illumination control board are an Arduino Nano board [36] and a Texas Instruments TLC59401 [37]. The Arduino Nano is a complete, breadboard-friendly microcontroller development board based on the Microchip ATmega328P microcontroller [38,39]. The Texas Instruments TLC59401 is an integrated 16-channel LED driver with dot correction and greyscale pulse width modulation (PWM) control enabling a convenient brightness control of LEDs without the need for external components like dropping resistors. Each output can be controlled separately (4096 steps) and has a drive capability of 120 mA. It operates as a constant-current sink and the desired current can be set using one external resistor only. In addition there are external PNP transistors (BC808-25 [40]) to drive the laser modules as

their operating current exceeds the maximum current of the TLC59401. The reflected light illuminators are connected to one of the PWM outputs on the Arduino Nano using some external n-channel MOSFET transistors (AO3418 [41]) to drive them. The whole control board is interfaced using a simple, fixed-length, text-based serial protocol to control each of the individual LEDs/laser modules as well as the reflected light illuminators, to set a whole stripe at once and to turn off all illuminators again. On the PC side there is a graphical user interface based capturing control software which facilitates an easy and straight forward data acquisition. At the moment, the capturing process is initiated manually once the data subject placed their hand/finger in the sensor. This process will be automated in the future as well.

The brightness control algorithm controls each of the single light transmission illuminator's laser modules as well as the reflected light illuminators as a whole. We decided to implement a simple, iterative algorithm based on a comparison against a target grey level, which works as follows—at first the laser centres have to be configured, including the determination of the area of influence for each laser, which is the area in the image a single laser illuminates. Then all lasers are set to an initial intensity level/brightness value which is half of their maximum intensity (I_{max}). The live image of the camera is analysed and the current grey level in the circle of influence of each laser is determined ($GL_{current}$) and compared against the set target grey level (GL_{target}). The new brightness value is then set according to: $I_{n+1} = I_n + I_{corr}$, where I_{n+1} is the new intensity level, I_n is the current intensity level and $I_{corr} = \frac{GL_{target} - GL_{current}}{GL_{max}} \cdot \frac{I_{max}}{2 \cdot n}$, where GL_{max} is the maximum grey value and n is the current iteration. The iteration stops if either the target grey level GL_{target} has been reached or if no more intensity changes are possible. The algorithm finishes in at most $log_2(I_{max})$ iterations. Both, the Arduino Nano firmware as well as the capturing software, including our brightness control algorithm are available on request as well.

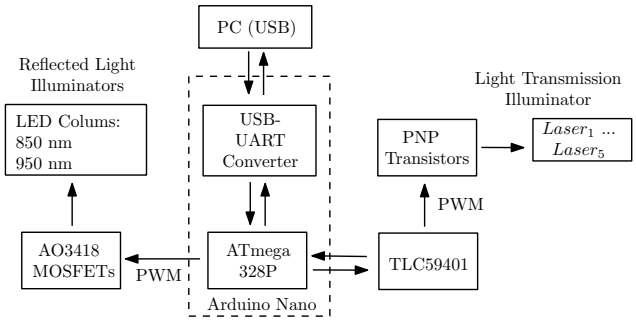

Figure 5. Schematic structure of the illumination control board.

2.1.4. Frame, Housing and Touchscreen

The outer frame is assembled using Coaxis® [42] aluminium profiles. The Coaxis® system is easy to use with several different profiles and connectors, which can be put together in many different ways. Another advantage is that this system provides a good stability and durability. On top of the aluminium frame there are laser cut plywood (4 mm beech wood) boards as side walls/cover. Figure 2 right shows the outside of the housing including its dimensions. A Waveshare 7inch HDMI LCD (C) touchscreen [43] is located the top front part of the capturing device. This touchscreen is connected to the acquisition PC and displays the live image stream from the camera, including an overlay of the optimal finger/hand position in order to help the data subjects in positioning their fingers/hand and also displays other information about the data acquisition, for example, which finger/hand to place next. The next revision of the capturing device will be a fully embedded one, that is, there is no need

for an external PC and the whole data acquisition can be controlled using the device itself with the help of the integrated touchscreen display.

2.2. PLUSVein-Contactless Finger and Hand Vein Data Set

To validate our proposed capturing device design and to show the good recognition performance that can be achieved, we established a data set with the help of this device. Due to the contactless acquisition, these datasets are challenging in terms of finger/hand normalisation to compensate for the different types of finger/hand misplacements contained in the data (tilts, bending, in-planar and non-planar rotations). The dataset will be publicly available for research purposes together with the publication of this paper (http://www.wavelab.at/sources/PLUSVein-Contactless/). It contains two subsets—a palmar finger and a palmar hand vein one, including 42 subjects, 6 fingers/2 hands per subject and 5 images per finger/hand in one session. Hence, the finger vein subset contains 1260 images and the hand vein one contains 840 images (2 illumination configurations, 850 and 950 nm, 420 images each) in total. The raw images have a resolution of 1280 × 1024 pixels and are stored in 8 bit greyscale png format. The visible area of the finger in the images is 600 × 180 pixels and for the hand 750 × 750 pixels on average. Some example images are shown in Figure 6. The age and information about the handedness of the data subjects was recorded as well. Besides this information, no other sensitive private information about the subjects was collected. All subjects gave their informed consent for inclusion before they participated in the study. The study was conducted in accordance with the Declaration of Helsinki, and the protocol was approved by the Ethics Committee of the University of Salzburg (PLUSVein Contactless Data Acquisition 2019).

Figure 6. Example images of the PLUSVein-Contactless finger (**left**) and hand (**right**) vein dataset.

2.3. Finger and Hand Vein Recognition Tool-Chain

The recognition tool-chain includes all steps of a biometric recognition system starting with the extraction of the region of interest (ROI) to pre-processing, feature extraction and comparison, which are depicted in Figure 7 and described in the following. In addition, the utilised image quality assessment methods and biometric fusion, especially score level fusion, are explained as well. All of the utilised methods are implemented within our open source vein recognition framework PLUS OpenVein Toolkit (http://www.wavelab.at/sources/OpenVein-Toolkit/).

ROI Extraction

The key aim of the region of interest (ROI) extraction is to select the best suitable image part for the subsequent feature extraction and to automatically normalise the used finger/hand region in a way to avoid shifts, rotations and to account for scale changes. The ROI extraction and finger/hand normalisation is a crucial step, especially in contactless acquisition, to account for the higher degree of freedom and to compensate the different types of finger/hand misplacements. Different ROI extraction methods have been utilised for finger and hand vein images.

For the finger vein images, the finger is aligned and normalised according to a modified version of the method proposed by Lu et al. [44]. This alignment places the finger in the same position in every image, having the same finger width (different scales due to different finger positions). At first the finger outlines (edge between finger and the background of the image) are detected and the centre line (in the middle of the two finger lines) is determined. Afterwards, the centre line of the finger is rotated and translated in a way that it is placed in the middle of the image and the image region outside of the finger is masked out by setting the pixels to black. Then the finger outline is normalised to a pre-defined width. The final step is the actual extraction of a rectangular ROI of a fixed size (450 × 150 pixels) with its top border located at the fingertip. These steps are visualised in Figure 8.

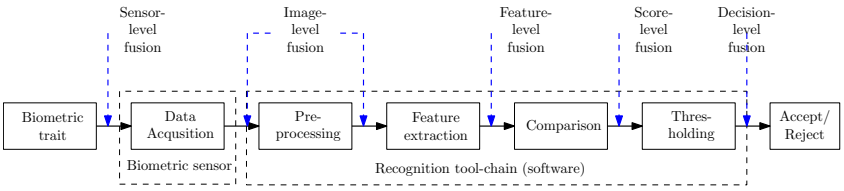

Figure 7. Biometric recognition tool-chain and different levels of biometric fusion.

The ROI method for hand vein images is a modified and extended version of the approach proposed by Zhou and Kumar [45]. At first the hand region is segmented by binarising the image using a local adaptive thresholding technique. Then the local minima and maxima points in the image are found. The local maxima correspond to the finger tips while the local minima correspond to the finger valleys. For the palmar view and the left hand, the second and fourth minima corresponds to the valley between the index and middle finger and the ring and the pinky finger, respectively. A line is fitted between those two valley points and then the image is rotated such that this line becomes horizontal. Afterwards, a square ROI is fitted inside the hand area, with its centre at the centre of mass of the hand (foreground in the segmented image). The size of the square ROI is adjusted such that its size is the maximum square without including any background pixels. The hand ROI extraction steps are shown in Figure 9. As a last step, the ROI image is scaled to a size of 384 × 384 pixels.

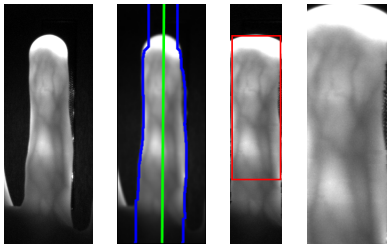

Figure 8. Finger vein region of interest (ROI) extraction process, from left to right: input image, finger outline and centre line detection, finger aligned, masked and normalised ROI boundary, final ROI.

Pre-Processing

Pre-processing approaches try to enhance the low contrast and improve the image quality.

Simple **Contrast Limited Adaptive Histogram Equalisation** (**CLAHE**) [46] or other local histogram equalisation techniques are most prevalent for this purpose. Global contrast equalisation techniques tend to over-amplify bright areas in the image while some other dark areas are not sufficiently enhanced. A localised contrast enhancement technique like CLAHE is a suitable baseline

tool to enhance the vein images as they exhibit unevenly distributed contrast. CLAHE has an integrated contrast limitation (clip limit) which should avoid the amplification of noise.

High Frequency Emphasis Filtering (**HFEF**) [47] tries to enhance the vein images in the frequency domain. At first the discrete Fourier transform of the image is computed, followed by the application of a Butterworth high-pass filter in the frequency domain. Afterwards the inverse Furier transform is computed to give prominence to the vein texture. In order to improve the image contrast the authors also apply a global histogram equalisation as a final step. We applied CLAHE instead of the global histogram equalisation.

Circular Gabor Filter (**CGF**) as proposed by Zhang and Yang [48] is another finger vein image enhancement technique which is rotation invariant and achieves an optimal joint localisation in both the spatial and the frequency domain. The authors originally suggested using grey level grouping for contrast enhancement and to reduce illumination fluctuations. Afterwards an even symmetric circular Gabor filter is applied to further attenuate the vein ridges in the image. Gabor filters are widely used to enhance images containing a high amount of texture and to analyse image texture information. In contrast to usual Gabor filters, a CGF does not have a direction, thus it amplifies the vein ridges in each direction. The bandwidth and the sigma of the CGF has to be tuned according to the visible vein information in the images (vein width in pixels).

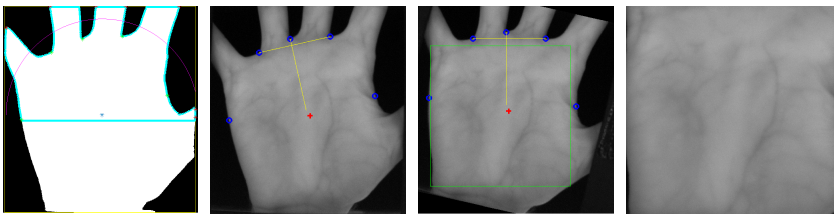

Figure 9. Hand vein ROI extraction process, from left to right: Segmented hand including outline and minima/maxima points, appropriate finger valleys and centre of mass selected, rotationally aligned hand image with maximum possible ROI fitted, final extracted ROI.

Furthermore, the images were resized to half of their original size, which not only speeded up the comparison process but also improved the results. For more details on the preprocessing methods the interested reader is referred to the authors' original publications. Each of the above mentioned pre-processing techniques is at least used for one of the feature extraction methods, but not necessarily with the same parameters for each method. The actual methods and parameters used for each feature extraction method are stated in the settings files (cf. Section 2.4).

Feature Extraction

Three vein pattern based techniques, which aim to extract the vein pattern from the background resulting in a binary image (vein pattern based methods) followed by a comparison of these binary images using a correlation measure and a general purpose key-point based technique were used, which are all algorithms well-established finger vein recognition algorithms.

Maximum Curvature (MC [49]) is a curvature based approach which is insensitive to varying vein widths as it aims to emphasise only the centre lines of the veins. At first the centre positions of the veins are extracted by determining the local maximum curvature in cross-sectional profiles obtained by calculating the first and second derivatives in four directions—horizontal, vertical and the two oblique directions. Each profile is classified as either being concave or convex. Vein lines are indicated by local maxima in concave profiles, hence only the concave ones are used. A score is assigned to each centre position which corresponds to the width and curvature of the maxima region. Afterwards, the centre positions of the veins are connected using a filtering operation in all four directions taking the

8-neighbourhood of pixels into account to account for misclassifications at the first step due to noise and other imperfections in the images. The output feature vector is essentially a binary image which is obtained by thresholding the recorded score values using the median of all scores as a threshold.

Principal Curvature (PC [50]) is another curvature based approach, which is not based on the derivates but on the gradient field of the image. Hence, the first step is the calculation of the gradient field. Hard thresholding to filter out small gradients by setting their values to zero is performed to prevent amplification of small noise components. Afterwards the normalised gradient field is obtained by normalising the magnitude to 1 at each pixel, which is then smoothed by applying a Gaussian filter. The actual principal curvature calculation is then done based on this smoothed normalised gradient field by computing the Eigenvalues of the Hessian matrix at each pixel. The two Eigenvalues are the principal curvatures and the corresponding Eigenvectors of the Hessian matrix represent the directions of the maximum and minimum curvature. The bigger Eigenvalue corresponds to the maximum curvature among all directions and is recorded and further used. The final step is again a threshold-based binarisation of the principal curvature values to obtain the output feature vector which is essentially a binary vein image.

Gabor Filter (GF [4]) is a Gaussian kernel function modulated by a sinusoidal plane wave. Gabor filters are inspired by the human visual system's multichannel processing of visual information. Several 2D even symmetric Gabor filters with different orientations (in $\frac{\pi}{k}$ steps where k is the number of orientations) form a filter bank. The image is filtered using this filter band to extract k different feature vectors. The single feature vectors from the previous step are fused and thresholded to get a resulting feature vector. To remove small noise components, this vector is further post-processed using morphological operations, resulting in the final output feature vector, which is again a binary image.

Scale Invariant Feature Transform (SIFT [51]) is a key-point based technique. In contrast to the three vein pattern based ones, key-point based techniques use information from the most discriminative points as well as consider the neighbourhood and context information around these points. This is achieved by extracting key-point locations at stable and distinct points in the image and then assigning a descriptor to each detected key-point location. The approach we used is based on the general purpose SIFT descriptor in combination with additional key-point filtering along the finger boundaries. This filtering is done to suppress information originating from the finger shape (outside boundary) instead of the vascular pattern. We originally presented this additional key-point filtering in Reference [52].

Comparison

The three vein pattern based features (MC, PC and GF) are compared using an extended version of the approach proposed by Miura et al. [49]. The input features (binary vein images) are not registered to each and only coarsely aligned (by the preceding ROI extraction). To account for small shifts and rotations, the correlations between the input feature vector and in x- and y-direction shifted as well as rotated versions of the reference feature vector are calculated. The final output score is the maximum among those individual correlation values, representing the best possible overlay/match between the two feature vectors. For the SIFT feature vectors a typical approach for key-point based features is utilised. At first the nearest neighbour for each key-point is found by simply calculating the distance between this key-point and all key-points in the reference feature vector. The nearest neighbours/best correspondences is the one with the highest similarity score. If this score is below a set threshold, the key-point does not have a matching one in the reference feature vector. The final comparison score is the ratio of the matched points and the maximum number of detected key-points in both images (which is the maximum number of possible matches).

Vein Specific Image Quality Assessment

In contrast to fingerprint recognition where there are standardised quality metrics like the NIST Fingerprint Image Quality (NFIQ) [53] and the newer version NFIQ 2.0, there are no standardised metrics in finger- and hand-vein recognition yet. Thus, the finger- and hand-vein images were analysed

using GCF [54] as it is a general image contrast metric and hence, independent of the image content. With the help of GCF the image contrast can be quantified exclusively disregarding the actual image content. As we aim to quantify the image quality of vein images, of course two vein specific NIR image quality metrics, namely the approach proposed by Wang et al. [55] (Wang17) and the approach proposed by Ma et al. [56] (HSNR) were included as well. The first approach evaluates the vein image quality fusing a brightness uniformity and a clarity criterion, which is obtained by analysing the local pixel neighbourhoods. The HSNR approach, which is especially tailored for non-contact finger vein recognition, simulates the human visual system by calculating an HSNR index and integrates an effective area index, a finger shifting index and a contrast index to arrive at the final image quality value.

Score Level Fusion

According to the ISO/IEC TR 24722:2015 standard [57], biometric fusion can be regarded as a combination of information from multiple sources, that is, sensors, characteristic types, algorithms, instances or presentations in order to improve the overall system's performance and to increase the systems robustness. Biometric fusion can be categorised according to the level of fusion and the origin of input data. The different levels of fusion correspond to the components of a biometric recognition system—sensor-level, image-level, feature-level, score-level and decision-level fusion, which are indicated in Figure 7. Sensor-level fusion is also called multisensorial fusion and describes using multiple sensors for capturing samples of one biometric instance [57]. This can either be done by the sensor itself or during the biometric processing chain. Hence, we perform sensor-level fusion as our capturing device acquires finger as well as two different kinds of hand vein images. The actual fusion is done during the biometric processing chain at score level (fusing the output scores of the individual modalities—finger veins, hand veins 850nm and hand veins 950nm).

The following combinations of different acquired modalities are evaluated:

1. Hand veins 850 nm + hand veins 950 nm
2. Hand veins 850 nm + finger veins
3. Hand veins 950 nm + finger veins
4. Hand veins 850 nm + hand veins 950 nm + finger veins

Note that, for the combinations including finger veins, only one finger is included in the fusion. We evaluated the combinations including a finger for all fingers of the respective hand and used the best performing finger, which turned out to be the middle finger for both hands. Acquiring images of several, distinct fingers takes more time as only one finger is captured at a time, the same applies to acquiring both hands. Thus, we restricted to the evaluated combinations to the above listed ones which do not considerably increase the acquisition time. The actual score level fusion is performed using the BOSARIS tool-kit [58], which provides a MATLAB based framework for calibrating, fusing and evaluating scores from binary classifiers and has originally been developed for automatic speaker recognition. A 5 fold random split of training and test data with 20 runs was used to train and fuse the scores using BOSARIS. The reported performance results are the average values of the 20 individual runs.

2.4. Experimental Setup and Evaluation Protocol

The evaluation is split into three parts—image quality assessment, baseline recognition performance evaluation for the individual subsets and recognition performance evaluation of the fusion combinations. The image quality assessment and the baseline recognition performance evaluation is done separately for the finger dataset and the two hand vein datasets (850 nm and 950 nm illuminator). The three image quality assessment schemes are evaluated for each individual image per dataset. The results are the average values over the whole dataset, that is, there is a single value for the finger vein and the hand vein 850 nm as well as the hand vein 950 nm dataset for each image quality metric. For the recognition performance DET plots as well as the EER (the point where the FMR equals the

FNMR), the FMR1000 (the lowest FNMR for FMR = 0.1%) and the ZeroFMR (the lowest FNMR for FMR = 0%) are provided. At first the parameters for the pre-processing and feature extraction are optimised on a training dataset. Each dataset is divided into two roughly equal sized subsets, based on the contained subjects, that is, all fingers/hands of the same person are in one subset. The best parameters are determined on each subset and then applied to the other subset for determining the comparison scores. This ensures a full separation of the training and test set. The final results are based on the combined scores of both test runs. The FVC2004 [59] test protocol is applied for calculating the comparison scores in order to determine the FMR/FNMR: for the genuine scores, all possible genuine comparisons are evaluated, resulting in $n_{gen} = \frac{5\cdot(5-1)}{2} \cdot (42 \cdot 6) = 2520$ and $n_{gen} = \frac{5\cdot(5-1)}{2} \cdot (42 \cdot 2) = 840$ genuine scores for the finger and hand vein subset, respectively. For the impostor scores only the first template of a finger/hand is compared against the first template of all other fingers/hands, resulting in $n_{imp} = \frac{(42\cdot6)\cdot(42\cdot6-1)}{2} = 31{,}626$ impostor comparisons for the finger vein subset as well as $n_{imp} = \frac{(42\cdot2)\cdot(42\cdot2-1)}{2} = 3486$ impostor comparisons for the hand vein ones. The EER/FMR1000/ZeroFMR values are given in percentage terms, for example, 0.47 means 0.47%. The full results including the image quality values for each single image, the comparison scores and plots as well as the settings and script files to reproduce the experiments can be downloaded here: http://www.wavelab.at/sources/Kauba19c/.

3. Results

This section presents the results of the image quality assessment as well as the recognition performance evaluation on the acquired datasets and the score level fusion combination of the data sets.

3.1. Image Quality Assessment

Table 1 lists the image quality assessment results for the three tested metrics, namely GCF, Wang17 and HSNR. The GCF values range from 0 to 8, the Wang17 values from 0 to 1 and the HSNR values from 0 to 100. Higher values correspond to higher image quality. Note that a cross-modality comparison (finger vs. hand veins) using those metrics does not lead to meaningful results as the underlying input data (images) are fundamentally different. To enable a meaningful quality assessment and a comparison with other, available finger and hand vein dataset, we evaluated several other finger and hand vein datasets by using the same quality metrics. The evaluated finger vein datasets include SDUMLA-HMT [60], HKPU-FID [4], UTFVP [61], MMCBNU_6000 [44], FV-USM [62] and PLUSVein-FV3 [27]. The image quality was evaluated for the following hand vein datasets—Bosphorus Hand Vein [63], Tecnocampus Hand Image [64], Vera Palm Vein [65] and PROTECT HandVein [66]. The discussion of the image quality assessment results is done in Section 4.

Table 1. Image quality assessment results for the proposed datasets (bold face) and several available finger- and hand vein datasets. Best results per quality metric and modality are highlighted **bold face**.

	dataset	GCF	Wang17	HSNR
Finger Vein	**Finger Vein**	**1.72**	0.256	**92.16**
	SDUMLA-HMT [60]	0.986	0.165	80.32
	HKPU-FID [4]	1.46	0.166	88.13
	UTFVP [61]	1.47	**0.356**	87.15
	MMCBNU_6000 [44]	1.52	0.121	87.39
	FV-USM [62]	0.69	0.136	83.35
	PLUSVein-FV3 [27]	1.48	0.306	89.78
Hand Vein	**Hand Vein 850 nm**	1.42	**0.682**	90.43
	Hand Vein 950 nm	1.87	0.656	**91.76**
	Bosphorus Hand Vein [63]	2.69	0.329	86.12
	Tecnocampus Hand Image [64]	2.31	0.373	54.33
	Vera Palm Vein [65]	1.31	0.43	85.09
	PROTECT HandVein [66]	**2.8**	0.563	82.43

3.2. Recognition Performance

The recognition performance results should serve as a baseline for further experiments/research conducted on these contactless finger and hand vein datasets. Table 2 lists the performance results in terms of EER, FMR1000 and ZeroFMR where the best results per subset (finger vein, hand vein 850 nm and hand vein 950 nm) are highlighted **bold face**. The corresponding DET plots are shown in Figure 10.

It is evident that MC performed best on all subsets in terms of EER, FMR1000 as well as ZeroFMR except for the finger vein one where it performed second best in terms of EER (but still best in terms of FMR1000 and ZeroFMR). The overall best performance was achieved on the hand vein 850 nm subset using MC and resulting in an EER of 0.35%. In terms of EER, on the finger vein subset SIFT performed best, followed by MC and GF while PC performed worst. On the hand vein 850 nm subset, PC performed second best, followed by SIFT and GF performed worst, while on the 950 nm subset SIFT performed second best, followed by PC and again, GF performed worst.

Table 2. Single modality recognition performance results.

Modality		MC	PC	GF	SIFT
Finger Vein	EER [%]	5.61	8.22	6.63	**3.66**
	FMR1000 [%]	**13.12**	23.99	18.39	16.61
	ZeroFMR [%]	**18.75**	42.19	28.76	36.11
Hand Vein 850 nm	EER [%]	**0.35**	0.95	1.55	0.95
	FMR1000 [%]	**0.95**	1.67	2.26	1.9
	ZeroFMR [%]	**1.67**	2.26	2.74	2.74
Hand Vein 950 nm	EER [%]	**0.38**	0.83	0.72	0.82
	FMR1000 [%]	**0.59**	1.43	1.19	1.67
	ZeroFMR [%]	**1.07**	1.67	1.67	2.02

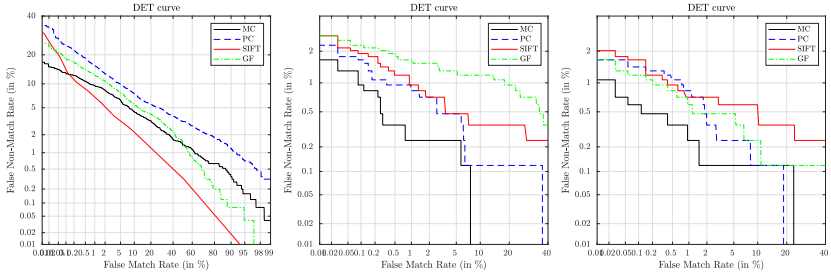

Figure 10. DET plots for finger vein (**left**), hand vein 850 nm (**middle**) and hand vein 950 nm (**right**).

3.3. Biometric Fusion Results

Table 3 shows the results for the tested fusion combination together with the relative performance increase of the combination. The relative performance increase (RPI) refers to the best performing single modality included in the fusion combination (usually the hand vein 850 or hand vein 950 nm result). Each fusion combination improved the results over the respective baseline ones. The overall best results of the tested fusion combinations was the combination of hand vein 850 nm + middle finger achieving an EER of 0.03% which corresponds to a relative performance increase of 1183%. The average improvement in terms of EER (over all feature types) compared to the best baseline (hand veins 850 nm) result for combination 1 is 148%, for combination 2 it is 373%, for combination 3 the average improvement is 140% and for combination 4 it is 365%.

Table 3. Score level fusion recognition performance results and improvement over baseline results. Best EER result (combination 2 for MC, combination 1 for PC, 3 for GF and 4 for SIFT) per feature type is highlighted **bold face**.

Combination			MC	RPI	PC	RPI	GF	RPI	SIFT	RPI
1	Hand 850 Hand 950	EER [%]	0.24	44%	**0.16**	405%	0.60	19%	0.37	123%
		FMR1000 [%]	0.36	162%	0.21	586%	0.77	54%	0.65	155%
		ZeroFMR [%]	0.70	139%	4.90	−66%	0.92	82%	1.49	35%
2	Hand 850 Middle Finger	EER [%]	**0.03**	1183%	0.57	65%	0.64	144%	0.48	98%
		FMR1000 [%]	0.01	7862%	0.97	71%	1.19	90%	0.52	268%
		ZeroFMR [%]	0.14	1112%	1.32	72%	1.70	61%	0.79	246%
3	Hand 950 Middle Finger	EER [%]	0.14	171%	0.37	122%	**0.48**	50%	0.26	218%
		FMR1000 [%]	0.14	333%	0.71	102%	0.74	61%	0.37	352%
		ZeroFMR [%]	0.28	289%	1.28	30%	1.11	51%	2.35	-14%
4	Hand 850 Hand 950 Middle Finger	EER [%]	0.04	849%	0.22	272%	0.57	26%	**0.20**	311%
		FMR1000 [%]	0.00	-	0.36	298%	0.62	91%	0.30	449%
		ZeroFMR [%]	0.17	861%	11.47	-85%	0.74	127%	2.08	-3%

4. Discussion

At first, we discuss the image quality of our datasets in comparison with other publicly available finger- and hand-vein datasets. The evaluation results are listed in Table 1. Considering finger veins, our dataset achieved the best results for GCF and HSNR while it is ranked third for Wang17. These results confirm decent image quality in terms of contrast and also a good image quality in terms of vein specific properties. Considering hand veins our 850 nm data set achieved the best results for Wang17 and the second best ones for HSNR, while the 950 nm dataset achieved the best results for HSNR and second best for Wang17. In terms of GCF, both hand vein data sets are only ranked second and third to last, indicating that the general image contrast is lower than for other datasets. However, the vein specific quality metrics still indicate good image quality, despite the inferior image contrast compared to the other datasets. There are several works in the literature [67–70] that confirm that quality metric results do not necessarily have to correlate with recognition accuracy. The recognition accuracy is the most important aspect of a sensor design and dataset, thus we decided to focus on the recognition accuracy evaluation instead of evaluating only the image quality only. Also note that other data set and sensor papers do not report the image quality, thus a direct comparison is not possible based on the image quality.

In the following, we compare our recognition performance evaluation results to other results reported in the literature. Matsuda et al. [12] reported an EER of 0.19% for their walk through style finger vein recognition system. [11] et al. reported an EER of 1.74% for their systems in case of finger veins only. Kim et al. [10] arrived at an EER of 3.6% for their NIR laser based contactless acquisition set-up. Sierro et al. [9] did not present any performance evaluation of their dataset. None of the mentioned authors disclosed their dataset, so their results are not reproducible. As we aim for reproducibility, all the results listed in Tables 4 and 5 are evaluated on publicly available finger and hand vein datasets and we base our discussion on those results only.

Table 4 lists performance results (in terms of the EER unless indicated otherwise) achieved on various finger vein datasets, ordered by the year of publication, where the last row corresponds to the results presented in this work. The listed results are the best reported ones from the original dataset authors given that they were available and indicated by "-" if they were not available. Note that all of the listed datasets, except the one presented in this work, have been acquired in a non contactless way. Especially compared to the PLUSVein-FV3 dataset, which has been acquired using the same type of NIR enhanced camera and NIR laser modules, the results on our proposed dataset are clearly inferior (5.61% EER vs. 0.06% EER). However, given the increased level of difficulty and challenges of this new, contactless finger vein dataset, the results are still in an acceptable range. The proposed acquisition device design and thus, the acquired dataset, allows for more degrees of

freedom in terms of finger/hand movement and thus, more unrestricted finger/hand positioning. This introduces different kinds of finger/hand misplacements, including tilts, bending, in-planar and non-planar rotations. Prommegger et al. showed, that especially those kinds of misplacements cause severe performance degradations for other publicly available datasets [7,71], especially for the SDUMLA-HMT finger vein dataset [60]. Also note that our results should only serve as a baseline and allow room for further improvements. We did not apply any special kind of finger misplacement corrections. If advanced correction schemes are applied, the results can of course be improved.

Table 4. Performance results of other publicly available finger vein datasets, ordered by publication year, "-" means that this information is not available. The "cla" column indicates contactless acquisition.

Name and Reference	Images/Subjects	cla	Feature Type	Performance (EER)	Year
PKU [72]	50,700/5208	no	WLD [72]	0.87%	2008
THU-FVFDT [73]	6540/610	no	MLD [73]	98.3% ident. rate	2009
SDUMLA-HMT [60]	3816/106	no	Minutia [74]	98.5% recogn. rate	2010
HKPU-FID [4]	6264/156	no	Gabor Filter [4]	0.43% (veins only)	2011
UTFVP [61]	1440/60	no	MC [49]	0.4%	2013
MMCBNU_6000 [44]	6000/100	no	-	-	2013
CFVD [75]	1345/13	-	-	-	2013
FV-USM [62]	5940/123	no	POC and CD [62]	3.05%	2013
VERA FV-Spoof [76,77]	440/110	no	MC [49]	6.2%	2014
PMMDB-FV [26]	240/20	no	MC [49]	9.75%	2017
PLUSVein-FV3 [27]	3600/60	no	MC [49]	0.06%	2018
Contactless FingerVein	840/42	**yes**	MC [49]	3.66%	2019

Regarding contactless hand vein recognition, Michael et al. [22] report an EER of 0.71% using palm veins only. Zhang et al. [23] only evaluate the KC value as measure of the registration between two feature vectors and thus, as an indicator for the recognition performance but they did not evaluate the actual recognition performance. The highest KC value they achieved was 1.1039. Fletcher et al. [24] reported an EER of 6.3% for their fully contactless hand vein based system for health patient identification. Table 5 summarises the achieved recognition performance for several publicly available hand vein recognition datasets, where the last row corresponds to the best results we achieved on our proposed contactless one so far. Note that, except for our proposed dataset and the PROTECT Mobile HandVein [25] dataset, all datasets have been acquired in a non contactless way. In the light of that and taking into account that we used only simple but well-established vein recognition schemes, the achieved recognition performance on our dataset is clearly competitive with other results reported in the literature. It is more than ten times better than the results published for the PROTECT Mobile HandVein [25] dataset and the results published by Fletcher et al. [24], and still twice as good as the results reported by Michael et al. [22], even though the only kind of hand normalisation we applied was the adaptive ROI extraction, correcting different scales, that is, different distances between the camera and the hand. No further tilt or non-planar rotation correction was applied. Again, note that our performance results should only serve as a baseline and can of course be improved.

Table 5. Related performance results of publicly available hand vein recognition datasets, ordered by publication year. The "cla" column indicates contactless acquisition.

Name and Reference	Images/Subjects	cla	Feature Type	Performance (EER)	Year
CIE [18]	2400/50	no	Thresholding [78]	1.1%	2011
Bosphorus Hand Vein [63]	1575/100	no	Geometry [79]	2.25%	2011
CASIA Multispectral [21]	7200/100	no	LBP/LDP [80]	0.09%	2011
Tecnocampus Hand Image [64]	6000/100	no	BDM [64]	98% recogn. rate	2013
Vera Palm Vein [65]	2200/110	no	LBP [81]	3.75%	2015
PROTECT HandVein [66]	2400/40	no	SIFT [51]	0.093%	2018
PROTECT Mobile HandVein [25]	920/31	**yes**	MC [49]	4.13%	2018
Contactless HandVein	420/42	**yes**	MC [49]	0.35%	2019

While the achieved baseline results for the contactless hand vein dataset are quite competitive compared to the contact-based hand vein datasets, the results for the contactless finger vein datasets are clearly inferior to the ones that can be achieved for contact-based finger vein recognition. Contactless finger vein recognition is more challenging than contactless hand vein one for several reason. One reason is that the finger has a much smaller area than the palm of the hand. Thus, small misplacements can lead to a reduced visibility of the vein patterns and a reduced image quality in general, making the recognition more difficult. Moreover, the vascular pattern structure within the finger is more fine-grained than within the palm of the hand. Hence, tilts, rotation and bending of the finger have a more severe effect on the acquired images in terms of the resulting distortions present in the image, again leading to complications during the recognition process. These challenges have to be tackled by suitable normalisation and correction schemes in order to improve the recognition performance for the contactless finger vein data.

The sensor level fusion results clearly indicate that by combining different acquisition modes (finger vein, hand vein 850nm and hand vein 950 nm) the recognition performance can be considerably improved. By combining the hand vein images in the two different wavelengths, the average performance improvement over the best baseline one is 148%. By combining one finger and one hand sample, the best results (MC) are improved by 1183% and 171% over the baseline results for 850 nm and 950 nm hand veins, respectively. By combining all three modes the results were improved as well and are more than 8 times better than the best baseline one (MC). Hence, applying sensor level fusion is an easy way to further enhance the recognition performance of our capturing device.

5. Conclusions

We proposed a new capturing device, which is able to acquire finger as well as hand vein images in a fully contactless way. Contactless acquisition has many advantages in terms of hygiene and user acceptance. In addition to the design and technical details of the acquisition device, we also provide a novel, contactless finger and hand vein dataset available for research purposes (can be downloaded here: http://www.wavelab.at/sources/PLUSVein-Contactless/). This dataset is the first available contactless finger vein dataset and one of the first available contactless hand vein datasets. It is a challenging dataset due to the contactless acquisition allowing for more unrestricted finger/hand movement and the resulting finger/hand misplacements. An image quality assessment using three vein tailored metrics has been conducted and confirmed the decent image quality which can be achieved using our proposed capturing device. Moreover, a recognition performance evaluation using several well-established vein recognition schemes has been carried out on this dataset in order to provide baseline results for further research. Those baseline results are competitive for the hand vein data (EER of 0.35%) and within range of other biometric technologies for the finger vein data (EER of 3.66%). Furthermore, biometric sensor level fusion experiments have been conducted to show the additional improvement in the recognition performance which can be achieved by combining finger vein and hand vein data (resulting in an overall best EER of 0.03%).

Our future work includes some improvements on the capturing device itself. The next version of the device should be an embedded device, eliminating the need for an additional PC to control the acquisition process. The capturing device has a built-in touch screen display already which can be used to control it via the graphical user interface. The only thing which is currently missing is the porting of the capturing software to an embedded platform like the Raspberry Pi and the automated start of the capturing process once the data subjects placed their finger/hand. Furthermore, we will extend our contactless finger and hand vein dataset. We are currently acquiring additional subjects and plan to enlarge the dataset to include a total of at least 100 subjects by the end of 2019. Moreover, we aim to do a thorough analysis on which types of finger/hand misplacements are present in the dataset, similar to the work has been done for other finger vein datasets [71]. Based on this analysis we will be able to apply different correction and normalisation schemes in order to improve the recognition performance.

Author Contributions: Conceptualization, C.K. and B.P.; methodology, C.K.; software, C.K. and B.P.; validation, C.K. and B.P.; formal analysis, C.K.; investigation, C.K. and B.P.; resources, C.K., B.P. and A.U.; data curation, C.K. and B.P.; writing—original draft preparation, C.K.; writing—review and editing, C.K.; visualization, C.K.; supervision, A.U.; project administration, C.K. and A.U.; funding acquisition, A.U.

Funding: This research was funded by European Union's Horizon 2020 research and innovation program under grant agreement number 700259, project PROTECT - Pervasive and UseR Focused BiomeTrics BordEr ProjeCT. This research received further funding by the Austrian Science Fund (FWF) and funding by the Salzburg state government, project no. P32201—Advanced Methods and Applications for Fingervein Recognition. Open Access Funding provided by the Austrian Science Fund (FWF)

Acknowledgments: First of all we really appreciate the spent time and effort of all the participants during our data collection and want to express our gratitude for their voluntary participation. Furthermore, we want to thank our colleagues Michael Linortner and Simon Kirchgasser who helped during the data acquisition. The Open Access Funding was kindly provided by the Austrian Science Fund (FWF).

Conflicts of Interest: The authors declare no conflict of interest. The funders had no role in the design of the study; in the collection, analyses, or interpretation of data; in the writing of the manuscript, or in the decision to publish the results.

Abbreviations

The following abbreviations are used in this manuscript:

ATM	Automated Teller Machine
CCD	Charge Coupled Device
CMOS	Complimentary Metal Oxid Semiconductor
COTS	Commercial Off The Shelf
DET	Detection Error Tradeoff
EER	Equal Error Rate
FMR	False Match Rate
FNMR	False Non Match Rate
LED	Light Emitting Diode
NIR	Near Infrared
PTFE	Polytetrafluoroethylene
PWM	Pulse Width Modulation
ROI	Region Of Interest

References

1. Fujitsu Laboratories Ltd. Fujitsu Develops Technology for World's First Contactless Palm Vein Pattern Biometric Authentication System. Available online: https://www.fujitsu.com/global/about/resources/news/press-releases/2003/0331-05.html (accessed on 6 October 2019).
2. Hitachi-Omron Terminal Solutions, Corp. Taiwan's CTBC Bank Adopts Finger Vein Authentication Solution for ATMs - Hitachi News. Available online: http://www.hitachi-omron-ts.com/news/pdf/201607-001.pdf (accessed on 20 June 2018).

3. Hitachi Group, Corp. Finger Vein Technology for Bank BPH (Poland) - Hitachi Europe News. Available online: http://www.hitachi.eu/en-gb/case-studies/finger-vein-technology-bank-bph-poland (accessed on 20 June 2018).
4. Kumar, A.; Zhou, Y. Human identification using finger images. *Image Process. IEEE Trans.* **2012**, *21*, 2228–2244.
5. Corporation, M. Mofiria FVA-U3SXE Finger Vein Reader Data Sheet. Available online: https://www.mofiria.com/wp/wp-content/uploads/2017/08/FVA-U3SXE.pdf (accessed on 20 June 2018).
6. Corporation, M. Mofiria FVA-U4BT Finger Vein Reader Data Sheet (FVA-U4ST Is the Same Device Except for the USB Instead of Bluetooth Connection). Available online: https://www.mofiria.com/wp/wp-content/uploads/2017/08/FVA-U4BT_E.pdf (accessed on 20 June 2018).
7. Prommegger, B.; Kauba, C.; Linortner, M.; Uhl, A. Longitudinal Finger Rotation - Deformation Detection and Correction. *IEEE Trans. Biom. Behav. Identity Sci.* **2019**; pp. 1–17, doi:10.1109/TBIOM.2019.2902020.
8. Corporation, H. Hitachi H-1 Finger-Vein Scanner Product Page. Available online: http://www.hitachi.co.jp/products/it/veinid/global/products/embedded_devices_u.html (accessed on 20 June 2018).
9. Sierro, A.; Ferrez, P.; Roduit, P. Contact-less palm/finger vein biometrics. In Proceedings of the 2015 International Conference of the Biometrics Special Interest Group (BIOSIG), Darmstadt, Germany, 9–11 September 2015; pp. 1–12.
10. Kim, J.; Kong, H.J.; Park, S.; Noh, S.; Lee, S.R.; Kim, T.; Kim, H.C. Non-contact finger vein acquisition system using NIR laser. *Proc. SPIE* **2009**, *7249*, doi:10.1117/12.810563.
11. Raghavendra, R.; Raja, K.B.; Surbiryala, J.; Busch, C. A low-cost multimodal biometric sensor to capture finger vein and fingerprint. In Proceedings of the 2014 IEEE International Joint Conference on Biometrics (IJCB), Clearwater, FL, USA, 29 September–2 October 2014; pp. 1–7.
12. Matsuda, Y.; Miura, N.; Nonomura, Y.; Nagasaka, A.; Miyatake, T. Walkthrough-style multi-finger vein authentication. In Proceedings of the 2017 IEEE International Conference on Consumer Electronics (ICCE), Las Vegas, NV, USA, 8–10 January 2017; pp. 438–441.
13. Hitachi Group, Corp. Making Society Safe and Convenient with High-Precision Walkthrough Finger Vein Authentication. Available online: https://www.hitachi.com/rd/portal/contents/story/fingervein/index.html (accessed on 6 October 2019).
14. Zhang, D.; Kong, W.K.; You, J.; Wong, M. Online palmprint identification. *IEEE Trans. Pattern Anal. Mach. Intell.* **2003**, *25*, 1041–1050.
15. Zhang, Y.B.; Li, Q.; You, J.; Bhattacharya, P. Palm vein extraction and matching for personal authentication. In Proceedings of the International Conference on Advances in Visual Information Systems, Shanghai, China, 28–29 June 2007; pp. 154–164.
16. Badawi, A.M. Hand Vein Biometric Verification Prototype: A Testing Performance and Patterns Similarity. *IPCV* **2006**, *14*, 3–9.
17. Distler, M.; Jensen, S.; Myrtue, N.G.; Petitimbert, C.; Nasrollahi, K.; Moeslund, T.B. Low-cost hand vein pattern recognition. In Proceedings of the IEEE International Conference on Signal and Information Processing (CSIP), Shanghai, China, 28 October 2011; pp. 1–4.
18. Kabacinski, R.; Kowalski, M. Vein pattern database and benchmark results. *Electron. Lett.* **2011**, *47*, 1127–1128, doi:10.1049/el.2011.1441.
19. Fujitsu Limited. Fujitsu Identity Management and PalmSecure Whitepaper. 2015. Available online: https://www.fujitsu.com/nz/Images/PalmSecure_white_paper-eu-en.pdf (accessed on 6 October 2019).
20. Fujitsu Limited. Fujitsu PalmSecure Datasheet. Available online: https://www.fujitsu.com/global/Images/PalmSecure_Datasheet.pdf (accessed on 6 October 2019).
21. Chinese Academy of Sciences' Institute of Automation (CASIA). CASIA Multispectral Palmprint V1.0. Available online: http://biometrics.idealtest.org/dbDetailForUser.do?id=6 (accessed on 6 October 2019).
22. Michael, G.K.O.; Connie, T.; Teoh, A.B.J. A contactless biometric system using palm print and palm vein features. In *Advanced Biometric Technologies*; IntechOpen: London, UK, 2011.
23. Zhang, Q.; Zhou, Y.; Wang, D.; Hu, X. Personal authentication using hand vein and knuckle shape point cloud matching. In Proceedings of the 2013 IEEE Sixth International Conference on Biometrics: Theory, Applications and Systems (BTAS), Arlington, VA, USA, 29 September–2 October 2013; pp. 1–6, doi:10.1109/BTAS.2013.6712702.

24. Fletcher, R.R.; Raghavan, V.; Zha, R.; Haverkamp, M.; Hibberd, P.L. Development of mobile-based hand vein biometrics for global health patient identification. In Proceedings of the IEEE Global Humanitarian Technology Conference (GHTC 2014), San Jose, CA, USA, 10–13 October 2014; pp. 541–547.
25. Debiasi, L.; Kauba, C.; Prommegger, B.; Uhl, A. Near-Infrared Illumination Add-On for Mobile Hand-Vein Acquisition. In Proceedings of the IEEE 9th International Conference on Biometrics: Theory, Applications, and Systems (BTAS2018), Redondo Beach, CA, USA, 22–25 October 2018; pp. 1–9.
26. University of Reading. PROTECT Multimodal DB Dataset. 2017. Available online: http://projectprotect.eu/dataset/ (accessed on 6 October 2019)
27. Kauba, C.; Prommegger, B.; Uhl, A. Focussing the Beam—A New Laser Illumination Based dataset Providing Insights to Finger-Vein Recognition. In Proceedings of the IEEE 9th International Conference on Biometrics: Theory, Applications, and Systems (BTAS2018), Los Angeles, CA, USA, 22–25 October 2018; pp. 1–9.
28. IDS Imaging Development Systems GmbH. UI-ML3240-NIR NIR-Enhanced Industrial Camera Data Sheet. Available online: https://en.ids-imaging.com/IDS/datasheet_pdf.php?sku=AB00442 (accessed on 6 October 2019).
29. Corporation, F. Fujifilm HF9HA-1B Product Page. Available online: http://www.fujifilmusa.com/products/optical_devices/machine-vision/2-3-15/hf9ha-1b/index.html (accessed on 20 June 2018).
30. Corporation, M. MIDOPT LP780 NIR Pass-Through Filter Product Page. Available online: http://midopt.com/filters/lp780/ (accessed on 20 June 2018).
31. Aliexpress. TO-18 300 mW 808 nm NIR Laser Diode Product Page. Available online: https://www.aliexpress.com/item/5Pcs-lot-High-Quality-808nm-300mW-High-Power-Burning-Infrared-Laser-Diode-Lab/32272128336.html?spm=a2g0s.9042311.0.0.27424c4drx8E2d (accessed on 20 June 2018).
32. Aliexpress. Double IC Two Road ACC Circuit Laser Dode Driver Board 650nm 2.8-5v Adjustable Constant Current 0-390mA 780nm 808nm 980nm Laser Product Page. Available online: https://www.aliexpress.com/item/Double-IC-Two-Road-ACC-Circuit-laser-Dode-Driver-Board-650nm-2-8-5v-Adjustable-Constant/32818824875.html?spm=a2g0s.9042311.0.0.27424c4drx8E2d (accessed on 20 June 2018).
33. Aliexpress. 10x Focusable 1230 Metal Housing w Lens for TO-18 5.6mm Laser Diode LD Product Page. Available online: https://www.aliexpress.com/item/10x-Focusable-1230-Metal-Housing-w-Lens-for-TO-18-5-6mm-Laser-Diode-LD/32665828682.html?spm=a2g0s.9042311.0.0.27424c4drx8E2d (accessed on 20 June 2018).
34. Osram Opto Semiconductors AG. Osram SFH-4550 850 nm High Power Infrared LED Data Sheet. Available online: https://dammedia.osram.info/media/resource/hires/osram-dam-5580407/SFH%204550_EN.pdf (accessed on 20 June 2018).
35. Vishay Semiconductors. TSUS540 Series Infrared Emitting Diode, 950 nm, GaAs Data Sheet. Available online: https://www.vishay.com/docs/81056/tsus5400.pdf (accessed on 20 June 2018).
36. Arduino LLC. Arduino Nano Manual. Available online: https://www.arduino.cc/en/uploads/Main/ArduinoNanoManual23.pdf (accessed on 20 June 2018).
37. Texas Instruments Corporation. Texas Instruments TLC59401 16-Channel LED Driver with Dot Correction and Greyscale PWM Control Data Sheet. Available online: http://www.ti.com/lit/ds/sbvs137/sbvs137.pdf (accessed on 20 June 2018).
38. Microchip Corporation. Microchip AVR ATmega328P 8-Bit Microcontroller Product Page. Available online: https://www.microchip.com/wwwproducts/en/ATmega328P (accessed on 20 June 2018).
39. Microchip Corporation. Microchip AVR ATmega328P 8-Bit Microcontroller Full Data Sheet. Available online: http://ww1.microchip.com/downloads/en/DeviceDoc/Atmel-7810-Automotive-Microcontrollers-ATmega328P_Datasheet.pdf (accessed on 20 June 2018).
40. ON Semiconductor. BC808 PNP SMD General Purpose Transistor Data Sheet. Available online: http://www.onsemi.com/pub/Collateral/BC808-25LT1-D.PDF (accessed on 20 June 2018).
41. Alpha&Omega Semiconductor. AO3418 30V N-Channel MOSFET SMD Data Sheet. Available online: http://aosmd.com/pdfs/datasheet/AO3418.pdf (accessed on 20 June 2018).
42. alfer aluminium GmbH. Combitech Coaxis Online Product Catalog. Available online: https://products.alfer.com/out/media/97010.pdf (accessed on 6 October 2019).
43. Waveshare. Waveshare 7inch HDMI LCD (C) Wiki Page. Available online: http://www.waveshare.net/wiki/7inch_HDMI_LCD_(C) (accessed on 6 October 2019).

44. Lu, Y.; Xie, S.J.; Yoon, S.; Wang, Z.; Park, D.S. An available database for the research of finger vein recognition. In Proceedings of the 2013 6th International Congress on Image and Signal Processing (CISP), Hangzhou, China, 16–18 December 2013; Volume 1, pp. 410–415.
45. Zhou, Y.; Kumar, A. Human identification using palm-vein images. *IEEE Trans. Inf. Forensics Secur.* **2011**, *6*, 1259–1274.
46. Zuiderveld, K. Contrast Limited Adaptive Histogram Equalization. In *Graphics Gems IV*; Heckbert, P.S., Ed.; Morgan Kaufmann: Burlington, MA, USA, 1994; pp. 474–485.
47. Zhao, J.; Tian, H.; Xu, W.; Li, X. A New Approach to Hand Vein Image Enhancement. In Proceedings of the Second International Conference on Intelligent Computation Technology and Automation, ICICTA'09, Zhangjiajie, China, 10–11 October 2009; Volume 1, pp. 499–501.
48. Zhang, J.; Yang, J. Finger-vein image enhancement based on combination of gray-level grouping and circular Gabor filter. In Proceedings of the International Conference on Information Engineering and Computer Science, Wuhan, China, 19–20 December 2009; pp. 1–4.
49. Miura, N.; Nagasaka, A.; Miyatake, T. Extraction of finger-vein patterns using maximum curvature points in image profiles. *IEICE Trans. Inf. Syst.* **2007**, *90*, 1185–1194.
50. Choi, J.H.; Song, W.; Kim, T.; Lee, S.R.; Kim, H.C. Finger vein extraction using gradient normalization and principal curvature. *Proc. SPIE* **2009**, *7251*, 9, doi:10.1117/12.810458.
51. Lowe, D.G. Object recognition from local scale-invariant features. In Proceedings of the Seventh IEEE International Conference on Computer Vision (CVPR'99), Kerkyra, Greece, 20–27 September 1999; Volume 2, pp. 1150–1157.
52. Kauba, C.; Reissig, J.; Uhl, A. Pre-processing cascades and fusion in finger vein recognition. In Proceedings of the International Conference of the Biometrics Special Interest Group (BIOSIG'14), Darmstadt, Germany, 10–12 September 2014.
53. Tabassi, E.; Wilson, C.; Watson, C. Nist fingerprint image quality. *NIST Res. Rep. NISTIR7151* **2004**, *5*.
54. Matkovic, K.; Neumann, L.; Neumann, A.; Psik, T.; Purgathofer, W. Global Contrast Factor-a New Approach to Image Contrast. *Comput. Aesthet.* **2005**, *2005*, 159–168.
55. Wang, C.; Zeng, X.; Sun, X.; Dong, W.; Zhu, Z. Quality assessment on near infrared palm vein image. In Proceedings of the 2017 32nd Youth Academic Annual Conference of Chinese Association of Automation (YAC), Hefei, China, 19–21 May 2017; pp. 1127–1130.
56. Ma, H.; Cui, F.P.; Oluwatoyin, P. A Non-Contact Finger Vein Image Quality Assessment Method. *Appl. Mech. Mater.* **2013**, *239*, 986–989.
57. ISO/IEC JTC 1/SC 37 . Information Technology – Biometrics – Multimodal and Other Multibiometric Fusion. *ISO/IEC TR 24722:2015*, **2015**.
58. Brümmer, N.; de Villiers, E. The BOSARIS toolkit. *arXiv* **2013**, arXiv:1304.2865.
59. Maio, D.; Maltoni, D.; Cappelli, R.; Wayman, J.L.; Jain, A.K. *FVC2004: Third Fingerprint Verification Competition*; Springer: Berlin/Heidelberg, Germany, 2004; Volume 3072, pp. 1–7.
60. Yin, Y.; Liu, L.; Sun, X. SDUMLA-HMT: A multimodal biometric database. In *Biometric Recognition*; Springer: Berlin/Heidelberg, Germany, 2011; pp. 260–268.
61. Ton, B.; Veldhuis, R. A high quality finger vascular pattern dataset collected using a custom designed capturing device. In Proceedings of the International Conference on Biometrics, ICB 2013, Madrid, Spain, 4–7 June 2013.
62. Asaari, M.S.M.; Suandi, S.A.; Rosdi, B.A. Fusion of band limited phase only correlation and width centroid contour distance for finger based biometrics. *Expert Syst. Appl.* **2014**, *41*, 3367–3382.
63. Bogazici University. Bosphorus Hand Database. Available online: http://bosphorus.ee.boun.edu.tr/hand/Home.aspx (accessed on 6 October 2019).
64. Faundez-Zanuy, M.; Mekyska, J.; Font-Aragonès, X. A new hand image database simultaneously acquired in visible, near-infrared and thermal spectrums. *Cogn. Comput.* **2014**, *6*, 230–240.
65. Tome, P.; Marcel, S. On the Vulnerability of Palm Vein Recognition to Spoofing Attacks. In Proceedings of the 8th IAPR International Conference on Biometrics (ICB), New Delhi, India, 29 March–1 April 2015.
66. Kauba, C.; Uhl, A. Shedding Light on the Veins - Reflected Light or Transillumination in Hand-Vein Recognition. In Proceedings of the 11th IAPR/IEEE International Conference on Biometrics (ICB'18), Gold Coast, Australia, 20–23 February 2018; pp.1– 8.

67. Li, G.; Yang, B.; Busch, C. Autocorrelation and dct based quality metrics for fingerprint samples generated by smartphones. In Proceedings of the 2013 18th International Conference on Digital Signal Processing (DSP), Fira, Greece, 1–3 July 2013; pp. 1–5.
68. Yang, B.; Li, G.; Busch, C. Qualifying fingerprint samples captured by smartphone cameras. In Proceedings of the 2013 IEEE International Conference on Image Processing, Melbourne, Australia, 15–18 September 2013; pp. 4161–4165.
69. Hämmerle-Uhl, J.; Pober, M.; Uhl, A. Systematic evaluation methodology for fingerprint-image quality assessment techniques. In Proceedings of the 2014 37th International Convention on Information and Communication Technology, Electronics and Microelectronics (MIPRO), Opatija, Croatia, 26–30 May 2014; pp. 1315–1319.
70. Hämmerle-Uhl, J.; Pober, M.; Uhl, A. General purpose bivariate quality-metrics for fingerprint-image assessment revisited. In Proceedings of the 2014 IEEE International Conference on Image Processing (ICIP), Paris, France, 27–30 October 2014; pp. 4957–4961.
71. Prommegger, B.; Kauba, C.; Uhl, A. On the Extent of Longitudinal Finger Rotation in Publicly Available Finger Vein datasets. In Proceedings of the 12th IAPR/IEEE International Conference on Biometrics (ICB'19), Crete, Greece, 4–7 June, 2019; pp. 1–8.
72. Huang, B.; Dai, Y.; Li, R.; Tang, D.; Li, W. Finger-vein authentication based on wide line detector and pattern normalization. In Proceedings of the 2010 20th International Conference on Pattern Recognition (ICPR), Istanbul, Turkey, 23–26 August 2010; pp. 1269–1272.
73. Yang, W.; Yu, X.; Liao, Q. Personal authentication using finger vein pattern and finger-dorsa texture fusion. In Proceedings of the 17th ACM international conference on Multimedia, Beijing, China, 19–24 October 2009; pp. 905–908.
74. Ong, T.S.; Teng, J.H.; Muthu, K.S.; Teoh, A.B.J. Multi-instance finger vein recognition using minutiae matching. In Proceedings of the 2013 6th International Congress on Image and Signal Processing (CISP), Hangzhou, China, 16–18 December 2013; Volume 3, pp. 1730–1735, doi:10.1109/CISP.2013.6743955.
75. Zhang, C.; Li, X.; Liu, Z.; Zhao, Q.; Xu, H.; Su, F. The CFVD reflection-type finger-vein image database with evaluation baseline. In *Biometric Recognition*; Springer: Berlin/Heidelberg, Germany, 2013; pp. 282–287.
76. Tome, P.; Vanoni, M.; Marcel, S. On the Vulnerability of Finger Vein Recognition to Spoofing. In Proceedings of the IEEE International Conference of the Biometrics Special Interest Group (BIOSIG), Darmstadt, Germany, 10–12 September 2014.
77. Vanoni, M.; Tome, P.; El Shafey, L.; Marcel, S. Cross-database evaluation using an open finger vein sensor. In Proceedings of the 2014 IEEE Workshop on Biometric Measurements and Systems for Security and Medical Applications (BIOMS) Proceedings, Rome, Italy, 17 October 2014; pp. 30–35.
78. Shahin, M.; Badawi, A.; Kamel, M. Biometric authentication using fast correlation of near infrared hand vein patterns. *Int. J. Biol. Med Sci.* **2007**, *2*, 141–148.
79. Yuksel, A.; Akarun, L.; Sankur, B. Hand vein biometry based on geometry and appearance methods. *IET Comput. Vis.* **2011**, *5*, 398–406.
80. Mirmohamadsadeghi, L.; Drygajlo, A. Palm vein recognition with local binary patterns and local derivative patterns. In Proceedings of the 2011 International Joint Conference on Biometrics (IJCB), Washington, DC, USA, 11–13 October 2011; pp. 1–6.
81. Mirmohamadsadeghi, L.; Drygajlo, A. Palm vein recognition with local texture patterns. *Iet Biom.* **2014**, *3*, 198–206.

Chapter 3
OpenVein—An Open-Source Modular Multipurpose Finger Vein Scanner Design

Christof Kauba, Bernhard Prommegger and Andreas Uhl

Abstract One of the main prerequisites in finger vein research is the availability of comprehensive, available finger vein datasets. In order to capture such datasets, a biometric scanner device tailored to capture the vascular patterns is essential. A sophisticated scanner design is the key to achieve a good image quality, robustness against external influences and finally to arrive at a competitive recognition performance. In this chapter, a fully open-source, modular and multipurpose finger vein scanner design is proposed. Two novel finger vein scanners are derived from this basic design. Both are able to capture reflected light and light transmission illuminated images from the dorsal as well as the palmar side. Three fingers are captured at once. The first scanner is based on widely used near-infrared LEDs as its light source, the second one on near-infrared laser modules. Despite their advantages in touchless operation, near-infrared laser modules have hardly been used in finger vein recognition so far. Our scanner design has proven to accomplish an excellent recognition performance using common finger vein recognition schemes. All details regarding the two scanner devices, including technical drawings of all parts, models of the 3D printed parts, control board schematics, the microcontroller firmware, the capturing software, parts list as well as assembly and setup instructions, are available free of charge for research purposes. This should facilitate interested researchers to rebuild such a scanner device for capturing finger vein data on their own.

Keywords Finger vein scanner · Open-source biometric sensor device · Light transmission · Reflected light · Open finger vein dataset · Dorsal · Palmar · Scanner assembly details

C. Kauba ( ) · B. Prommegger · A. Uhl
Department of Computer Sciences, University of Salzburg, Jakob-Haringer-Str. 2, 5020 Salzburg, Austria
e-mail: ckauba@cs.sbg.ac.at

B. Prommegger
e-mail: bprommeg@cs.sbg.ac.at

A. Uhl
e-mail: uhl@cs.sbg.ac.at

A. Uhl et al. (eds.), *Handbook of Vascular Biometrics*, Advances in Computer Vision and Pattern Recognition, https://doi.org/10.1007/978-3-030-27731-4_3

3.1 Introduction

Vascular pattern based biometrics, as a new and emerging biometric trait, deals with the patterns formed by the blood vessels located inside the human body, i.e. it is an internal biometric trait. These vascular patterns are not visible to the naked eye, thus a specifically designed capturing device, usually denoted as biometric scanner or biometric sensor, is necessary to sample this biometric [16]. The haemoglobin contained in the blood flowing through the vessels has a higher light absorption coefficient within the near-infrared (NIR) spectrum than the surrounding tissue. Hence, the vascular patterns can be rendered visible as dark lines in the captured images with the help of NIR illumination and NIR-sensitive cameras but not by using commodity off-the-shelf digital cameras as they usually have a built-in NIR blocking filter. The most common body parts considered include fingers [7, 27, 28, 32, 39], hands [6, 8, 36, 37, 42] and also wrists [21]. In the following, we will focus on the recognition of vascular patterns inside the human fingers, commonly denoted as finger vein recognition.

Finger vein scanner devices are already equipped in commercial products, like automated teller machines (ATMs) in Japan [10], for authentication of bank customers in Poland [9], for securing online banking transactions at home in the UK [29] and as an alternative to fingerprint-based authentication systems in general. Almost all commercial-off-the-shelf (COTS) finger vein scanner devices do not permit access to the captured finger vein images. Instead, they only provide a biometric template, encoded in a proprietary format defined by the manufacturer of the scanner device, which can only be used within the software framework provided by the manufacturer. This situation leads to a vendor lock-in, which is not desired for the operator. Moreover, it makes recognition performance evaluations possible, but these biometric templates do neither allow for the development of biometric template protection and biometric workload reduction schemes (see Chap. 12) nor enable a systematic evaluation of the template's properties in regards to external influences and changes in the vein pattern (robustness evaluation). Hence, these templates and the COTS scanners are only of little use in biometric research.

An important requirement for doing research on any biometric trait is the availability of comprehensive datasets. However, the number of finger vein datasets available to the research community is limited and there is still a lack of large, available finger vein databases. In order to establish a dataset that is of value for research purposes, a finger vein scanner that provides access to the raw vein images is essential. The design of such a scanner device is a crucial point if it comes to image quality, robustness against external influences, user convenience and consequently to a good recognition performance. Only a specifically designed finger vein scanner is able to provide high-quality vein images enabling a competitive recognition performance. The main contribution of this chapter is our proposed design of two open-source, multipurpose finger vein scanners. Both scanners are based on the same modular design. They are one of the first finger vein scanners (besides the scanner proposed by Raghavendra et al. in [26]) that are able to capture three fingers at once in order to speed up the

data acquisition process and to minimise longitudinal pose variations (see [23] for an in-depth discussion of the problems due to longitudinal finger rotation). Both are equipped with a light transmission (also called transillumination) as well as a reflected light illuminator allowing to capture light transmission and reflected light images. Hence, these scanners are the first ones that are able to capture both reflected light and light transmission images. Both scanners capture high-resolution and high-quality finger vein images providing a high recognition performance. Furthermore, both of the mainly used views of the finger, dorsal and palmar, can be captured. The two scanners only differ in the type of transillumination light source: the first scanner utilises NIR light-emitting diodes (LEDs) while the second one is based on NIR laser modules. NIR laser modules are not common in finger vein recognition despite the advantages they offer. They enable an increased range of vertical finger movement while preserving a good image contrast and quality compared to LEDs which is especially important if touchless operation is desired.

Our proposed scanner design is fully open source. All of the housing parts and mounting brackets are either 3D-printed or laser-cut plywood parts and can be reproduced with low expenditure. While this chapter covers all the important design key points and describes each of the scanner parts, all technical details of the scanner together with detailed assembly and setup instructions are available in a public repository. This includes part lists, data sheets of the individual parts, technical drawings of the housing parts, models of the 3D printed parts, the schematics and board layout of the illumination controller, the firmware of the illumination controller and the capturing software. By open sourcing all details of our proposed scanner design, other researchers working in the field of finger vein biometrics can benefit from our design. They can get and/or make all the parts needed to construct a finger vein scanner based on our design, follow the instructions and assemble the scanner on their own which enables them to capture high-quality finger vein images and facilitate their own research. The use of our proposed scanner design and the reproduction of the finger vein scanner itself is free of charge for research purposes. The modular design of the scanner allows to exchange, modify and improve the individual parts easily. With the help of other researchers we are confident that our scanner design will continue to improve over time.

The second advantage that comes with a fully open-source scanner design is the ability to establish a large, publicly available finger vein dataset. We already established a finger vein dataset captured using the two scanners based on our design which is available for research purposes [34]. This dataset confirms the decent recognition performance that can be achieved using a scanner based on our design. For more details, see [12, 13]. Together with other researchers and research institutions, we plan to extend this dataset in order to establish a comprehensive, publicly available finger vein dataset for research purposes. Researchers already owning a scanner based on our design and interested in a collaboration can contribute to the dataset by providing us their captured finger vein samples. Such an extensive, collaborative dataset will stimulate the research on finger vein biometrics. Moreover, large finger vein datasets are vital in order to develop and test finger vein indexing schemes, template protection schemes and runtime efficient identification schemes.

The rest of this chapter is organised as follows: Sect. 3.2 gives an overview on the basic design principles of finger vein scanners, followed by a review of commercial finger vein scanners and related research on finger vein scanners as well as datasets. Section 3.3 discusses all important details and individual parts of our proposed finger vein scanner design. Section 3.4 presents our open finger vein dataset captured using the scanners built according to our design. Section 3.5 concludes this chapter together with an outlook on future work, especially on further improving the scanner design and extending our open finger vein dataset.

3.2 Finger Vein Scanners

Finger vein recognition belongs to vascular pattern based biometrics. As the name suggests, these biometrics are based on the vascular pattern, formed by the blood vessel structure inside the human body. Finger vein recognition deals with the vascular pattern inside the human fingers. This pattern has to be made visible and captured by a suitable biometric scanner device in order to enable biometric recognition. The deoxinated haemoglobin in the blood flowing through the blood vessels absorbs light within the NIR spectrum while the surrounding tissue has a much lower light absorption coefficient within that spectrum. Thus, the vascular pattern can be rendered visible with the help of an NIR light source in combination with an NIR-sensitive image sensor.

Consequently, the most important parts of a finger vein scanner are an NIR light source and an NIR-sensitive image sensor or camera. The NIR light source usually consists of NIR LEDs (light-emitting diodes) with a light emission peak wavelength between 750 and 950 nm. In addition to the NIR camera and the NIR light source, either an NIR pass-through filter or an optically opaque box to reduce the influence of ambient light is beneficial. To assist the capture subject in positioning of the finger, most finger vein scanners contain some kind of finger positioning support or finger guide unless they are meant for fully touchless operation.

3.2.1 Light Source Positioning

Two types of illumination are distinguished, based on the relative positioning of the image sensor, the finger and the illuminator: light transmission, also called transillumination and reflected light. Figure 3.1 shows both variants.

Light transmission: the image sensor and the illuminator are placed on opposite sides of the finger. The light penetrates the skin on the side of the finger next to the illuminator, runs through the finger tissue, where it gets reflected, refracted, dispersed, scattered and absorbed. A fraction of the emitted light emerges on the opposite side of the finger and gets captured by the image sensor. As the light has to travel through the whole finger, higher light intensities are needed compared to reflected light, thus

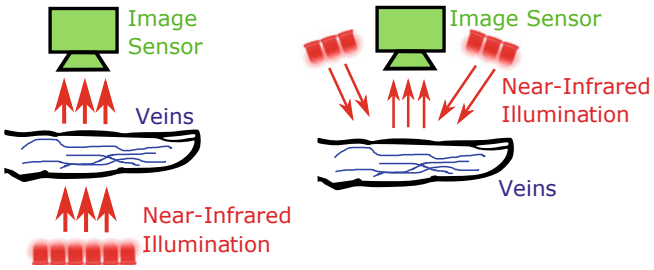

Fig. 3.1 Light source and image sensor positioning, left: light transmission, right: reflected light. Reflected light enables smaller scanner devices while light transmission renders more details of the vascular pattern visible due to the higher penetration depth inside the finger tissue

leading to higher power consumption. Due to the placement of the illuminator and the image sensor opposite to each other, the scanner devices are bigger compared to reflected light ones. Note that the positioning of the image sensor and the illuminator perpendicular to each other (in an angle of 90°) is sometimes called light dispersion. We consider this still as light transmission as it is just a kind of light transmission caused due to scattering and refraction. The light travels sideways through the finger and the fraction of the light which is emitted on the image sensor side of the finger gets captured.

Reflected light: the image sensor and the illuminator are placed on the same side of the finger, either dorsal or palmar. The light originates from the illuminator, a small part gets reflected directly at the finger's surface, the remaining part penetrates the skin and tissue and gets reflected, refracted and scattered there. The fraction of the light emerging at the same side of the finger is captured by the image sensor. Reflected light based scanners need less light intensity. Thus, they have a lower power consumption and can be built in a smaller manner as the light source and image sensor are positioned next to each other. However, the penetration depth of the light is lower than for light transmission, and thus less details of the vascular patterns become visible. Nevertheless, in finger vein recognition, light transmission is used almost exclusively.

3.2.2 Two Main Perspectives of the Finger—Dorsal and Palmar

The main perspectives or views from which the finger is captured are dorsal and palmar (also called ventral). Dorsal images are taken from the back or dorsal side of the hand while palmar images are taken from the palm or bottom side of the hand. Figure 3.2 shows both capturing perspectives. Of course there are several more views around the finger that could be captured like the side views, but finger vein

Fig. 3.2 Two main perspectives on the finger. Left: palmar view, right: dorsal view

recognition mainly deals with palmar images, with some exceptions where the dorsal view is used.

3.2.3 Commercial Finger Vein Scanners

Here we present some common COTS finger vein scanners. As in finger vein recognition, light transmission in combination with palmar images is used almost exclusively, so all COTS scanners are based on this set-up as well (some COTS scanners have the light source and the camera arranged perpendicular to each other which the manufacturers call light dispersion). As motivated in the introduction, the COTS scanners do not provide access to the captured vein images but only output a template encoded in a proprietary format. Figure 3.3 shows some widely used COTS finger vein scanners. The major two companies providing finger vein authentication solutions are Hitachi Ltd. and Mofiria Ltd. Their technologies are patented and non-disclosed. Hence, not many details are known about these scanners, except that they are based on the light transmission principle and capture palmar images. The M2-FingerVein™ reader [52] is basically a rebranded version of the original Hitachi H-1 (or PCT-KCUA011) USB finger vein scanner [51]. According to the M2SYS website, it "scans the inner surface of the finger", is "resistant to criminal temper-

Fig. 3.3 COTS finger vein scanners, from left to right: M2SYS M2-FingerVein™ reader, Mofiria FVA-U4ST, Mofiria FVA-U3SX

ing", achieves a "high accuracy", "less than 0.01% for the FRR, less than 0.0001% for the FAR and 0% for the FTE", uses a "unique and constant" biometric trait and provides "fast authentication speed". However, the scanner design and details are undisclosed making it hard to verify those claims. The scanner provides "fast authentication speed" indeed but especially bearing in mind that this scanner is not able to prevent longitudinal finger rotation [23], the claimed FRR and FAR values are doubtful. Moreover, it has been shown that commercial scanners are susceptible to presentation attacks [30], hence the claim "resistant to criminal tempering" might only refer to tempering with the scanner hardware and authentication software. The Mofiria FVA-U3SX [57] and the FVA-U4ST [58] are based on Mofiria's "unique reflective dispersion method" and an "automatic finger position adjustment ensures both comfortable usability and high accuracy authentication without firmly fixing the finger position on the unit" according to their respective data sheets. Both are small, fast and comfortable USB-powered finger vein scanners that provide two enrolment methods. The FVA-U3SX has an electrostatic sensor to detect the presence of the finger on the scanner. Note the compact size of all the commercial scanners and the semi- or full-open scanner housing. Scanners built in an open manner have been shown to increase the capture subjects' acceptance and convenience.

3.2.4 *Finger Vein Prototype Scanners and Datasets in Research*

Due to the fact that almost all COTS finger vein scanners do not provide access to the raw finger vein images and that the datasets established by the commercial companies are non-disclosed, researchers began to construct their own finger vein scanners and established several finger vein datasets. Table 3.1 gives an overview of several available as well as unpublished finger vein datasets in chronological order. It lists the number of subjects and fingers per subject that were captured, the total number of images contained in the dataset, the number of capturing sessions, the image resolution and the scanner used to capture the images. The first publicly available finger vein dataset was established by the Peking University (PKU) [11] in 2008 using their own prototype scanner (*PKU Proto*). The Seoul National University (SNU) [15] established the first non-contact finger vein dataset in 2009. They built their own touchless prototype scanner (*SNU Proto*). The dataset was captured using two different scanners, an LED and a laser-based one. The Norwegian Biometrics Laboratory collected the GUC45 [5], a multi-modal database comprising finger vein, finger knuckle and fingerprint images using their two prototype scanners (*GUC Proto 1* and *GUC Proto 2*) in 2009. This database is only available semi-publicly, i.e. that visitors at the Norwegian Biometrics Laboratory can access and use the database. The second database established in 2009 is the THU-FVFDT [40] provided by the University of Tsinghua, captured using their self-designed prototype scanner (*Tsinghua Proto*). It contains finger vein as well as finger dorsal texture images. In 2010, the SDUMLA-HMT [41], a multi-modal biometric database including finger

Table 3.1 Finger vein datasets acquired for research purposes

Name	Dors/palm	Avail.	Subjects	Fingers	Images	Sessions	Year	Scanner
PKU [11]	Palmar	Yes	5208	4	50,700	1	2008	PKU Proto
SNU-LP-FV [15]	Palmar	No	10	1	200	1	2009	SNU Proto
GUC45 [5]	Palmar	Semi	45	10	10080	12	2009	GUC Proto 1/2
THU-FVFDT [40]	Palmar	Yes	610	2	6540	2	2009	Tsinghua Proto
SDUMLA-HMT [41]	Palmar	Yes	106	6	3816	1	2010	Wuhan Proto
HKPU-FID [16]	Palmar	Yes	156	4	6264	2	2011	HKPU Proto
KTDeaduk-FV [17]	Palmar	No	30	8	2400	1	2011	KTDeaduk Proto
S-EMB-Laser-FV [18]	Palmar	No	100	6	6000	1	2012	Shandong EL Proto
UTFVP [32]	Palmar	Yes	60	6	1440	2	2013	Twente Proto
MMCBNU_6000 [19]	Palmar	Yes	100	6	6000	1	2013	Chonbuk Proto
CFVD [43]	Palmar	Yes	13	6	1345	2	2013	Shandong Proto
Shandong. Univ [38]	Palmar	No	34	6	4080	2	2013	Wuhan Proto
FV-USM [1]	Palmar	Yes	123	4	5940	2	2013	Sains Proto
VERA FV-Spoof [30]	Palmar	Yes	110	2	440	2	2014	Twente Proto
GUC-FPFV-DB [25]	Palmar	No	41	6*	1500	1	2014	GUC-FPFV Proto
GUC-Dors-FV-DB [24]	Dorsal	Semi	125	4	5000	1	2015	GUC-Dors Proto
PMMDB-FV [33]	Dorsal	Yes	20	4	240	1	2017	PLUSVein-V2
PLUSVein-FV3 [12]	Dorsal	Yes	60	6	3600	1	2018	PLUS OpenVein

vein images, was released by the University of Shandong. They utilised a custom prototype scanner provided by the University of Wuhan (*Wuhan Proto*) during their finger vein data collection. In 2011, the HKPU finger vein database [16] captured using their own prototype scanner (*HKPU Proto*) was released by the Hong Kong Polytechnical University. The KTDeaduk-FV finger vein database [17] was collected by the KT Daeduk Research Center in Korea in cooperation with the Korea Science Academy of KAIST in 2011 too. This database was captured with their own prototype scanner (*KTDeaduk Proto*). It has not been published so far. The Shandong University acquired a finger vein dataset using their prototype embedded finger vein scanner (*Shandong EL Proto*). This dataset has not been published though. In 2013, several finger vein databases have been established. The University of Twente published the UTFVP finger vein database [32], captured with the help of their prototype

scanner (*Twente Proto*). The Chonbuk University in South Korea used their prototype scanner (*Chonbuk Proto*) to establish the MMCBNU_6000 finger vein database [19]. The Shandon University released the CFVD [43], the first reflected light finger vein database acquired using their prototype scanner (*Shandong Proto*). The Shandong University established a second finger vein database [38] using a prototype scanner provided by the University of Wuhan (*Wuhan Proto*) but did not make this database available. The FV-USM database [1] published by the University of Sains in Malaysia was acquired using their custom-designed scanner (*Sains Proto*) and also released in 2013. In 2014, the Idiap Research Institute in Switzerland established the first finger vein spoofing attack database, VERA Finger Vein Spoofing [30] using the same scanner design as it has been used to capture the UTFVP (*Twente Proto*). The Norwegian Biometrics Laboratory designed another finger vein scanner prototype (*GUC-FPFV Proto*), able to capture fingerprint and finger vein images at the same time. In 2014, they captured the GUC-FPFV-DB [25] but they did not make it available * in Table 3.1 indicates that for most but not for all subjects 6 fingers have been captured as there are subjects with less than 6 captured fingers. In 2015, the Norwegian Biometrics Laboratory designed another finger vein scanner which captures dorsal images (*GUC-Dors Proto*) and created the first dorsal finger vein database [24]. Again they did not fully release this database for the research community. It is only semi-public, i.e. available for visitors at the Norwegian Biometrics Laboratory. In 2017, together with our partners from the PROTECT project the team at PLUS (Paris Lodron University of Salzburg) established a multi-modal biometric database PMMDB [33]. Among other biometric traits, this database contains dorsal finger vein images captured with the predecessor of our proposed scanner design (*PLUSVein-V2*), and is publicly available. Our most recent finger vein database is the PLUSVein-FV3 [12], captured using the scanner design presented in this chapter (*PLUS OpenVein*). This database is publicly available as well. Note that except the GUC-Dors-FV-DB [24] established by the Norwegian Biometrics Laboratory, the PMMDB-FV [33] and the PLUSVein-FV3 dataset [12], which have been captured by members of PLUS, all finger vein datasets are palmar ones. Figure 3.4 shows some example images for the available finger vein datasets (except for PKU and CFVD). We will not go into further details about the databases but focus on the corresponding scanner devices in the following.

Table 3.2 gives some details about the scanners that were used to acquire the finger vein databases listed in Table 3.1, including the equipped camera, focal length of the lens (column: lens), additional filter, the illuminator peak wavelength (column: illumin., note that all illuminators except the one of the *SNU Proto,* the *Shandong EL Proto* and the *PLUS OpenVein* are LED based) as well as if the illuminator is a reflected light or light transmission type (column: r/t) as far as the information is available for the respective finger vein scanner device (– in the table indicates that this information is not available). All of the listed finger vein scanners except the *Shandong Proto* and our proposed scanner *PLUS OpenVein* (which is able to use both reflected light as well as light transmission) use light transmission to capture the images. The *PKU Proto* scanner consists of a 1/3-in. greyscale CMOS camera and an advanced illumination control system using an LED-based illuminator. Apart

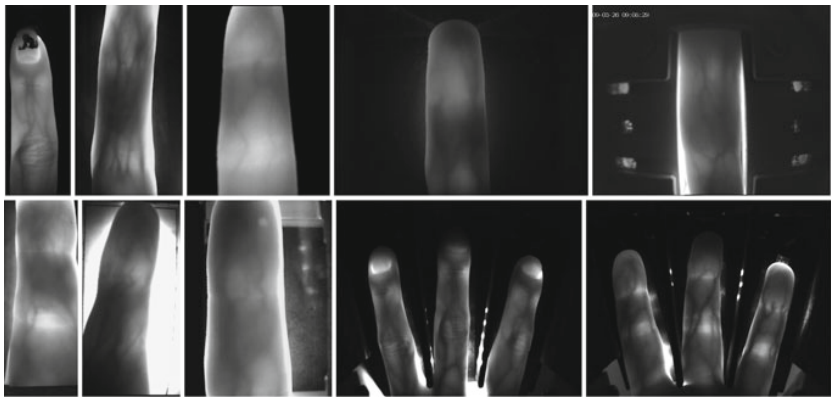

Fig. 3.4 Example images from several available finger vein datasets, left-to-right, top-to-bottom row (all images have been rotated such that the finger is in vertical position pointing upwards): PMMDB-FV, UTFVP, MMCBNU_6000, FV-USM, THU-FVFDT, VERA FV-Spoofing, HKPU-FID, SDUMLA-HMT, PLUSVein-FV3 dorsal, PLUSVein-FV3 palmar

from those details there is no additional information about the camera, the LEDs or the equipped infrared filter available. There are two variants of the touchless scanner prototype developed by the Seoul National University, *SNU Proto*. This touchless scanner should prevent the cross-contamination of skin diseases. The first one is based on conventional 850 nm LEDs as light source, the second one is based on an 830 nm NIR laser. The NIR lasers are manufactured by Lasiris Laser in StokerYale, Canada. A laser line generator lens (E43-475 from Edmund optics in Singapore) with a fixed pan angle is added in order to generate a line laser from the spot laser. This should enable a uniform illumination along the finger. Both scanners are based on light transmission and use a GF 038B NIR CCD Camera from ALLIED Vision Technologies, Germany. The camera is equipped with an additional IR-pass filter. The first two scanner prototypes developed by the Norwegian Biometrics Laboratory in 2009, *GUC Proto* 1 and *GUC Proto* 2 both use a CCD camera in combination with an NIR-pass filter. 850 nm LEDs and 940 nm LEDs are used in the first and second scanners, respectively. Besides this basic information, also the arrangement of the LEDs, their view range and the physical design of the scanners are described in the respective papers. The *Tsinghua Proto* uses two arrays of 890 nm LEDs, one mounted above the top-left and the other one above the top-right of the finger. It has two cameras, one located at the bottom of the device (below the finger), equipped with an IR filter with a cut-off wavelength of 1000 nm to capture the finger vein images and another camera situated on the top of the device (above the finger) to capture the dorsal texture images. The *Wuhan Proto* scanner is based on a near-infrared CCD camera including an additional NIR-pass filter with a wavelength of 900 nm. The light source consists of 790 nm LEDs. The scanner device has a groove in the shell of the device used to guide the finger's orientation. No detailed information about the camera and the illumination control is available. The *HKU Proto* scanner

Table 3.2 Finger vein scanners that were used to acquire the datasets in Table 3.1—means that the information was not available

Name	Camera	Resolution	Lens (mm)	Filter	Illumin.	r/t
PKU Proto	1/3–in. CMOS cam	512 × 384	–	IR filter	–	t
SNU Proto	GF 038B NIR, AVT	768 × 492	–	IR-pass filter	830/850	t
GUC Proto 1	CCD camera	512 × 240	–	NIR-pass filter	850 nm	t
GUC Proto 2	CCD camera	512 × 240	–	NIR-pass filter	940 nm	t
Tsinghua Proto	industrial camera	720 × 576	–	IR filter 1000 nm	890 nm	t
Wuhan Proto	NIR CCD camera	320 × 240	–	NIR-pass 900 nm	790 nm	t
HKPU Proto	NIR camera	512 × 256	–	NIR-pass filter	850 nm	t
KTDeaduk Proto	–	640 × 480	–	NIR-pass 750 nm	850 nm	t
Shandong EL Proto	NIR camera	580 × 600	–	NIR-pass 800 nm	808 nm	t
Twente Proto	C-Cam BCi5	1280 × 1024	12	B+W 093 930 nm	850 nm	t
Chonbuk Proto	cam w. NIR filter rem.	640 × 480	–	NIR-pass filter	850 nm	t
Shandong Proto	–	640 × 480	–	NIR-pass 850 nm	850 nm	r
Sains Proto	Sony PSEye cam	640 × 480	–	IR-pass filter	850 nm	t
GUC-FPFV Proto	DMK 22BUC03 CMOS	744 × 480	8	none	870 nm	t
GUC-Dors Proto	monochrome CMOS	744 × 480	8	none	920 nm	t
PLUSVein-V2	IDS UI-ML1240-NIR	1280 × 1024	9	none	850 nm	t
PLUS OpenVein	IDS UI-ML1240-NIR	1280 × 1024	9	NIR-pass 850 nm	multiple	t+r

exposes the dorsal side to NIR frontal illuminators consisting of LEDs with a peak wavelength of 850 nm. It has two cameras, an NIR camera in combination with an NIR filter to capture the vein images and one webcam to capture the finger texture. It does neither use a finger guide nor pegs to align the finger, so it can be regarded as semi-touchless device. Again, there are no details about the specific type of camera, LEDs or NIR filter available. The *KTDaeduk Proto* scanner is equipped with a CCD camera, including an additional NIR passing filter with a cut-off wavelength of 750 nm, located at the bottom of the device. A hot mirror is used to be able to mount the camera horizontally, and thus to reduce the height of the device. The NIR

illuminator is located at the top of the device, above the dorsal side of the finger, and based on 850 nm LEDs. In addition, the scanner has a finger guidance to assist the capture subject in positioning his finger correctly. The *Shandong EL Proto* is the main part of an embedded finger vein recognition system. It is based on the light transmission principle but uses three NIR laser diodes with a peak wavelength of 808 nm instead of LEDs due to their stronger permeability and higher optical output power compared to LEDs. The scanner is equipped with a monochromatic NIR camera and an additional NIR-pass filter with a cut-off frequency of 800 nm to block daylight. A plate of 10 mm thick, transparent acryl is located above the NIR laser diodes to serve as a platform for positioning the finger and to remove uneven illumination. The whole scanner/finger vein recognition system is controlled by a DSP based mainboard. The *Twente Proto* is the best documented scanner so far. Its light source consists of 8 Osram SFH4550 LEDs (the same type we use for the reflected light illuminator) with a peak wavelength of 850 nm, situated on top of the dorsal side of the finger. Each LED is intensity controlled individually by a simple control loop to achieve a uniform illumination intensity along the finger. The camera is a C-Cam BCi5 monochrome CMOS camera, fitted with a Pentax H1214-M machine vision lens having a focal length of 12 mm. An additional infrared filter with a cut-off wavelength of 930 nm (type B+W 093) is mounted on the lens. The scanner device uses an Edmund Optics NT41-405 first surface mirror to minimise the height of the scanner. However, this scanner device is still quite bulky. Detailed information about the scanner design can be found in the Master's thesis of Ton [31]; however, based solely on the published details it is not possible to construct a ready-to-use scanner in a straightforward way. The *Twente Proto* scanner is described in Chap. 5 [35] of this book. Section 6 of Chap. 5 [35] also presents a novel finger vein acquisition device proposed by the University of Twente. This new version of the scanner is much more compact compared to the *Twente Proto* one. It is based on a Raspberry Pi as processing board and three Raspberry Pi camera modules as image sensors. It consists of three NIR LED strips that can be positioned in a semicircle from 0–180°. Thus, this scanner is able to capture multi-perspective finger vein images (cgf. Chap. 13 [22]) and allows for 3D finger vein reconstruction. The team at the University of Twente is currently investigating the optimal illumination and settings for the 3D finger vein reconstruction. The *Chonbuk Proto* scanner is equipped with a camera including an additional infrared light passing filter and an array of 850 nm infrared LEDs located above the finger. The camera is a modified COTS camera where the NIR blocking filter was replaced by an NIR pass-through filter. It has a finger holder with a hole in the backside of the scanner serving as a finger placement unit. This prototype scanner is quite small with a size of $68 \times 54 \times 101$ mm. The *Shandong Proto* is the only scanner prototype besides out PLUS OpenVein scanner that is based on reflected light. It consists of a camera, an NIR pass-through filter with a cut-off wavelength of 850 nm and an NIR light source based on 850 nm LEDs. This is the only information that is available for this prototype scanner. The *Sains Proto* scanner has three units of 850 nm NIR LEDs, placed in a row on the top section of the scanner, serving as light source. A Sony PSEye camera is mounted at the bottom section of the scanner. It does not use any pegs or finger guides. The capture

subject has to touch the back wall of the scanner with their finger only. The *GUC-FPFV Proto* scanner is able to capture finger vein and fingerprint images at once. It is designed to be a low-cost device, consisting of a DMK 22BUC03 monochrome CMOS camera, fitted with a T3Z0312CS 8 mm lens and an LED-based illuminator made of 40 Vishey Semiconductors TSSF5210 870 nm NIR LEDs. The scanners have additional physical structures made of aluminium foil to channel and focus the luminous flux in order to provide enough light intensity to penetrate the whole finger. The scanner device has a size of 180 × 110 × 70 mm. The *GUC-Dors Proto* scanner is designed to capture dorsal finger vein images. It uses the same camera and lens as the *GUC-FPFV Proto* (DMK 22BUC03 monochrome CMOS camera, fitted with a T3Z0312CS 8 mm lens) but 920 nm LEDs instead of 850 nm ones. The light source is placed 10 mm away from the finger placement holder and the camera is placed 100 mm away from the finger. This is the only information available about that scanner, not even an image is depicted in the paper. The *PLUSVein-V2* scanner is also designed to capture dorsal finger vein images but could be easily used to capture palmar images as well. It is based on an IDS Imaging UI-ML-1240NIR NIR-enhanced industrial camera fitted with a Fujifilm HF9HA-1B 9 mm lens (the same as in our design of the *PLUS OpenVein* scanner). No additional NIR pass-through filter is used, instead the scanner is embedded in a wooden box to block the ambient light. The light transmission illuminator consists of 8 Osram SFH 4253-Z 850 nm LEDs. Each LED is brightness controlled individually by an automatic brightness control algorithm in order to achieve an optimal illumination along the finger.

For most of the above-mentioned finger vein scanner prototypes, except the *Twente Proto*, only very few details are available. Thus, it is not possible to reproduce those scanners in a straightforward manner. Our *PLUS OpenVein* scanner is the first finger vein scanner that is able to capture both reflected light and light transmission images. Moreover, it is designed to capture dorsal as well as palmar images. Most important though: its design is fully open source. Our scanner design is explained in detail in the following section.

3.3 PLUS OpenVein Finger Vein Scanner

This section presents our proposed, fully open-source finger vein scanner design, called PLUS OpenVein. At first, the advantages of our scanner design and the differences to existing finger vein scanners are discussed, followed by a detailed explanation of the individual scanner parts. The finger vein scanner design consists of the following main components: an NIR-enhanced camera together with a lens and an NIR pass-through filter, an NIR light transmission illuminator including an illuminator bracket, an NIR reflected light illuminator, an illuminator control board, a finger placement unit and a modular wooden housing. The functional interaction of each of the individual scanner parts, specified by the scanner design, is as important as the choice of each of the individual parts in order to achieve a good finger vein image quality, and consequently a high recognition performance.

3.3.1 Advantages and Differences to Existing Designs

The following list summarises the main advantages and differences of the proposed design over the existing ones presented in Sect. 3.2.4:

- Modular and easy to reproduce design: Most finger vein scanners in research do not place any importance on enabling changes of their individual parts. The PLUS OpenVein is a modular finger vein scanner design, i.e. its individual parts can be replaced, modified and improved easily. All of the housing parts and mounting brackets are either 3D-printed or laser-cut plywood parts. One the one hand, this enables each researcher owning a 3D printer to reproduce the scanner (the laser-cut parts can also be reproduced using a jigsaw). On the other hand, it is easy to modify and improve those parts to individual needs as only the 3D models have to be edited.
- Dorsal/palmar images as well as light transmission/reflected light: although it is easy to capture dorsal images using a scanner meant to capture palmar ones by simply turning the finger around, it is hard to maintain the same longitudinal rotation angle at each capture. Moreover, all exisiting finger vein scanner designs exhibit either light transmission or reflected light only. Our finger vein scanner design is a multipurpose one as it is able to capture dorsal as well as palmar (by rotating the hand 180° around its longitudinal axis), with the finger placement unit especially shaped to prevent unwanted longitudinal finger rotation [23] and achieve a defined finger position for each image capture. Furthermore, it is equipped with two types of illuminators, a light transmission as well as a reflected light one, to acquire palmar and dorsal finger vein images during a single acquisition.
- Three fingers are captured simultaneously: All COTS scanners as well as all research prototype scanners listed in Table 3.2 capture only one finger at a time. The PLUS OpenVein scanner design is the first proposed finger vein scanner that is designed to capture three fingers (index, middle and ring finger) at once to speed up the data acquisition process.
- NIR laser module based scanner version: NIR laser modules exhibit several advantages over NIR LEDs, especially in contactless operation as described in Sect. 3.3.3.2. However, all COTS finger vein scanners as well as the majority of scanners used in research are based on NIR LEDs. We derived two versions of our PLUS OpenVein finger vein scanner design, one is based on a standard NIR LED light transmission illuminator while the second one is based on an NIR laser module illuminator. Both scanners are derived from the same basic structure and differ only in their illuminator, the illuminator control board and the illuminator bracket.
- Finger placement unit to prevent finger misplacement: In [23], we showed that longitudinal finger rotation can easily occur with most types of finger vein scanners and has a severe impact on the recognition performance too. Bearing that in mind, we designed our finger placement unit to prevent most possible kinds of finger misplacements, especially longitudinal finger rotation. This finger placement unit is described in Sect. 3.3.6.

- Open-source scanner design: As mentioned in Sect. 3.2.4, not many details are available for most of the finger vein scanner designs in research, apart from a few exceptions (e.g. the design of Ton [31]). Our scanner design is the first true open-source one. All technical details of the scanner parts, the data sheets, the software as well as more detailed descriptions and instructions for constructing and setting up the scanner can be found in our public repository: http://www.wavelab.at/sources/PLUS-OpenVein, making it a fully open-source scanner design. Our license agreement permits the free of charge use, modifications and reproduction finger vein scanners based on our design for research and non-profit purposes.
- The main disadvantage of our scanner design is its higher price compared to other designs which are based on low-cost camera modules, like the new Twente Proto [35], the *GUC-FPFV Proto* [25], the *GUC-Dors Proto* [24] and the one proposed in [26]. On the one hand, the high-quality industrial NIR enhanced camera allows for a higher image quality and contrast compared to the low-cost cameras. On the other hand, the camera module can be easily replaced by any other suitable camera module thanks to our modular design, effectively reducing the total costs of the scanner device to the same level as other low-cost scanner devices. Hence, in practice, this is not really a disadvantage.

Figure 3.5 shows both of the scanners fully assembled and with the right and front side of the scanner half open including labelled parts. The outside dimensions of the LED version and the laser module based scanner are 146 × 175 × 258 mm and 146 × 175 × 306 mm, respectively. Each individual scanner part together with its advantages over similar designs and the design decisions is explained in the following.

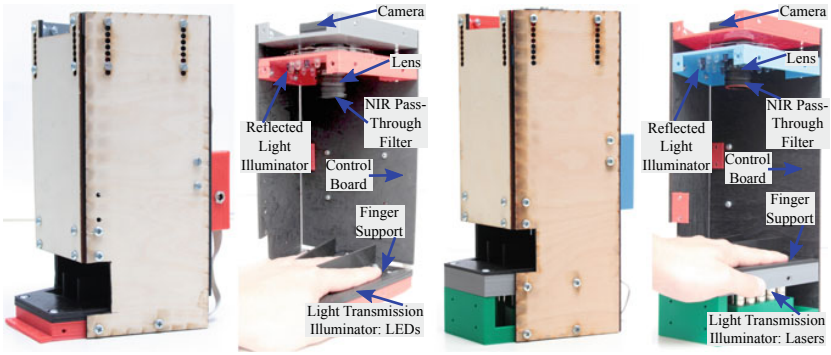

Fig. 3.5 PLUS OpenVein finger vein scanner, left: LED version, right: laser module version

3.3.2 Image Sensor, Lens and Additional Filter

The IDS Imaging UI-ML1240-NIR camera [60] was chosen as image sensor. It has a max. resolution of 1280 × 1024 pixels and a max. frame rate of 25 fps. It is based on the EV76C661ABT CMOS monochrome image sensor, having a colour depth of 8 bit, a max. resolution of 1.31 megapixels, with a pixel size of 5.3 µm and a sensor diagonal of 1/1.84 in. The main advantage of this camera compared to modified webcams and other visible light cameras is that it is an NIR-enhanced industrial camera. It is specifically designed to achieve a high quantum efficiency within the NIR spectrum. Note the higher quantum efficiency within 800–900 nm of the NIR version compared to the monochrome one, both depicted in Fig. 3.6 left. This wavelength range includes the peak wavelengths of our NIR LEDs (850 nm) and NIR laser modules (808 nm) equipped in the light transmission illuminator. Most COTS and consumer cameras that are designed for the visible wavelength spectrum are sensitive in the NIR spectrum too, but they are equipped with NIR blocking filters in order to avoid unwanted colour effects caused by NIR light (the sunlight contains an NIR wavelength spectrum part too which would stain the images blue to violet). The NIR blocking filter can be removed, enabling the camera to capture NIR images, but those modified cameras are less sensitive than a special NIR-enhanced camera. Due to its increased NIR sensitivity, an NIR-enhanced camera achieves a higher image contrast in the NIR spectrum than a visible wavelength one. On the contrary, a special NIR-enhanced industrial camera is several orders of magnitude more expensive than a modified webcam solution, posing a disadvantage for this type of camera in terms of costs. However, advantages in terms of image quality predominated, and thus the use of an NIR-enhanced camera was the preferred option for our finger vein scanner design. Note that the camera holder bracket can be modified for the use of different camera models easily.

The camera is equipped with a Fujifilm HF9HA-1B 9 mm fixed focal lens [50]. The lens has a manual iris and is C-Mount compatible. The short focal length of 9 mm

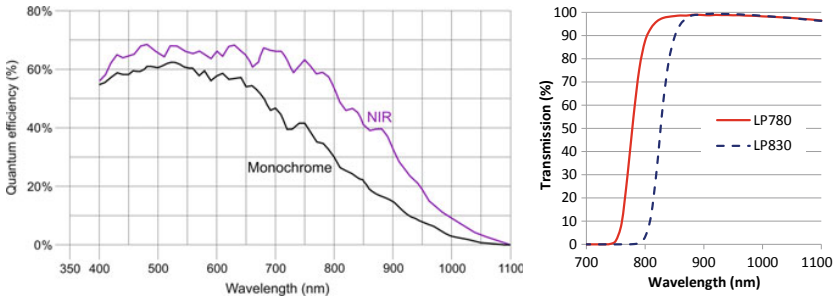

Fig. 3.6 Left: quantum efficiency charts for the UI-ML-1240-NIR (black line) and the UI-ML-1240-M (purple line), taken from the data sheet [60], right: filter chart for the MIDOPT FIL LP780/27 (solid red line) and LP830/27 (dashed blue line) NIR pass-through filter

is necessary to maintain a short distance between the camera and the finger which is desired in order to reduce the overall size of the scanner device. A lens with an increased focal length has less image distortions but requires a larger distance from the finger, thus increasing the overall size of the scanner. A shorter focal length reduces the minimum distance to the finger but increases the image distortions, especially at the image boundaries. Thus, we decided to use a 9 mm focal length as the best trade-off between the distance to the finger, i.e. the overall scanner dimensions, and the image distortions introduced by the lens itself. A MIDOPT FIL LP830/27 [56] and a MIDOPT FIL LP780/27 [55] NIR pass-through filter for the LED and the laser-based version of the scanner, respectively, are mounted on top of the lens. The filter chart of the LP830, depicted in Fig. 3.6 right as dashed blue line, fits well with the emission spectrum (cf. Fig. 3.9) of the NIR LEDs (peak wavelength of 860 nm) and the filter chart of the LP780 (solid red line in Fig. 3.6) fits well with the NIR laser modules (peak wavelength of 808 nm). This additional NIR pass-through filter helps to reduce the influence of ambient light and further improves the quality of the vein images. Currently, the wooden scanner housing is still needed for stability reasons, to comply with safety regulations for the laser-based version of the scanner and to further reduce the influence of the ambient light in case of direct sunlight shining on the scanner. For the next, slightly improved version of the scanner design, the NIR pass-through filters will be replaced by the MIDOPT BN850 Narrow Near-IR Bandpass Filter [54] and the MIDOPT BN810 Narrow Near-IR Bandpass Filter [53] for the LED version of the scanner and the laser module version of the scanner, respectively. These filters are more effective in reducing the ambient light's influence and enable the removal of the wooden scanner housing without impacting the image quality for indoor use of the scanner and at least a reduction of the housing's side plates dimensions if outdoor use is desired. On the other hand, the NIR pass-through filter increases the total costs of the scanner, especially the narrow bandpass filter. If the scanner is used in indoor environments only, where the influence of ambient light can be controlled, it is possible to refrain from using and NIR pass-through filter for cost reasons. To achieve an optimal image quality, we recommend to use the additional NIR pass-through filter though.

The last part of the camera assembly is the camera holder bracket, depicted in Fig. 3.7 together with the camera, the lens and the NIR pass-through filter, which is mounted on the very top of the scanner. The camera holder bracket is again a custom-developed, 3D-printed part which can be easily modified for mounting different cameras.

3.3.3 Light Transmission Illuminator

There are two different versions of the light transmission illuminator: one based on NIR LEDs and the other one based on NIR laser modules. The scanner equipped with the laser modules is bigger due to the larger size of the laser module based illuminator compared to the LED-based one and due to the minimal distance of

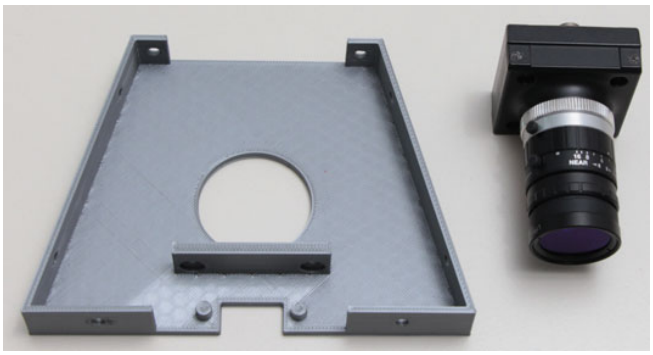

Fig. 3.7 Camera holder bracket (left), IDS NIR-enhanced camera + Fujifilm 9 mm lens and NIR pass-through filter (right)

about 30 mm between the laser modules and the finger surface which is necessary to adjust the optimal focal length of the laser modules. Both illuminators consist of three stripes, one stripe underneath each finger. These stripes are mounted with the help of a custom-developed, 3D-printed, illuminator bracket, depicted in Fig. 3.8 top for the LED version (the two parts are then screwed together to hold the LEDs in place) and Fig. 3.8 bottom for the laser module based version. This bracket is located underneath the finger placement unit.

3.3.3.1 LED-Based Version

The LED-based light transmission illuminator has three stripes consisting of 8 Osram SFH-4253-Z SMD LEDs [65] each. The stripes are depicted in Fig. 3.8 top-right. The LEDs have a radiation half-angle of $\pm 60°$, a peak wavelength of 860 nm and a max. radiant intensity of 13 mW/sr. The emission spectrum of the LEDs is depicted in Fig. 3.9 left. These LEDs were chosen as their peak wavelength is within the recommended wavelength band for vascular pattern recognition and because they are standard, low-cost electronic components. They are placed in a distance of 7.5 mm next to each other, which has been determined to be the optimal distance during our tests in order to provide a sufficient and uniform illumination along the finger. Each LED can be brightness controlled separately and independently from the other LEDs in order to achieve an optimal image contrast. The health and safety requirements for NIR LEDs are defined in the IEC-62471 standard on "Photobiological safety of lamps and lamp systems" [3]. The standard defines limits in terms of radiation intensity and duration to prevent Corneal Hazard as well as Retinal Thermal Hazard. The Renesas Electronics application note AN1737 [67] shows an example calculation for an LED similar to the ones equipped in our scanner design, a distance of the LED and eyes of 200 mm and a radiation duration of 10 s. In this case, the safety factor for the Corneal and the Retinal Thermal Hazard is 4×10^6 and 2×10^5, respectively, i.e.

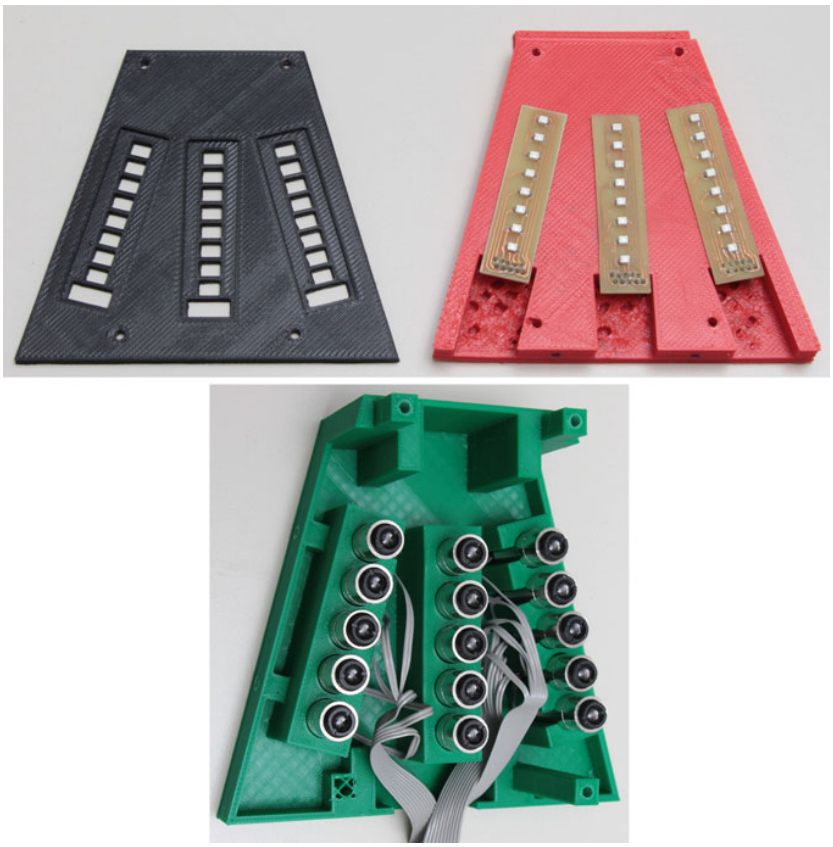

Fig. 3.8 Illuminator mounting bracket, top: LED version (two parts) + single LED stripes, bottom: laser version including the laser modules

the radiation level is at least 10^5 times below the critical limit. Moreover, our scanner housing prevents any direct exposure of the eye to the LED radiation. Hence, our scanner complies with the health and safety regulations.

3.3.3.2 Laser Module Based Version

The second version of the light transmission illuminator is based on laser modules instead of LEDs and consists of three stripes of five laser diodes [46] including an adjustable constant-current laser diode driver PCB [45] and a TO-18 housing with a focus adjustable lens [44] for each of the laser modules (the combination of laser diode + control PCB + housing is denoted as laser module or laser). The laser diodes

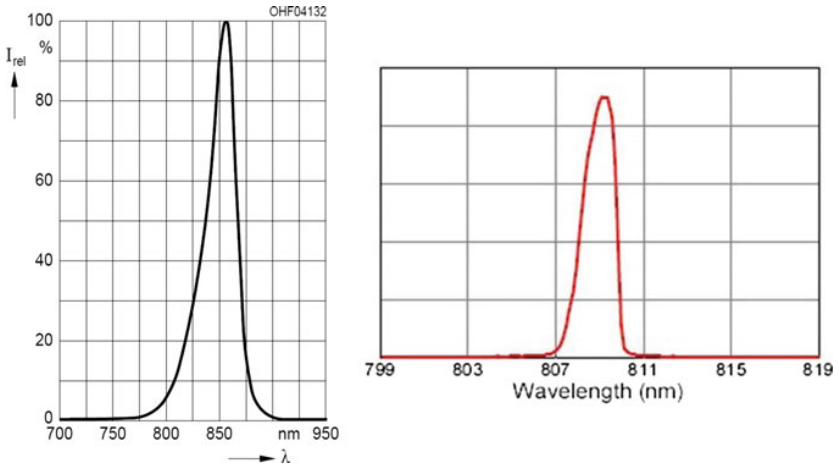

Fig. 3.9 Emission spectrum of the light transmission illuminator NIR LEDs (left) and the NIR laser modules (right), taken from the data sheet [65]

are TO-18 type (diameter 5.6 mm), and have a peak wavelength of 808 nm and an optical output power of 300 mW. These laser diodes belong to Class 3B according to the IEC 60825-1 standard [4]. The guidelines on laser health and safety require that any direct exposure to the laser beam has to be avoided for this laser class. To be compliant with these regulations, the housing of the scanner design is built in a way to ensure that no exposure of the eyes to the laser beam is possible. The emission spectrum of the laser diodes can be seen in Fig. 3.9 right. Note that their emission spectrum is narrower than the spectrum of the LEDs facilitating the use of narrow bandpass filters instead of NIR longpass filters, leading to further attenuation of the ambient light. The main advantages of the laser diodes/laser modules over the LEDs are their higher optical output power and their narrow radiation half-angle. This enables a higher degree of vertical finger movement without degrading the image quality, which is especially important if a full touchless operation is desired. The broad radiation half-angle of the LEDs leads to over-illuminated areas at the finger outline while the contrast in the vein regions is decreased as soon as the finger is not placed directly on top of the illuminator. Due to the narrow radiation half-angle of the laser modules (note that the laser diodes itself do not have such a narrow radiation angle, instead the focus adjustable lens included in the housing makes such a narrow angle possible), the main part of the luminous flux stays inside the centre regions of the finger (where most of the veins are) and thus the contrast in these regions remains stable if the finger is moved upwards (away from the illuminator). Figure 3.10 shows a comparison between the LED (left) and the laser module (right) based scanner. It can be clearly seen that for the LED version the contrast gets lower the further away the finger is from the illuminator while it remains high for the laser module based version. The disadvantage of using laser modules instead of LEDs is

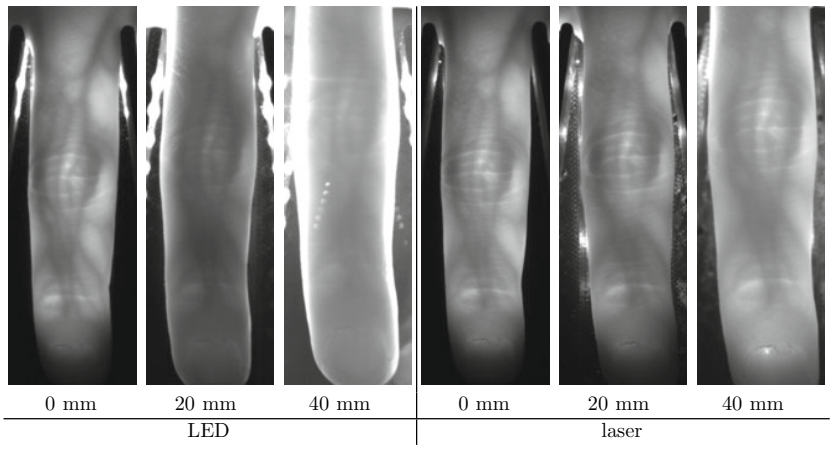

Fig. 3.10 Finger vein images captured with our scanners showing illumination issues due to vertical finger movement (0, 20 and 40 mm away from the scanner surface): note the bright areas along the finger boundaries and the reduced contrast of the vein region the further away the finger gets from the scanner surface for the LED scanner images (left) compared to the laser scanner ones (right) (image originally published in [12], © 2018 IEEE)

their high price. A single laser module is about 15–20 times more expensive than a single LED. In non-contactless operation, the image quality of the laser modules is only slightly better compared to LEDs. Hence, for the current version of the scanner, we recommend the LED-based version to cut down costs. If the scanner design is adopted towards a touchless version, laser modules are the preferred option.

3.3.4 Reflected Light Illuminator

The reflected light illuminator is composed of three different types of LEDs, 850 nm (Osram SFH 4550 LEDs [66] with a radiation half-angle of $\pm 3°$ and a max. radiant intensity of 700 mW/sr), 950 nm (Vishay Semiconductors CQY 99 [69] with a radiation half-angle of $\pm 22°$ and a max. radiant intensity of 35 mW/sr) and warm white daylight ones (Luckylight 504WC2E-W6-3PC [61] with a radiation half-angle of $\pm 15°$ and a typical luminous intensity of 23000 mcd), eight pieces each. These three types of LEDs are all standard, low-cost electronic parts. The two NIR types have peak wavelengths that are within the recommended spectrum for vascular pattern recognition and the warm white daylight one is commonly used in many different applications. The LEDs are mounted in a circle on the reflected light illuminator bracket (depictedn in Fig. 3.11), situated on top of the scanner device around the camera lens. The LEDs are arranged in an alternating manner, i.e. each 850 nm LED is followed by a 950 nm one, then a warm white one, then a 850 nm one and so on.

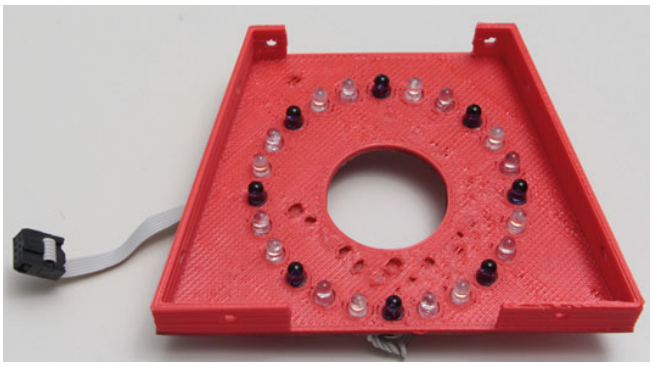

Fig. 3.11 Reflected light illuminator: 850, 950 nm and warm white daylight LEDs are arranged in an alternating manner around a circle. The camera lens is put through the circular hole in the middle of the bracket

This design turned out to be optimal in terms of uniform illumination regardless which of the three illuminators is turned on. Each of the 850 nm and the 950 nm eight tuples of LEDs can be brightness controlled separately, but not each individual LED. The warm white daylight LEDs can only be turned on at a fixed intensity (no brightness control). The reflected light illuminator enables the capturing of reflected light finger vein images. The warm white daylight LEDs are mainly meant for use during adjusting and testing and not during finger vein image acquisition. However, they can be utilised to capture additional finger texture images.

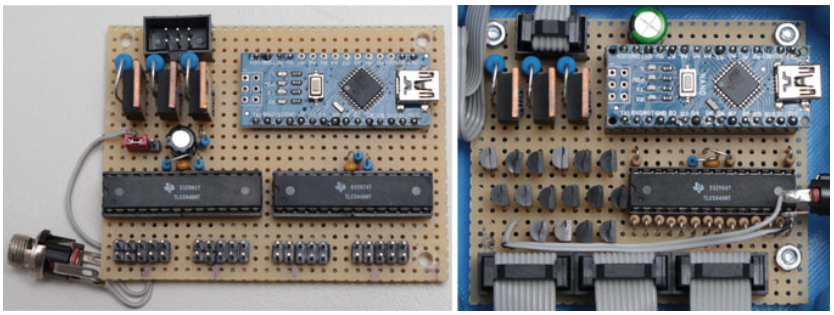

Fig. 3.12 Illuminator brightness control board prototype, left: LED version, right: laser module version

3.3.5 *Illuminator Brightness Control Board*

Figure 3.12 (left: LED version, right: laser module version) shows an image of the first prototype brightness control PCB board built using THT (through-hole-technology) parts. The final version is based on SMD (surface-mounted device) parts. Its two main components are an Arduino Nano board [48] and a Texas Instruments TLC59401/TLC5940PWP [68] (the THT version of the board uses the old version, the TLC5940). The Arduino Nano is a complete, breadboard-friendly microcontroller development board based on the Microchip ATmega328P microcontroller [63], including an integrated USB to UART converter and several external components necessary to operate the ATmega328P. The ATmega328P offers several built-in components, like analog and digital outputs, timers, UART, I2C, SPI Interface, etc. Most important for our application are the six PWM outputs and the UART interface. More details on the ATmega328P can be found in the data sheet [62]. The Texas Instruments TLC5940 is an integrated 16-channel LED driver with dot correction and greyscale PWM control enabling a convenient brightness control of LEDs without the need for external components like dropping resistors. Each output can be controlled separately (4096 steps) and has a drive capability of 120 mA. It operates as a constant-current sink and the desired current can be set using only one external resistor. It is controlled using a serial data interface. As every single LED of the three stripes of eight LEDs each (24 LEDs in total) is desired to be controlled individually, two of these TLC5940 are equipped on the LED version of the control board as each TLC5940 has 16 outputs. In Fig. 3.13, a schematic overview of the control board is depicted. The control board is connected to the PC over the USB interface. The data sent over USB is converted to UART compatible data, received by the Arduino Nano (or the ATmega328P to be precise) which controls the 2 TLC5940s. Each output of the TLC5940 is directly connected to an LED. The LED and the laser module version differ. The laser modules exhibit a higher current consumption than

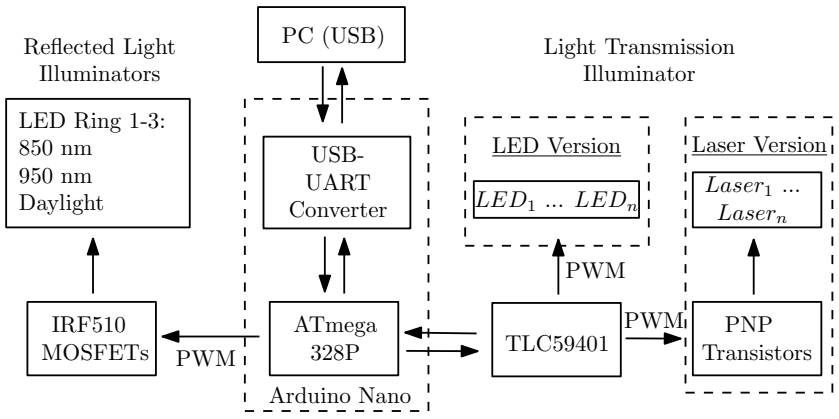

Fig. 3.13 Schematic structure of the control PCB

the LEDs that would exceed the maximum of 120 mA provided by the TLC5940. Thus, external PNP transistors (CDIL BC327-25 [49] for the THT version of the board and ON Semiconductor BC808-25 SMD [64] for the final SMD version) in combination with suitable base dropping resistors are added. The laser modules are not directly connected to the TLC5940 but to the PNP transistors. The laser module version has only one TLC5940 as there are 15 laser modules in total (compared to the LED version with 24 LEDs). Furthermore, two of the PWM outputs on the Arduino Nano board are used to brightness control the reflected light illuminator. One digital output is utilised to turn the warm white daylight reflected light illuminator on and off. There are additional N-Channel MOSFETs (International Rectifier IRF510 [70] for the THT version and Alpha&Omega Semiconductor AO3418 [47] for the final SMD version) and dropping resistors on both versions of the control board for the reflected light illuminators. The complete schematic and board layout as well as all data sheets for the final SMD version can be found in our public repository.

3.3.5.1 Arduino Firmware

The Arduino Nano or to be more precise the ATmega328P microcontroller on which it is based can be programmed in several different programming languages and development environments. We decided to use C++ together with the Arduino IDE to be able to utilise all the convenient Arduino libraries. There is a library for the TLC5940 included in the Arduino framework. Using this library the TLC5940 can be easily interfaced and controlled. It handles the serial protocol of the TLC5940 and setting/receiving of the brightness level values. It uses two out of the three internal timers of the ATmega328P, so if the TLC5940 library is utilised, only two of the six available PWM outputs on the Arduino Nano remain available for use (thus, we went on without being able to brightness control the warm white daylight reflected light in order to avoid adding another external hardware part). We implemented a simple protocol to interface each of the individual LEDs/laser modules as well as the reflected light illuminators, to set a whole stripe at once and to turn off all illuminators again. The Arduino Nano is recognised as USB serial port on the PC and a fixed-length text-based serial protocol, allowing for easy debugging, is used to send the command to the brightness control board. Details about the protocol as well as the brightness control board firmware can be found in our repository.

3.3.6 Finger Placement Unit

To provide an intuitive interaction with the scanner device and to help the capture subject at positioning their fingers correctly, the scanner has a finger guide or a finger placement unit. As the scanner captures the index, middle and ring fingers simultaneously, it is important that all three fingers are aligned with the underneath illumination stripes. This is especially important for the LED version of the scanner

in order to avoid overexposed areas along the finger outline (refer to Sect. 3.3.3.2 for details on the advantages of the lasers over the LEDs). The finger placement unit, depicted in Fig. 3.14, is a custom-developed, 3D-printed part with three elliptically shaped grooves, each with a rectangular hole in the centre of the groove which is situated above the location where the LEDs or laser modules are placed. These grooves guide the capture subject at placing their fingers correctly and enable a natural and comfortable finger placement position during the capturing process, regardless if the fingers are placed in palmar or dorsal direction. Moreover, the finger placement unit was designed to prevent most kinds of finger misplacement, including tilts, planar finger rotation, horizontal shifts and especially longitudinal finger rotation by requiring the capture subject to place their finger flat on the placement unit with the fingers aligned to the grooves. In addition, the placement unit has two walls in between the index and middle and the middle and ring finger, respectively. These walls in combination with the shape of the grooves lead to a slightly spread position of the fingers, which makes an easy segmentation of the single fingers possible. Moreover, they block the diffuse light emitted sideways from the fingers which would otherwise lead to overexposed areas along the finger boundaries. In order to arrive at an optimal size and shape of the finger positioning support we performed several tests with male and female subjects, different age groups and different ethnicities (European, Asian, African). The current design is suitable for a broad range of people, especially for the average European and also for most adult Asian people. However, there might be some modifications necessary for younger Asian people with small hands/fingers. As it is a 3D-printed part, these adjustments to better suit different groups of people can be done easily. Note that adjustments have to be made to the LED/laser mounting brackets (see Sect. 3.3.3) too if the finger placement unit is changed.

3.3.7 Housing Parts

The housing for the PLUS OpenVein finger vein scanner was designed for two reasons. The first version of the scanner did not include an NIR pass-through filter, thus the housing was necessary to shield the scanner from the ambient light and improve the image contrast. Second, the wooden housing serves as a frame for mounting all the brackets and parts and putting the whole scanner assembly together. The housing consists of four wooden parts: two side panels, one front panel and one back panel which are connected using 3D-printed mounting brackets. The parts for the LED-based version are shown in Fig. 3.15. The laser module based version ones are not shown but only differ in their height (which are larger than the LED ones). There is an additional 3D-printed housing to accommodate the brightness control PCB which is mounted on the backplane (depicted in Fig. 3.5). The wooden parts are cut out of 4 mm plywood using a laser cutter. The current version of the scanner includes an NIR pass-through filter, so the wooden housing is mainly for stability and mounting reasons (except if the scanner is exposed to direct sunlight, then the

Fig. 3.14 Finger placement unit: the finger-shaped grooves guide the capture subject in placing their fingers correctly. The walls are blocking diffuse emitted light from adjacent fingers, the light transmission illuminators are placed underneath the rectangular holes

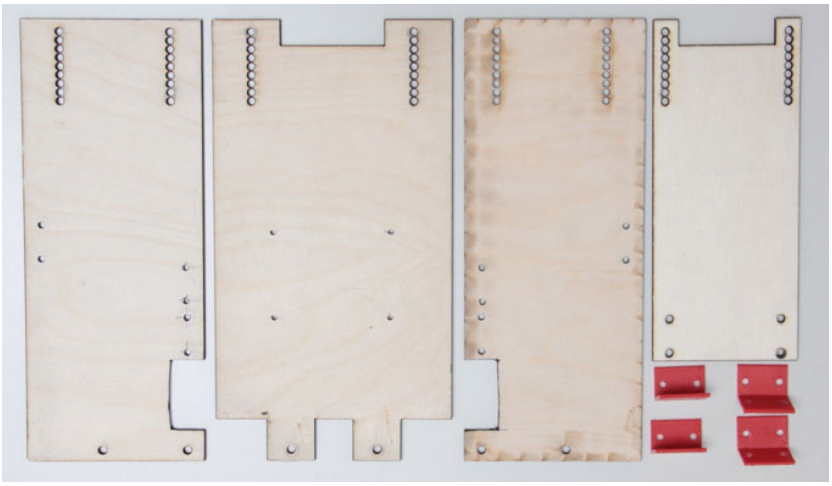

Fig. 3.15 Housing parts of the LED-based scanner

housing is necessary to reduce the influence of the ambient light too). As studies showed that the capture subjects' acceptance and convenience is higher for scanner devices built in a semi-open or fully open manner, we are planning to design a second version of the housing which has smaller side and front panels (semi-open design).

3.3.8 Capturing Software

So far, all the hardware parts of the scanner including the brightness controller firmware have been described. There is still one important thing missing, the scanner control software for capturing actual finger vein images. Our control software is based on the IDS Imaging uEye Software Suite [59] as the image sensor is an IDS camera. Their framework is available for Windows- and Linux-based operating systems. We implemented our capturing software for Windows using C# and Microsoft Visual Studio 2015. A screenshot of the capturing software can be seen in Fig. 3.16. Its functionality can be divided into four main parts:

1. Initial scanner calibration: During initial scanner calibration the LED/laser module centres are set with the help of 3D-printed calibration sticks. This is essential for the automated brightness control algorithm to work correctly.
2. Setting camera parameters: Here several camera parameters, e.g. frame rate, white balance, gain, pixel clock, exposure time, etc. can be set.
3. Controlling the illumination sources: the light sources (light transmission and reflected light) can be either be controlled manually and individually or automatically. The manual control is only meant for troubleshooting purposes and tests while usually the automatic brightness control is applied.
4. Image capturing: The image capturing process is designed to be semi-automated and convenient for a typical finger vein data collection. Some general settings, e.g. the directory to save the captured images, which kind of images (dorsal/palmar, left/right hand, light transmission/reflected light), how many images per kind and the desired average grey level can be set in advance. Then the session ID and the subject ID are set. Afterwards a single image can be captured or a fully automatic capturing run can be started. During the fully automatic capturing run, the desired number of images is captured and the software prompts to pull the hand out of the scanner and put it in again after each image. After all images per hand/side are captured, the software prompts to insert the next hand or change the side of the hand until all images for the current subject are captured. The illuminator brightness is adjusted automatically before each captured image according to the algorithm described in the following.

3.3.8.1 Automated Brightness Control Algorithm

In order to achieve an optimal image contrast especially in the vein regions, an automatic brightness control algorithm was developed. This algorithm controls each of the single light transmission illuminator LEDs/laser modules as well as the reflected light illuminators as a whole. After several tests with different image qualities and image contrast metrics, we opted for a simple, iterative algorithm based on a comparison against a target grey level. This algorithm works as follows: at first, the LED/laser centres have to be configured once as described below. This includes the determination of the area of influence for each LED/laser, which is the area in the image

a single LED/laser illuminates (defined by a circle with a certain radius). Then all LEDs/lasers are set to an initial intensity level/brightness value which is half of their maximum intensity (I_{max}). The live image of the camera is analysed and the current grey level within the area of influence of each LED/laser is determined ($GL_{current}$) and compared against the set target grey level (GL_{target}). The new brightness value is then set according to $I_{n+1} = I_n + I_{corr}$, where I_{n+1} is the new intensity level, I_n is the current intensity level and $I_{corr} = \frac{GL_{target} - GL_{current}}{GL_{max}} \cdot \frac{I_{max}}{2 \cdot n}$, where GL_{max} is the maximum grey value and n is the current iteration. The iteration stops if either the target grey level GL_{target} has been reached or if no more intensity change is possible. The algorithm finishes in at most $log_2(I_{max})$ iterations. Thus, it is fast enough for real-time applications while preserving a good performance in terms of uniform image contrast.

3.4 PLUSVein-FV3 Finger Vein Dataset

To demonstrate the high recognition performance that can be achieved by using our proposed scanner design, we established a dataset using both of our scanners, the LED-based version and the laser-based one. This dataset has already been published [12] and is available at: http://www.wavelab.at/sources/PLUSVein-FV3/. The first version contained dorsal finger vein images captured from 60 subjects, 6 fingers

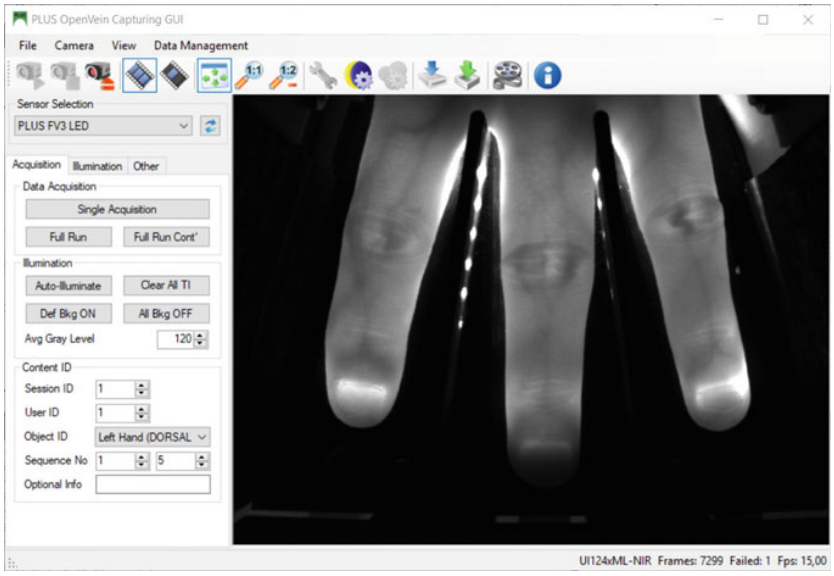

Fig. 3.16 Main window of the PLUS OpenVein finger vein capturing software

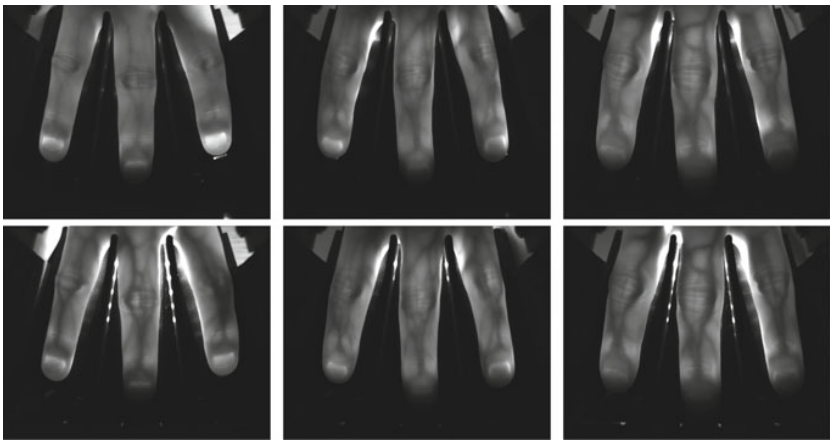

Fig. 3.17 PLUSVein-FV3 example images, top: laser module based scanner, bottom: LED-based scanner

per subject and 5 images per finger in one session, summing up to a total of 3600 images from 360 individual fingers (1800 per scanner). Our scanners capture three fingers at once, so the 3600 images are actually extracted from 1200 raw finger vein images which were separated into three images corresponding to each individual finger. Those single finger images have a resolution of 420 × 1024 pixels and are stored in 8-bit greyscale png format. Some example images are shown in Fig. 3.17. In our previous work [12], we reported the recognition performance numbers that can be achieved using the dorsal images of our dataset, and thus our scanner design. We arrived at EERs as low as 0.028% and 0.111% for MC [20]/PC [2] and a SIFT-based approach [14], respectively, with these simple but well-established finger vein recognition schemes. In the meanwhile, we extended the dataset to contain palmar finger vein images captured from the same subjects too. Thus, it now includes a total of 7200 images, 1800 per scanner and per view (palmar/dorsal). In another recently published work [13], we compared the performance of palmar versus dorsal images. We showed that the best view in terms of recognition accuracy depends on the feature extraction algorithm, resulting in EER of 0.08% for the palmar images using MC and an EER of 0.08% for the dorsal images using SIFT. These performance figures approve the sophisticated and deliberate design of our finger vein scanners.

We are still extending our dataset in-house. The most recent version consists of about 100 subjects so far. The main reason for open sourcing our finger vein scanner design was to help other researchers working in the field of finger vein biometrics by sharing our custom-developed scanner design with them. The second most important reason is that we are interested in collaborations to extend our dataset and evolve it to an extensive, open finger vein dataset available for research purposes. If there are several reproductions of the scanner based on our design out there, every researcher having such a scanner device at hand and interested in participating could just provide

the captured vein images and we will then include them in a new release of the open finger vein dataset.

We are currently discussing options for a suitable online platform to handle such a collaboration efficiently as well as trying to clarify the legal aspects (the consent forms have to include the right to merge the single datasets together which of course includes sharing the finger vein data with other partners in different countries and under different legislations) of sharing the finger vein images. We are confident that these two issues can be resolved soon.

3.5 Conclusion

This chapter proposes a new finger vein scanner design. After the introduction, the basic principle of a finger vein scanner is outlined, followed by a review on commercial finger vein scanners, available research finger vein datasets and the corresponding finger vein scanners used to establish these datasets. The main contribution of this chapter are the details about our fully open-source, modular, multipurpose finger vein scanner design. Our finger vein scanner design is based on commercial-off-the-shelf parts, a custom-developed brightness control board and custom-designed 3D-printed parts as well as laser-cut plywood parts. It is modular as each individual part can be replaced, modified and improved easily. This scanner is the first finger vein scanner that is able to capture reflected light as well as light transmission images. Moreover, it is able to capture three fingers at once (index, middle and ring finger) from the dorsal and palmar view (by rotating the hand around 180°). Thus, we call it a multipurpose finger vein scanner. Two different versions of the basic design are presented, one based on a conventional NIR LED illuminator, the second one based on NIR laser modules. Laser modules have not gotten much attention in finger vein recognition so far, despite their advantages especially if it comes to touchless operation. All the individual parts are described together with their design decisions. Our scanner design is fully open source: all technical details of the scanner design, including data sheets, parts lists, technical drawings and 3D models of the housing parts, firmware and software together with detailed assembly and setup instructions can be found in a public repository: http://www.wavelab.at/sources/PLUS-OpenVein. The use of our scanner design and the reproduction of the finger vein scanner according to our design is free of charge for research purposes. Thanks to our fully open-source design, other researchers can easily reproduce our scanner and utilise this scanner for their own finger vein data collection, meaning they are no longer dependent from publicly available datasets. Moreover, they can contribute their modifications and improvements to our scanner design as well. To confirm the decent recognition performance that can be achieved using our scanner design, we established a dataset using our two scanners. This dataset currently contains 7200 images from 360 individual fingers and is publicly available for research purposes at: http://www.wavelab.at/sources/PLUSVein-FV3.

3.5.1 Future Work

Although the current scanner design has been proven to be competitive in terms of recognition accuracy and usability, we still strive to improve it. The first improvement will be a rather small one. We will replace the NIR pass-through filter with an NIR bandpass filter for both versions of the scanner. This helps in further reducing the influence of the ambient light and is advantageous if it comes to the next improvement. The next change to the scanner design will include a removal of the side plates and the front plate to arrive at a more open or at least semi-open design. Scanners designed in an open manner have been shown to increase the capture subjects' acceptability and convenience. Instead of removing the side plates completely we are thinking of making them only half of their current width such that the scanner becomes semi-open while still retaining its mechanical stability. The second improvement we are currently working on is the integration of the capturing software on a Raspberry Pi microcomputer as a first step towards a stand-alone, embedded finger vein scanner device which only requires an external power source but no additional PC for acquiring the images. The next step towards this stand-alone design is an additional touchscreen display, mounted at the front plate of the scanner device, connected to the Raspberry Pi and used to control the whole data acquisition process. Thanks to our fully open-source design, other researchers can contribute their modifications and improvements to our scanner design too.

Furthermore, we plan to establish a comprehensive, publicly available finger vein dataset for research purposes. Researchers who are interested in a contribution to this new finger vein dataset can simply build a scanner based on our open-source design, acquire finger vein images on their own and then contribute to the dataset by providing us their captured finger vein data. Such an extensive, available, collaborative finger vein dataset will be beneficial for the whole finger vein research community and is vital in order to achieve further progress in finger vein recognition. We are currently also extending the first version of our already available finger vein dataset in-house. Together with our partners and other researchers who are willing to contribute and build a scanner based on our design, we are confident that we will establish a comprehensive, open finger vein dataset from which the whole finger vein research community will benefit.

Acknowledgements This project has received funding from the European Union's Horizon 2020 research and innovation program under grant agreement No. 700259, project PROTECT—Pervasive and UseR Focused BiomeTrics BordEr ProjeCT.

References

1. Asaari MSM, Suandi SA, Rosdi BA (2014) Fusion of band limited phase only correlation and width centroid contour distance for finger based biometrics. Expert Syst Appl 41(7):3367–3382
2. Choi JH, Song W, Kim T, Lee SR, Kim HC (2009) Finger vein extraction using gradient normalization and principal curvature. Proc SPIE 7251:9. https://doi.org/10.1117/12.810458
3. Commission IE et al (2006) IEC 62471: 2006. IEC Photobiological safety of lamps and lamp systems, Geneva
4. Commission IE et al (2007) Safety of laser products-part 1: equipment classification and requirements. IEC 60825–1
5. Daniel H (2012) Vascular pattern recognition and its application in privacy–preserving biometric online–banking system. PhD thesis, PhD dissertation, Gjovik University College
6. Eng PC, Khalil-Hani M (2009) Fpga-based embedded hand vein biometric authentication system. In: TENCON 2009 IEEE region 10 conference, pp 1–5
7. Fadhil RI, George LE (2017) Finger vein identification and authentication system. LAP Lambert Academic Publishing, Germany
8. Fletcher RR, Raghavan V, Zha R, Haverkamp M, Hibberd PL (2014) Development of mobile-based hand vein biometrics for global health patient identification. In: IEEE global humanitarian technology conference (GHTC 2014), pp 541–547
9. Hitachi Group, Corp (2018) Finger vein technology for Bank BPH (Poland)—Hitachi Europe News. http://www.hitachi.eu/en-gb/case-studies/finger-vein-technology-bank-bph-poland. Accessed 20 June 2018
10. Hitachi-Omron Terminal Solutions, Corp (2018) Taiwan's CTBC bank adopts finger vein authentication solution for ATMs—Hitachi News. http://www.hitachi-omron-ts.com/news/pdf/201607-001.pdf. Accessed 20 June 2018
11. Huang B, Dai Y, Li R, Tang D, Li W (2010) Finger-vein authentication based on wide line detector and pattern normalization. In: 20th international conference on pattern recognition (ICPR) 2010. IEEE, pp 1269–1272
12. Kauba C, Prommegger B, Uhl A (2018) Focussing the beam—a new laser illumination based data set providing insights to finger-vein recognition. In: Proceedings of the IEEE 9th international conference on biometrics: theory, applications, and systems (BTAS2018), Los Angeles, California, USA, pp 1–9
13. Kauba C, Prommegger B, Uhl A (2018) The two sides of the finger—dorsal or palmar—which one is better in finger-vein recognition? In: Proceedings of the international conference of the biometrics special interest group (BIOSIG'18), Darmstadt, Germany
14. Kauba C, Reissig J, Uhl A (2014) Pre-processing cascades and fusion in finger vein recognition. In: Proceedings of the international conference of the biometrics special interest group (BIOSIG'14), Darmstadt, Germany
15. Kim J, Kong HJ, Park S, Noh S, Lee SR, Kim T, Kim HC (2009) Non-contact finger vein acquisition system using NIR laser. In: Sensors, cameras, and systems for industrial/scientific applications X, vol 7249. International Society for Optics and Photonics
16. Kumar A, Zhou Y (2012) Human identification using finger images. IEEE Trans Image Process 21(4):2228–2244
17. Lee EC, Jung H, Kim D (2011) New finger biometric method using near infrared imaging. Sensors 11(3):2319–2333
18. Liu Z, Song S (2012) An embedded real-time finger-vein recognition system for mobile devices. IEEE Trans Consum Electron 58(2):
19. Lu Y, Xie SJ, Yoon S, Wang Z, Park DS (2013) An available database for the research of finger vein recognition. In: 6th international congress on image and signal processing (CISP), 2013 , vol 1. IEEE, pp 410–415
20. Miura N, Nagasaka A, Miyatake T (2007) Extraction of finger-vein patterns using maximum curvature points in image profiles. IEICE Trans Inf Syst 90(8):1185–1194

21. Pascual JES, Uriarte-Antonio J, Sanchez-Reillo R, Lorenz MG (2010) Capturing hand or wrist vein images for biometric authentication using low-cost devices. In: Proceedings of the sixth international conference on intelligent information hiding and multimedia signal processing (IIH-MSP 2010), pp 816–819
22. Prommeger B, Kauba C, Uhl A (2019) A different view on the finger–multi-perspective score level fusion in finger-vein recognition. In: Uhl A, Busch C, Marcel S, Veldhuis R (eds) Handbook of vascular biometrics. Springer Science+Business Media, Boston, MA, USA, pp 395–434
23. Prommegger B, Kauba C, Uhl A (2018) Longitudinal finger rotation—problems and effects in finger-vein recognition. In: Proceedings of the international conference of the biometrics special interest group (BIOSIG'18), Darmstadt, Germany
24. Raghavendra R, Busch C (2015) Exploring dorsal finger vein pattern for robust person recognition. In: 2015 international conference on biometrics (ICB), pp 341–348. https://doi.org/10.1109/ICB.2015.7139059
25. Raghavendra R, Raja KB, Surbiryala J, Busch C (2014) A low-cost multimodal biometric sensor to capture finger vein and fingerprint. In: IEEE international joint conference on biometrics (IJCB), 2014. IEEE, pp 1–7
26. Raghavendra R, Venkatesh S, Raja K, Busch C (2018) A low-cost multi-finger vein verification system. In: proceedings of international conference on imaging systems and techniques (IST 2018), Karkow, Poland
27. Shaheed K, Liu H, Yang G, Qureshi I, Gou J, Yin Y (2018) A systematic review of finger vein recognition techniques. Information 9:213
28. Ting E, Ibrahim M (2018) A review of finger vein recognition system. J Telecommun Electron Comput Eng 10(1–9):167–171
29. Today BT (2014) Uk banking customers ready for finger biometrics authentication. Biom Technol Today 2014(9):3–12. 10.1016/S0969-4765(14)70138-9 http://www.sciencedirect.com/science/article/pii/S0969476514701389
30. Tome P, Vanoni M, Marcel S (2014) On the vulnerability of finger vein recognition to spoofing. In: IEEE international conference of the biometrics special interest group (BIOSIG). URL http://publications.idiap.ch/index.php/publications/show/2910
31. Ton B (2012) Vascular pattern of the finger: biometric of the future? sensor design, data collection and performance verification. Master's thesis, University of Twente
32. Ton B, Veldhuis R (2013) A high quality finger vascular pattern dataset collected using a custom designed capturing device. In: International conference on biometrics, ICB 2013. IEEE. URL http://doc.utwente.nl/87790/
33. University of Reading (2017) PROTECT multimodal DB dataset. http://projectprotect.eu/dataset/
34. University of Salzburg (2018) PLUSVein-FV3 finger-vein data set. http://www.wavelab.at/sources/PLUSVein-FV3
35. Veldhuis R, Spreeuwers L, Ton B, Rozendal S (2019) A high quality finger vein dataset collected using a custom designed capture device. In: Uhl A, Busch C, Marcel S, Veldhuis R (eds) Handbook of vascular biometrics. Springer Science+Business Media, Boston, MA, USA, pp 145–158
36. Wang J, Wang G (2017) Quality-specific hand vein recognition system. IEEE Trans Inf Forensics Secur 12(11):2599–2610
37. Watanabe M, Endoh T, Shiohara M, Sasaki S (2005) Palm vein authentication technology and its applications. In: Proceedings of the biometric consortium conference, Citeseer, pp 19–21
38. Xi X, Yang G, Yin Y, Meng X (2013) Finger vein recognition with personalized feature selection. Sensors 13(9):11243–11259
39. Yang L, Yang G, Yin Y, Zhou L (2014) A survey of finger vein recognition. In: Chinese conference on biometric recognition (CCBR'14), vol 8833. Springer LNCS, pp 234–243
40. Yang W, Yu X, Liao Q (2009) Personal authentication using finger vein pattern and finger-dorsa texture fusion. In: Proceedings of the 17th ACM international conference on Multimedia. ACM, pp 905–908

41. Yin Y, Liu L, Sun X (2011) Sdumla-hmt: a multimodal biometric database. In: Biometric recognition, pp 260–268
42. Yuksel A, Akarun L, Sankur B (2011) Hand vein biometry based on geometry and appearance methods. IET Comput Vis 5(6):398–406
43. Zhang, C., Li, X., Liu, Z., Zhao, Q., Xu, H., Su, F.: The cfvd reflection-type finger-vein image database with evaluation baseline. In: Biometric recognition. Springer, pp 282–287

Online References and Data Sheets

44. Aliexpress (2018) 10x focusable 1230 metal housing w lens for TO-18 5.6 mm laser diode LD product page. https://www.aliexpress.com/item/10x-Focusable-1230-Metal-Housing-w-Lens-for-TO-18-5-6mm-Laser-Diode-LD/32665828682.html?spm=a2g0s.9042311.0.0.27424c4drx8E2d. Accessed 20 June 2018
45. Aliexpress (2018) Double IC two road ACC circuit laser diode driver board 650 nm 2.8–5 v adjustable constant current 0-390 mA 780 nm 808 nm 980 nm laser product page. https://www.aliexpress.com/item/Double-IC-Two-Road-ACC-Circuit-laser-Dode-Driver-Board-650nm-2-8-5v-Adjustable-Constant/32818824875.html?spm=a2g0s.9042311.0.0.27424c4drx8E2d. Accessed 20 June 2018
46. Aliexpress: TO-18 300 mW 808 nm NIR laser diode product page. https://www.aliexpress.com/item/5Pcs-lot-High-Quality-808nm-300mW-High-Power-Burning-Infrared-Laser-Diode-Lab/32272128336.html?spm=a2g0s.9042311.0.0.27424c4drx8E2d. Accessed 20 June 2018
47. Alpha & Omega Semiconductor (2018) AO3418 30V N-Channel MOSFET SMD data sheet. http://aosmd.com/pdfs/datasheet/AO3418.pdf. Accessed 20 June 2018
48. Arduino LLC: Arduino Nano manual. https://www.arduino.cc/en/uploads/Main/ArduinoNanoManual23.pdf. Accessed 20 June 2018
49. Continental Device India Limited (2018) BC327-25 PNP TO-92 silicon planar epitaxal transistor data sheet. http://pdf.datasheetcatalog.com/datasheet_pdf/continental-device-india-limited/BC327_to_BC338-40.pdf. Accessed 20 June 2018
50. Corporation, F.: Fujifilm HF9HA-1B product page. http://www.fujifilmusa.com/products/optical_devices/machine-vision/2-3-15/hf9ha-1b/index.html. Accessed 20 June 2018
51. Corporation H (2018) Hitachi H-1 finger-vein scanner product page. http://www.hitachi.co.jp/products/it/veinid/global/products/embedded_devices_u.html. Accessed 20 June 2018
52. Corporation M (2018) M2SYS M2-finger-vein reader product page. http://www.m2sys.com/finger-vein-reader/. Accessed 20 June 2018
53. Corporation M (2018) MIDOPT BN810 810 nm narrow near-IR bandpass filter product page. http://midopt.com/filters/bn810/. Accessed 20 June 2018
54. Corporation M (2018) MIDOPT BN850 850 nm narrow near-IR bandpass filter product page. http://midopt.com/filters/bn850/. Accessed 20 June 2018
55. Corporation M (2018) MIDOPT LP780 NIR pass-through filter product page. http://midopt.com/filters/lp780/. Accessed 20 June 2018
56. Corporation M (2018) MIDOPT LP830 NIR pass-through filter product page. http://midopt.com/filters/lp830/. Accessed 20 June 2018
57. Corporation M (2018) Mofiria FVA-U3SXE finger vein reader data sheet. https://www.mofiria.com/wp/wp-content/uploads/2017/08/FVA-U3SXE.pdf. Accessed 20 June 2018
58. Corporation M (2018) Mofiria FVA-U4BT finger vein reader data sheet (FVA-U4ST is the same device except for the USB instead of Bluetooth connection). https://www.mofiria.com/wp/wp-content/uploads/2017/08/FVA-U4BT_E.pdf. Accessed 20 June 2018
59. IDS Imaging Development Systems GmbH (2018) uEye software suite product and download page. https://de.ids-imaging.com/download-ueye-win32.html. Accessed 20 June 2018

60. IDS Imaging Development Systems GmbH (2018) UI-ML1240-NIR NIR-enhanced industrial camera data sheet. https://de.ids-imaging.com/IDS/datasheet_pdf.php?sku=AB00184. Accessed 20 June 2018
61. Lucky Light Electronics Co., Ltd. (2018) 504WC2E-W6-3PC 5 mm round with flange type warm white LED technical data sheet. https://www.luckylight.cn/media/component/datasheet/504WC2E-W6-3PC.pdf. Accessed 20 June 2018
62. Microchip Corporation (2018) Microchip AVR ATmega328P 8-bit microcontroller full data sheet. http://ww1.microchip.com/downloads/en/DeviceDoc/ATmega328_P%20AVR%20MCU%20with%20picoPower%20Technology%20Data%20Sheet%2040001984A.pdf. Accessed 20 June 2018
63. Microchip Corporation (2018) Microchip AVR ATmega328P 8-bit microcontroller product page. https://www.microchip.com/wwwproducts/en/ATmega328P. Accessed 20 June 2018
64. ON Semiconductor (2018) BC808 PNP SMD general purpose transistor data sheet. http://www.onsemi.com/pub/Collateral/BC808-25LT1-D.PDF. Accessed 20 June 2018
65. Osram Opto Semiconductors AG (2018) Osram SFH-4253-Z 850 nm NIR SMD LED data sheet. https://media.osram.info/media/resource/hires/osram-dam-2496162/SFH%204253.pdf. Accessed: 20 June 2018
66. Osram Opto Semiconductors AG (2018) Osram SFH-4550 850 nm high power infrared LED data sheet. https://dammedia.osram.info/media/resource/hires/osram-dam-5580407/SFH%204550_EN.pdf. Accessed 20 June 2018
67. Renesas Electronics (2019) Application Note AN1737—eye safety for proximity sensing using infrared light-emitting diodes. https://www.renesas.com/eu/en/doc/application-note/an1737.pdf. Accessed 20 Jan 2019
68. Texas Instruments Corporation (2018) Texas instruments TLC59401 16-channel LED driver with dot correction and greyscale PWM control data sheet. http://www.ti.com/lit/ds/sbvs137/sbvs137.pdf. Accessed 20 June 2018
69. Vishay Semiconductor (2018) TSUS540 series infrared emitting diode, 950 nm, GaAs data sheet. https://www.vishay.com/docs/81056/tsus5400.pdf. Accessed 20 June 2018
70. Vishay Siliconix (2018) IRF510 Hexfet power MOSFET T0-220 data sheet. https://www.vishay.com/docs/91015/sihf510.pdf. Accessed 20 June 2018

IEEE TRANSACTIONS ON BIOMETRICS, BEHAVIOR, AND IDENTITY SCIENCE, VOL. 1, NO. 2, APRIL 2019

Longitudinal Finger Rotation—Deformation Detection and Correction

Bernhard Prommegger, Christof Kauba, Michael Linortner, and Andreas Uhl

***Abstract*—Finger vein biometrics is becoming more and more popular. However, longitudinal finger rotation, which can easily occur in practical applications, causes severe problems as the resulting vein structure is deformed in a non-linear way. These problems will become even more important in the future, as finger vein scanners are evolving toward contact-less acquisition. This paper provides a systematic evaluation regarding the influence of longitudinal rotation on the performance of finger vein recognition systems and the degree to which the deformations can be corrected. It presents two novel approaches to correct the longitudinal rotation, one based on the known rotation angle. The second one compensates the rotational deformation by applying a rotation correction in both directions using a pre-defined angle combined with score level fusion and works without any knowledge of the actual rotation angle. During the experiments, the aforementioned approaches and two additional are applied: one correcting the deformations based on an analysis of the geometric shape of the finger and the second one applying an elliptic pattern normalization of the region of interest. The experimental results confirm the negative impact of longitudinal rotation on the recognition performance and prove that its correction noticeably improves the performance again.**

***Index Terms*—Finger vein recognition, longitudinal finger rotation, finger rotation detection, finger rotation correction, biometric fusion.**

I. Introduction

VASCULAR pattern based biometric systems, commonly denoted as vein biometrics, offer several advantages over other well-established biometric recognition systems. In particular, hand and finger vein systems have become a serious alternative to fingerprint based ones for several applications. Vein based systems use the structure of the blood vessels inside the human body, which becomes visible under near-infrared (NIR) light. As the vein structure is located inside the human body, it is resistant to abrasion and external influences on the skin. Furthermore, a lifeness detection to detect presentation attacks can be performed easily [1].

Manuscript received September 10, 2018; revised January 15, 2019; accepted February 14, 2019. Date of publication March 7, 2019; date of current version April 19, 2019. This work was supported in part by the European Union's Horizon 2020 Research and Innovation Program under Grant 700259, and in part by the FFG KIRAS Project AUTFingerATM under Grant 864785. This paper was recommended for publication by Associate Editor D. Maio upon evaluation of the reviewers' comments. *(Corresponding author: Bernhard Prommegger.)*

The authors are with the Department of Computer Sciences, University of Salzburg, 5020 Salzburg, Austria (e-mail: bprommeg@cs.sbg.ac.at; ckauba@cs.sbg.ac.at; mlinortner@cs.sbg.ac.at; uhl@cs.sbg.ac.at).

Digital Object Identifier 10.1109/TBIOM.2019.2902020

The performance of finger vein recognition systems suffers from different internal and external factors. Internal factors include the design and configuration of the sensor itself, especially the NIR light source and the camera module. External factors include environmental conditions (e.g., temperature and humidity) and deformations due to misplacement of the finger, typically including shifts, tilt, bending and longitudinal rotation which will be further examined in this work.

Performance degradations caused by various types of finger misplacement are not new and have been addressed in several publications. The need for a robust finger vein image normalisation including rotational alignment has already been mentioned by Kumar and Zhou in 2012 [1]. Chen *et al.* [2] state that deformation correction can be done either during pre-processing, feature extraction or comparison. Moreover, the physical design of the sensor can help to avoid misplacements of the finger. Prommegger *et al.* [3] showed, that longitudinal finger rotation has a severe influence on the recognition performance of a finger vein recognition system. There are several approaches that try to reduce the influence of these issues during the processing of the vein patterns. Kumar and Zhou [1] introduced a finger alignment based on the finger boundary to overcome finger translation and rotation. Lee *et al.* [4] proposed a system utilizing a minutia based alignment together with local binary patterns as feature extraction method. Huang *et al.* [5] improved the resistance against longitudinal rotation by applying an elliptic pattern normalization to the input images. Matsuda *et al.* [6] proposed a feature-point based recognition system introducing a finger-shape model and a non-rigid registration method. They achieved robustness against longitudinal rotation up to $\pm 30°$. Yang *et al.* [7] introduced a finger vein recognition framework including an anatomy structure analysis based vein extraction algorithm and integration matching strategy. Chen *et al.* [2] introduced an approach that detects different types of finger deformation by analysing the shape of the finger, e.g., around the longitudinal axis, and corrects them using linear and non-linear transformations. Besides these software based solutions, there are some hardware-based ones which aim to prevent finger misplacements in the first place, during acquisition, rather than correcting them afterwards. Kauba *et al.* [8] presented a finger vein scanner that captures three fingers at once and requires the subject to place the fingers in a flat, aligned position on a finger shaped guiding surface. This reduces longitudinal finger rotation, planar finger rotation as well as finger shifts to a minimum. To the best of our knowledge, there is no method that satisfactory solves the problem

of longitudinal finger rotation. Problems resulting from finger misplacements, e.g., longitudinal rotation, will receive more attention in the future as finger vein systems evolve towards contact-less operation.

The main contribution of our work is the systematic analysis to which extent a longitudinal finger rotation can be compensated and which impact such a correction has on the recognition accuracy of the finger vein recognition system. This analysis extends the authors previous work [3], [9]. Therefore, we evaluate four different methods to correct the longitudinal rotaion, where the first and the last on are proposed in this work:

1) A correction using the actual rotation angle provided by the data set and a circular projective correction. This approach has not been applied in finger vein recognition and serves as a reference for the effectiveness of the other rotation compensation methods.
2) A method proposed by Chen *et al.* [2] that analyses the geometric shape of the finger and corrects the deformations based on the results.
3) Elliptic pattern normalization of the region of interest as proposed by Huang *et al.* [5].
4) A new method proposed in this article that compensates the rotational deformations without the knowledge of the actual rotation angle by applying a rotation correction in both directions using a pre-defined angle combined with score level fusion.

To verify the effectiveness of the proposed approach (4), it is also applied on two commonly used finger vein data sets, namely UTFVP [10] and SDUMLA-HMT [11].

The rest of this paper is organized as follows: Longitudinal finger rotation and its problems caused for finger vein recognition systems are described in more detail in Section II. Section III explains all details of the used rotation compensation methods. Section IV explains the processing tool-chain and the used data set together with the experimental set-up. Furthermore it includes the experimental results together with a discussion. Section V concludes the paper along with an outlook on future work.

II. Longitudinal Finger Rotation

While capturing finger vein images, the finger's placement on the scanner is not necessarily done in an optimal way. Such misplacements result in deformations of the vein structure, affecting the performance of a finger vein recognition system. Fig. 1 shows the orientations of the x, y and z axis with respect to the finger. The different types of misplacements include:

- shifts of the finger in x- and y-direction (planar shifts)
- shifts of the finger in z-direction (distance to the camera, scaling)
- planar rotation of the finger (in the xy-plane)
- tilts of the finger (finger tip and finger root are not in the same xy-plane)
- finger bending and
- rotation around the longitudinal axis of the finger (y-axis).

As described in the authors' previous work [3], some of the problematic misplacements can be reduced or even completely prevented during acquisition by adding simple support structures on the scanner, e.g., guiding walls to prevent planar shifts. Moreover, they can be corrected by the biometric processing chain during pre-processing (finger alignment during ROI extraction) or feature extraction and comparison (using x- and y-direction shifted and rotated versions of the extracted templates). Almost all currently available commercial off-the-shelf (COTS) sensors are equipped with such support structures, but most of them are still not able to prevent a rotation around the y-axis (longitudinal finger rotation). Thus, longitudinal finger rotation cannot be ruled out and poses a severe problem to finger vein recognition systems. Fig. 2 shows an example of the longitudinal finger rotation while using a COTS scanner. In a supervised acquisition scenario, the user can be guided to place the finger correctly. However, in unsupervised operation of the scanner, such longitudinal rotations are highly likely to occur. As finger vein scanner development tends towards contact-less operation, the problem of finger misplacement is getting more serious due the increased degrees of freedom and the inability to use guiding structures.

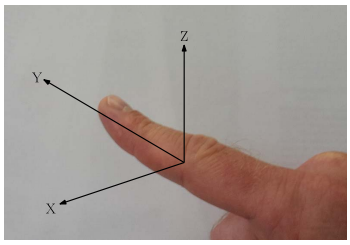

Fig. 1. Definition of the axes of a finger in a three-dimensional space.

Fig. 2. Finger rotation example using a commercial off-the-shelf scanner (rotation counter-clockwise, originally published in [3]).

The captured vein structure is a projection of the vessel structure in the 3D space onto a 2D plane. If the finger is rotated along its longitudinal axis, the vein pattern is deformed according to a non-linear transformation. Fig. 3. shows the effect of longitudinal finger rotation on the vein pattern. The finger cross section (top row) is rotated from $-30°$ to $+30°$. As a result of this rotation, the projected pattern of the veins (bottom row) changes as well. Depending on the relative position of the veins to each other and the rotation angle, some of the captured veins might merge into a single one. The vein structures of $-30°$ (left), $0°$ (middle) and $30°$ (right) are completely

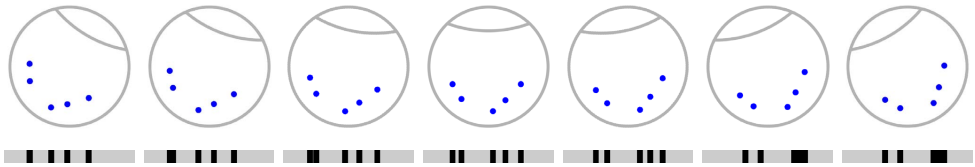

Fig. 3. Longtitudinal finger rotation principle: A schematic finger cross section showing five veins (blue dots) rotated from −30° (left) to +30° (right) in 10° steps. The projection (bottom row) of the vein pattern is different according to the rotation angle following a non-linear transformation (originally published in [3]).

different. Widely used vein recognition schemes can handle such deformations only to a certain extent [3]. If the deformations caused by the longitudinal rotation are corrected, the negative impact can be reduced, but not completely mitigated.

III. Finger Rotation Compensation

As longitudinal finger rotation decreases the performance of a finger vein recognition system, it is beneficial to compensate the deformations caused by this rotation. In this study, four different approaches to tackle this problem are discussed and analysed. The first approach which has not been applied in finger vein recognition sp far assumes that the longitudinal rotation angle is known and compensates the deformation by applying a non-linear transformation in the opposite direction. This kind of analysis was only possible because the *PLUSVein Finger Rotation data set* (PLUSVein-FR) provides the actual angle of the longitudinal finger rotation. The results of this method can be used as a reference for the evaluation of the effectiveness of the other rotation correction methods as the results of this method will be close to the possible best achievable results. The second approach, proposed by Chen *et al.* [2], tries to detect the finger rotation by analysing the finger shape and again correcting it using a non-linear transformation. The third method applies an elliptic pattern normalization (EPN) [5] of the acquired image to reduce the deformations. The last approach is a novel approach proposed by the authors. It applies a rotation compensation in both directions using a fixed angle together with a maximum rule score level fusion. Its main advantage is that no prior knowledge of the actual rotation angle is required.

A. Rotation Compensation for Known Rotation Angle

For an accurate correction of the vein pattern the position of the veins in the 2D image as well as the shape of the finger and the depth of the veins within the finger has to be known. As this information is not available in general, both need to be estimated. We approximate the shape of the finger as a circle like Matsuda *et al.* did in [6]. We further assume, that the veins are located on the skin surface instead of underneath the skin. Therefore, the vein pattern is projected back on the outer circle of the finger. Fig. 4 depicts this principle. The left image shows a schematic cross section of a finger acquired with a longitudinal rotation $\varphi_{rotate} = 25°$. The blue dots represent the veins in their proper position, the red ones those that are projected onto the skin. The bar below is a visualization of the

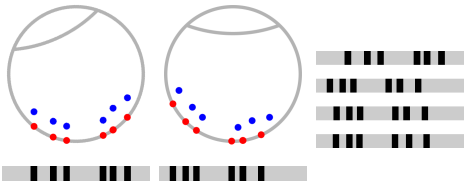

Fig. 4. Principle of rotation correction with known rotation angle. Left: finger rotated with 25°. The blue points depict the veins inside the finger, the red points the veins projected on the finger shape. The bar below is the projected vein pattern. Middle: the finger rotated into the palmar view. The bar below is the rotation corrected vein pattern, which corresponds to the veins estimated on the finger surface. On the right side the vein patterns are visualized below each other. From top to bottom: rotated vein pattern, corrected vein pattern, corrected pattern shifted for the highest correlation to the palmar pattern (bottom row).

vein pattern, where the black areas correspond to the veins. In the middle image, the finger is rotated back into the ideal palmar position ($\varphi_{rotate} = 0°$). It is clearly visible that the blue and red dots are not perfectly aligned with each other. From top to bottom, the right side shows the vein patterns of the acquired image (same as on the left side), the rotated pattern (same as in the middle), a shifted version of the rotated pattern and the original pattern that would have been acquired without the presence of longitudinal rotation. The rotation corrected pattern is clearly more similar to the original pattern than the acquired one. The additional shift is applied to achieve a higher correlation between the corrected patterns and the original one.

The position of a pixel within the vein pattern is defined by its x-coordinate x_r and the corresponding y-coordinate y_r, which is calculated by (1)

$$y_r = \sqrt{r^2 - x_r^2} \tag{1}$$

where r is the approximated radius of the finger. r is half the finger width, which corresponds to half of the height of the extracted finger ROI. The rotation back into the palmar view is calculated by applying the rotation matrix given in (2).

$$\begin{bmatrix} x_p \\ y_p \end{bmatrix} = \begin{bmatrix} cos(-\varphi_{rotate}) & -sin(-\varphi_{rotate}) \\ sin(-\varphi_{rotate}) & cos(-\varphi_{rotate}) \end{bmatrix} * \begin{bmatrix} x_r \\ y_r \end{bmatrix} \tag{2}$$

x_p and y_p are the corrected coordinates of the vein pixel in the palmar view and φ_{rotate} is the rotation angle. If the veins are located on the skin surface and the finger radius is known exactly, this method is accurate. In practice, the blood vessels

are inside the finger and the finger outline detection my not be completely accurate, thus there remains a small deviation.

B. Geometric Shape Analysis Based Finger Rotation Deformation Detection and Correction

Chen *et al.* [2] proposed a method to detect and correct finger deformations based on a geometric shape analysis (GADC). They distinguished three types of finger deformations: finger tilt, finger bending and longitudinal finger rotation. In this work only longitudinal finger rotation, which Chen *et al.* called a type 3 deformation, is discussed. For the shape analysis they defined several parameters, on the basis of which they calculated statistical measures of the finger. These parameters are described in Section II of the original paper. The detection of a type 3 deformation is based on the bending at the proximal inter-phalangeal joint. If the absolute difference of the upper and lower angle of the finger outline at the joint, α_{upp_joint1} and α_{down_joint1}, is larger than a defined threshold $t_{3rotate}$, a deformation of type 3 is present and the image has to be corrected. The rotation correction is applied either in the one or the other direction using a fixed sampling scheme. Thus, the same fixed correction is applied independent of the actual rotation angle. A detailed description of the rotation detection and correction scheme can be found in [2].

C. Elliptic Pattern Normalization

Huang *et al.* [5] proposed a normalization of the vein pattern in the feature space. The method is based on the hypothesis, that the cross section of a finger approximately resembles an ellipsis and that the veins which are captured by the finger vein scanner are located close to the finger surface. Their normalization essentially corresponds to a rolling of the finger, which reduces the non-linear deformation of the vein structure across the entire width of the finger. After this correction is applied, a horizontal shift of the images during comparison corresponds to a rotation of the finger. They applied the elliptic normalization in the feature space using a vein pattern based feature extraction. As this paper also investigates algorithms that are not vein pattern based, an elliptic correction in the feature space is not feasible for all of them. Therefore, the correction is applied in the image space. This way the normalization can be used for all algorithms under investigation. For more details on this method, the interested reader is referred to the original work [5].

D. Rotation Compensation Using a Fixed Angle

In real world scenarios, the longitudinal rotation angle is unknown and its estimation is a difficult task. Hence, a method that does not require the rotation angle to correct the images would be beneficial. As shown in [3], commonly used recognition schemes tolerate rotations of at least $\pm 10°$. Thus, a system that is able to keep the deformations caused by the longitudinal rotation within this range is desirable.

The proposed method for correcting longitudinal finger rotation is based on rotations of the image in both directions using a fixed compensation angle. The final score is calculated using a maximum rule score level fusion of the three comparisons (original, non-rotated image and the two rotated versions).

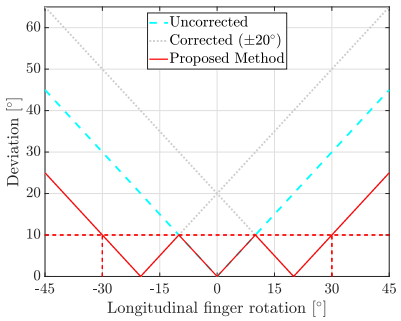

Fig. 5. Deviation of the rotated finger to the palmar view with an correction angle $\varphi_{corr} = 20°$.

It is assumed that the enrolment data is acquired in a constrained environment. Thus, the longitudinal rotation of the enrolment data should be close to 0°. During the image acquisition, the finger can be positioned either correctly (no rotation) or rotated to the left or to right side. In order to reduce the rotational deviation between the two samples, comparisons using the captured sample itself with respect to the unmodified enrolled sample and its rotated versions in both directions are applied. The angle of the applied rotation φ_{corr} is defined in advance. The applied rotation compensation is the same as explained in Section III-A: the finger is approximated as a circle and the image is projected on this circle prior to applying the rotation correction.

Fig. 5 illustrates how this approach reduces the rotational deviation with φ_{corr} = 20°. The dashed cyan line shows the deviation of the rotation for the original data. The dotted grey lines represent the deviation of the data corrected with $\pm\varphi_{corr}$. The red line corresponds to the minimum deviation of all images to the enrolled one. It can be seen that the rotational angle of the sample compared to the original deviation is reduced. For example, if the probe sample is rotated $\varphi = 30°$ from the enrolled sample, the following comparisons are done:

1) The probe sample against the unmodified enrolled sample: rotation angle between the compared images: 30°.
2) The probe sample against the enrolled image rotated with φ_{corr}: rotation angle of $-\varphi+\varphi_{corr} = -30°+20° = 10°$.
3) The probe sample against the enrolled image rotated with $-\varphi_{corr}$: rotation angle of $-\varphi - \varphi_{corr} = -30° - 20° = 50°$.

If $\varphi_{corr} = 20°$, the deviation does not exceed 10° if the rotation angle stays within a range of $\pm 30°$. This deviation can be handled by commonly used recognition schemes and thus, the performance degradation can be kept at an acceptable level. The best choice for φ_{corr} depends on the actual application and the scanner device. The useful range of φ_{corr} is in the range of 5° to 25° for most applications.

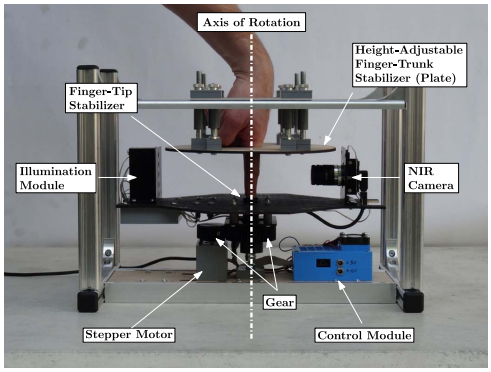

Fig. 6. Basic principle of the multi-perspective finger vein scanner used to acquire the *PLUSVein-FR* data set (originally published in [9], © 2018 IEEE).

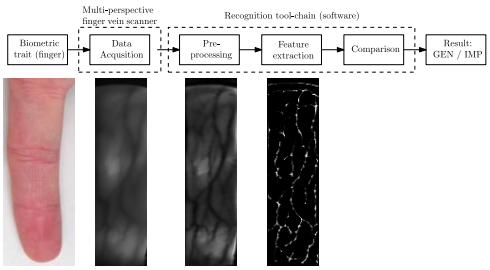

Fig. 7. Basic components of a biometric recognition system (originally published in [3]).

IV. Experiments

During the experiments, the four rotation compensation approaches described in Section III are applied on the *PLUSVein finger rotation data set*, which is described in the following subsection. Furthermore, to verify effectiveness of the proposed fixed angle method, it is applied on the publicly available finger vein data sets UTFVP [10] und SDUMLA-HMT [11].

A. PLUSVein Finger Rotation Data Set

The *PLUSVein Finger rotation data set* (PLUSVein-FR) has been acquired using a custom designed multi-perspective finger vein scanner as depicted in Fig. 6. It provides finger vein images all around the finger (360°) with a resolution of 1°. The finger is placed in the center of the scanner (axis of rotation), whereas the NIR camera (right side) and the NIR illumination unit (left side) are placed on opposite sides of the finger (light transmission). The different projections of the finger are acquired by rotating the camera and the illumination module around the finger.

The data set contains finger images captured from 63 different subjects, 4 fingers per subject, which sums up to a total of 252 unique fingers. Each finger is acquired 5 times. This results in 1.260 images per perspective. In this work, we use the perspectives in the range of ±45° around the palmar view in steps of 1°. For more details on the data set and the multi-perspective finger vein scanner, the interested reader is referred to the authors previous publications [3], [9]. The data set is publicly available for research purposes at http://wavelab.at/sources/PLUSVein-FingerRotationDataSet.

B. Recognition Tool-Chain

The components of the recognition tool-chain are visualized in Fig. 7, which are the same as in the authors previous work [9]: First, the biometric trait is acquired by the multi-perspective finger vein scanner as a video sequence. The subsequent tool-chain consists of pre-processing (ROI (region of interest) extraction and image enhancement), feature extraction and comparison. At first the frames corresponding to 1° steps are extracted from the video sequences. Afterwards each image is processed individually: the ROI is extracted and the finger outline is detected using an edge detection algorithm. Then a straight line is fitted to the center of the finger. Based on this line, the finger is aligned (rotated and vertically shifted) such that it is in horizontal position and the center line of the finger is in the middle of the image. The area outside of the finger lines is masked out (pixels set to black). Afterwards, the image is cut to a pre-defined length of 1100 pixels. The height of the finger is normalized to a height of 300 pixels throughout the whole length of the finger image. To avoid artifacts at the image borders, 10 pixels are cut off on each side. The resulting ROI has a size of 280×1080 pixels. Fig. 8 visualizes this process. The top image shows the finger with the center and finger lines, the bottom image shows the final ROI. Furthermore, to improve the visibility of the vein patterns **High Frequency Emphasis Filtering** (HFE) [12], **Circular Gabor Filter** (CGF) [13] and simple **CLAHE** (local histogram equalisation) [14] are used as pre-processing techniques. For more details on the pre-processing methods refer to [15]. This study compares four simple and one advanced vein pattern based feature extraction methods which is based on the analysis of the anatomy structure of the veins. **Maximum Curvature** (MC) [16], **Principal Curvature** (PC) [17], **Wide Line Detector** (WLD) [5] and **Gabor Filter** (GF) [1] aim to extract the vein pattern from the background resulting in a binary image, followed by a comparison of these binary images. Comparing the binary feature images is done using a correlation measure, calculated between the input images and in x- and y-direction shifted and rotated versions of the reference image. The more sophisticated vein pattern based method, **Finger Vein Recognition With Anatomy Structure Analysis** (ASAVE), proposed by Yang *et al.* [7], is a finger vein recognition framework which includes an anatomy structure analysis based vein extraction algorithm and an integration matching strategy. In addition, two keypoint based recognition schemes, a **SIFT** [15] based technique with additional keypoint filtering and **Deformation-Tolerant Feature-Point Matching** (DTFPM) proposed by Matsuda *et al.* [6] are evaluated.

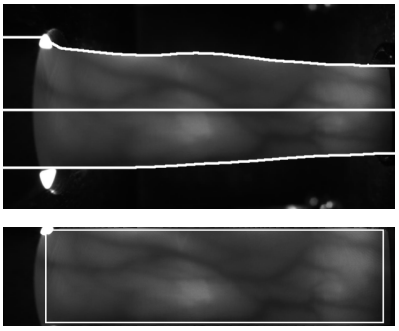

Fig. 8. ROI extraction - top: finger line detection. The straight line in the middle represents the center of the finger at which it is horizontally aligned. The top and bottom lines are the detected finger outlines which separate the finger from the background. The region between the lines is regarded as finger region. Bottom: the finger region is transformed to a fixed height. Afterwards the ROI, visualized as white square, of a fixed size is cut out.

TABLE I
NUMBER OF COMPARISONS FOR EACH SUBSETS

Name	Subjects	Genuine	Impostor	Total
Subset 1	32	3200	16384	19584
Subset 2	31	3100	15376	18476
Total	63	6300	31760	38060

C. Evaluation Protocol

To quantify the performance, the EER, the FMR100 (the lowest FNMR for FMR $\leq$ 1%), the FMR1000 (the lowest FNMR for FMR $\leq$ 0,1%) as well as the ZeroFMR (the lowest FNMR for FMR $=$ 0%) are used. The data set is divided into two roughly equal sized subsets. The division is based on the contained subjects, i.e., all fingers of the same person are in one subset. Each subset is used to determine the parameters which are then applied to the other subset. This ensures a 100% separation of the data used for determining the optimal parameters and the actual test set. The evaluation within the subsets follows the test protocol of the FVC2004 [18]: for calculating the genuine scores, all possible genuine comparisons are performed. For calculating the impostor scores, only the first image of each finger is compared to the first image of all other fingers. The resulting number of comparisons for both subsets are listed in Table I. The final results are evaluated based on the combined scores (genuine and impostor) of both test runs. The parameter optimization is executed only for the original, unmodified data set. The same parameter settings are applied for all experiments on the modified versions of the data sets too.

To quantify the decrease in performance for the rotated finger vein images, the relative performance degradation (RPD), which is calculated as stated in equation (3), is used:

$$RPD = \frac{EER_x - EER_{ref}}{EER_{ref}}. \quad (3)$$

EER_{ref} is the EER of the reference data set and EER_x the EER of the evaluated data set. A RPD of 0 means no change in performance, a RPD of 1 corresponds to an EER increase to its doubled value. For a negative RPD, the performance increased. For the evaluation of the performance increase due to rotation correction, the relative performance increase (RPI) as in equation (4) is calculated:

$$RPI = \frac{EER_{ref} - EER_x}{EER_x}. \quad (4)$$

Again, EER_{ref} is the EER of the reference data set and EER_x the EER of the evaluated data set. A RPI of 0 means no change in the performance, a RPI of 1 corresponds to a drop in the EER to half of its value. For a negative RPI, the performance decreased. All values are given in percentage terms, e.g., 2.35 means 2.35%.

An implementation of the complete tool-chain as well as the used configuration files and results (EER, FMR100, FMR1000 and ZeroFMR) are available for download at: http://www.wavelab.at/sources/Prommegger19a.

TABLE II
BASELINE PERFORMANCE RESULTS AT THE PALMAR VIEW FOR THE DIFFERENT RECOGNITION SCHEMES ORDERED BY RECOGNITION PERFORMANCE

Feature	EER	FMR100	FMR1000	ZeroFMR
MC	0.37 ($\pm$0.09)	0.30	0.43	0.84
PC	0.77 ($\pm$0.13)	0.70	1.37	1.92
DTFPM	0.87 ($\pm$0.14)	0.83	2.27	6.85
WLD	0.92 ($\pm$0.14)	0.92	1.29	2.80
GF	1.02 ($\pm$0.15)	1.02	1.70	2.61
SIFT	1.80 ($\pm$0.20)	2.05	4.10	6.97
ASAVE	2.96 ($\pm$0.25)	3.91	5.74	15.07

D. Baseline Results

In order to quantify the change of the recognition performance due to rotation correction, the results of the unmodified PLUSVein-FR are calculated. In finger vein recognition usually the palmar perspective is used [10], [11], [19]–[22]. The performance of the data set achieved at this view is stated in Table II. The results are comparable to other publicly available finger vein data sets: MC achieves the best recognition rate with an EER of 0.37%, followed by PC, DTFPM, WLD, GF and SIFT while ASAVE, with an EER of 2.96%, performs worst.

The images captured at the different rotation angles from $-45°$ to $45°$ are compared to the palmar view (no rotation, $0°$). The trend of the absolute EER is shown in Fig. 9. MC, PC and WLD follow the same trend: They start at an EER $<$ 1% and keep quite a stable performance up to $\pm 15°$, where their EER is still $<$ 1.5%. Higher rotations lead to a fast drop of the performance. At a rotation of $\pm 45°$, their EER is $>$ 40%. The trend of GF, the fourth of the simple vein pattern based methods, is similar, but its performance degradation is more prominent. Both keypoint based methods are more robust against longitudinal rotation. DTFPM shows the overall best performance and outperforms all vein pattern based methods for rotation angles higher than $\pm 30°$. At $\pm 45°$ its EER is still $<$ 20%. SIFT outperforms the other methods starting at $\pm 35°$ and achieves an EER of $<$ 30% at $\pm 45°$. The more sophisticated ASAVE framework shows no advantage over the simple vein pattern based methods: It starts at a higher baseline EER

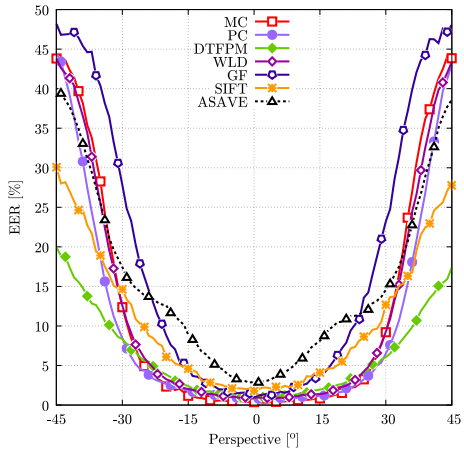

Fig. 9. Trend of the EER across the different rotation angles (0° corresponds to the palmar view) for the original, unmodified data set from −45° to 45°.

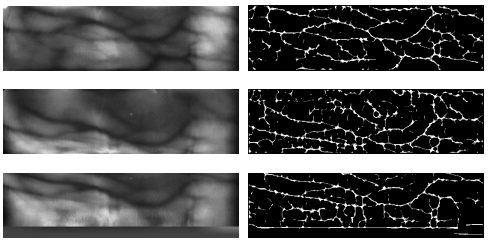

Fig. 10. ROI (left) and extracted MC features (right) of sample images of the PLUSVein-FR. First row: palmar view (0°), second row: 25° rotated view, bottom row: rotation corrected version of the 25° rotated image.

of 3% and its performance degrades towards higher rotation angles too, arriving at an EER of about 40% at ±45° as well.

As already shown in [3], all recognition schemes are able to tolerate a longitudinal finger rotation up to ±10°, while still achieving an acceptable performance. The EER values as well as the RPD for selected perspectives are stated in Table III. This table lists the performance indicators for all applied rotation correction methods and recognition schemes. The RPD is always calculated with respect to the palmar view (0°) of the same recognition scheme and rotation correction method. This allows a direct comparison of the different methods. Since the recognition results for rotations in both directions are almost symmetrical, the table only contains values for positive rotation angles.

E. Rotation Compensation for Known Rotation Angle

As mentioned in Section IV-A, for the PLUSVein-FR the exact angle of the longitudinal finger rotation is known. This fact can be exploited to apply an actual correction of the longitudinal finger rotation as described in Section III-A. Fig. 10

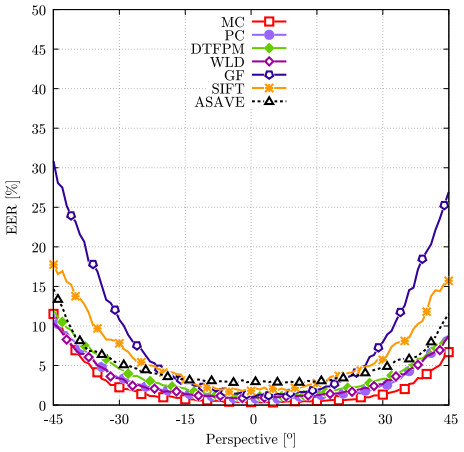

Fig. 11. Trend of the EER across the different rotation angles applying an exact longitudinal finger rotation compensation (0° corresponds to the reference, palmar view) from −45° to 45°.

depicts the ROI (left side) and the extracted MC features (right side) for different views. The images in the top row are from the palmar view, the middle shows the ones from a 25° rotated finger and the bottom row its corrected version. It is clearly visible that the vein structure of the rotated image (middle row) is a deformed version of the palmar one (top row). The vein structures of the rotation corrected images in the bottom row are more similar to the palmar images than the uncorrected ones. The part of the corrected ROI image that contains no information (due to the transform) is filled with the average grey level of the image.

Fig. 11 depicts the trend of the EER for the corrected images. For all methods, the drop in the recognition performance is less pronounced than without rotation compensation. Again, MC, PC and WLD show a similar trend: Up to a rotation angle of ±30° the EER stays below 3%. Even for a rotation of ±45° their EER is still below 9%. The performance of keypoint based algorithms increases as well, but not to the same extent as for MC, PC and WLD. These algorithms are already tolerant against longitudinal rotation, and thus, the potential for improvement due to rotation correction is smaller. Neither DTFPM, nor SIFT outperform the three simple vein pattern based methods. ASAVE benefits most from this correction: With a maximum RPD of $< 300\%$ over the whole range of ±45°, it exhibits the lowest performance degradation. Although, due to its low baseline performance, all methods except SIFT and GF still outperform ASAVE in terms of absolute EER. Again, GF shows the fastest performance degradation among all algorithms. These results indicate, that especially simple vein pattern based methods get the most out of the longitudinal rotation compensation. They are even able to outperform more sophisticated methods like DTFPM. Keypoint based methods, which are robust against rotation to some level, do only benefit from the correction to a small extent.

TABLE III
PERFORMANCE RESULTS IN TERMS OF EER AND RPD OF ALL CORRECTION METHODS AND RECOGNITION SCHEMES. THE RPD IS ALWAYS CALCULATED WITH RESPECT TO THE PALMAR VIEW (0°) OF THE SAME RECOGNITION SCHEME AND ROTATION CORRECTION METHOD. THE HIGHLIGHTED RESULTS (BOLD FACE) REPRESENT THE BEST RECOGNITION RATES FOR A RECOGNITION SCHEME AT THE SPECIFIED ROTATION ANGLE

Method	Rotation angle	No Correction		Known Angle		GADC		EPN		Fixed Angle		Fixed Angle + EPN	
		EER	*RPD*	*EER*	*RPD*	*EER*	*RPD*	*EER*	*RPD*	*EER*	*RPD*	*EER*	*RPD*
MC	0°	0.37	—	0.37	—	0.59	—	**0.17**	—	0.28	—	0.21	—
	5°	0.41	13.15	0.34	-8.26	0.81	37.29	0.17	0.97	0.30	6.18	**0.16**	-23.26
	10°	0.63	73.37	0.49	34.51	0.96	62.32	0.25	47.24	0.32	12.37	**0.19**	-7.75
	15°	0.84	130.68	0.52	42.86	1.11	86.94	**0.32**	84.36	0.38	33.71	0.34	62.80
	20°	1.54	320.82	0.62	68.94	2.05	246.62	0.67	286.94	0.62	117.99	**0.44**	115.50
	25°	3.25	788.35	0.99	169.35	4.42	646.06	1.13	555.40	1.00	252.26	**0.75**	262.02
	30°	9.21	2415.79	1.32	260.14	11.66	1866.52	1.99	1051.57	1.46	413.50	**1.05**	407.75
	35°	23.68	6372.16	2.03	453.54	25.21	4152.94	4.61	2570.63	2.55	798.34	**1.74**	746.51
	40°	37.39	10119.38	3.93	974.29	37.85	6284.78	10.88	6205.09	5.19	1724.77	**2.88**	1296.93
	45°	43.84	11882.56	6.69	1728.68	43.51	7239.77	25.19	14500.85	9.66	3299.00	**4.62**	2145.00
PC	0°	0.77	—	0.77	—	0.86	—	0.51	—	0.65	—	**0.46**	—
	5°	0.75	-2.67	0.76	-0.59	0.78	-9.23	0.51	0.04	0.65	0.00	**0.43**	-6.94
	10°	0.89	15.81	0.87	13.73	0.98	14.36	0.49	-3.45	0.92	41.17	**0.41**	-10.42
	15°	1.13	47.05	1.11	44.97	1.26	46.40	0.52	3.19	0.97	48.53	**0.46**	0.00
	20°	1.65	114.89	1.48	92.45	1.81	110.97	0.81	59.38	1.34	105.15	**0.63**	37.50
	25°	3.26	324.80	1.62	111.15	3.84	346.83	1.21	137.66	1.70	161.28	**0.86**	87.16
	30°	6.52	748.56	2.56	232.94	8.37	873.41	1.94	281.33	2.44	274.26	**1.16**	152.09
	35°	15.36	1897.84	3.93	411.87	17.91	1983.44	3.67	623.05	3.79	481.61	**1.78**	286.81
	40°	30.37	3851.08	6.06	688.84	31.64	3580.94	9.13	1697.57	5.45	736.03	**2.84**	517.36
	45°	43.01	5496.60	8.75	1038.17	42.97	4898.52	20.34	3903.85	8.46	1199.25	**3.98**	766.32
DTFPM	0°	0.87	—	0.87	—	1.21	—	1.00	—	**0.81**	—	0.94	—
	5°	1.02	17.23	1.16	32.78	1.55	27.63	1.43	43.49	**0.98**	21.74	1.32	40.58
	10°	1.40	60.34	1.35	54.67	1.97	62.64	1.79	79.82	**0.98**	20.75	1.45	53.82
	15°	1.96	124.60	1.52	73.39	2.85	135.10	1.85	85.83	**1.44**	78.66	1.52	61.62
	20°	2.65	203.56	2.00	128.99	3.86	218.31	2.32	132.46	**1.89**	133.40	1.97	109.50
	25°	4.16	375.71	**2.38**	172.86	5.14	323.97	3.68	269.44	2.87	255.74	3.12	231.59
	30°	6.05	591.73	**3.31**	278.31	7.43	512.76	5.79	480.59	4.35	438.76	5.16	448.71
	35°	9.12	943.91	**4.53**	417.93	10.62	775.74	8.10	711.94	6.78	739.54	7.14	658.74
	40°	13.50	1445.01	**6.37**	628.50	14.70	1111.82	9.78	881.15	9.74	1105.54	8.64	818.49
	45°	17.33	1883.09	**8.66**	891.01	18.35	1413.10	12.81	1184.81	13.83	1612.08	11.50	1122.53
WLD	0°	0.92	—	0.92	—	1.13	—	0.72	—	0.78	—	**0.65**	—
	5°	0.84	-8.61	1.02	9.90	1.28	12.95	0.75	4.51	0.79	2.26	**0.57**	-12.23
	10°	1.10	18.87	1.11	20.42	1.37	20.98	0.84	17.64	1.03	32.92	**0.70**	7.09
	15°	1.38	49.90	1.24	34.32	1.61	42.83	0.91	26.85	1.14	47.12	**0.87**	33.49
	20°	2.30	149.57	1.46	58.43	2.69	137.91	1.31	82.31	1.47	89.50	**1.14**	75.06
	25°	4.25	360.57	2.01	117.74	5.54	390.24	1.92	168.44	2.00	157.62	**1.49**	128.60
	30°	9.29	905.55	2.64	185.55	11.85	949.21	2.89	304.11	2.63	239.51	**1.99**	204.40
	35°	21.26	2202.19	3.88	319.93	23.47	1977.35	5.43	658.91	3.98	413.17	**2.60**	298.77
	40°	35.06	3696.61	6.22	573.82	35.86	3074.41	12.08	1587.46	6.03	677.38	**4.12**	531.52
	45°	43.34	4593.00	8.72	843.73	43.31	3734.29	24.35	3301.41	10.24	1219.98	**5.98**	815.63
GF	0°	1.02	—	1.02	—	2.15	—	0.40	—	0.76	—	**0.38**	—
	5°	1.50	47.55	1.29	27.41	2.81	30.95	0.60	51.87	1.02	33.54	**0.46**	20.50
	10°	2.34	130.05	1.52	50.01	4.01	86.47	0.67	67.88	1.32	72.96	**0.41**	7.95
	15°	3.90	283.84	1.94	90.97	5.20	142.12	0.97	144.29	1.87	145.91	**0.59**	53.55
	20°	7.16	604.34	2.93	188.74	8.88	313.38	1.77	343.63	2.91	281.76	**1.00**	161.08
	25°	13.57	1234.95	4.80	372.34	15.53	622.82	2.87	620.23	5.02	559.12	**1.63**	327.61
	30°	23.21	2183.73	7.95	681.83	25.30	1077.10	5.57	1300.74	8.32	992.67	**2.84**	643.92
	35°	37.14	3554.99	12.59	1138.61	37.79	1658.20	10.57	2556.57	14.09	1749.70	**4.79**	1156.47
	40°	46.26	4452.59	19.42	1810.58	46.45	2061.23	20.10	4951.93	21.49	2722.22	**8.22**	2053.95
	45°	48.05	4628.08	26.92	2549.20	48.05	2135.60	34.55	8585.07	28.78	3678.84	**12.74**	3238.87
SIFT	0°	1.80	—	1.80	—	2.02	—	1.32	—	1.54	—	**1.25**	—
	5°	2.30	28.26	2.05	14.14	2.46	22.14	1.42	7.83	1.72	11.83	**1.37**	9.34
	10°	2.56	42.53	2.19	21.80	2.75	36.10	1.80	36.72	2.43	57.96	**1.71**	36.39
	15°	4.11	129.08	2.78	54.57	4.27	111.53	2.40	82.42	3.08	99.82	**2.19**	75.02
	20°	5.51	206.72	3.68	105.09	6.66	229.92	3.46	162.95	3.48	125.56	**2.49**	99.44
	25°	8.65	381.87	4.36	142.66	9.02	347.11	4.25	222.54	5.41	251.16	**3.78**	202.50
	30°	12.69	606.56	5.72	218.46	12.99	543.57	6.16	367.81	8.74	467.17	**5.05**	303.86
	35°	16.32	808.88	8.11	351.76	17.11	747.91	8.70	560.13	11.59	652.31	**7.89**	531.20
	40°	22.96	1178.52	11.81	557.49	23.38	1058.67	11.52	774.49	17.10	1010.00	**10.15**	711.13
	45°	27.77	1446.86	**15.70**	774.65	27.83	1279.11	16.46	1149.28	22.84	1382.10	15.94	1174.38
ASAVE	0°	2.96	—	2.96	—	3.27	—	1.65	—	1.70	—	**1.34**	—
	5°	3.66	23.83	3.01	1.77	4.12	26.17	1.91	15.41	1.83	8.09	**1.46**	9.56
	10°	5.57	88.29	2.87	-3.02	6.03	84.71	2.70	63.39	2.24	31.89	**1.65**	23.41
	15°	8.12	174.78	2.98	0.70	8.56	162.14	4.29	159.54	2.47	45.53	**2.11**	58.06
	20°	10.54	256.54	3.40	15.04	11.34	247.16	6.44	289.15	3.22	89.84	**3.08**	130.70
	25°	11.87	301.71	**3.89**	31.63	13.06	299.75	8.19	395.30	5.29	211.86	4.70	251.85
	30°	14.57	392.87	**4.78**	61.84	16.28	398.43	10.01	505.31	9.51	460.02	7.16	435.72
	35°	20.66	598.91	**5.85**	97.88	22.78	597.45	11.40	589.44	15.33	803.39	10.53	687.56
	40°	30.83	943.09	**7.08**	139.41	31.61	867.82	14.61	783.26	19.70	1060.49	15.08	1028.66
	45°	38.58	1205.26	**11.51**	289.26	38.39	1075.56	22.94	1287.11	21.43	1162.75	19.60	1366.53

F. Rotation Compensation Using Geometric Shape Analysis

In this experiment, the performance of the method proposed in [2] is analysed as described in Section III-B. As neither an implementation nor the data set on which the shape analysis is based are available, the results on the original data cannot be reproduced. The main task of this approach is the detection of

TABLE IV
ACCURACY OF JOINT DETECTION USING A SLIDING WINDOW APPROACH AS PROPOSED IN [23]. THE PERCENTAGE IS THE DEVIATION OF THE DETECTED JOINT RELATIVE TO THE GROUND TRUTH WITH RESPECT TO THE LENGTH OF THE FINGER

	Deviation within			
	0-5%	5-10%	10-20%	>20%
Joint 1	74.80	6.36	9.78	9.06
Joint 2	51.67	27.42	13.20	7.71

TABLE V
STATISTICAL DATA OF THE FINGER GEOMETRY ON THE PLUSVEIN-FR DATA SET AS DEFINED IN TABLE 2 OF [2]

Gen	Fing	Value	Min	Mean	Max	Std Dev
M	Idx	$r_{root-tip}$	0.97	1.21	1.59	0.091
		r_{joints}	1.06	1.16	1.27	0.040
		$r_{joint1-tip}$	1.07	1.18	1.38	0.058
		$r_{root-joint1}$	0.86	1.02	1.16	0.055
		α	171.55	176.93	181.89	1.675
	Mid	$r_{root-tip}$	0.87	1.07	1.34	0.086
		r_{joints}	1.01	1.15	1.28	0.053
		$r_{joint1-tip}$	0.96	1.18	1.36	0.064
		$r_{root-joint1}$	0.74	0.91	1.15	0.072
		α	164.43	174.24	184.95	2.945
F	Idx	$r_{root-tip}$	0.94	1.25	1.63	0.126
		r_{joints}	1.05	1.19	1.32	0.056
		$r_{joint1-tip}$	1.02	1.20	1.43	0.073
		$r_{root-joint1}$	0.86	1.04	1.29	0.088
		α	170.41	176.62	181.68	2.405
	Mid	$r_{root-tip}$	0.87	1.07	1.36	0.096
		r_{joints}	1.05	1.18	1.32	0.054
		$r_{joint1-tip}$	0.99	1.19	1.40	0.062
		$r_{root-joint1}$	0.73	0.90	1.12	0.073
		α	168.81	173.92	182.11	2.329
All	All	$r_{root-tip}$	0.87	1.15	1.63	0.127
		r_{joints}	1.01	1.17	1.32	0.053
		$r_{joint1-tip}$	0.96	1.19	1.43	0.065
		$r_{root-joint1}$	0.73	0.97	1.29	0.095
		α	164.43	175.45	184.95	2.739

the finger lines and joints. For the joint detection, Chen *et al.* used a sliding window approach presented in [23]. As this algorithm did not provide satisfactory results for our data set, the joints as well as the roots and tips of the finger were marked manually. When comparing the manually determined values with those of the sliding window approach, large deviations are noticeable. Table IV states the results in detail. For joint 1 (proximal inter-phalangeal joint), 75% of the detected joints are within a range of 5% of the length of the finger (distance between finger root and -tip), for joint 2 (distal inter-phalangeal joint) only 52% are within this range. For joint 1 and joint 2, around 9% and nearly 8% of the detected joint positions are more than 20% off from the manually selected position, respectively.

The statistical measures obtained for the PLUSVein-FR are depicted in Table V. The values differ from the ones by Chen *et al.*, especially the angle α at the proximal inter-phalangeal joint is larger. The standard deviations differ as well: For the distance and diameter ratio values ($r_{root-tip}$, r_{joints}, $r_{joint1-tip}$ and $r_{root-joint1}$), the obtained one is 10 times higher, for α it is more than 10 times lower. These differences might result from the difference in the number of subjects and the subjects' ethnicity. Their data set consists of 12 Asian subjects (6 female and 6 male) only, whereas the PLUSVein-FR consists of 63 (27 female, 36 men) mainly European people.

Based on this statistical data, the geometric finger analysis to detect the finger rotation is executed for all rotation angles.

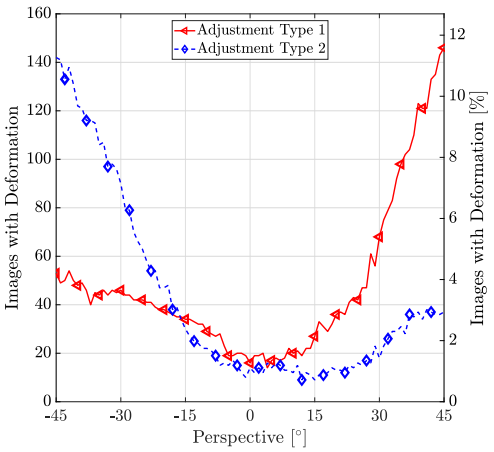

Fig. 12. Number of images with a detected longitudinal finger rotation (type 3 deformation) using the method presented in [2]. Left y-axis: absolute number of deformed images detected, right y-axis: value in percent (the total number of images is 1260).

Fig. 12 illustrates the number of detected images exhibiting longitudinal finger rotation. At a rotation angle of ±30°, less than 6% of the input images are detected as rotated, whereas for more than 2% a wrong (opposite direction) rotation is detected. Even at ±45° only 12% of the images are classified to contain a type 3 deformation. Thus, this method is clearly not applicable to the PLUSVein-FR. One reason therefore might be due to the placement of the finger. Chen *et al.* used a device where the finger is placed over its entire length on the scanner, while the PLUSVein-FR was captured with a device where only the fingertip and the finger trunk rests. The rest of the finger does not touch any part of the scanner. When placing a finger onto a surface, the finger is slightly deformed. This deformation influences the geometric properties on which Chen *et al.*'s algorithm is based. Due to the improper rotation detection, the recognition performance is not significantly improved compared to the unmodified data set. On the contrary, the performance even slightly decreases. This result seems to be valid as, e.g., for the SDUMLA-HMT Chen *et al.* only achieved an average RPI of 22% over all 7 investigated algorithms when applying corrections for all three analysed finger deformations. For MC, the RPI was 7% only (the EER decreased from 2.44% to 2.38%). These results indicate, that the performance gain will be even smaller if only a single correction is applied. The trend for GADC is basically the same as for the baseline results in Fig. 9, hence there is no separate visualization for GADC. However, the performance trend for GADC is depicted in the plots of Fig. 17, where all recognition schemes are compared.

G. Rotation Compensation Using Elliptic Pattern Normalization

In this part of the experiment, the EPN as proposed by Huang *et al.* [5] and described in Section III-C is applied.

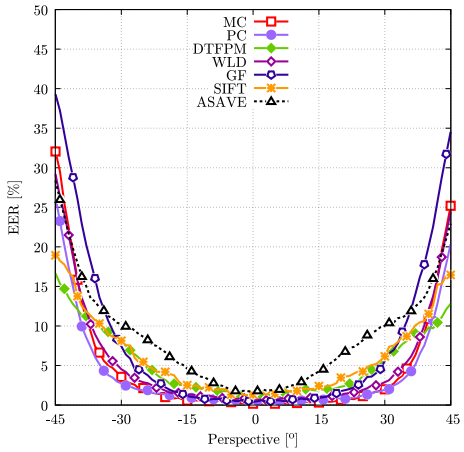

Fig. 13. Trend of the EER across the different rotation angles after applying EPN in the range of $-45°$ to $45°$.

Fig. 13 depicts the trend of the EER for elliptic input image normalization. The area in which the performance remains almost stable becomes larger for all recognition schemes. All algorithms, but especially MC, PC and WLD, show an increased robustness against longitudinal rotation. For MC, PC and WLD, the point at which the performance begins to degrade sharply, shifts to $> \pm 30°$ and to $> \pm 25°$ for GF. For DTFPM and SIFT, the performance curve flattens out compared to the unmodified data set. The same holds for ASAVE, which achieves the worst performance in terms of EER.

H. Rotation Compensation Using a Fixed Rotation Angle

The last part of the experiments is devoted to the analysis of the proposed rotation compensation method based on a fixed rotation angle as described in Section III-D. The top plot of Fig. 14 shows the functional principle using MC features for $\varphi_{corr} = 20$. It shows five different lines: one line for the trend of the EER of the unmodified data set, two lines for the $\pm\varphi_{corr}$ rotated images, the result of the maximum rule score level fusion from the original and the two fixed angle corrected scores and as a reference and a line for the performance using the known rotation angle for correction. Within the region of $\pm\varphi_{corr}$, the fused results are equal to the exact correction. Outside this region they stick to the angle corrected lines. That the performance of the proposed method is close to the performance of the known angle approach confirms the effectiveness of the approach. To show the influence of the pre-defined rotation angle φ_{corr} on the results, it is varied between 5°, 10°, 15°, 20° and 25° and applied on the PLUSVein-FR. The results are visualized in the bottom plot of Fig. 14: in essence, all curves follow the same trend, but the rotation angle at which the performance starts to decrease rapidly rises with an increasing φ_{corr}.

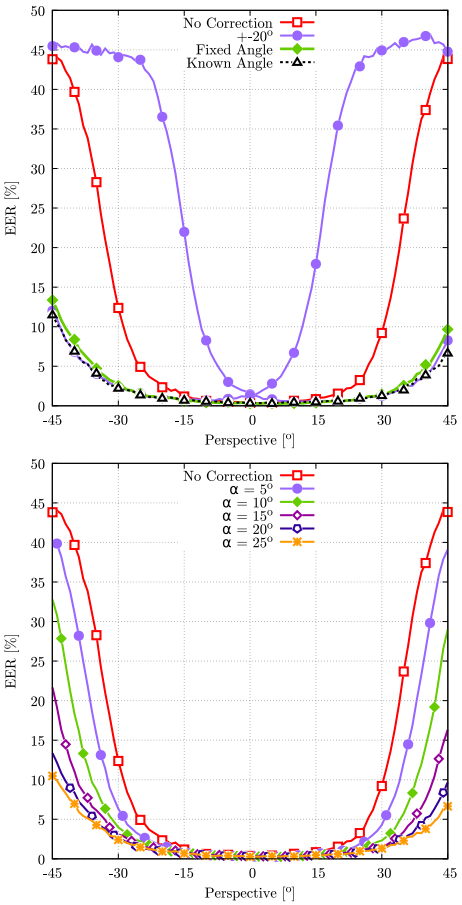

Fig. 14. Trend of the EER across the different perspectives applying a rotation compensation using a fixed rotation angle using MC features. Top: details for $\varphi = 20°$, bottom: the influence of varying φ from 5° to 25° in steps of 5°.

In the next experiment, the proposed fixed angle approach is applied on two different data sets with a correction angle of $\varphi_{corr} = 20°$: first to the original PLUSVein-FR and second to the PLUSVein-FR after elliptical pattern normalization has been performed. As all analysed recognition schemes are able to tolerate rotations to at least $\pm 10°$ a φ_{corr} of 20° is chosen, which keeps the effective rotation angle below 10° within a range of $\pm 30°$. Fig. 15 shows the results for both data sets. The top plot visualizes the EER values for the original data set. By applying the proposed approach, all evaluated recognition schemes achieve superior results compared to the original data set. The performance degradation is slower which, leading to flatter EER curves. Especially vein pattern based methods,

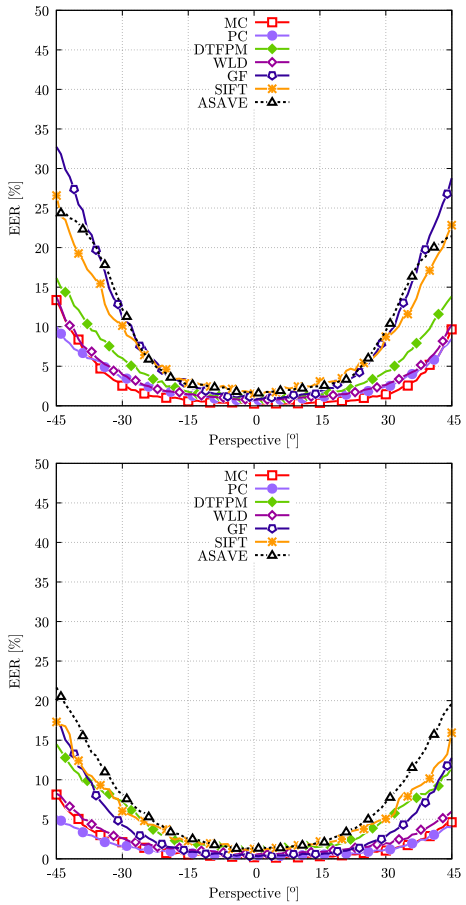

Fig. 15. Trend of the EER across the different perspectives applying a rotation compensation using a fixed rotation angle using MC features. Top: fixed angle compensation $\varphi = 20°$, bottom: fixed angle compensation combined with EPN.

namely MC, PC and WLD, benefit from this approach: there is no sharp drop in their performance any more: PC's EER stays below 10% over the whole range, MC's and WLD's below 14%. DTFPM achieves an EER just above 15% at ±45°, which is worse than the vein pattern based methods. SIFT and ASAVE arrive at EERs around 25%, GF at less than 35% for this rotation angle. The results for applying the proposed method together with EPN, which are depicted at the bottom of Fig. 15, are even superior. The curves are flatter compared to the original data set. The EER for PC stays below 5% over the whole range of ±45°, for MC and WLD below 10%, for DTFPM below 15% and for GF and SIFT below 20%. For the worst-performing algorithm, ASAVE, the EER only slightly exceeds 20%.

TABLE VI
EVALUATION RESULTS FOR THE METHOD PROPOSED IN SECTION III-D ON THE UTFVP DATA SET

Fixed Rotation Angle					
α	EER	FMR100	FMR1000	ZeroFMR	RPI
—	0.38 (±0.08)	0.23	0.50	2.19	—
±5°	0.14 (±0.05)	**0.09**	**0.14**	1.22	174.80
±10°	**0.14 (±0.05)**	0.10	0.17	**1.06**	**175.60**
±15°	0.16 (±0.05)	0.12	0.19	1.37	144.50
±20°	0.24 (±0.06)	0.14	0.42	2.50	57.35
±25°	0.30 (±0.07)	0.24	0.47	1.91	29.56
±30°	0.34 (±0.08)	0.26	0.49	2.08	11.49
±35°	0.50 (±0.09)	0.40	0.89	2.48	-24.14
±40°	1.89 (±0.18)	2.73	6.35	21.13	-79.81
±45°	7.39 (±0.34)	14.72	22.88	34.31	-94.83
Fixed Rotation Angle + EPN					
α	EER	FMR100	FMR1000	ZeroFMR	RPI
—	0.35 (±0.08)	0.24	0.56	2.16	—
±5°	**0.17 (±0.05)**	0.14	**0.19**	**0.66**	**100.80**
±10°	0.21 (±0.06)	0.16	0.24	1.01	67.39
±15°	0.17 (±0.05)	**0.12**	0.26	1.32	100.80
±20°	0.19 (±0.06)	0.16	0.30	1.35	81.84
±25°	0.21 (±0.06)	0.17	0.24	1.60	66.77
±30°	0.28 (±0.07)	0.19	0.35	1.55	24.90
±35°	0.31 (±0.07)	0.23	0.54	1.81	10.83
±40°	0.61 (±0.10)	0.45	1.61	14.20	-42.79
±45°	0.87 (±0.12)	0.80	1.75	7.60	-59.98

I. Verification of the Fixed Rotation Angle Approach

To verify the effectiveness of the proposed fixed angle approach, it is applied on the publicly available UTFVP [10] and SDUMLA-HMT [11] data sets. Both data sets consist of finger vein images acquired from the palmar perspective. Again, we use the original data set and its elliptic normalized version during the experiments. φ_{corr} is varied from 5° to 45° in steps of 5°. This part of the experiment is only performed for MC features.

By visual inspection, the UTFVP data set seems to exhibit little to no longitudinal rotation, whereas the extent of longitudinal finger rotation within SDUMLA-HMT seems to be higher. Table VI lists the results for the UTFVP data set. The baseline EER without any rotation correction is 0.38%. Using the fixed angle correction approach, the EER reaches its minimum of 0.14% for $\varphi_{corr} = 10°$ and keeps below 0.34% until $\varphi_{corr} \leq 30°$. With a further increase of φ_{corr}, the performance drops faster and hits an EER of 7.39%. FMR100, FMR1000 and ZeroFMR follow approximately the same trend. The last column shows the *RPI* with respect to the baseline EER. At its maximum, the relative performance increase is 175%. By applying EPN on the data set the EER without fixed angle correction arrives at 0.35%, corresponding to an RPI of 20% compared to the baseline performance on the unchanged data set. When combining both methods, the best result with an EER of 0.17% is achieved for $\varphi_{corr} = 5°$. This corresponds to an RPI of 100% and 145% compared to the elliptic normalized data set without fixed angle correction and to the original unmodified data set, respectively.

The results for the SDUMLA-HMT data set are listed in Table VII. The baseline EER is 4.19% for the unmodified data set. By applying the proposed approach with increasing φ_{corr}, the EER steadily drops until $\varphi_{corr} = 25°$ where it reaches its minimum of 1.62%. If φ is further increased, the EER increases rapidly to an EER around 9.5%. Again, FMR100,

TABLE VII
EVALUATION RESULTS FOR THE METHOD PROPOSED IN SECTION III-D ON THE SDUMLA-HMT DATA SET

Fixed Rotation Angle					
α	EER	FMR100	FMR1000	ZeroFMR	RPI
—	4.19 (±0.13)	5.29	7.01	52.78	—
±5°	3.13 (±0.12)	3.93	5.62	63.36	33.71
±10°	2.41 (±0.10)	2.85	4.30	55.24	73.95
±15°	2.01 (±0.09)	2.41	3.50	**51.88**	108.10
±20°	1.72 (±0.09)	1.97	3.14	52.10	143.80
±25°	**1.62 (±0.09)**	**1.84**	**3.11**	60.29	**157.90**
±30°	1.71 (±0.09)	2.02	3.36	56.76	144.40
±35°	2.00 (±0.09)	2.45	4.55	73.00	109.00
±40°	3.96 (±0.13)	6.55	13.49	80.94	5.71
±45°	9.54 (±0.20)	17.94	27.67	85.68	-56.10
Fixed Rotation Angle + EPN					
α	EER	FMR100	FMR1000	ZeroFMR	RPI
—	2.18 (±0.10)	2.55	3.63	46.43	—
±5°	1.61 (±0.08)	1.80	2.94	53.17	35.94
±10°	1.49 (±0.08)	1.59	2.38	42.30	46.86
±15°	1.29 (±0.08)	1.36	2.13	**40.57**	69.41
±20°	1.11 (±0.07)	1.13	**1.90**	42.40	96.60
±25°	**1.05 (±0.07)**	**1.06**	1.94	49.46	**108.80**
±30°	1.25 (±0.07)	1.36	2.35	47.94	74.25
±35°	1.52 (±0.08)	1.74	2.94	52.21	43.67
±40°	1.82 (±0.09)	2.17	4.05	64.33	20.23
±45°	2.18 (±0.10)	2.93	5.77	61.49	0.12

FMR1000 and ZeroFMR show approximately the same trend. The maximum *RPI* is 158% for $\varphi_{corr} = 25°$. By applying EPN on the data set, the EER arrives at 2.18%, which corresponds to an RPI of 92% compared to the baseline performance. Combining both methods further improves the results, hitting the best performance at $\varphi_{corr} = 25°$ with an EER of 1.05%. The resulting RPI is 109% and 300% with respect to the elliptic normalized data set and to the original unmodified data set, respectively.

As the rotation angle of 25°, where the best result is achieved, seems to be relatively high, we checked the result for plausibility by visually inspecting the images manually. It turned out that there are quite a view samples exhibiting a high degree of longitudinal rotation. Fig. 16 shows such an example (sample number 2 and 3 of the left ring finger from subject #6). The top row shows the original images from the data set. It is clearly visible that the two finger images are rotated versions of each other. The second and third row show the ROI of the left and right sample, respectively. The bottom row is the rotation corrected right image using a rotation angle of 25°. The vein pattern of the rotated version of the right image is clearly more similar to sample #2 than the original features of sample #3.

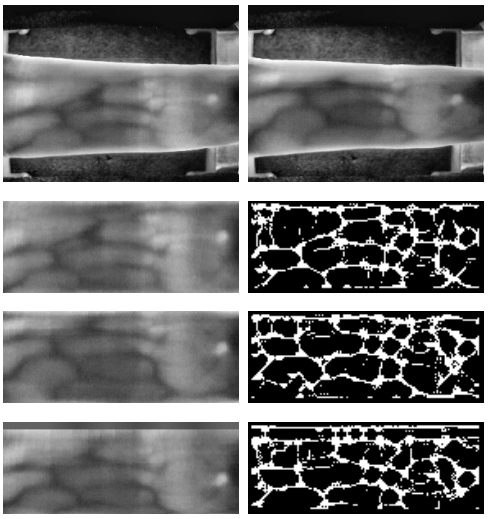

Fig. 16. Example of two samples from the same finger of the SDUMLA-HMT data set. Top row: original images, row 2: ROI and extracted features from the left sample, row 3: right sample, bottom row: rotated version of the right sample using a rotation angle of 25°.

J. Comparison of Rotation Compensation Methods

To enable a better comparison of the different rotation correction approaches' performance gain for each recognition scheme, Fig. 17 depicts their trends grouped per scheme. As all simple vein pattern based methods (MC, PC, WLD, GF) follow the same general behaviour, only MC is visualized. Table VIII lists the EER and the RPI with respect to the baseline performance of the unmodified data set at the palmar view for all correction / recognition scheme combinations for some selected perspectives.

The top-left figure gives the performance for MC. Like all vein pattern based methods, MC highly benefits from the rotation compensation. Without rotation correction, MC is able to achieve a relatively stable recognition rates up to a rotation angle of ±15°. For higher rotation angles, the performance drops faster, and starts to drop rapidly at ±25°. At ±45°, the EER is close to 45%. The recognition rate can be improved noticeably by applying a correction based on the actual known rotation angle. Hereby, the range, in which the performance is stable can be increased to ±30°. Even at ±45° the EER is still around 10%, which corresponds to an RPI of 600%. An application of GADC type 3 correction has no positive effect at all. On the contrary, the performance even slightly degrades. Similar to applying a correction using the known rotation angle, also EPN extends the stable region. However, starting at a rotation angle of ±30°, the recognition rate starts to decrease rapidly. Applying the proposed fixed angle method with a pre-defined rotation correction angle of $\varphi_{corr} = 20°$ achieves similar results to the known angle method. The best results are accomplished by combining the fixed angle method with EPN. This combination even outperforms the known angle correction method. The worst EER at −45° is still 8%.

The DTFPM results are visualized in the top-right subplot. DTFPM is designed to be robust against longitudinal finger rotation. As a result, all curves are shallowed compared to MC. Even using the original, non-corrected data set yields EERs of $< 20\%$ over the whole tested range. Applying a correction using the known rotation angle doubles the performance, resulting in a maximum EER of about 10% at ±45°. Again, the application of GADC yields a slight deterioration of the performance. Elliptic normalization, the fixed angle method

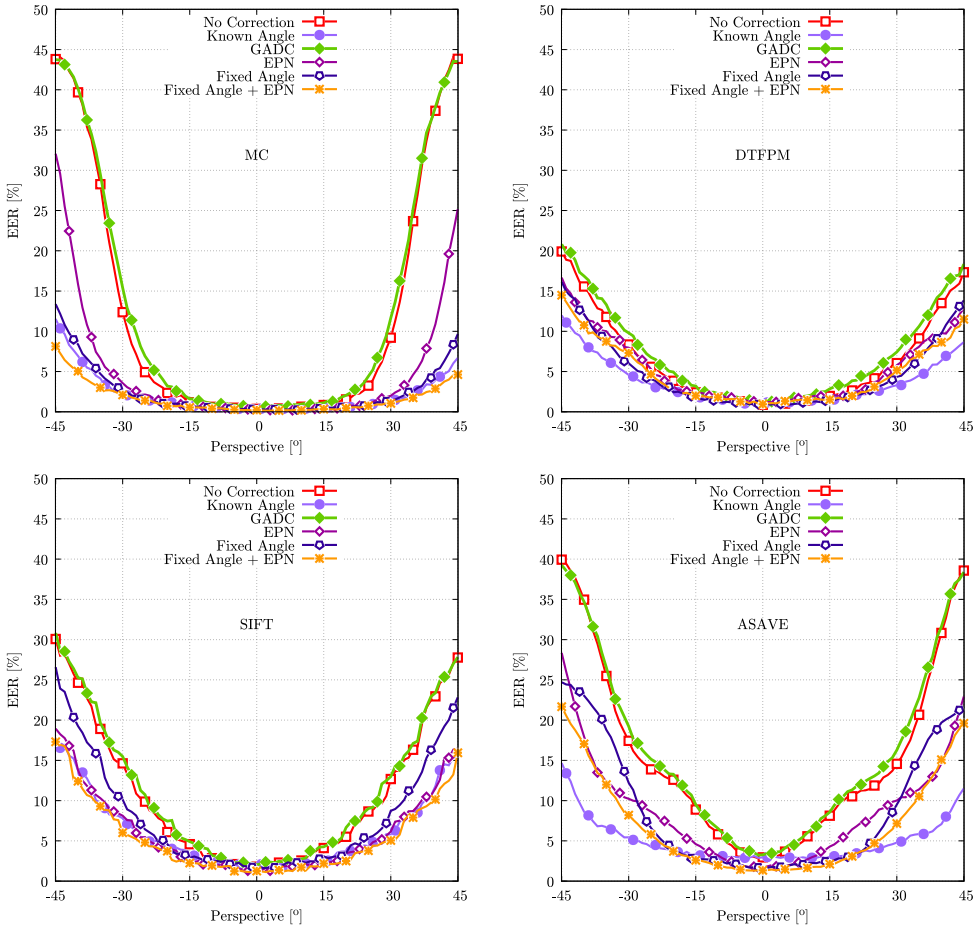

Fig. 17. Trend of the EER across the different perspectives applying different rotation compensation approaches for the same recognition scheme. Top left: MC, top right: DTFPM, bottom left: SIFT, bottom right: ASAVE.

and the combination of both are superior to no correction but inferior to the known angle method. The proposed fixed angle method achieves the best results among these methods for DTFPM.

Similar to DTFPM, SIFT is more robust against longitudinal finger rotation than vein pattern based methods. This leads to a similar behaviour for the different correction methods, although with raised EER rates: A correction using the known rotation angle flattens the EER curve, achieving an EER of just above 15% at ±45° (instead of 30% without correction). GADC does not improve the results at all. The proposed method also reduces the resulting EERs, but not to the same extent as the known angle method. EPN achieves roughly the same recognition rates as the correction using the known angle. The combination of elliptic normalization and the fixed angle method achieves the overall best results. The results are depicted in the bottom-left plot.

The bottom-right chart shows the results for ASAVE. The known angle correction achieves pretty stable results within the range of ±40° with an EER below 8%. For higher rotation angles the performance drops sharply until it reaches its maximum EER of 15% at −45°. Again, GADC does not gain any performance increase compared to the performance of the original data set. Elliptic normalization shallows the EER curve and achieves EERs below 10% up to ±30°. For higher rotation angles its performance decreases rapidly and arrives at an EER of 23% at ±45°. The proposed method is

TABLE VIII
PERFORMANCE RESULTS IN TERMS OF EER AND RPD OF ALL CORRECTION METHODS AND RECOGNITION SCHEMES. THE RPI IS ALWAYS CALCULATED WITH RESPECT TO THE BASELINE PERFORMANCE OF THE UNMODIFIED DATA SET AT THE PALMAR VIEW FOR ALL CORRECTION / RECOGNITION SCHEME COMBINATIONS. THE HIGHLIGHTED RESULTS (BOLD FACE) REPRESENT THE BEST RECOGNITION RATES FOR A RECOGNITION SCHEME AT THE SPECIFIED ROTATION ANGLE

Method	Rotation angle	No Correction		Known Angle		GADC		EPN		Fixed Angle		Fixed Angle + EPN	
		EER	RPI	EER	RPI	EER	RPI	EER	RPI	EER	RPI	EER	RPI
MC	0°	0.37	—	0.37	—	0.59	-38.28	**0.17**	112.05	0.28	28.75	0.21	77.65
	5°	0.41	—	0.34	23.33	0.81	-49.13	0.17	137.62	0.30	37.19	**0.16**	161.92
	10°	0.63	—	0.49	28.90	0.96	-34.07	0.25	149.68	0.32	98.65	**0.19**	233.88
	15°	0.84	—	0.52	61.47	1.11	-23.84	**0.32**	165.33	0.38	122.12	0.34	151.72
	20°	1.54	—	0.62	149.10	2.05	-25.06	0.67	130.62	0.62	148.55	**0.44**	246.90
	25°	3.25	—	0.99	229.82	4.42	-26.51	1.13	187.42	1.00	224.69	**0.75**	335.93
	30°	9.21	—	1.32	598.55	11.66	-21.04	1.99	363.26	1.46	530.78	**1.05**	780.21
	35°	23.68	—	2.03	1069.22	25.21	-6.07	4.61	413.90	2.55	827.58	**1.74**	1258.25
	40°	37.39	—	3.93	851.27	37.85	-1.21	10.88	243.70	5.19	621.04	**2.88**	1199.62
	45°	43.84	—	6.69	555.26	43.51	0.77	25.19	74.03	9.66	353.88	**4.62**	848.20
PC	0°	0.77	—	0.77	—	0.86	-10.59	0.51	51.26	0.65	17.98	**0.46**	67.14
	5°	0.75	—	0.76	-2.09	0.78	-4.13	0.51	47.17	0.65	14.83	**0.43**	74.82
	10°	0.89	—	0.87	1.83	0.98	-9.46	0.49	81.44	0.92	-3.22	**0.41**	116.07
	15°	1.13	—	1.11	1.43	1.26	-10.19	0.52	115.55	0.97	16.81	**0.46**	145.78
	20°	1.65	—	1.48	11.66	1.81	-8.93	0.81	103.94	1.34	23.58	**0.63**	161.22
	25°	3.26	—	1.62	101.18	3.84	-15.00	1.21	170.37	1.70	91.82	**0.86**	279.37
	30°	6.52	—	2.56	154.87	8.37	-22.06	1.94	236.61	2.44	167.50	**1.16**	462.62
	35°	15.36	—	3.93	290.30	17.91	-14.27	3.67	317.96	3.79	305.27	**1.78**	763.27
	40°	30.37	—	6.06	400.87	31.64	-4.03	9.13	232.48	5.45	457.58	**2.84**	969.69
	45°	43.01	—	8.75	391.72	42.97	0.11	20.34	111.44	8.46	408.21	**3.98**	979.76
DTFPM	0°	0.87	—	0.87	—	1.21	-27.93	1.00	-12.34	**0.81**	8.18	0.94	-7.07
	5°	1.02	—	1.16	-11.71	1.55	-33.81	1.43	-28.38	**0.98**	4.17	1.32	-22.50
	10°	1.40	—	1.35	3.66	1.97	-28.95	1.79	-21.83	**0.98**	43.66	1.45	-3.12
	15°	1.96	—	1.52	29.53	2.85	-31.15	1.85	5.95	**1.44**	36.00	1.52	29.15
	20°	2.65	—	2.00	32.56	3.86	-31.27	2.32	14.47	**1.89**	40.70	1.97	34.66
	25°	4.16	—	**2.38**	74.35	5.14	-19.14	3.68	12.88	2.87	44.67	3.12	33.33
	30°	6.05	—	**3.31**	82.85	7.43	-18.65	5.79	4.44	4.35	38.90	5.16	17.16
	35°	9.12	—	**4.53**	101.55	10.62	-14.09	8.10	12.71	6.78	34.52	7.14	27.86
	40°	13.50	—	**6.37**	112.08	14.70	-8.12	9.78	38.04	9.74	38.64	8.64	56.33
	45°	17.33	—	**8.66**	100.11	18.35	-5.55	12.81	35.31	13.83	25.31	11.50	50.75
WLD	0°	0.92	—	0.92	—	1.13	-18.25	0.72	29.02	0.78	19.02	**0.65**	41.42
	5°	0.84	—	1.02	-16.85	1.28	-33.86	0.75	12.82	0.79	6.36	**0.57**	47.24
	10°	1.10	—	1.11	-1.29	1.37	-19.67	0.84	30.36	1.03	6.43	**0.70**	56.97
	15°	1.38	—	1.24	11.60	1.61	-14.20	0.91	52.46	1.14	21.26	**0.87**	58.80
	20°	2.30	—	1.46	57.53	2.69	-14.24	1.31	76.62	1.47	56.74	**1.14**	101.62
	25°	4.25	—	2.01	111.52	5.54	-23.19	1.92	121.36	2.00	112.78	**1.49**	184.92
	30°	9.29	—	2.64	252.15	11.85	-21.65	2.89	221.04	2.63	252.50	**1.99**	367.17
	35°	21.26	—	3.88	448.23	23.47	-9.40	5.43	291.39	3.98	433.94	**2.60**	716.45
	40°	35.06	—	6.22	463.45	35.86	-2.22	12.08	190.28	6.03	481.27	**4.12**	750.19
	45°	43.34	—	8.72	397.28	43.31	0.06	24.35	78.01	10.24	323.15	**5.98**	624.84
GF	0°	1.02	—	1.02	—	2.15	-52.71	0.40	155.42	0.76	33.43	**0.38**	166.30
	5°	1.50	—	1.29	15.80	2.81	-46.72	0.60	148.15	1.02	47.42	**0.46**	226.07
	10°	2.34	—	1.52	53.36	4.01	-41.66	0.67	250.00	1.32	77.48	**0.41**	467.51
	15°	3.90	—	1.94	100.99	5.20	-25.04	0.97	301.31	1.87	108.26	**0.59**	565.66
	20°	7.16	—	2.93	143.93	8.88	-19.43	1.77	305.52	2.91	146.17	**1.00**	618.42
	25°	13.57	—	4.80	182.63	15.53	-12.67	2.87	373.42	5.02	170.24	**1.63**	731.35
	30°	23.21	—	7.95	192.10	25.30	-8.26	5.57	316.43	8.32	178.87	**2.84**	717.49
	35°	37.14	—	12.59	195.09	37.79	-1.70	10.57	251.41	14.09	163.65	**4.79**	674.64
	40°	46.26	—	19.42	138.28	46.45	-0.39	20.10	130.17	21.49	115.24	**8.22**	462.84
	45°	48.05	—	26.92	78.47	48.05	0.00	34.55	39.05	28.78	66.95	**12.74**	277.09
SIFT	0°	1.80	—	1.80	—	2.02	-11.01	1.32	36.31	1.54	16.53	**1.25**	43.56
	5°	2.30	—	2.05	12.36	2.46	-6.56	1.42	62.14	1.72	33.65	**1.37**	68.40
	10°	2.56	—	2.19	17.02	2.75	-6.81	1.80	42.11	2.43	5.15	**1.71**	50.03
	15°	4.11	—	2.78	48.20	4.27	-3.63	2.40	71.17	3.08	33.59	**2.19**	87.90
	20°	5.51	—	3.68	49.55	6.66	-17.27	3.46	58.99	3.48	58.46	**2.49**	120.77
	25°	8.65	—	4.36	98.58	9.02	-4.09	4.25	103.64	5.41	59.91	**3.78**	128.68
	30°	12.69	—	5.72	121.87	12.99	-2.31	6.16	105.87	8.74	45.17	**5.05**	151.15
	35°	16.32	—	8.11	101.19	17.11	-4.61	8.70	87.67	11.59	40.79	**7.89**	106.71
	40°	22.96	—	11.81	94.45	23.38	-1.81	11.52	99.28	17.10	34.22	**10.15**	126.27
	45°	27.77	—	**15.70**	76.85	27.83	-0.19	16.46	68.78	22.84	21.62	15.94	74.25
ASAVE	0°	2.96	—	2.96	—	3.27	-9.49	1.65	78.74	1.70	74.16	**1.34**	121.18
	5°	3.66	—	3.01	21.68	4.12	-11.16	1.91	91.79	1.83	99.52	**1.46**	150.00
	10°	5.57	—	2.87	94.15	6.03	-7.74	2.70	105.97	2.24	148.63	**1.65**	237.44
	15°	8.12	—	2.98	172.88	8.56	-5.13	4.29	89.24	2.47	228.84	**2.11**	284.51
	20°	10.54	—	3.40	209.91	11.34	-7.05	6.44	63.76	3.22	227.09	**3.08**	241.82
	25°	11.87	—	**3.89**	205.17	13.06	-9.05	8.19	44.97	5.29	124.34	4.70	152.53
	30°	14.57	—	**4.78**	204.54	16.28	-10.50	10.01	45.54	9.51	53.28	7.16	103.49
	35°	20.66	—	**5.85**	253.19	22.78	-9.30	11.40	81.20	15.33	34.74	10.53	96.29
	40°	30.83	—	**7.08**	335.70	31.61	-2.45	14.61	111.09	19.70	56.54	15.08	104.41
	45°	38.58	—	**11.51**	235.32	38.39	0.49	22.94	68.20	21.43	80.02	19.60	96.86

able to keep the recognition rates stable between $\pm 20°$. For higher rotation angles the performance degrades sharply. Once more, the best results are achieved by using a combination of EPN and the proposed method. Although, for ASAVE the performance results in this case are noticeable worse compared to the correction using the known angle.

TABLE IX
RANKING OF THE ROTATION CORRECTION METHODS UNDER INVESTIGATION BASED ON THE EXPERIMENTAL RESULTS PER RECOGNITION SCHEME

Rotation correction	No Corr	Known Angle	GADC	EPN	Fixed Angle	Fixed Angle + EPN
MC	5	2	6	4	3	1
PC	5	2	6	4	3	1
DTFPM	5	1	6	4	2	3
WLD	5	2	6	4	3	1
GF	5	2	6	4	3	1
SIFT	5	2	6	3	4	1
ASAVE	5	1	6	4	3	2

K. Ranking of Rotation Correction Methods

Table IX gives the ranking of the applied rotation correction methods per recognition scheme. Regarding the single approaches, the correction using the known rotation angle achieves the best results. Although, in practical applications the known angle method cannot be applied as the rotation angle is usually not known. Thus, the most appropriate approach is the proposed fixed angle method on its own. However, a combination of the proposed approach and the EPN further improves the results. Especially for vein pattern based schemes, the results achieved by the proposed method are only slightly worse than the known angle approach. Except for SIFT, EPN on its own leads to inferior results compared to the proposed method. GADC even degrades the recognition rates compared to applying no correction.

The results of the different rotation correction approaches indicate that simple vein pattern based methods get the most out of rotation correction. MC, PC as well as WLD outperform all other recognition schemes after applying a rotation compensation using the exact rotation angle, elliptic normalization, the fixed angle method or a combination of the latter two.

L. Runtime Evaluation for Fixed Angle Approach

The rotation correction introduces additional processing steps. Thus, the runtime costs are relevant in a practical application. As the rotation compensation is applied during biometric enrolment, the additional cost are two comparisons and the maximum rule score level fusion at the biometric recognition. If the approach is combined with EPN, this step needs to be considered too. Note, that the implementations of the recognition algorithms used in these experiments are not optimized for runtime performance. Hence, the determined durations are only indicators for the additional costs imposed due to the proposed approach. Table X lists the average processing times for the different steps in the recognition tool-chain. It can be seen that the additional runtime of the steps added by this approach (two comparisons and the maximum score level fusion) is negligible compared to the other steps. Therefore, the total duration, as shown in Table XI, is only slightly higher. As the processing of the elliptical correction takes noticeably longer, its application increases the overall duration perceptibly. The runtime analysis shows, that the fixed angle correction approach on its own is suitable for real-time applications.

TABLE X
THE AVERAGE TIME OF COST FOR EVERY RELEVANT STEP IN THE RECOGNITION TOOL-CHAIN

Method	EPN [ms]	PP [ms]	FE [ms]	Comparison [ms]	Fusion [ms]
MC	89.942	29.705	293.114	2.621	0.006
PC	89.942	28.185	4.367	2.452	0.006
DTFPM	89.942	4.842	341.537	3.278	0.006
WLD	89.942	16.179	24.221	2.483	0.006
GF	89.942	84.456	6.107	2.472	0.006
SIFT	89.942	83.569	23.076	2.761	0.006
ASAVE	89.942	17.887	113.711	2.560	0.006

TABLE XI
THE AVERAGE TIME OF COST FOR A SINGLE COMPARISON USING NO ROTATION CORRECTION, THE FIXED ANGLE APPROACH AND THE FIXED ANGLE APPROACH AFTER APPLYING EPN

Method	No Correction	Fixed Angle		Fixed Angle + EPN	
	[s]	[s]	Increase [%]	[s]	Increase [%]
MC	0.325	0.331	1.61	0.421	29.25
PC	0.035	0.040	14.03	0.130	270.98
DTFPM	0.350	0.356	1.88	0.446	27.60
WLD	0.043	0.048	11.60	0.138	221.34
GF	0.093	0.098	5.32	0.188	102.00
SIFT	0.109	0.115	5.05	0.205	87.26
ASAVE	0.134	0.139	3.82	0.229	70.86

V. CONCLUSION

We systematically investigated the extent to which longitudinal finger rotation can be compensated and the impact of the correction on the recognition accuracy of a finger vein recognition system. Therefore, we evaluated two novel correction approaches and two other ones from the literature. The first approach has not been applied to finger vein recognition before and exploits the fact that for the PLUSVein-FR data set the angle of the longitudinal rotation is known. It applies a rotation compensation using a circular projection based on this known angle. As second approach we evaluated a method proposed by Chen *et al.* [2] that analyses the geometric shape of the finger and based on this results, detects deformations and corrects them. The third approach applies an elliptic pattern normalization as proposed in [5].

In real world scenarios the longitudinal rotation angle is unknown and its estimation is a difficult task. The fourth approach, is a novel method that is able to correct longitudinal finger rotation deformation without any knowledge or estimation of the actual angle of rotation, which is its main advantage.

The results of the known angle approach showed that a correction of the rotation is possible up to $\pm 30°$, achieving reasonable recognition results. It turned out that especially vein pattern based algorithms, e.g., MC and PC, benefit from this rotation correction. The approach based on the geometric shape analysis, did not achieve satisfactory results on our data set at all. By applying EPN, all recognition schemes under investigation achieved superior results compared to applying no correction. By successfully applying the newly proposed fixed angle method on three different data sets (PLUSVein-FR, UTFVP and SDUMLA-HMT), we confirmed its effectiveness. The analysis of the computational cost showed, that the fixed angle correction approach is also suitable for real-time applications. A combination with EPN further improved the results

and achieved the best robustness against longitudinal finger rotation for all recognition schemes. However, EPN is more computational expensive than the proposed approach.

We further confirmed that simple, vein pattern based recognition schemes in combination with our proposed correction method outperform more sophisticated and complex recognition algorithms and rotation detection frameworks. For example, PC with elliptic normalization and our proposed fixed angle compensation approach reduces the impact of longitudinal finger rotation noticeably. In biometrics there is a general trend towards contact-less as well as on-the-move acquisition. Hence, recognition tool-chains that are robust against different finger misplacements and the resulting deformations will become essential.

Our future work will include further analysis of deformations caused by different finger misplacements and the development of methodologies improving the robustness against them. Furthermore, we will analyse the presence of finger rotation in commonly used publicly available finger vein data sets.

REFERENCES

[1] A. Kumar and Y. Zhou, "Human identification using finger images," *IEEE Trans. Image Process.*, vol. 21, no. 4, pp. 2228–2244, Apr. 2012.

[2] Q. Chen, L. Yang, G. Yang, and Y. Yin, "Geometric shape analysis based finger vein deformation detection and correction," *Neurocomputing*, vol. 311, pp. 112–125, Oct. 2018.

[3] B. Prommegger, C. Kauba, and A. Uhl, "Longitudinal finger rotation—Problems and effects in finger-vein recognition," in *Proc. Int. Conf. Biometrics Special Interest Group (BIOSIG)*, Darmstadt, Germany, 2018, pp. 1–11.

[4] E. C. Lee, H. C. Lee, and K. R. Park, "Finger vein recognition using minutia-based alignment and local binary pattern-based feature extraction," *Int. J. Imag. Syst. Technol.*, vol. 19, no. 3, pp. 179–186, 2009.

[5] B. Huang, Y. Dai, R. Li, D. Tang, and W. Li, "Finger-vein authentication based on wide line detector and pattern normalization," in *Proc. IEEE 20th Int. Conf. Pattern Recognit. (ICPR)*, 2010, pp. 1269–1272.

[6] Y. Matsuda, N. Miura, A. Nagasaka, H. Kiyomiu, and T. Miyatake, "Finger-vein authentication based on deformation-tolerant feature-point matching," *Mach. Vis. Appl.*, vol. 27, no. 2, pp. 237–250, 2016.

[7] L. Yang, G. Yang, Y. Yin, and X. Xi, "Finger vein recognition with anatomy structure analysis," *IEEE Trans. Circuits Syst. Video Technol.*, vol. 28, no. 8, pp. 1892–1905, Aug. 2018.

[8] C. Kauba, B. Prommegger, and A. Uhl, "The two sides of the finger—Dorsal or palmar—Which one is better in finger-vein recognition?" in *Proc. Int. Conf. Biometrics Special Interest Group (BIOSIG)*, Darmstadt, Germany, 2018, pp. 1–5.

[9] B. Prommegger, C. Kauba, and A. Uhl, "Multi-perspective finger-vein biometrics," in *Proc. IEEE 9th Int. Conf. Biometrics Theory Appl. Syst. (BTAS)*, Los Angeles, CA, USA, 2018, pp. 1–9.

[10] B. T. Ton and R. N. J. Veldhuis, "A high quality finger vascular pattern dataset collected using a custom designed capturing device," in *Proc. Int. Conf. Biometrics (ICB)*, 2013, pp. 1–5. [Online]. Available: http://doc.utwente.nl/87790/

[11] Y. Yin, L. Liu, and X. Sun, "SDUMLA-HMT: A multimodal biometric database," in *Biometric Recognition*. Heidelberg, Germany: Springer, 2011, pp. 260–268.

[12] J. Zhao, H. Tian, W. Xu, and X. Li, "A new approach to hand vein image enhancement," in *Proc. 2nd Int. Conf. Intell. Comput. Technol. Autom. (ICICTA)*, vol. 1, 2009, pp. 499–501.

[13] J. Zhang and J. Yang, "Finger-vein image enhancement based on combination of gray-level grouping and circular Gabor filter," in *Proc. IEEE Int. Conf. Inf. Eng. Comput. Sci. (ICIECS)*, 2009, pp. 1–4.

[14] K. Zuiderveld, "Contrast limited adaptive histogram equalization," in *Graphics Gems IV*, P. S. Heckbert, Ed. San Diego, CA, USA: Morgan Kaufmann, 1994, pp. 474–485.

[15] C. Kauba, J. Reissig, and A. Uhl, "Pre-processing cascades and fusion in finger vein recognition," in *Proc. Int. Conf. Biometrics Special Interest Group (BIOSIG)*, Darmstadt, Germany, Sep. 2014, pp. 1–6.

[16] N. Miura, A. Nagasaka, and T. Miyatake, "Extraction of finger-vein patterns using maximum curvature points in image profiles," *IEICE Trans. Inf. Syst.*, vol. 90, no. 8, pp. 1185–1194, 2007.

[17] J. H. Choi, W. Song, T. Kim, S.-R. Lee, and H. C. Kim, "Finger vein extraction using gradient normalization and principal curvature," in *Proc. SPIE Image Process. Mach. Vis. Appl.*, vol. 7251, 2009, Art. no. 725111. [Online]. Available: https://doi.org/10.1117/12.810458

[18] D. Maio, D. Maltoni, R. Cappelli, J. L. Wayman, and A. K. Jain, "FVC2004: Third fingerprint verification competition," in *Proc. 1st Int. Conf. Biometric Authentication (ICBA)*, 2004, pp. 1–7.

[19] M. S. M. Asaari, S. A. Suandi, and B. A. Rosdi, "Fusion of band limited phase only correlation and width centroid contour distance for finger based biometrics," *Expert Syst. Appl.*, vol. 41, no. 7, pp. 3367–3382, 2014.

[20] Y. Lu, S. J. Xie, S. Yoon, Z. Wang, and D. S. Park, "An available database for the research of finger vein recognition," in *Proc. 6th Int. Congr. Image Signal Process. (CISP)*, vol. 1, 2013, pp. 410–415.

[21] P. Tome, M. Vanoni, and S. Marcel, "On the vulnerability of finger vein recognition to spoofing," in *Proc. IEEE Int. Conf. Biometrics Special Interest Group (BIOSIG)*, Sep. 2014, pp. 1–10. [Online]. Available: http://publications.idiap.ch/index.php/publications/show/2910

[22] W. Yang, X. Yu, and Q. Liao, "Personal authentication using finger vein pattern and finger-dorsa texture fusion," in *Proc. 17th ACM Int. Conf. Multimedia*, 2009, pp. 905–908.

[23] L. Yang, G. Yang, Y. Yin, and R. Xiao, "Sliding window-based region of interest extraction for finger vein images," *Sensors*, vol. 13, no. 3, pp. 3799–3815, 2013.

Bernhard Prommegger received the M.Sc. degree in applied image and signal processing from the University of Salzburg and the University of Applied Sciences Salzburg in 2014 and the DI (Austrian equivalent to M.Sc.) degree in information technology and systems management from the University of Applied Sciences Salzburg in 2015. He is currently pursuing the Ph.D. degree in applied image and signal processing with the Department of Computer Sciences, University of Salzburg, where he is currently a Research Assistant. His main research interest is in vascular biometrics, especially multiperspective finger vein biometrics.

Christof Kauba received the B.Eng. and M.Sc. degrees and the Ph.D. degree in applied information technology from the University of Salzburg, Austria, in 2013, 2015, and 2018, respectively, where he is a Post-Doctoral Researcher with the Department of Computer Sciences. His research interests include image and video processing, image forensics and biometrics, especially biometric sensor design as well as finger- and hand-vein biometrics.

Michael Linortner received the DI (Austrian equivalent to M.Sc.) degree in information technology and systems management from the University of Applied Sciences Salzburg in 2017. He is currently a Research Assistant with the Department of Computer Sciences, University of Salzburg. His main research interest is in vascular biometrics, especially finger vein biometrics.

Andreas Uhl is a Professor with the Department of Computer Sciences, University of Salzburg, where he heads the Multimedia Processing and Security Lab. His research interests include image and video processing and compression, wavelets, media security, medical imaging, biometrics, and number-theoretical numerics.

Chapter 10
Different Views on the Finger—Score-Level Fusion in Multi-Perspective Finger Vein Recognition

Bernhard Prommegger, Christof Kauba and Andreas Uhl

Abstract In finger vein recognition, the palmar view of the finger is used almost exclusively, with some exceptions where the dorsal view is utilised. Only little attention has been paid to all other views around the finger's longitudinal axis. We established a multi-perspective finger vein dataset comprising of views all around the finger's longitudinal axis, captured using our self-developed rotating multi-perspective finger vein capture device. The performance of the single views is evaluated using common finger vein recognition algorithms. Based on these single view scores, several score-level fusion experiments involving different fusion strategies are carried out in order to determine the best performing set of views and feature extraction methods to be fused in terms of recognition accuracy while minimising the number of views involved. Our experimental results show that the recognition performance can be significantly improved over the best performing single view one with as few as two views and two-feature extraction methods involved.

Keywords Finger vein recognition · Multi-perspective fusion · Biometric fusion · Score-level fusion · Multi-algorithm fusion · Multi-perspective finger vein capture device · Finger vein dataset

B. Prommegger ( ) · C. Kauba · A. Uhl
Department of Computer Sciences, University of Salzburg,
Jakob-Haringer-Str. 2, 5020 Salzburg, Austria
e-mail: bprommeg@cs.sbg.ac.at

C. Kauba
e-mail: ckauba@cs.sbg.ac.at

A. Uhl
e-mail: uhl@cs.sbg.ac.at

A. Uhl et al. (eds.), *Handbook of Vascular Biometrics*, Advances in Computer Vision and Pattern Recognition, https://doi.org/10.1007/978-3-030-27731-4_10

10.1 Introduction

Finger vein recognition as one representative of vascular pattern biometrics deals with the vascular pattern inside the fingers of a human. Since one of the first mentions of finger veins as a biometric trait in academia by Kono [1] in 2000, they have received much attention not only from academia but also from industry. Commercial off-the-shelf (COTS) finger vein capture devices, as well as most research papers solely, use the palmar (front side of the finger) view in combination with light transmission (the light source and the image sensor are placed on opposite sides of the finger) as illumination source. Multi-perspective finger vein recognition deals with two or more arbitrary perspectives around the finger's longitudinal axis. Despite the advantages of multi-perspective finger vein biometrics over single view ones, these additional perspectives have not got much attention so far. Moreover, there is no publicly available multi-perspective finger vein dataset yet.

This chapter is based on our previous work [2] where we designed a novel, multi-perspective finger vein capture device in order to establish the first multi-perspective finger vein data set. This dataset comprises of images captured all around the finger's longitudinal axis in 1° steps. Based on this dataset, each of the different views has been evaluated individually and some simple fusion experiments have been conducted. The main focus of this chapter is on the fusion of multiple perspectives and feature extraction methods in order to determine the best performing combination in terms of recognition accuracy by employing a more advanced multi-sample score-level fusion scheme as well as by applying further fusion strategies in terms of view and feature combinations. We analyse all possible pairs and triples of perspectives and all possible combinations of the used feature extraction methods. In addition, we combine the best results of our multi-perspective and multi-algorithm fusion experiments to one single combined fusion. Our main goal is to minimise the number of views and feature extraction methods involved, while maximising the recognition accuracy. A typical multi-perspective finger vein capture device contains one image sensor and one light source situated at the right position per desired view. The more views are to be captured, the more camera and illumination modules have to be equipped, thus increasing the production costs, the complexity and the overall size of the finger vein capture device. If the number of desired perspectives is further increased, the construction of a suitable capture device is no longer feasible without the need of rotating parts. Our current multi-perspective finger vein capture device is such a rotating device, making it more susceptible to malfunctions and external influences than a capture device containing no rotating parts. Moreover, the capturing time is increased as the capture device has to rotate all around the finger. Hence, it is beneficial to reduce the number of different views to be captured to a minimum in order to reduce the complexity and production costs of the biometric capture device and to avoid the need for a rotating device while still preserving the advantages of a multi-perspective capture device.

The rest of this chapter is structured as follows: Sect. 10.2 starts with a description of multi-perspective finger vein biometrics including related work regarding other

views than the palmar and dorsal one in finger vein recognition. Our multi-perspective finger vein capture device design is described in Sect. 10.3. Section 10.4 introduces our multi-perspective finger vein dataset captured with the aforementioned device. Section 10.5 gives an overview of biometric fusion in general followed by related work on biometric fusion in finger vein recognition. Section 10.6 explains our experimental set-up, including the finger vein recognition tool chain as well as the fusion framework we utilised and lists the experimental results, followed by a results discussion. Section 10.7 concludes this paper an gives and outlook on future work.

10.2 Multi-perspective Finger Vein Biometrics

The majority of the available finger vein recognition schemes as well as all available COTS finger vein capture devices deal with the palmar (also called ventral) view of the finger. There are only some exceptions where the dorsal view is used. Raghavendra and Busch [3] proposed the first dorsal finger vein acquisition and a complete recognition tool chain including several different feature extraction schemes. In the scope of the PROTECT project (http://www.projectprotect.eu), we acquired the first publicly available dorsal finger vein dataset [4] using the predecessor of our open-source finger vein capture device. In [5], we established a larger dorsal finger vein dataset captured using both of our proposed open-source finger vein capture devices, which design is decribed in Chap. 3 of this book [6].

There are more views around the finger than the palmar and dorsal one that can be captured. A single finger is an elliptical cylinder-shaped object, hence, there are all possible views around its longitudinal axis (360° of rotation) available. Multi-perspective finger vein recognition describes the use of two or more of these perspectives around the finger's longitudinal axis. Multi-perspective finger vein recognition has several advantages over the single perspective one: The vein patterns of the palmar and dorsal view as well as of the perpendicular views are independent from each other [7]. By fusing more than one perspective that is independent enough from each other (i.e. the rotation angle between the single perspectives has to differ enough for the perspectives to be independent of each other), the overall recognition performance can be increased easily. Tome et al. [8, 9] showed that finger vein and hand vein recognition systems are susceptible to a simple type of presentation attack. By using a paper printout of the vein pattern, they were able to successfully spoof several finger vein capture devices. This paper printout is a flat, 2D representation of the vein pattern. If a biometric capture device takes finger vein images from different perspectives, such simple 2D printout attack finger vein presentation will not be identified as bona fide finger vein presentation. Thus, a multi-perspective finger vein capture device is successfully able to prevent this kind of presentation attack. However, multi-perspective finger vein recognition bears some disadvantages too: The biometric capture devices get more complex, either more than one camera and illumination module are needed, or the capture device has to be build in a rotating manner. This leads to higher production costs of multi-perspective capture devices

and especially rotating capture devices are more error prone due to the moving parts. Another disadvantage is the bigger size of a multi-perspective capture device compared to single perspective ones. The multiple image sensors/illuminator modules or the rotating parts need more space than just a single image sensor in combination with one illumination module.

Lu et al. [10] proposed a multi-perspective finger vein recognition system using two cameras. The cameras are placed at an angle of 60° next to each other, each camera is located 30° apart from the palmar view. They applied feature—as well as score-level fusion using the two views captured simultaneously by the two cameras and were able to improve the recognition performance of the single view ones. Zhang et al. [11] employed a binocular stereoscopic vision device to do 3D point cloud matching of hand veins and knuckle shape. Their capture device set-up consist of two cameras, placed in a relative position of about 45° next to each other, each one equipped with an NIR-pass filter. There is only a single light transmission illuminator placed underneath the palm of the hand. The 3D point clouds are generated by extracting information from the edges of the hand veins and knuckle shapes and then compared utilising a kernel correlation method, especially designed for unstructured 3D point clouds. The authors claim that their proposed method is faster and more accurate compared to 2D vein recognition schemes. In [12] the authors propose a 3D hand vein capturing system based on a rotating platform and a fixed NIR camera. The camera is located above the hand, the hand is put on a handle with an integrated light transmission illuminator. This handle is mounted on a rotating plate. Then the plate rotates around the z-axis. However, the degree of rotation is limited due to the limited movement of the hand in this position. A 3D point cloud is generated from the single view images and matched using kernel correlation. This should help to overcome hand registration and posture change problems present in hand vein recognition if only 2D vein patterns/images are available.

Nevertheless, true multi-perspective finger vein recognition (evaluating more than two different views around the finger) has not been investigated so far, except for our previous work [2]. One reason herefore might be the lack of available multi-perspective finger vein datasets. In order to acquire such a dataset a suitable biometric capture device, able to capture the different views to be acquired, is essential. Capturing these additional perspectives could be done by utilising either a COTS capture device or one of the capture devices proposed in other works by simply turning the finger around its longitudinal axis. However, it is difficult to position the finger in the correct rotational angle. Thus, rotating the finger itself implies the disadvantage of an inaccurate rotation angle and deviations in the rotation angle across different iterations, leading to a low repeatability and a low quality dataset. In order to acquire a suitable multi-perspective finger vein dataset comprising of images captured in several, defined perspectives, either a biometric capture device comprising of several cameras and illumination modules, able to capture more than one view simultaneously, or a rotating biometric capture device able to capture these views consecutively, is necessary. If only a limited number of perspectives are involved, a suitable biometric capture device can be built without any rotating parts, just by equipping an individual image sensor and an associated illumination module per desired

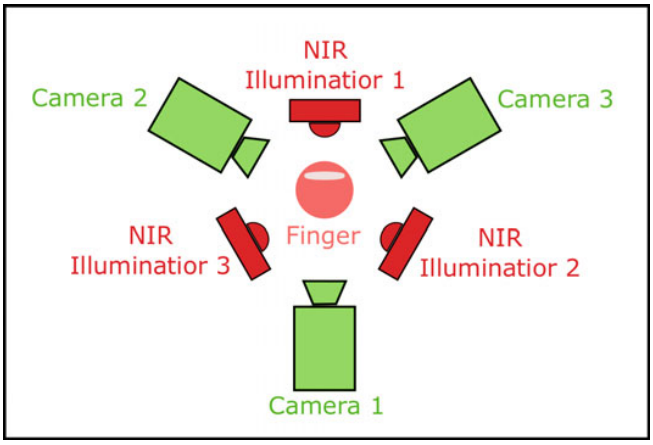

Fig. 10.1 Multi-perspective finger vein set-up exhibiting three different perspectives based on three image sensors and three illuminator modules

view (an example with three different views is shown in Fig. 10.1). The illumination intensity has to be adjusted per view as the path to penetrate the finger is different for each individual view, requiring a stronger or weaker illumination depending on the distance. If more perspectives are desired, rotating the capture device around the finger while the finger remains in a fixed position during the acquisition process is the only feasible option.

The design and construction of a practicable biometric capture device is a complex task. Furthermore, the actual data acquisition is a tedious and time-consuming work. In our previous paper [2], we proposed a rotating multi-perspective finger vein capture device that is able to capture the finger all around its longitudinal axis (360°). We established a multi-perspective finger vein dataset consisting of 252 individual fingers. Based on this dataset, we evaluated the different views around the finger in 5° steps and concluded that the palmar followed by the dorsal one achieve the best single view recognition performance. Moreover, we applied a simple score-level fusion strategy and showed that the recognition performance can be improved by fusing more than one view. This chapter is an extension of our previous work. Based on our proposed multi-perspective finger vein capture device, we refine and extend our previous results by the following:

- Improving the recognition tool chain to improve the single view results, especially the ROI extraction and by including a new recognition scheme proposed by Matsuda et al. [13].
- Employing an advanced score-level fusion framework (BOSARIS [14]).
- Exploring different fusion strategies in terms of which views to include in the fusion.
- Evaluating multi-algorithm fusion per view (fusion is done at score level).

- Combining multi-perspective and multi-algorithm fusion.

The purpose of our evaluations is to maximise the recognition performance while minimising the number of single views involved. If only a limited number of views is involved, the capture device can be built without the need for any rotating parts just by equipping an individual image sensors and an illumination modules per desired view. A biometric capture device which relies on rotating parts is more error prone and more susceptible to external influences, the rotation speed can vary due to increased friction or it can be completely blocked if the finger is not properly inserted. The rotating parts exhibit a higher wear than non-moving parts and are thus more prone to failures. Moreover, the acquisition time of a rotating capture device is higher compared to a non-rotating one as the device needs to rotate around the finger in order to capture the different views. Furthermore, a capturing device exhibiting a closed box design, where the capture subject has to put his finger into a "black hole" poses psychological disadvantages and leads to discomfort. Hence, in practical applications of multi-perspective finger vein biometrics only a capture device built in a non-rotating and open manner is feasible. Consequently, we aim to identify the best combination of two or three views to include in the fusion in order to build such a multi-perspective finger vein capture device based on fixed, non-moving parts only. Figure 10.1 shows the schematic principle of such a capture device for three perspectives: it consists of three independent image capturing pairs, each consisting of its own NIR illumination module and NIR camera.

10.3 Multi-perspective Finger Vein Capture Device

In order to acquire a multi-perspective finger vein dataset, we designed a custom finger vein capture device tailored to this purpose. For more details on the general principle of a finger vein scanner and the vascular pattern recognition basics, the interested reader is referred to our open finger vein scanner chapter [6] and the introductory chapter [15] of this book, respectively. Our multi-perspective finger vein capture device is able to capture images from all around the finger's longitudinal axis (360°). An illustration of the unwrapped finger vein capture device with all its parts labelled can be seen in Fig. 10.2. Its outside dimensions (of the aluminium frame including the rotating part) are 258 × 325 × 455 mm (width × height × depth). The rotating part (rotator) has a diameter of 380 mm. The device consists of an aluminium frame, where the rotation motor and the control board are located and a rotator, which rotates around the finger. The rotating part is connected to a stepping motor by two cogwheels. These cogwheels have a gear ratio of 1:5/3 (motor to rotor). The stepping motor (SY42STH47-1684A [16]) which drives the rotator has 200 steps per full rotation (1.8° per single step). We use a micro-stepping of 1/16, thus one step corresponds to 0.0675°. Hence, it is possible to capture a maximum of 5333 different perspectives of the finger. Located on the right side of the device is the image sensor, an IDS Imaging UI-1240ML-NIR industrial NIR-enhanced camera

[17]. It has a max. resolution of 1280 × 1024 pixels, a max. frame rate of 25 fps and is equipped with a Fujiflim HF9HA-1b 9 mm 2/3" wide-angle lens [18]. To reduce the influence of ambient light, an additional NIR long-pass filter (MIDOPT LP780 [19], with a cut-off wavelength of about 750 nm and a useful range of 780–1000 nm) is mounted on top of the camera lens. The illumination module is located on the opposite side of the image sensor (the left side in Fig. 10.2). Our multi-perspective finger vein capture device is based on the light transmission principle. Instead of typical NIR LEDs the illumination module consists of five NIR laser modules with a peak emission wavelength of 808 nm placed in a strip. Laser diodes have several advantages over LEDs, especially, if the finger is not placed directly on top of the illumination module as mentioned in Chapter [6]. Due to the rotating principle of the biometric capture device, it is not possible for the finger to touch the illumination module, which prevents the use of LEDs without impacting the image quality. Each laser module consists of a NIR laser diode, a control PCB for the laser diode and a housing with a focus-adjustable lens. The plane of focus of the laser modules is set at the axis of rotation where the finger is placed, leading to the highest possible amount of illumination at the position of the finger. Each of the laser modules can be brightness controlled separately (by adjusting the operating current) and independently, enabling a uniform illumination along the whole finger. The finger is put into the capture device at its axis of rotation (in the centre of the image in Fig. 10.2). A fingertip stabiliser (a custom 3D printed part which inside is shaped like the outside of a fingertip) is located at the inside bottom of the rotating part and a height-adjustable finger trunk stabiliser, which is basically a wooden plate with a hole in the middle is located above the rotating part. These finger stabilisers help to reduce finger movements during one acquisition run to a minimum. The finger is put into the capture device so that its tip is inside the fingertip stabiliser, pushing the height-adjustable plate down. Afterwards, this individual finger height is fixed using four screws on the top of the scanner and remains fixed until a new finger is to be captured. All parts except the stepping motor, the camera including the lens and NIR long-pass filter) are self-designed and manufactured by ourselves, including several 3D printed parts, the wooden housing of the rotating part, the housing of the control board, the control board itself and the aluminium frame.

The acquisition process is semi-automated. At first, the subject has to put the finger into the device. Then the height of the finger trunk stabiliser plate has to be adjusted and the operator initiates one capturing run (360° around the finger's longitudinal axis), starting the automated part of the acquisition process.

During this automated data acquisition part, the illumination for each laser module is set automatically by the help of an automated brightness control algorithm. This algorithm tries to achieve a sufficient and uniform illumination along the finger in order to obtain an optimal image contrast. It evaluates the average grey level of the image area around the centre of each laser module i ($GL^i_{current}$) and compares this value to a predefined target grey level (GL^i_{target}). If there is a deviation between these two values, the operating current of the corresponding laser module is adjusted: $I^i_{corr} = \frac{GL^i_{target} - GL^i_{current}}{GL_{\max}} \cdot \frac{I_{\max}}{2 \cdot n}$, where $GL_{\max}$ is the maximum grey value (255 for 8 bit

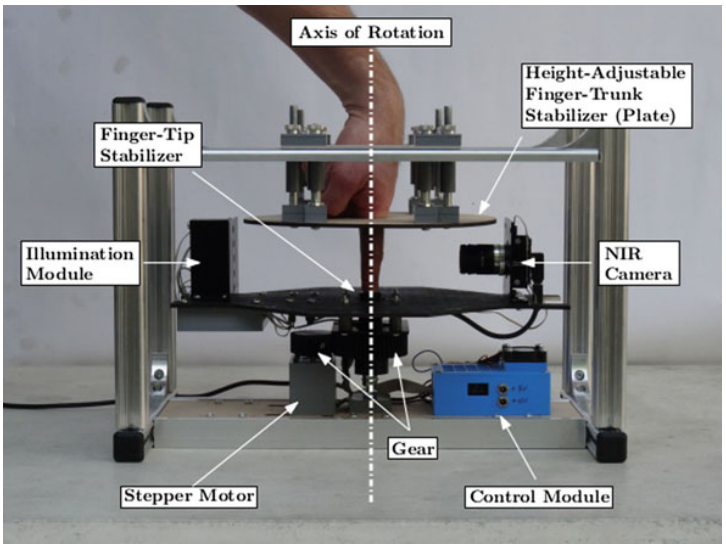

Fig. 10.2 Self-designed multi-perspective finger vein capture device (image originally published in [2], ©2018 IEEE)

images) and n is the number of the current iteration. Initially, all laser modules are set to half of their maximum operating current $I_{\max}$ (corresponding to its maximum intensity). The algorithm finishes in at most $\log_2(I_{\max})$ steps.

After the optimal intensity level for each laser module is set, the video sequence recording is started. The rotator starts to rotate around the finger and an indicator LED is turned on to synchronise the video stream. The rotation is stopped when the rotator reaches its start position again and at this point the indicator LED is turned off. A few frames later the video sequence recording is stopped too. The videos are recorded in the MP4 container format using the MJPG video codec with a frame rate of 15 fps and YUV colour space. The speed of the rotation and the video frame rate are synchronised such that a defined resolution (in degree) of images per full rotation (video frames) is met and the desired degree steps can later be extracted from single, individual frames without the need for temporal interpolation. The set illumination intensity remains the same for the whole capturing run until all perspectives are captured. This ensures the compatibility and comparability of the single, individual perspectives to each other. The different projections in 1° steps corresponding to single video frames are then extracted out of the video sequence. The capture device's indicator LED is utilised to synchronise the video frames with the beginning and the end of the rotation. In theory, there should be 361 images per full rotation run (0° and 360° is captured separately). Due to slight variations in the rotation speed and the video frame rate, there are between 357 and 362 frames instead of 361. Thus, it

became necessary to map the frame with the minimum deviation from the desired rotational angle to the corresponding perspective, resulting in a maximum deviation of 0.5° from the desired rotation angle.

10.4 Multi-perspective Finger Vein Dataset

With the help of our self-designed multi-perspective finger vein capture device, we established a multi-perspective finger vein dataset in order to be able to conduct our multi-perspective score-level fusion experiments. This dataset currently consists of 63 subjects, 4 fingers per subject (index and middle finger of the left and right hand) and 5 runs per finger. The thumb and the pinky finger were not included as they are too short compared to the index and middle. The ring finger was skipped as well as it turned out to be too uncomfortable for the subjects to put it in the capture device for the whole capturing process. The finger was removed and inserted in the device again after each run. During each run, a video sequence of a full 360° rotation with a target resolution of 1° (each frame corresponds to a 1° step) is captured. Figure 10.3 shows the capture device during the data acquisition process. The acquisition process takes approximately 45 s per capture attempt, hence it takes about 15 min to capture a single subject, including all four fingers, 5 runs per finger. The whole dataset consists of $63 \times 4 \times 5 \times 361 = 454{,}860$ images in total. The extracted video frames have a resolution of 1024×1280 pixels and are 8-bit greyscale images stored in png format.

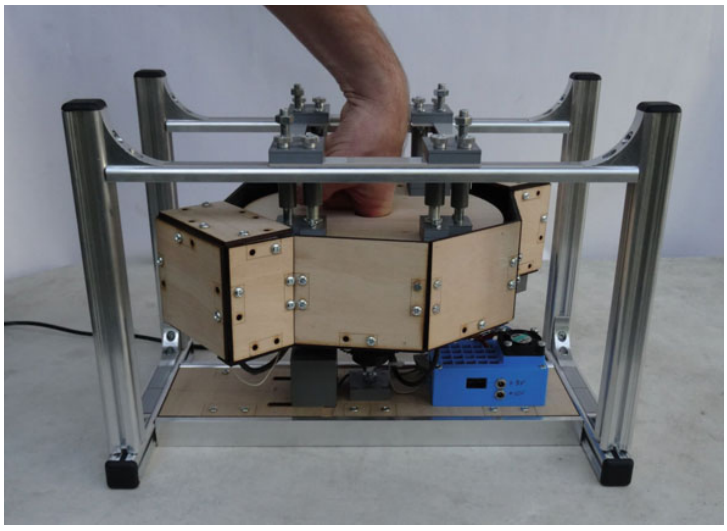

Fig. 10.3 Data acquisition with the multi-perspective finger vein capture device (image originally published in [2], ©2018 IEEE)

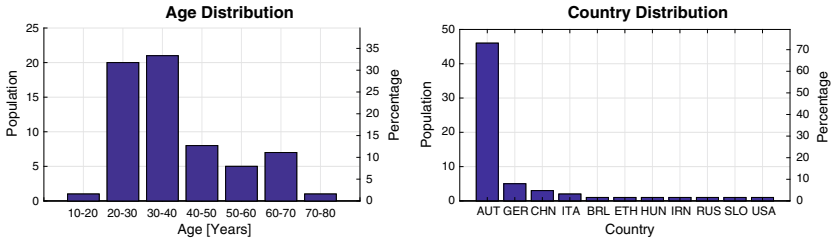

Fig. 10.4 Age (left, image originally published in [2], ©2018 IEEE) and country of origin distribution (right) for the multi-perspective finger vein dataset

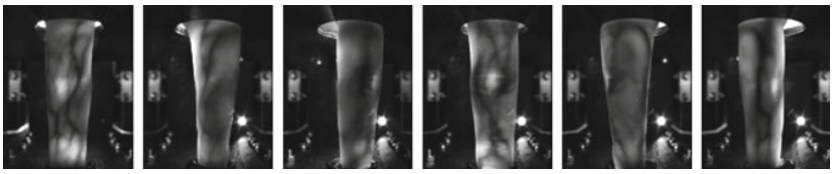

Fig. 10.5 Multi-perspective finger vein dataset example images, from left to right: 0°, 60°, 120°, 180°, 240°, 300° (image originally published in [2], ©2018 IEEE)

The finger is always located in the centre area of the image, thus the images are then cropped to 650 × 1280 pixels to retain the usable finger area only. Figure 10.5 shows some example images in different perspectives from 0° to 300°. It can be clearly seen that the visible vein lines vary among the different perspectives. The black part at the centre top area in the images results from the finger trunk stabilisation plate, which is pushed in further or less depending on the length of the finger.

The gender distribution of the 63 subjects is almost balanced with 27 (42.7%) female and 36 (57.3%) male subjects. The subjects represent a good cross section among all different age groups, as the age distribution, depicted in Fig. 10.4 left, shows. There is only a slight overhang among the 20–40 year old subjects. The youngest subject was 18 and the oldest one 79 years old. The subjects are from 11 different countries (Austria, Brazil, China, Ethiopia, Hungary, Iran, Italy, Russia, Slovenia, USA) while the majority of subjects are white Europeans (73%). The origin country distribution is depicted in Fig. 10.4 right. The dataset is available for research purposes and can be downloaded at http://wavelab.at/sources/PLUSVein-FR/.

10.5 Biometric Fusion

Like every typical biometric recognition system, a finger vein recognition system consists of five steps/modules: image acquisition, preprocessing, feature extraction, comparison and the final decision. This recognition tool chain is depicted in Fig. 10.6.

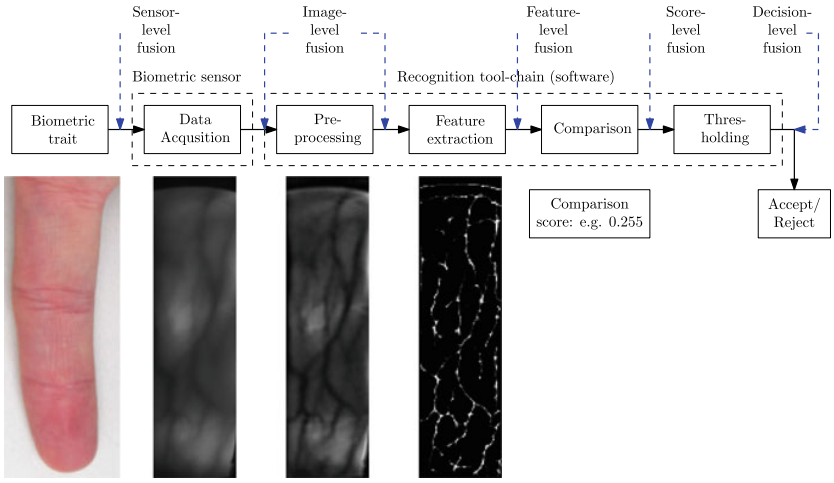

Fig. 10.6 Basic components of a biometric recognition system including the different levels of fusion by taking the example of finger veins (second row)

There are two modes, enrolment and authentication. Authentication includes both, verification as well as identification. During enrolment one or several finger vein images are captured and the extracted biometric templates are stored in a database. During authentication a new template is extracted from a newly captured image and compared against one or more templates stored in the database. The result is a comparison score. Finally the decision module outputs for the capture subject an "accept" or "reject" depending on the evaluation of the comparison score against a threshold.

According to the ISO/IEC TR 24722:2015 standard [20], biometric fusion can be regarded as a combination of information from multiple sources, i.e. sensors, characteristic types, algorithms, instances or presentations in order to improve the overall system's performance and to increase the systems robustness.[1] Biometric fusion can be categorised according to the level of fusion and the origin of input data. The different levels of fusion correspond to the components of a biometric recognition system:

- Sensor-level fusion: is also called multisensorial fusion and describes using multiple sensors for capturing samples of one biometric instance [20]. This can either be done by the sensor itself or during the biometric processing chain. An example of sensor-level fusion are finger vein images that have been captured using different wavelength of near-infrared light and fused by merging the different wavelength bands to obtain one single output image. This can be done by a single biomet-

[1]Recognition performance is just one aspect. PAD performance (robustness against presentation attacks) is another aspect to keep in mind.

ric capture device. Another example is the acquisition and fusion of fingerprint images captured using optical, electrostatic and acoustic sensors.

- Image-level fusion: during data acquisition, the biometric capture device itself might be able to capture multiple samples of the same biometric trait and combine those samples to a single output sample. Image-level fusion corresponds to fusing several images captured from the same biometric trait but not necessarily within the sensor device. Image-level fusion can also be applied after preprocessing so the input to the fusion module is the preprocessed images. One example of image-level fusion is a finger vein capture device that captures more than one finger simultaneously and combines the images from the individual fingers into a single output image, which is also called multi-instance.
- Feature-level fusion: during template creation, several meaningful features, describing the biometric trait's properties, are extracted from the preprocessed images and stored in a feature vector, commonly denoted as biometric template. Feature-level fusion combines several such feature vectors to form a new, higher dimensional feature vector which should represent a subject's biometric traits in a different and more discriminant way. Dimensionality reduction methods are beneficial in combination with feature-level fusion to extract the most significant and discriminative features and to save storage space.
- Score-level fusion: during the comparison step, two templates are compared against each other and a similarity or dissimilarity score is calculated. Score-level fusion combines two or more of those scores into a new, single score. The input scores can originate from different comparison modules. They should either be compatible with each other (e.g. all are similarity scores exhibiting the same range of possible values) or else a score normalisation technique has to be applied during the fusion.
- Decision-level fusion: the output of the decision module is a binary one, which can be interpreted as match/non-match or accept/reject. Decision-level fusion combines two or more of these binary output decisions to a single output one. Usually, majority of voting schemes are employed at decision-level fusion. Note that at the decision level, the least information is available (only a binary decision), compared to the other levels of fusion.

Regarding the origin of the input data, biometric fusion can be categorised into:

- Multi-modal fusion: multiple different types of biometric traits from the same subject is fused together. A popular example is the fusion of information from fingerprints and finger veins or iris and periocular.
- Multi-instance fusion: multiple instances of the same type of biometric trait are fused together. For example, several finger vein images from different fingers of the same subject or information from both irises of one subject are fused together.
- Multi-presentation fusion: multiple samples of the same instance of biometric trait is captured and fused, e.g. several finger veins of the same finger is captured and fused together.

- Multi-algorithmic fusion: multiple feature representations are generated using the same input data, e.g. several different finger vein features are extracted with different algorithms from the same input image and fused together.

There is no direct dependency between the origin of the input data and the level of fusion that is employed.

10.5.1 Fusion in Finger Vein Recognition

This subsection provides an overview of related work in biometric fusion involving finger veins. The first subsection discusses several single modality fusion approaches. The second subsection lists multi-modality fusion approaches which include finger veins among other biometric traits.

10.5.1.1 Single Modality (Finger Vein Only) Fusion

Table 10.1 gives an overview of related work on single modality fusion in finger vein recognition, i.e. only data from finger veins is utilised during fusion at different levels. The table lists the level of fusion applied, the origin of the input data to the fusion, the number of images and subjects contained in the used dataset, the reported biometric performance (EER if not stated otherwise) and the year of publication, sorted according to fusion level and year of publication. All the related works listed in Table 10.1 are described in the following.

Yang and Jia [21] presented a multispectral finger vein fusion approach by fusing enhanced finger vein images captured in different wavelengths. They applied an image denoising method followed by image registration and a brightness adjustment prior to the image-level fusion of images captured in six different wavelength bands. Their image-level fusion strategy operates pixel-wise and is based on an improved regional energy integration method in the spatial domain. The comparison scores are obtained by phase-only correlation. They achieved a minimum EER of 11.02% by fusing all six bands.

Guan et al. [22] applied feature-level fusion to Wavelet transform based vein image features. The high- and low-frequency Wavelet features are obtained independently and then fused by a simple nearest-neighbour rule. They did several experiments using different training set sizes and arrived at a maximum recognition rate of 94.35%. Yang and Zhang [23] proposed a feature-level scheme using global and local features. The local features are extracted using a Gabor filter framework and the global ones using 2D invariant moments. The fusion itself is performed by a weighted fusion strategy based on canonical correlation analysis. They reported a lowest FAR of 1.15% and a FRR of 2.47% for their fused features. Gupta and Gupta [24] proposed a feature-level fusion approach of two distinct binary vein features (the features are binary vein images). The first type of features is extracted using repeated

Table 10.1 Related work in single modality finger vein fusion, ordered according to fusion level and year of publication

Reference	Fusion level	Origin	Images/subjects	Performance (EER)	Year
[21]	Image	Multi-sample	5760/60	11.02%	2012
[22]	Feature	Single-sample	2044/292 (fingers)	Recognition rate: 94.35%	2009
[23]		Single-sample	640/64	FAR: 1.15%, FRR: 2.47%	2010
[24]		Single-sample	3132/156	2.98%	2015
[26]		Single-sample	1440/60	0.19%	2016
[27]	Score	Single-sample	1200/100	0.28%	2010
[28]		Multi-instance	1440/80	0.83% (fusion of 3 fingers)	2012
[29]		Single-sample	4000/50	0.011%	2012
[30]		Single-sample	4080/30	1.56%	2013
[31]		Single-sample	4260/71 (680/85)	2.63%/0.78%	2013
[32]		Single-sample	3804/634 (fingers)	2.84%	2013
[33]		Single-sample	1440/60	0.27%	2014
[2]		Multi-sample	454860/63	0.04%	2018
[35]	Decision	Single-sample	1620/54	FAR: 0.0086% at 1% FRR	2009

line tracking [25]. The second type of features is obtained by multi-scale matched filtering. A variational approach is proposed to fuse both feature extraction methods. The score calculation is conducted by first aligning the two input images with the help of an affine transformation. The affine transformation matrix is found using a gradient descent optimisation based on a sum of squared differences cost function. The authors report a minimum EER of 2.98%. Kauba et al. [26] used different binary vein feature extraction schemes and applied several advanced feature-level fusion schemes (COLLATE, STAPLE, STAPLER), which were originally proposed for segmentation of magnetic resonance imaging (MRI) brain images together with simple average and majority voting based fusion in the finger vein domain. They conducted two different sets of experiments exhibiting two different fusion strategies. In the first one, only a single feature extraction scheme was used with a set of several different feature extraction parameters per input image. The output features

obtained for the individual parameters where then fused together. In the second set, different feature extraction schemes were applied per input image and their outputs were fused. The authors showed that both strategies (single feature extractor as well as multiple feature extractors) lead to an improvement in the recognition accuracy. The best EER achieved for the first strategy was 0.29% and for the second one 0.19% compared to the best EER for the single features of 0.47%.

Zhou and Kumar [27] proposed a score-level fusion scheme for palm vein recognition based on multiple representations. They extracted four different kinds of features, two based on their proposed representations. The first ones are using Hessian phase information from the vein images, the second ones using localised Radon transform to generate a kind of orientation encoding. The other two ones are based on Ordinal Code and a Laplacian representation, respectively. These four feature representations are compared individually to get the output scores which are then fused by applying a heuristic fusion rule. The authors arrived at a minimum EER of 0.28%. Yang et al. [28] did a score-level fusion of extracted features from multiple fingers of the same subject. They used LBP based features and a Hamming distance based comparison module to generate the scores. These scores are then fused using a simple sum rule in combination with triangular norm. Their best reported EER of 0.83% was achieved by fusion ring, middle and index finger using Frank's t-norm. In [29] Kang Park used local as well as global vein features in combination with score-level fusion. The local features are extracted by the help of LBP and compared using the Hamming distance. The global ones are Wavelet transform based features which are compared using the Euclidean distance. The comparison scores are then fused with the help of a radial basis function based support vector machine. Park reported a best achieved EER of 0.0011%. Liu et al. [30] proposed a score-level fusion scheme including pixel as well as super-pixel based finger vein features. LBP, vein pattern structure based and vein minutiae based features form the pixel based features. The super-pixel based image segmentation is done using the SLIC method. Histogram, gradient and entropy features extracted from the super-pixel based segmentation are then combined and form the super-pixel based features. An Euclidean distance based comparison of both individual features is performed to calculate the comparison scores. These scores are normalised and fused by using the weighted average fusion strategy. The weights are tuned to achieve an optimal EER. They reported a minimum EER of 1.56%. Qin et al. [31] applied score-level fusion to multiple representations of the same finger vein pattern. The vein pattern is represented by three different types of features: finger vein shape based, finger vein orientation based and SIFT feature point based features. The former two are subregion partitioned and subregion compared with the help of the SIFT based features, which are treated individually, leading to three comparison scores. The scores are normalised using the Z-score normalisation and then fused by applying a weighted-sum rule based fusion as well as a support vector machine based fusion. They achieved minimum EERs of 2.63 and 0.78%. Lu et al. [32] proposed a score-level fusion scheme based on Gabor features. Usually, the individual filter responses obtained from the Gabor filter bank are weighted and/or directly combined into a single output feature. Instead, the authors extract and compare the output of each single Gabor filter channel separately.

The corresponding comparison scores are then fused using a simple weighted-sum rule. The authors were able to get an EER of 2.84% using their proposed method. Kauba et al. [33] tested different preprocessing cascades in order to improve the individual performance of the single finger vein feature extraction schemes. Binary and SIFT/SURF based features were compared individually to obtain the output scores. These scores were normalised using Min-Max normalisation and then fused using weighted sum/product/average/minimum/maximum fusion rule. The best fusion rule in terms of lowest EER was chosen accordingly. They were able to achieve a minimum EER of 0.27% with the help of score-level fusion compared to a minimum EER of 0.47% for the single features. In our previous work [2], we performed a multi-sample score-level fusion of several different perspectives around the finger. Therefore, we established a multi-perspective finger vein dataset with the help of our self-designed multi-perspective finger vein capture device, described in Sects. 10.4 and 10.3, respectively. Several different perspectives starting from 2 up to 72 were fused at score-level for 4 different kinds of extracted features using a simple sum-rule based fusion. We achieved a best overall EER of 0.039% for the fusion of 18 different views and Maximum Curvature [34] features.

Yang et al. [35] proposed a decision-level fusion approach based on three different finger vein feature representations. They extracted a topological feature, a local moment based feature and a vein shape based feature. These features were compared individually by means of a nearest cosine classifier outputting the class which the input feature belongs to. These output decisions were then fused by the help of the Dempster–Shafer algorithm. The authors reported a lowest FAR of 0.0086% at a FRR of 1%.

10.5.1.2 Multi-modality Fusion Including Finger Veins

In addition to the single modality fusion approaches, several multi-modality fusion approaches including finger veins as one of the involved biometric traits were proposed. Table 10.2 gives an overview of these approaches, including the reference to the original publication, the fusion level, the involved biometric traits, the number of subjects in the dataset used, the reported performance (EER if not stated otherwise) and the year of publication. Most approaches fuse finger-related biometrics, including fingerprint, finger texture, finger shape, finger knuckle and finger veins. There are only two approaches involving other biometrics than finger-related ones. Razzak et al. [36] fused face and finger veins and He et al. [37] fused face, fingerprints and finger veins. Both applied score-level fusion. The number of involved traits varies between at least two and at most four. Fingerprint is the most prominent one [37–46] besides finger veins that is included in the fusion followed by finger texture [38, 43, 45, 47–49] as the second most prominent one and finger shape [42, 43, 50–52] as the third one. The majority of the approaches is based on feature-level and score-level fusion, there are only two decision-level fusion approaches compared to eight

Table 10.2 Related work in finger vein fusion, multi-modality fusion involving finger veins, ordered according to fusion level and year of publication

References	Fusion level	Involved traits	Subjects	Performance (EER)	Year
[40]	Feature	Fingerprint, finger veins	40	1.85% FRR and 0.97% FAR	2011
[44]		Fingerprint, finger veins	64	1.35% FAR at 0% FRR	2012
[46]		Fingerprint, finger veins	40	1.485%	2012
[48]		Finger texture, finger veins	220	0.45%	2012
[49]		Finger texture, finger veins	220	0.435%	2014
[43]		Finger texture, finger shape, fingerprint, finger veins	100	0.00796%	2015
[45]		Finger texture, fingerprint, finger veins	300	0.415%	2016
[51]	Score	Finger shape, finger veins	816	0.075%	2010
[37]		Face, fingerprint, finger veins	510	99.8% GAR at 0.01% FAR	2010
[36]		Face, finger veins	35	5% FAR and 92.4% GAR	2010
[47]		Finger texture, finger veins	312	0.08%	2012
[52]		Finger shape, finger veins	120	4%	2013
[50]		Finger shape, finger veins	492	1.78%	2014
[42]		Finger shape, fingerprint, finger knuckle, finger veins	100	0.0319%	2014
[38]		Finger texture, fingerprint, finger veins	378	0.109%	2015
[41]	Decision	Fingerprint, finger veins	33	1.86%	2011
[39]	Feature/decision	Fingerprint, finger knuckle, finger veins	165	0.04%	2016

feature-level and eight score-level ones. All proposed fusion approaches showed a significant improvement in the recognition accuracy of the fusion compared to using finger veins only.

10.6 Experimental Analysis

This section describes the experimental part of this chapter. At first, the used subset of the dataset introduced in Sect. 10.4 is explained. Afterwards, the finger vein recognition tool chain which is employed during the experimental analysis is described. This is followed by a presentation of the fusion strategy and the applied score-level fusion framework. Afterwards, the experimental protocol to determine the FAR and FRR and consequently the recognition performance in terms of EER/FMR1000/ZeroFMR is explained. Then the results of the individual fusion strategies are given and discussed. Finally, this section is concluded with an overall results discussion.

10.6.1 Finger Vein Dataset

To reduce the amount of data during the fusion, we used a subset of the multi-perspective finger vein dataset [2] only. Not all 360 different perspectives are evaluated, but only each fifth one is considered. Thus, there is a total of 73 different perspectives ($\frac{360°}{5°/step} = 72$ plus the last one which is $360° = 0°$ again results in 73). All 63 capture subjects, 4 fingers per subject and 5 images per view and finger are considered. This results in a total of $73 \times 63 \times 4 \times 5 = 91{,}980$ images instead of 454,860 for the total dataset.

10.6.2 Finger Vein Recognition Tool chain

The finger vein recognition tool chain includes all steps of a biometric recognition system starting with the extraction of the Region of Interest (ROI) to preprocessing, feature extraction and comparison. The input data are the images of the different individual perspectives acquired from the 3D capture device, the output is a comparison score that can be used to determine whether the provided finger belongs to a certain (enrolled) data subject or not.

ROI Extraction

Prior to the ROI extraction, the finger is aligned and normalised. The alignment should place the finger always in the same position in the image, independent of the relative position of the finger during the acquisition. To achieve this, the finger lines (edge between finger and the background of the image) are detected and the centre

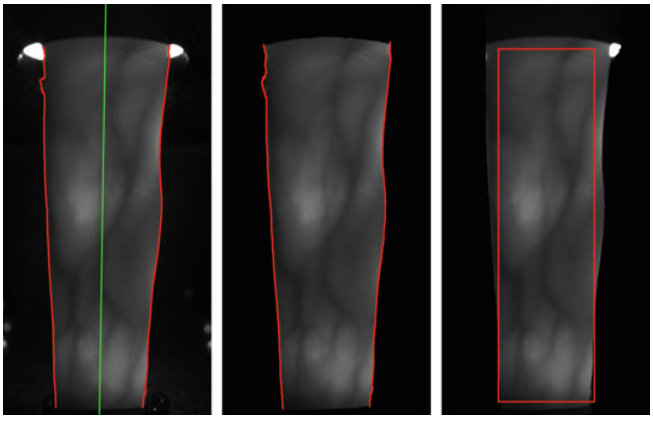

Fig. 10.7 ROI extraction process (images originally published in [2], ©2018 IEEE)

line (in the middle of the two finger lines) is determined. Afterwards, the centre line of the finger is rotated and translated in a way that it is placed in the middle of the image and the image region outside of the finger is masked by setting the pixels to black. The final step is to extract a rectangular ROI of a fixed size (1100 × 300 pixel) from a fixed position. The three steps are visualised in Fig. 10.7. The implementation used is based on the method proposed in [53].

Preprocessing

Preprocessing tries to enhance the low contrast and improve the image quality. In the following the preprocessing methods, we employed in our finger vein recognition tool chain are explained.

Simple **CLAHE** [54] or other local histogram equalisation techniques are most prevalent according to the literature for this purpose. A localised contrast enhancement technique like CLAHE is a suitable baseline tool to enhance the vein images as they exhibit unevenly distributed contrast. CLAHE has an integrated contrast limitation (clip limit) which should avoid the amplification of noise.

High-Frequency Emphasis Filtering (**HFEF**) [55], originally proposed for hand vein image enhancement tries to enhance the vein images in the frequency domain. At first, the discrete Fourier transform of the image is computed, followed by the application of a Butterworth high-pass filter of order n. The authors originally proposed to use a global histogram equalisation but we decided to apply CLAHE instead.

Circular Gabor Filter (**CGF**) as proposed by Zhang and Yang [56] is another finger vein image enhancement technique which is rotation invariant and achieves an optimal joint localisation in both, the spatial and the frequency domain. The authors originally suggested to use grey level grouping for contrast enhancement but we again apply CLAHE instead.

Furthermore, the images were resized to half of their original size, which not only speeded up the comparison process but also improved the results. For more details on

the preprocessing methods, the interested reader is referred to the authors' original publications.

Feature Extraction

We used five different feature extraction methods. The first three techniques discussed aim to extract the vein pattern from the background resulting in a binary image (vein pattern based methods) followed by a comparison of these binary images using a correlation measure. All algorithms are well-established finger vein recognition algorithms. We used the publicly available implementations published in [5].

Maximum Curvature (MC [34]) aims to emphasise only the centre lines of the veins and is therefore insensitive to varying vein widths. The first step is the extraction of the centre positions of the veins by determining the local maximum curvature in cross-sectional profiles obtained in four directions: horizontal, vertical and the two oblique directions. The cross-sectional profile is determined based on the first and second derivates. Then each profile is classified as either being concave or convex, where only the local maxima belonging to a concave profile indicate a vein line. Afterwards, a score according to the width and curvature of the vein region is assigned to each centre position and recorded in a matrix called locus space. Due to noise or other distortions, some pixels may not have been classified correctly at the first step, thus the centre positions of the veins are connected using a filtering operation in all four directions taking the 8-neighbourhood of pixels into account. The final binary output image is obtained by thresholding of the locus space using the median as a threshold.

Principal Curvature (PC [57]): At first the gradient field of the image is calculated. In order to prevent the unwanted amplification of small noise components, a hard thresholding which filters out small gradients by setting their values to zero is done. Then the gradient at each pixel is normalised to a magnitude of 1 to get a normalised gradient field. This normalised gradient field is smoothed by applying a Gaussian filter. The next step is the actual principal curvature calculation. The curvatures are obtained from the Eigenvalues of the Hessian matrix at each pixel. The two Eigenvectors of the Hessian matrix represent the directions of the maximum and minimum curvature and the corresponding Eigenvalues are the principal curvatures. Only the bigger Eigenvalue which corresponds to the maximum curvature among all directions is used. The last step is a threshold based binarisation of the principal curvature values to arrive at the binary vein output image.

Gabor Filter (GF [47]): Gabor filters are inspired by the human visual system's multichannel processing of visual information and have been widely used in biometrics. A Gabor filter is a Gaussian kernel function modulated by a sinusoidal plane wave. Kumar and Zhou [47] proposed a Gabor filter based finger vein extraction approach. Therefore, a filter bank consisting of several 2D even symmetric Gabor filters with different orientations (in $\frac{\pi}{k}$ steps where k is the number of orientations) is created. k feature images are extracted by filtering the vein image using the different filter kernels contained in the Gabor filter bank. The final feature image is obtained by summing all the single feature images from the previous step and thresholding

the resulting feature image. This image is then post-processed using morphological operations to remove noise to get the final binary vein output image.

In contrast to the vein pattern based techniques described above, two key-point based techniques were used. Key-point based techniques try to use information from the most discriminative points as well as considering the neighbourhood and context information around these points by extracting key-point locations and assigning a descriptor to each detected key-point location.

The first one is a **Scale-Invariant Feature Transform** (SIFT [58]) based technique with additional key-point filtering along the finger boundaries to suppress information originating from the finger shape instead of the vascular pattern. This technique was originally proposed by Kauba et al. [33].

Deformation-Tolerant Feature Point Matching (DTFPM [13]): The second key-point based technique replaces the conventional SIFT descriptor and key-point detector by vascular pattern tailored ones. This method is robust against irregular shading and vein deformations due to posture changes. At first, the authors apply a technique originally proposed by Yang and Yang [59] for enhancing the vein images. Then a minimum-curvature map is calculated from the enhanced vein images based on Eigenvalue analysis. The feature point locations are determined from this curvature image (smaller Eigenvalue) at any point where the vein shape is non-linear. The feature descriptor takes the vein shape around the key-point location into account and is extracted from the so-called vein pattern map (larger Eigenvalue). The feature vector contains a quantification of the different vein directions inside a variable-sized window around the key-point location. The descriptor is normalised with the help of a finger shape model in a way that the descriptor area becomes smaller the closer the key-point location is to the finger boundaries. The authors claim that their proposed method is tolerant against several different types of finger posture changes, e.g. longitudinal finger rotation, translations and bending of the finger.

Comparison

For the comparison of the binary feature images we extended the approach in [25] and [34]. As the input images are neither registered to each other nor aligned, the correlation between the input image and in x- and y-direction shifted versions of the reference image is calculated. The maximum of these correlation values is normalised and then used as the final comparison score.

The SIFT features are compared by finding their nearest neighbours/best correspondences and calculating a score based on the distances between the corresponding key-points.

DTFPM employs a deformation tolerant comparison strategy by using non-rigid registration. At first, the correspondences between the key-points in the two images for comparison are found. These correspondences are filtered using a local and global histogram technique based on the relative distances between the corresponding key-points. After this filtering step, the key-point coordinates of one of the involved feature vectors are transformed by applying a non-rigid transformation based on an outlier-robust thin-plate spline model as proposed in [60]. Afterwards, the correspondences between the adjusted key-points are determined again. These updated

correspondences are filtered by a comparison of the descriptor distances with fixed thresholds. The final comparison score is determined as the ratio of the matched points and the sum of the number of detected key-points in both images.

10.6.3 Score-Level Fusion Strategy and Toolkit

We applied three different fusion strategies. The first strategy involves the fusion of all possible combinations of pairs of distinct views (which are $\binom{N}{k} = \binom{73}{2} = 2628$ combinations, 73 different views are considered) as well as all possible three tuples of distinct views (which are $\binom{73}{3} = 62196$ combinations) for each of the five-feature extraction methods. As motivated in the introduction, it is beneficial if the number of involved views is as little as possible to reduce the complexity and the production costs of the biometric capture device and to be able to build such a device without any moving parts. Thus, only pairs and three tuples are considered here. The second strategy employs the fusion of all possible combinations of feature extraction methods per view. There are $\binom{5}{2} + \binom{5}{3} + \binom{5}{4} + \binom{5}{5} = 26$ combinations per perspective, resulting in a total of 10,830 different fusion combinations. Here, our aim is to identify the best combination of features for each individual view which does not necessarily have to be the same across all the different views. The third strategy is a combination (fusion) of the best results obtained during the first and second one.

All three fusion strategies are applied at score-level. The second strategy could be applied at feature-level too, but not for all the involved feature extraction types as they are not compatible with each other. The feature-level fusion of MC, PC and GF is possible while the fusion of DTFPM and SIFT with any of the other feature extraction types is not possible. Feature-level fusion is not possible for the first strategy at all, as there is no meaningful way to combine the features of different perspectives, e.g. by merging the extracted vein lines or using majority voting as the visible vein lines differ for each view. Score-level fusion usually performs better than decision-level fusion, as there is more information available at the score level and there are more variants to fuse the individual scores. Hence, we decided to apply score-level fusion in all three fusion strategies.

In our previous work [2], a simple sum based fusion rule, without any weights for the input scores, was applied. In this work, a more advanced score-level fusion approach, namely the BOSARIS toolkit [14] is utilised. BOSARIS provides a MATLAB based framework for calibrating, fusing and evaluating scores from binary classifiers and has originally been developed for automatic speaker recognition. It can be applied to any biometric trait where two alternate classes are distinguished (genuine/impostor). The toolkit provides several functionalities, e.g. a normalised Bayes error rate plot, ROC and DET plots, including efficient algorithms to generate these plots for large score files, logistic regression solutions for the fusion of several subsystems, solutions for calibration (mapping scores to likelihood ratios), a logistic regression optimiser and an efficient binary score file format. During this work, we only harness the fusion capabilities of BOSARIS though. BOSARIS needs

a supervised training phase where combination weights are trained based on logistic regression in order to fuse multiple input systems into a single output one providing well-calibrated log-likelihood-ratios. This is achieved by employing a general purpose, unconstrained convex optimisation algorithm, which is used to train the logistic regression fusion and calibration methods. Hence, BOSARIS needs a training set of data to find the optimal combination of weights for the actual fusion in order to minimise the classification error and thus to maximise the recognition performance based on the fused output scores. BOSARIS has the option to set a target prior according to the costs of a miss and a false alarm for the training phase of the fusion. We set this target prior to 0.5 assuming that the costs of a miss and a false alarm are both weighted equally.

10.6.4 Evaluation Protocol

The experiments are split into four parts: in the first part, we analyse the recognition performance of all single perspectives. Every perspective is considered as a separate dataset. Here, we do not perform any cross-projection comparison. The images are processed as described in Sect. 10.6.2 and 73 projections all around the finger in 5° steps are extracted. The recognition performance is quantified in terms of the EER as well as the FMR1000 (the lowest FNMR for FMR = 0.1%) and the ZeroFMR (the lowest FNMR for FMR = 0%). The performance values are calculated for each single perspective. For the parameter optimisation, the data set is divided into two roughly equal-sized subsets. The division is based on the contained subjects, i.e. all fingers of the same person are in one subset. Each subset is used to determine the parameters which are then applied to the other subset. This ensures a 100% separation of the data used for determining the optimal parameters and the actual test set. The necessary comparison scores for the FAR/FRR calculation, which is the basis for the EER/FMR1000/ZeroFMR calculation, are determined according to the test protocol of the FVC2004 [61]: to compute the genuine scores, all possible genuine comparisons are done. Instead of computing all possible impostor scores only the first image of a finger is compared against the first image of all other fingers. The final results are evaluated based on the combined scores (genuine and impostor) of both test runs. The parameter optimisation is executed only for the palmar dataset. The same parameter settings are also applied for the experiments on the other perspectives. The resulting number of comparisons for both subsets are listed in Table 10.3. All performance-related result values are given in percentage terms, e.g. 0.04 means 0.04%.

In the second part of our experiments, we fuse different features originating from the same feature extraction method but extracted from different perspectives as described in Sect. 10.6.3. The third part of the experiments is dedicated to a multi-algorithm fusion. We fuse all possible combinations of the five employed feature extraction methods at score level based on the scores obtained during the first part of the experiments, resulting in 2-, 3-, 4- and 5-tuples. In the last part, we com-

Table 10.3 Number of comparisons for each subset

Name	Subjects	Genuine	Impostor	Total
Subset 1	32	1280	8128	9408
Subset 2	31	1240	7626	8866
Total	63	2520	15,754	18,274

bine the two strategies of multi-perspective and multi-algorithm fusion. Based on the results from the two individual fusion strategies we determine the best possible combinations/fusion of perspectives and feature extraction methods. All four parts are evaluated using the same protocol to determine the performance figures. For all fusion experiments, the input data are the comparison scores generated during the single perspective experiments. We apply a fivefold cross-validations procedure, where we use every fold once for the training of the fusion module. The determined fusion parameters are applied to the test data consisting of the four remaining folds. The final results are evaluated based on the combined scores (genuine and impostor) of all five test runs.

We provide the scores files for each individual perspective and feature extraction methods as well as a script to run BOSARIS and generate all the fused scores files and performance figures we used during our experiments. These files and the scripts can be downloaded at http://www.wavelab.at/sources/Prommegger19b/.

10.6.5 Single Perspective Performance Results

The single perspective analysis for MC, PC, GF and SIFT have already been carried out in our previous work [2]. We added DTFPM as an additional key-point based recognition scheme. We had to change our ROI extraction to make the ROIs compatible with DTFPM. Our previous ROI approach selected a fixed size rectangle placed at the centre of the finger, independent of the finger's width. DTFPM is sensitive to parts of the finger outline and background areas that are contained in the input images and expects the finger width normalised to the ROI height. Thus, we updated our ROI extraction scheme as described in Sect. 10.6.2 and recalculated the results for the already evaluated algorithms based on the new ROIs. Note that due to the new ROIs these updated results are different from our previous work. Figure 10.8 top shows the results in terms of EER. There are two lines for every method: the thin line shows the actual EER value, the thicker line is a smoothed version calculated based on the EER using a moving average filter of size 5, which should highlight the trend of the recognition performance. The images captured of neighbouring views contain quite a similar vein structures (note that our step-width is 5°), thus the recognition performance is similar too. The best results are obtained around the palmar (0°, 360°) and dorsal (180°) region. The results of the perspectives in-between are inferior. This

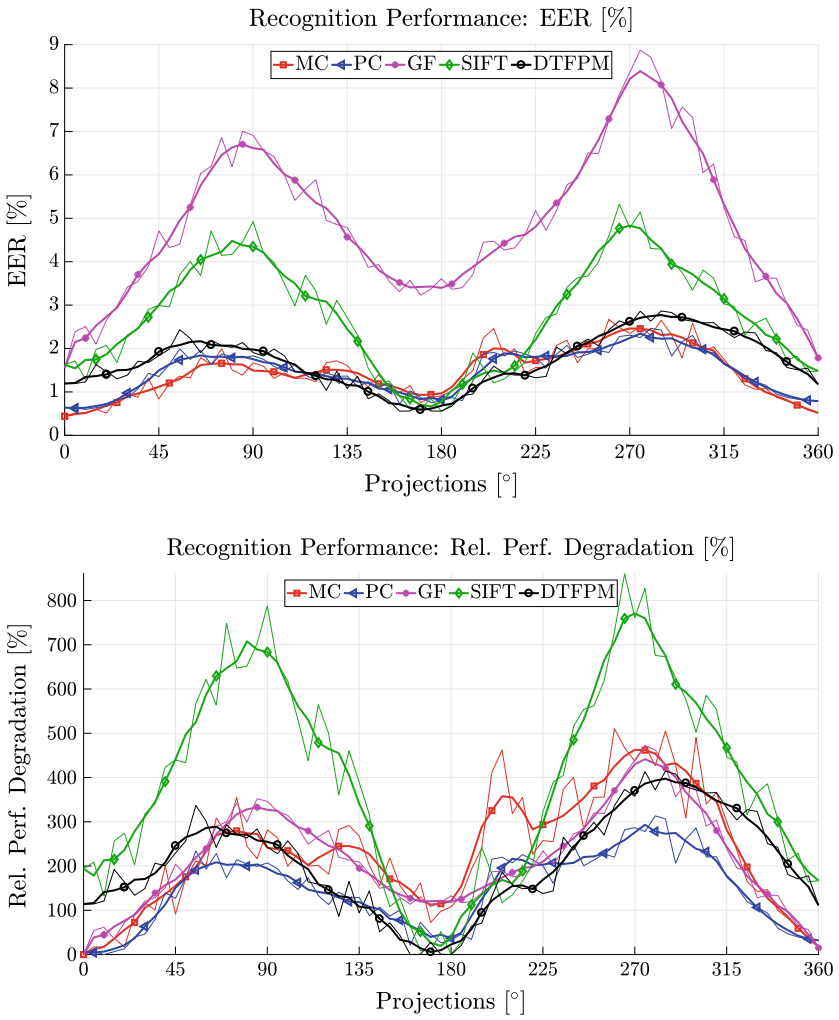

Fig. 10.8 Recognition performance for different projections: EER (top) and relative performance degradation in relation to the best performing view (bottom)

is due to the fact, that they contain fewer visible vein lines and thus fewer vein information than the palmar and dorsal view. Figure 10.9 shows the original ROI, the ROI after preprocessing and the extracted features (using MC) for the views 0°, 90°, 180° and 270°. It reveals that the 90° and 270° views contain less vein information than the palmar and dorsal view. Moreover, the vein extraction algorithms include some features related with the texture of the finger. This is especially visible at 180° where

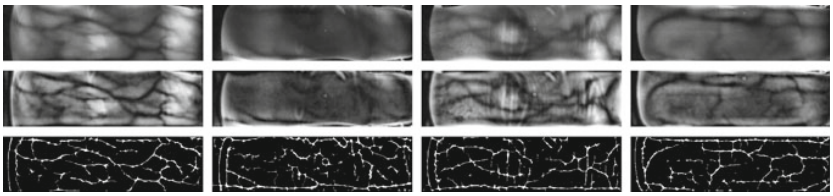

Fig. 10.9 ROI (first row), enhanced images (second row) and extracted MC features (third row) for different projections (originally published in [2], ©2018 IEEE). Note that there are less vein lines visible for 90° and 270° compared to 0° and 180°

some of the features are related with the finger knuckles instead of veins. These features are visible as horizontal lines in the feature image.

For the key-point based algorithms, especially SIFT, the palmar region exhibits a better performance than the other perspectives as well, but the best performance is achieved around the dorsal region. For SIFT this can be explained based on the employed preprocessing: only image (vein) enhancement and no vein extraction (binarisation) ahead of the SIFT key-point calculation is applied. Hence, the non-vein finger texture information is not suppressed in the input images of SIFT. Especially, the structure of finger knuckles seem to contain a lot of additional information which SIFT is able to exploit during feature extraction. Finger knuckles have been introduced by Zhang et al. [62] as an independent biometric characteristic. Yang et al. [63] experienced a similar behaviour. They fused the finger texture of the dorsal view with the vein structure of the palmar view which leads to an improvement in the recognition performance. Consequently, the additional information originating from the finger knuckles and the finger texture present at the dorsal view leads to the superior performance of SIFT for the dorsal view compared to the palmar one.

Table 10.4 lists the information regarding the best and worst perspective for each feature extraction method. MC, PC and GF perform best around the palmar view (note that 360° = 0°), while SIFT and DTFPM perform best around the dorsal view. The overall best result was achieved for MC at 0° with an EER of 0.44% (±0.15) where the number in brackets is the confidence interval. For all feature extraction methods, the worst results can be reported around 270°. The Relative Performance Degradation (RPD) of the different perspectives is visualised in Fig. 10.8 bottom. The RPD, stated in Eq. (10.1), is calculated with respect to the minimum EER (EER^{FT}_{min}) reached for a certain feature extraction method, where $EER^{FT}_{perspective}$ is the EER of the current perspective. The maximum performance degradation across the different algorithms is between 200 and 800%.

$$RPD^{FT}_{perspective} = \frac{EER^{FT}_{perspective} - EER^{FT}_{\text{min}}}{EER^{FT}_{\text{min}}} \tag{10.1}$$

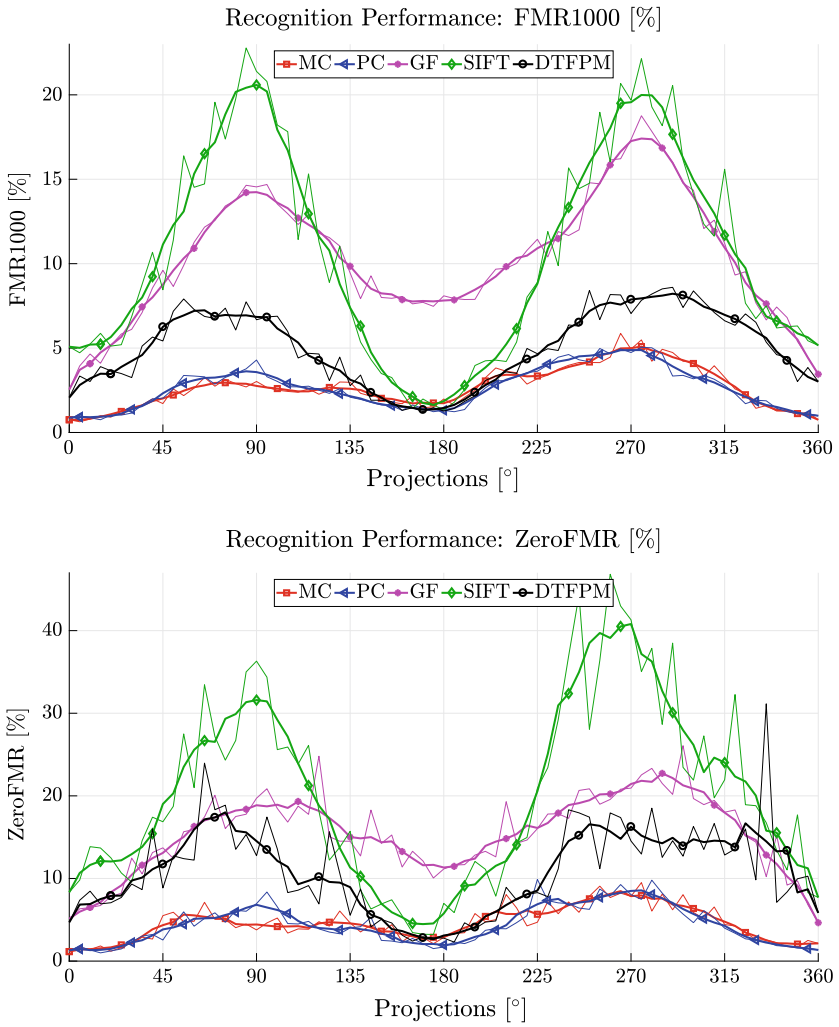

Fig. 10.10 Recognition performance among the different projections: FMR1000 (top), ZeroFMR (bottom)

The FMR1000 and ZeroFMR are visualised in Fig. 10.10 top and bottom, respectively. They follow the same trend as the EER: a good performance around the palmar and dorsal region and an inferior one for the views in between.

Table 10.4 Best/worst single perspective results per feature extraction method and single perspective

Feature type	Best perspective				Worst perspective			
	View	EER	FMR1000	ZeroFMR	View	EER	FMR1000	ZeroFMR
MC	0°	**0.44 (±0.15)**	0.76	1.15	260°	2.67 (±0.37)	4.46	7.69
PC	10°	0.60 (±0.18)	0.87	1.35	280°	2.47 (±0.36)	5.02	9.79
GF	0°	1.55 (±0.28)	2.54	5.13	275°	8.87 (±0.65)	18.76	22.54
SIFT	180°	0.55 (±0.17)	1.35	6.98	265°	5.33 (±0.53)	20.67	42.98
DTFPM	160°	0.56 (±0.17)	1.31	3.13	285°	2.87 (±0.38)	8.51	12.56

10.6.6 Multi-perspective Fusion Results

In the second part of our experiments, we analyse the impact of fusing the extracted features of the same feature extraction method from multiple perspectives (MPF). In detail, we evaluate the fusion of all possible pairs and three tuples.

The first part of this section deals with the fusion of all possible pairs. Figure 10.11 shows heat maps of the EER for all combinations per feature extraction method (top row: MC, PC, bottom row: GF, SIFT and DTFPM). The perspectives involved in the fusion are plotted on x- and y-axis, whereas the performance in terms of EER is visualised using a colour scheme from light/white which corresponds to a low EER (good performance) to dark/red which corresponds to a high EER (bad performance). The actual logarithmic scale is given in the colour bar on the right side of the plots. Note that the results are symmetric with regard to the main diagonal (45°). This diagonal corresponds to the single perspective performance results and is visible as dark line (high EER) in all five plots.

According to the performance analysis of the single perspectives (Sect. 10.6.5), the palmar and dorsal region perform best. Although, there are slight variations among the different feature extraction methods, the results obtained from the single perspectives are confirmed by the two-perspective fusion: a combination of two perspectives including the palmar (close to 0°, 360°) or dorsal (close to 180°) region always results in a good recognition performance. A fusion of two views in-between those two regions result in an inferior performance. For MC, PC and GF the EER for all fusion combinations including the palmar (area along the outer edges of the plot) and dorsal view (cross lines in the centre) perform better (light, white to yellow colours) than fusion combinations without these views (dark, orange to red colours), achieving the best results when both regions are fused (light, white colour).

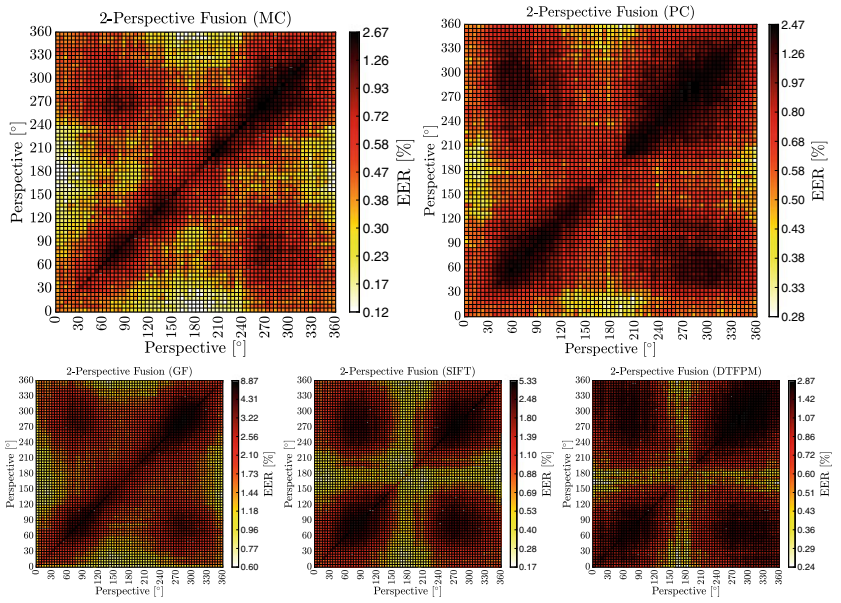

Fig. 10.11 Recognition performance for two-view fusion. Top row: MC (left), PC (right), bottom row: GF (left), SIFT (middle) and DTFPM (right)

Both key-point based methods show a different behaviour. The fusion of the palmar and dorsal region is still superior to all other fusion combinations, but SIFT and DTFPM perform well if the dorsal perspective is included in the fusion in general. This can also be seen in the plots as the 180° cross shows light, white to yellow colours which indicates a good performance. For SIFT, this is even more pronounced than for DTFPM.

Table 10.5 lists the best results in terms of EER, FMR1000 and ZeroFMR for each feature extraction method in detail. MC when fusing 0° and 180° achieves the overall best performance with an EER of 0.12%. For the evaluation of the results, the single perspective baseline EER and the relative performance increase (RPI) with respect to the baseline EER, as calculated in Eq. (10.2), are stated. The performance increase compared to the best single view result is between 110% (PC) and 270% (MC), which corresponds to a 2–3.5 times lower EER than the single perspective performance, respectively.

$$RPI = \frac{EER_{Baseline} - EER_{Fusion}}{EER_{Fusion}} \tag{10.2}$$

In addition to all pairs, all possible triples are evaluated. Table 10.6 shows the five best performing combinations per feature extraction method. Again the single perspective baseline EER and the relative performance increase is included. The highest

Table 10.5 Best two-perspective fusion results per feature extraction method. Best result is highlighted **bold font**. For comparability also the single perspective baseline EER and the relative performance improvement (based on the single perspective performance) is included

Feature type	2 Perspective fusion					Single perspective		Rel. Perf.
	View 1	View 2	EER	FMR1000	ZeroFMR	View	EER	Incr. [%]
MC	0°	180°	**0.12 (±0.08)**	0.12	0.16	0°	0.44	**264.90**
PC	10°	190°	0.28 (±0.12)	0.36	0.56	10°	0.60	113.14
GF	140°	360°	0.60 (±0.18)	0.80	1.56	0°	1.55	156.48
SIFT	165°	205°	0.17 (±0.09)	0.36	1.63	180°	0.55	229.72
DTFPM	0°	160°	0.24 (±0.11)	0.32	1.55	160°	0.56	132.27

recognition performance improvement is between 150% for PC and 1100% for MC which is in any case better than the best two-perspective fusion (see Table 10.5). The overall best result with an EER of 0.036% is achieved using MC when fusing the 5°, 170° and 235° view.

Table 10.6 also includes the perspectives of interest. It is striking, that once again a lot of combinations include perspectives close to the palmar (0°, 360°) and dorsal (180°) regions. Thus, we additionally analysed the occurrence of the palmar and dorsal view in the top 25 results for each feature extraction method. All angles within a certain range around 0° and 180° are mapped to the palmar and dorsal region, respectively. Three different mapping ranges are evaluated: $\pm 15°$ ($345° - 15°$, $165° - 195°$), $\pm 20°$ ($340° - 20°$, $160° - 200°$) and $\pm 25°$ ($335° - 25°$, $155° - 205°$). The results are presented in Table 10.7. It turns out that the best performing individual region (palmar for MC, PC, GF and dorsal for SIFT and DTFPM) is present in most of the top 25 fusion combinations. At a mapping range of $\pm 25°$ it is even included in at least 96% of the top 25 results. For this mapping range also the opposite region is part of at least 80% of the combinations, except for GF (only 24%). For GF, this can be explained by the big performance difference of palmar (~1.5%) and dorsal region (~3.6%).

In order to be able to decide whether a three-perspective fusion is beneficial compared to a two-perspective approach, one way is to calculate the significance of the recognition performance improvement. We use the method proposed in [64] to calculate a boundary for the significance from the achieved EERs. Table 10.8 lists the χ^2 values in detail. The following translations of χ^2 values into p_v values can be used to interpret the values stated in the table: $\chi^2 = 6.6$ corresponds to $p_v = 0.01 (\equiv 1\%)$, $\chi^2 = 7.9$ to $p_v = 0.005 (\equiv 0.5\%)$ and $\chi^2 = 10.8$ to $p_v = 0.001 (\equiv 0.1\%)$. Thus, all performance improvements exhibiting $\chi^2 > 6.6$ are regarded as significant. The resulting χ^2 values indicate that a fusion of two and three perspectives lead to

Table 10.6 Recognition performance for three-view fusion: five best results per feature extraction method. Best result per feature extraction method is highlighted **bold font**. For comparability also the single perspective baseline EER and the relative performance improvement (based on the single perspective performance) is included

Feature type	3 Perspective fusion						Single perspective		Rel. Perf.
	View 1	View 2	View 3	EER	FMR1000	ZeroFMR	View	EER	Impr. [%]
MC	5°	170°	235°	**0.036 (±0.04)**	0.040	0.240	0°	0.44	**1111.78**
	0°	210°	235°	0.036 (±0.04)	0.040	0.120			1107.27
	10°	165°	215°	0.039 (±0.05)	0.040	0.159			1019.25
	20°	160°	235°	0.039 (±0.05)	0.040	0.040			1014.94
	165°	235°	355°	0.039 (±0.05)	0.040	0.159			1014.94
PC	10°	175°	200°	**0.238 (±0.11)**	0.401	0.602	10°	0.60	**150.21**
	20°	205°	235°	0.239 (±0.11)	0.319	0.638			149.65
	175°	235°	360°	0.239 (±0.11)	0.399	0.518			149.65
	140°	190°	360°	0.239 (±0.11)	0.282	0.524			149.59
	155°	210°	360°	0.239 (±0.11)	0.399	0.839			149.45
GF	125°	225°	360°	**0.284 (±0.12)**	0.401	1.325	0°	1.55	**446.48**
	90°	205°	360°	0.313 (±0.13)	0.638	1.794			394.98
	75°	140°	360°	0.321 (±0.13)	0.442	1.165			383.32
	120°	220°	355°	0.321 (±0.13)	0.758	1.475			383.09
	120°	200°	360°	0.321 (±0.13)	0.481	0.882			382.82
SIFT	165°	205°	350°	**0.058 (±0.05)**	0.040	0.635	180°	0.55	**857.58**
	20°	170°	210°	0.075 (±0.06)	0.040	0.714			643.62
	170°	205°	350°	0.081 (±0.06)	0.079	0.476			585.30
	170°	205°	335°	0.081 (±0.06)	0.079	0.635			585.30
	140°	205°	350°	0.081 (±0.06)	0.079	0.714			585.30

(continued)

Table 10.6 (continued)

Feature type	3 Perspective fusion						Single perspective		Rel. Perf.
	View 1	View 2	View 3	EER	FMR1000	ZeroFMR	View	EER	Impr. [%]
DTFPM	5°	160°	280°	**0.159 (±0.09)**	0.559	1.837	160°	0.56	**249.88**
	0°	180°	295°	0.162 (±0.09)	0.439	1.276			243.31
	15°	160°	295°	0.162 (±0.09)	0.439	1.637			243.04
	0°	180°	185°	0.165 (±0.09)	0.437	1.033			237.24
	0°	180°	245°	0.169 (±0.09)	0.439	2.396			228.78

Table 10.7 Analysis of the occurrence of palmar and dorsal views per feature extraction method in the 25 best three-perspective fusions. Both means that palmar and dorsal are present at the same combination.

Feature type (%)	Max distance ±15°			Max distance ±20°			Max distance ±25°		
	Palmar	Dorsal	Both	Palmar	Dorsal	Both	Palmar	Dorsal	Both
MC	84.0	52.0	40.0	92.0	76.0	68.0	**100.0**	84.0	84.0
PC	92.0	68.0	68.0	**100.0**	68.0	68.0	**100.0**	80.0	80.0
GF	**100.0**	8.0	8.0	**100.0**	16.0	16.0	**100.0**	24.0	24.0
SIFT	80.0	88.0	68.0	84.0	88.0	72.0	92.0	96.0	88.0
DTFPM	92.0	60.0	56.0	**100.0**	**100.0**	**100.0**	**100.0**	**100.0**	**100.0**

a significant improvement compared to the single view performance, whereas the improvement for a three perspective fusion compared to fusing two views is lower but still significant for MC, GF and SIFT.

10.6.7 Multi-algorithm Fusion Results

This time different feature extraction methods per perspective are fused (MAF) instead of perspectives per feature extraction method. We evaluate all possible pairs, triples, quadruples and the combination of all five- feature extraction methods, resulting in 26 different combinations per perspective. Figure 10.12 shows the best fusion result per number of fused feature extraction methods. The best result, for example, two-feature extraction methods included in the fusion at 0° means that the best performing pair of features in terms of EER of all pairs calculated at 0° is depicted. It

Table 10.8 Estimated χ^2 from the EER for multi-perspective fusion. Best results per number of involved views is highlighted **bold font**

Feature extraction method	Best EER for [n] involved views			Significance $n_1 \rightarrow n_2$ (χ^2 value)		
	n = 1	n = 2	n = 3	n = 1→n = 2	n = 1→n = 3	n = 2→n = 3
MC	**0.44 (±0.15)**	**0.12 (±0.08)**	**0.036 (±0.04)**	33.415	62.660	8.265
PC	0.60 (±0.18)	0.28 (±0.12)	0.238 (±0.11)	21.264	28.576	0.622
GF	1.55 (±0.28)	0.60 (±0.18)	0.284 (±0.12)	**76.708**	**159.698**	**20.642**
SIFT	0.55 (±0.17)	0.17 (±0.09)	0.058 (±0.05)	36.650	72.755	10.054
DTFPM	0.56 (±0.17)	0.24 (±0.11)	0.159 (±0.09)	23.391	140.869	3.005

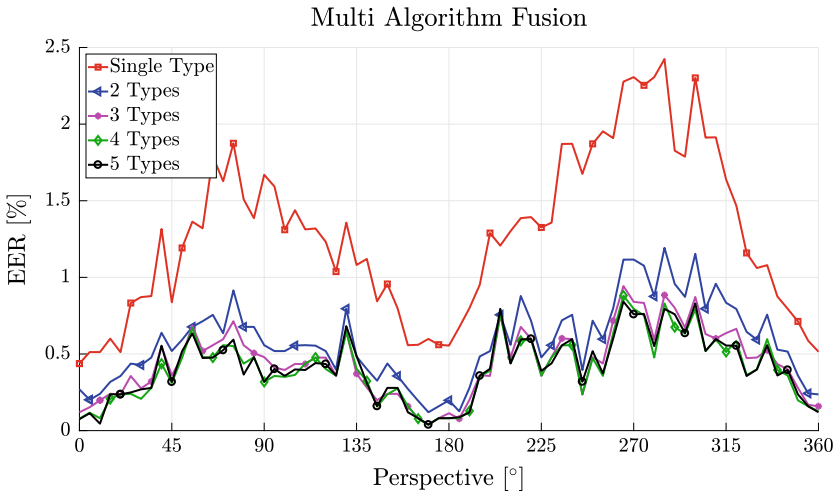

Fig. 10.12 Recognition performance for multi-algorithm fusion: best result in terms of EER per number of feature extraction methods fused is depicted for each perspective

can be seen that even the fusion of two-feature extraction methods increases the performance remarkably. Adding the third feature extraction method further improves the result, whereas fusing four- or five-feature extraction methods does not further improve the recognition performance significantly.

Table 10.9 lists the results of the MAF in more detail. The column occurrence states how often in terms of perspectives a feature extraction method combination performs superior to all other combinations of the same number of included feature

Table 10.9 Multi-algorithm fusion results per number of included features. Occurrence indicates the numbers of perspectives for which the specified combination achieves the best score, the given EER values are calculated over all perspectives. The two view columns state at which view the best and worst performance has been achieved. The best result per number of included feature extraction methods is highlighted **bold face**

# Features included	Feature types	Occurrences	Best		Avg	Worst	
			EER	View	EER	EER	View
1	MC	34 (46.58%)	**0.44 (±0.15)**	0°	1.46	2.67 (±0.37)	260°
	PC	19 (26.03%)	0.60 (±0.18)	10°	1.47	2.47 (±0.36)	280°
	DTFPM	16 (21.92%)	0.56 (±0.17)	160°	1.71	2.87 (±0.38)	285°
	SIFT	4 (5.48%)	0.55 (±0.17)	180°	2.75	5.33 (±0.53)	265°
	GF	–	1.55 (±0.28)	0°	4.89	8.87 (±0.65)	275°
2	PC, DTFPM	31 (42.47%)	0.20 (±0.10)	180°	0.66	1.32 (±0.26)	205°
	MC, DTFPM	22 (30.14%)	0.13 (±0.08)	185°	0.68	1.47 (±0.28)	285°
	MC, SIFT	11 (15.07%)	**0.12 (±0.08)**	170°	0.78	1.83 (±0.31)	265°
	SIFT, DTFPM	8 (10.96%)	0.16 (±0.09)	175°	1.04	2.08 (±0.33)	265°
	MC, PC	1 (1.37%)	0.32 (±0.13)	10°	0.95	1.95 (±0.32)	285°
	PC, SIFT	–	0.24 (±0.11)	180°	0.92	1.88 (±0.31)	265°
	GF, DTFPM	–	0.32 (±0.13)	180°	1.17	2.32 (±0.35)	265°
	GF, SIFT	–	0.40 (±0.14)	170°	1.63	3.56 (±0.43)	265°
	MC, GF	–	0.44 (±0.15)	0°	1.39	2.54 (±0.36)	300°
	PC, GF	–	0.51 (±0.16)	360°	1.28	2.32 (±0.35)	265°

(continued)

Table 10.9 (continued)

# Features included	Feature types	Occurrences	Best		Avg	Worst	
			EER	View	EER	EER	View
3	MC, SIFT, DTFPM	33 (45.21%)	**0.04 (±0.05)**	170°	0.50	0.99 (±0.23)	285°
	MC, PC, DTFPM	23 (31.51%)	0.12 (±0.08)	185°	0.52	1.23 (±0.25)	205°
	PC, SIFT, DTFPM	11 (15.07%)	0.12 (±0.08)	165°	0.53	0.96 (±0.22)	270°
	PC, GF, DTFPM	3 (4.11%)	0.23 (±0.11)	245°	0.62	1.31 (±0.26)	205°
	MC, GF, DTFPM	2 (2.74%)	0.16 (±0.09)	185°	0.66	1.47 (±0.28)	285°
	MC, PC, SIFT	1 (1.37%)	0.12 (±0.08)	170°	0.64	1.31 (±0.26)	265°
	MC, GF, SIFT	–	0.12 (±0.08)	170°	0.77	1.76 (±0.30)	265°
	GF, SIFT, DTFPM	–	0.12 (±0.08)	175°	0.82	1.68 (±0.30)	265°
	PC, GF, SIFT	–	0.25 (±0.11)	170°	0.82	1.71 (±0.30)	265°
	MC, PC, GF	–	0.32 (±0.13)	0°	0.94	1.91 (±0.31)	285°
4	MC, PC, SIFT, DTFPM	51 (69.86%)	**0.04 (±0.05)**	170°	0.42	0.88 (±0.21)	265°
	MC, PC, GF, DTFPM	10 (13.70%)	0.12 (±0.08)	185°	0.51	1.23 (±0.25)	205°
	MC, GF, SIFT, DTFPM	9 (12.33%)	0.04 (±0.05)	170°	0.50	1.07 (±0.24)	275°
	PC, GF, SIFT, DTFPM	3 (4.11%)	0.11 (±0.08)	185°	0.50	1.00 (±0.23)	265°
	MC, PC, GF, SIFT	–	0.09 (±0.07)	170°	0.63	1.32 (±0.26)	265°
5	MC, PC, GF, SIFT, DTFPM	73 (100.00%)	**0.04 (±0.05)**	170°	0.41	0.84 (±0.21)	265°

extraction methods. The minimum, average and maximum EER are determined based on the results for all perspectives of the given feature extraction method combination. Considering single feature extraction methods, MC or PC are included in more than 70% of the best results. GF is not included in any combination that performs best for any perspective. The results of fusing feature extraction method pairs clearly show that it is beneficial to fuse a vein pattern based algorithm (MC, PC, GF) to a key-point based one (SIFT, DTFPM). The combinations of either MC/PC and SIFT/DTFPM are leading to 98% of the best results in two-feature extraction methods fusion.

Table 10.10 Estimated χ^2 from the EER for multi-algorithm fusion

Nr of features EER	n = 1 0.44 (±0.15)	n = 2 0.12 (±0.08)	n = 3 0.04 (±0.05)	n = 4 0.04 (±0.05)	n = 5 0.04 (±0.05)
n = 1 0.44 (±0.15)	–	33.42	60.91	60.91	60.91
n = 2 0.12 (±0.08)	33.42	–	7.31	7.31	7.31
n = 3 0.04 (±0.05)	60.91	7.31	–	0	0
n = 4 0.04 (±0.05)	60.91	7.31	0	–	0
n = 5 0.04 (±0.05)	60.91	7.31	0	0	–

DTFPM (83%) is involved more often than SIFT (26%). Again, GF is not present in any of the best combinations. The overall best result with an EER of 0.04% is achieved when fusing MC, PC, SIFT and DTFPM. Once again, the analysis of the perspective, at which the best result is achieved, confirms, that views from the palmar (0°, 360°) and dorsal (180°) region perform best.

Same as for the two-perspective fusion, we also check the performance increase of three-perspective fusion on its significance. Table 10.10 lists the results in detail. The resulting χ^2 values indicate, that a fusion of two or more feature extraction methods is always beneficial compared to a single feature extraction method. The same holds true when comparing a two-feature extraction method fusion to a three, four or five one. However, applying a four or five feature-type fusion instead of a three feature-type one leads to no significant improvements anymore.

10.6.8 Combined Multi-perspective and Multi-algorithm Fusion

In this section, we combine multiple perspectives and multiple feature extraction methods into one combined fusion method (CMPMAF). For the selection of the relevant perspectives and feature extraction methods we considered the results for multi-perspective fusion (Sect. 10.6.6) and feature extraction method fusion (Sect. 10.6.7). Although the χ^2 values for the multi-perspective fusion in Table 10.8 are only boundaries, they still indicate that the performance increase from two to three perspectives is significant for MC, GF and SIFT. The drawback of adding additional perspectives is the added cost/complexity to the system (additional camera and illumination module, higher computational costs). Therefore, we decided that the significance of the improvement is not high enough to justify the extra effort. As

Table 10.11 Performance results: Fusion of vein pattern based with key-point based features for both, palmar and dorsal view. The best result is highlighted **bold face**

Feature types	Perspectives	EER	FMR1000	ZeroFMR
MC, SIFT	0°, 180°	**0.04 (±0.05)**	0.04	0.64
MC, DTFPM	0°, 180°	0.08 (±0.07)	0.08	0.12
PC, SIFT	0°, 180°	0.16 (±0.09)	0.16	0.32
PC, DTFPM	0°, 180°	0.16 (±0.09)	0.16	0.24
GF, SIFT	0°, 180°	0.20 (±0.10)	0.20	0.60
GF, DTFPM	0°, 180°	0.20 (±0.10)	0.20	0.28

a result of this, we only consider the two perspective fusion. The results presented in Fig. 10.11 and Table 10.5 show that the best results are achieved when fusing palmar and dorsal view. This behaviour can be confirmed when analysing the occurrence of certain perspectives of the three-perspective fusion: Table 10.7 states that the palmar and dorsal region is part of most of the top 25 results. Therefore, we selected 0° and 180° for our combined fusion.

For MAF, the significance analysis (see Table 10.10) indicates that the performance increase from a two to a three feature extraction method fusion is significant but would lead to additional computational costs (for score-level fusion, every feature extraction method needs to be processed by the whole processing chain up to the comparison). Thus, we decided to include the two-feature extraction method MAF into our combined fusion strategy only. Furthermore, the results listed in 10.9 state that 88% of the best two-feature extraction method fusion combinations include one vein pattern based (MC, PC, GF) and one key-point based (SIFT, DTFPM) feature. Therefore, we analysed all possible combinations of those feature extraction methods using both, palmar and dorsal view. Table 10.11 lists the results of the CMPMAF. We evaluated all six possible combinations and arrived at a best EER of 0.04% with a confidence interval of 0.05% for the combined fusion of MC and SIFT for palmar and dorsal view. This result is 11 times better than the best single perspective result (MC at 0° with an EER of 0.44%). All other combinations also perform well. The worst result with an EER of 0.20% is achieved when fusing GF with either SIFT or DTFPM. This is still more than two times better than the best single perspective result. For the sake of completeness, we also calculated the results of the best 3-, 4- and 5-MAF combinations with the palmar and dorsal view. These results, listed in Table 10.12, show that the EER can be further improved. The best result with an EER of 0 is achieved when fusing the scores of all five feature types.

Table 10.13 compares the performance of the best combined two-perspective two-algorithm fusion with the best results of all other fusion strategies. One can see that the calculated χ^2 indicates a significant performance improvement with respect to the single perspective, the 2-MPF and the 2-MAF strategy. All other fusion strategies achieved about the same EER.

Table 10.12 Performance results: Fusion of vein pattern based with key-point based features for both, palmar and dorsal view. The best result is highlighted **bold face**

Feature types	Perspectives	EER	FMR1000	ZeroFMR
MC, SIFT, DTFPM	000°, 180°	0.04 (±0.04)	0.00	0.36
MC, PC, SIFT, DTFPM	000°, 180°	0.01 (±0.01)	0.00	0.12
MC, PC, GF, SIFT, DTFPM	000°, 180°	**0.00 (±0.00)**	0.00	0.00

Table 10.13 Comparison of the best two-perspective two-algorithm fusion combination to the best result of the other fusion strategies including the relative performance improvement, the factor, by which the EER decreased and the boundary χ^2 for significance

Fusion strategy	EER	EER CMPMAF	Rel. Perf. Impr. [%]	Factor	χ^2
Single perspective	0.44 (±0.15)	0.04 (±0.05)	1000	11	60.91
2-MPF	0.12 (±0.08)		200	3	7.31
3-MPF	0.04 (±0.04)		0	1	0.00
2-MAF	0.12 (±0.08)		200	3	7.31
3-MAF	0.04 (±0.05)		0	1	0.00
4-MAF	0.04 (±0.05)		0	1	0.00
5-MAF	0.04 (±0.05)		0	1	0.00

10.6.9 Results Discussion

The evaluation of the independent recognition performances for different projections revealed, that indeed the widely used palmar perspective performed best, followed by the dorsal one performing second best. The views in-between exhibit a slightly worse performance, which is still acceptable. Our results indicate that the presence of finger texture and finger knuckles has a positive influence on the recognition performance. Figure 10.9 shows, that the well-established feature extraction algorithms not only extract features resulting from the finger veins but also from the skin texture of the finger and therefore inherently fuse texture and vein structure. The best single view result was achieved using MC features at the palmar view with an EER of 0.44%.

However, the main objective of this work was to find a suitable trade-off between the number of involved views and feature extraction methods and the recognition performance. In order to arrive at a design decision for a multi-perspective finger vein capture device, several aspects have to be considered: first of all, the gain in recognition accuracy, followed by the production costs and complexity of the biometric capture device which is directly related to the number of involved views and finally the computational complexity of the finger vein recognition system including

the capturing time, i.e. the total processing time, which is related to both, the number of different views and the number of different feature extraction methods involved. Adding more perspectives or feature extraction methods increases the complexity of the finger vein sensor and the recognition tool chain. For every feature extraction method, all steps of the recognition tool chain from preprocessing to comparison need to be executed. Adding further perspectives additionally increases the cost and complexity of the capture device's hardware by the need of either adding more camera/illumination modules (one per perspective) or a rotator that moves camera and illumination module into position. Ideally, the number of perspectives and feature extraction methods are kept to a minimum. Furthermore, additional aspects like an improved resistance against presentation attacks and an increased robustness against environmental influences should be included too. Therefore, the decision on how many perspectives and feature extraction methods are used has to be a trade-off between added cost/complexity and improvement of the recognition performance. Our proposed design is based on the findings during the fusion evaluations.

The multi-perspective fusion results showed that by fusing two independent views, in particular, the palmar and dorsal view, a significant performance gain can be achieved. Adding a second perspective improved the recognition performance between a factor 2–3.5, depending on the feature extraction method. The best result with an EER of 0.12% was achieved using MC features fusing the palmar and dorsal view. Adding a third view still improves the performance compared to two perspectives, but not to the same extent (significance) as from a single perspective to the 2-MPF. In this case, the best result of 0.036% EER was achieved using MC when fusing 5°, 170° and 235°. A biometric capture device able to capture the palmar and the dorsal view simultaneously can be built without any moving parts. Two cameras and two illumination modules are sufficient. Each additional view poses noticeable extra costs in terms of hardware (camera and illumination modules) and complexity of the capture device construction. Therefore, one must decide whether the improvement in accuracy justifies the extra effort. As our results show, the performance improvement from a 2-MPF to a 3-MPF is not as significant as from a single perspective to a 2-MPF, a two-perspective capture device, capturing the vein structure from the palmar and dorsal region is the best choice.

For MAF, a single perspective capturing device is sufficient. Such a biometric capture device can be built in a more compact and less expensive manner than a multi-perspective one. Moreover, existing finger vein capture devices acquiring images of the palmar view, can be utilised to apply multi-algorithm fusion too. However, adding an additional feature type to the MAF increases the computational cost. The MAF results showed, that the fusion of different feature extraction methods per single view improves the overall performance remarkably as well. The best results were obtained when fusing vein pattern based algorithms (especially MC and PC) with key-point based methods (SIFT, DTFPM). The best MAF result with an EER of 0.04% was achieved when fusing MC, SIFT and DTFPM in the dorsal region. Including more feature types does not improve the performance compared to the 3-MAF. As the computational complexity for the calculation and comparison of DTFPM features are higher than for the other features types, and the performance increase compared

to the best 2-MAF utilising MC and SIFT (EER = 0.12%) features is not as significant as from a single perspective to the 2-MAF, the best MAF option is a 2-MAF including MC and SIFT features.

In a third step, we combined MPF and MAF. By using the best performing perspectives of the two-perspective approach (palmar and dorsal) and combining them with a vein pattern based (MC, PC or GF) and a key-point based method (SIFT or DTFPM), we were able to achieve an EER of 0.04% utilising MC and SIFT. This corresponds to an improvement by a factor of 11 compared to the best single perspective performance, while achieving similar results as for the best MPF and MAF strategies. Adding more feature types to the combined fusion strategy further improved the result. Combining palmar and dorsal view together with all five feature types resulted in a perfect result with EER, FMR1000 and ZeroFMR of 0%.

A multi-perspective finger vein capture device is more resistant against presentation attacks, especially against simple paper printout based attacks. Depending on the actual construction of the multi-perspective capture device, it might also be more robust against contamination (e.g. dust and dirt, sun protection lotion or hand cream on the finger surface) of the finger due to the fact that more than one perspective is captured. Hence, the two-perspective capture device is the preferred option over the single perspective, multi-algorithm fusion one regarding these additional aspects.

Taking all the above-mentioned considerations into account, especially the additional advantages provided by a multi-perspective capture device in terms of resistance against presentation attack and robustness against external influences, the most preferable option is to design a two-perspective capture device capturing the palmar and the dorsal view applying a two-algorithm fusion including MC and SIFT features, whereas by including only one view the advantages of multi-perspective recognition can not be retained. The second feature extraction method can be included without involving additional hardware costs just by extending the recognition tool chain and putting up with the extended processing time, which makes the two-feature version beneficial in any case. This proposed finger vein capture device set-up arrives at an EER of 0.04%, which is a performance gain by a factor of 11 compared to the best single-view, single feature performance. Hence, this option provides an optimal trade-off between recognition accuracy, construction costs and processing time.

10.7 Conclusion and Future Work

In this chapter, we introduced multi-perspective finger vein recognition. For most work reported in the literature, only the palmar view is used in finger vein recognition. However, as the finger is an elliptically shaped cylinder, there are several other views available all around the finger's longitudinal axis. In order to be able to exploit these additional views, a suitable biometric capture device able to capture these different views is necessary. This chapter is based on our previous work [2], where we constructed a rotating, multi-perspective finger vein capture device which was then utilised to capture a multi-perspective finger vein data set. Based on this dataset, the

recognition performance of each view was evaluated individually. Then we applied three different score-level fusion strategies, the first one fusing all possible pairs and triples of distinct views, the second one fusing all different feature combinations per each single view and the third one combining the first two approaches. The first strategy was employed to find out the best performing pairs and three tuples of views in terms of recognition performance. The more views are desired to be captured, the higher the complexity and production costs of a suitable biometric capture device. At some point (a certain number of desired views), only a rotating device is able to capture the desired views. A rotating capture device bears several disadvantages, e.g. it is more prone to failures and has an increased capturing time. If only a limited number of views is involved, the production costs and the complexity of the biometric capture device are kept low. The second strategy was applied to investigate the best feature extraction method combination per view. The third strategy, which combines the first two approaches, was applied to find out if the recognition results can be further improved.

The single view evaluation results confirmed that the widely used palmar perspective, followed by the dorsal one (not taking views which are only a few degrees off from the palmar and dorsal view into account), achieves the best performance in finger vein recognition. All the perspectives in-between the palmar and dorsal one exhibit an inferior recognition performance to the palmar and dorsal one. Regarding the multi-perspective score-level fusion it turned out that a fusion of only two perspectives increases the recognition performance significantly, where a fusion of the palmar and the dorsal view performed best. Adding a third perspective still improves the results over the two perspective ones, but not to the same extent as the two perspective ones. The multi-algorithm fusion achieves similar results to the multi-perspective one, arriving at an EER of 0.04% for the combination of three-feature extraction methods. A pure multi-algorithm fusion is preferable in terms of hardware costs and capture device's complexity but does not exhibit the advantages of a multi-perspective recognition in regards to resistance against presentation attacks and increased robustness against external influences. By applying both fusion approaches at the same time for the best performing two perspectives (palmar and dorsal) and the best performing two distinct feature extraction methods (MC, a vein pattern based one and SIFT, a key-point based one), we were able to improve the recognition performance by a factor of 11 compared to the best single view result, achieving an EER of 0.04%.

Regarding recognition performance, hardware costs, processing time and robustness against presentation attacks and external influences the overall best option is to go for the combined multi-perspective and multi-algorithm fusion. In particular, a finger vein capture device capturing the palmar and the dorsal view including MC and SIFT features in a combined fusion provides the best trade-off between the above mentioned considerations and is, therefore, our preferred design decision.

Future Work

The first step will be the construction of a combined multi-perspective and multi-algorithm type fusion finger vein capture device to prove its applicability in real-life

applications of finger vein recognition. We plan to do extended tests with this device, regarding presentation attacks, robustness against external influences like changing ambient conditions as well as subject-related influences.

Besides the capture device construction, our future work will include further analysis using our multi-perspective finger vein dataset. There are several other aspects besides the single perspective performance and the fusion of multiple perspectives which can be evaluated based on this dataset. One example is the robustness evaluation of different finger vein recognition algorithms against longitudinal finger rotation, which we already performed in a separate work [65]. We showed that this kind of rotation poses a severe problem for most algorithms. Since for our dataset the longitudinal rotation angle is known, we will test different techniques to compensate the finger rotation, either by estimating the rotation angle based on the captured images only or by using the known rotation angle and then applying a rotation compensating transform.

Another interesting question is if the best performing view is consistent across different subjects/fingers. To perform this analysis we will extend our dataset to contain at least 100+ subjects and then conduct a subject/finger based analysis to find out if the palmar perspective is the best one for all or at least a majority of the subjects/fingers or if there are significant differences.

Another field of interest is finger vein recognition in the 3D space. Therefore, we want to reconstruct a 3D model of the finger vein structure based on multiple images captured in different perspectives and apply different feature extraction and comparison strategies.

Acknowledgements This project has received funding from the European Union's Horizon 2020 research and innovation programme under grant agreement No. 700259, project PROTECT—Pervasive and UseR Focused BiomeTrics BordEr ProjeCT.

References

1. Kono M (2000) A new method for the identification of individuals by using of vein pattern matching of a finger. In: Proceedings of fifth symposium on pattern measurement, Yamaguchi, Japan, pp 9–12
2. Prommegger B, Kauba C, Uhl A (2018) Multi-perspective finger-vein biometrics. In: Proceedings of the IEEE 9th international conference on biometrics: theory, applications, and systems (BTAS2018), Los Angeles, California, USA, pp 1–9
3. Raghavendra R, Busch C (2015) Exploring dorsal finger vein pattern for robust person recognition. In: 2015 international conference on biometrics (ICB), pp 341–348
4. University of Reading. PROTECT multimodal DB dataset, June 2017. http://projectprotect.eu/dataset/
5. Kauba C, Prommegger B, Uhl A (2018) Focussing the beam—a new laser illumination based data set providing insights to finger-vein recognition. In: Proceedings of the IEEE 9th international conference on biometrics: theory, applications, and systems (BTAS2018), Los Angeles, California, USA, pp 1–9

6. Kauba C, Prommegger B, Uhl A (2019) Openvein—an open-source modular multi-purpose finger-vein scanner design. In: Uhl A, Busch C, Marcel S, Veldhuis R (eds) Handbook of vascular biometrics. Springer Science+Business Media, Boston, MA, USA, pp 77–112
7. Gray H, Goss CM (1974) Anatomy of the human body. Am J Phys Med Rehabil 53(6):293
8. Tome P, Marcel S (2015) On the vulnerability of palm vein recognition to spoofing attacks. In: The 8th IAPR international conference on biometrics (ICB)
9. Tome P, Vanoni M, Marcel S (2014) On the vulnerability of finger vein recognition to spoofing
10. Lu Y, Yoon S, Park DS (2014) Finger vein identification system using two cameras. Electron Lett 50(22):1591–1593
11. Zhang Q, Zhou Y, Wang D, Hu X (2013) Personal authentication using hand vein and knuckle shape point cloud matching. In: 2013 IEEE Sixth international conference on biometrics: theory, applications and systems (BTAS). IEEE, pp 1–6
12. Qi Y, Zhou Y, Zhou C, Hu X, Hu X (2016) Vein point cloud registration algorithm for multi-pose hand vein authentication. In: 2016 IEEE international conference on identity, security and behavior analysis (ISBA). IEEE, pp 1–6
13. Matsuda Y, Miura N, Nagasaka A, Kiyomizu H, Miyatake T (2016) Finger-vein authentication based on deformation-tolerant feature-point matching. Mach Vis Appl 27(2):237–250
14. Brümmer N, De Villiers E (2013) The bosaris toolkit: theory, algorithms and code for surviving the new dcf.arXiv:1304.2865
15. Uhl A (2019) State-of-the-art in vascular biometrics. In: Uhl A, Busch C, Marcel S, Veldhuis R (eds). In: Handbook of vascular biometrics. Springer Science+Business Media, Boston, MA, USA, 3–62
16. Changzhou Songyang Machinery & Electronics New Technic Institute (2018) SY42STH47-1684A high torque hybrid stepping motor data sheet. https://www.pololu.com/file/0J714/SY42STH38-1684A.pdf. Accessed 20 June 2018
17. IDS Imaging Development Systems GmbH (2018) UI-ML1240-NIR NIR-enhanced industrial camera data sheet. https://de.ids-imaging.com/IDS/datasheet_pdf.php?sku=AB00184. Accessed 20 June 2018
18. Fujifilm Corporation (2018) Fujifilm HF9HA-1B product page. http://www.fujifilmusa.com/products/optical_devices/machine-vision/2-3-15/hf9ha-1b/index.html. Accessed 20 June 2018
19. Midopt Corporation (2018) MIDOPT LP780 NIR pass-through filter product page. http://midopt.com/filters/lp780/. Accessed 20 June 2018
20. International Electrotechnical Commission et al (2015) Multimodal and other multibiometric fusion. ISO/IEC TR 24722
21. Yang J, Jia Y (2012) A method of multispectral finger-vein image fusion. In: 2012 IEEE 11th international conference on signal processing (ICSP), vol 1. IEEE, pp 753–756
22. Guan F, Wang K, Mo H, Ma H, Liu J (2009) Research of finger vein recognition based on fusion of wavelet moment and horizontal and vertical 2dpca. In: 2nd international congress on image and signal processing, 2009 CISP'09. IEEE, pp 1–5
23. Yang J, Zhang X (2010) Feature-level fusion of global and local features for finger-vein recognition. In: 2010 IEEE 10th international conference on signal processing (ICSP). IEEE, pp 1702–1705
24. Gupta P, Gupta P (2015) An accurate finger vein based verification system. Digital Signal Process 38:43–52
25. Miura N, Nagasaka A, Miyatake T (2004) Feature extraction of finger-vein patterns based on repeated line tracking and its application to personal identification. Mach Vis Appl 15(4):194–203
26. Kauba C, Piciucco E, Maiorana E, Campisi P, Uhl A (2016) Advanced variants of feature level fusion for finger vein recognition. In: Proceedings of the international conference of the biometrics special interest group (BIOSIG'16), Darmstadt, Germany, pp 1–12
27. Zhou Y, Kumar A (2010) Contactless palm vein identification using multiple representations. In: 2010 fourth IEEE international conference on biometrics: theory applications and systems (BTAS). IEEE, pp 1–6

28. Yang Y, Yang G, Wang S (2012) Finger vein recognition based on multi-instance. Int J Digital Content Technol Appl 6(11)
29. Park KR (2012) Finger vein recognition by combining global and local features based on svm. Comput Inf 30(2):295–309
30. Liu F, Yang G, Yin Y, Xi X (2013) Finger-vein recognition based on fusion of pixel level feature and super-pixel level feature. In: Biometric recognition. Springer, pp 274–281
31. Qin H, Qin L, Xue L, He X, Chengbo Y, Liang X (2013) Finger-vein verification based on multi-features fusion. Sensors 13(11):15048–15067
32. Lu Y, Yoon S, Park DS (2013) Finger vein recognition based on matching score-level fusion of gabor features. J Korean Inst Commun Inf Sci 38(2):174–182
33. Kauba C, Reissig J, Uhl A (2014) Pre-processing cascades and fusion in finger vein recognition. In: Proceedings of the international conference of the biometrics special interest group (BIOSIG'14), Darmstadt, Germany, Sept 2014
34. Miura N, Nagasaka A, Miyatake T (2007) Extraction of finger-vein patterns using maximum curvature points in image profiles. IEICE Trans Inf Syst 90(8):1185–1194
35. Yang J, Shi Y, Yang J, Jiang L (2009) A novel finger-vein recognition method with feature combination. In: 2009 16th IEEE international conference on image processing (ICIP). IEEE, pp 2709–2712
36. Razzak MI, Yusof R, Khalid M (2010) Multimodal face and finger veins biometric authentication. Sci Res Essays 5(17):2529–2534
37. He M, Horng SJ, Fan P, Run RS, Chen RJ, Lai JL, Khan MK, Sentosa KO (2010) Performance evaluation of score level fusion in multimodal biometric systems. Pattern Recogn 43(5):1789–1800
38. Kang W, Chen X, Qiuxia W (2015) The biometric recognition on contactless multi-spectrum finger images. Infrared Phys Technol 68:19–27
39. Khellat-Kihel S, Abrishambaf R, Monteiro JL, Benyettou M (2016) Multimodal fusion of the finger vein, fingerprint and the finger-knuckle-print using kernel fisher analysis. Appl Soft Comput 42:439–447
40. Lin K, Han F, Yang Y, Zhang Z (2011) Feature level fusion of fingerprint and finger vein biometrics. In: International conference in swarm intelligence. Springer, pp 348–355
41. Park YH, Tien DN, Lee HC, Park KR, Lee EC, Kim SM, Kim HC (2011) A multimodal biometric recognition of touched fingerprint and finger-vein. In: 2011 international conference on multimedia and signal processing (CMSP), vol 1. IEEE, pp 247–250
42. Peng J, El-Latif AAA, Li Q, Niu X (2014) Multimodal biometric authentication based on score level fusion of finger biometrics. Optik-Int J Light Electron Opt 125(23):6891–6897
43. Peng J, Li Q, El-Latif AAA, Niu X (2015) Linear discriminant multi-set canonical correlations analysis (ldmcca): an efficient approach for feature fusion of finger biometrics. Multimed Tools Appl 74(13):4469–4486
44. Yang J, Zhang X (2012) Feature-level fusion of fingerprint and finger-vein for personal identification. Pattern Recogn Lett 33(5):623–628
45. Yang J, Zhong Z, Jia G, Li Y (2016) Spatial circular granulation method based on multimodal finger feature. J Electr Comput Eng
46. Yang Y, Lin K, Han F, Zhang Z (2012) Dynamic weighting for effective fusion of fingerprint and finger vein. PICA: Prog Intell Comput Appl 1(1):50–61
47. Kumar A, Zhou Y (2012) Human identification using finger images. IEEE Trans Image Proc 21(4):2228–2244
48. Yang W, Huang X, Liao Q (2012) Fusion of finger vein and finger dorsal texture for personal identification based on comparative competitive coding. In: 2012 19th IEEE international conference on image processing (ICIP). IEEE, pp 1141–1144
49. Yang W, Huang X, Zhou F, Liao Q (2014) Comparative competitive coding for personal identification by using finger vein and finger dorsal texture fusion. Inf Sci 268:20–32
50. Asaari MAM, Suandi SA, Rosdi BA (2014) Fusion of band limited phase only correlation and width centroid contour distance for finger based biometrics. Expert Syst Appl 41(7):3367–3382

51. Kang BJ, Park KR (2010) Multimodal biometric method based on vein and geometry of a single finger. IET Comput Vis 4(3):209–217
52. Xiaoming X, Yilong Y, Gongping Y, Xianjing M (2013) Personalized fusion method based on finger vein and finger contour. J Comput Res Dev 9:015
53. Lu Y, Xie SJ, Yoon S, Yang J, Park DS (2013) Robust finger vein ROI localization based on flexible segmentation. Sensors 13(11):14339–14366
54. Zuiderveld K (1994) Contrast limited adaptive histogram equalization. In: Heckbert PS (ed) Graphics gems IV. Morgan Kaufmann, pp 474–485
55. Zhao J, Tian H, Xu W, Li X (2009) A new approach to hand vein image enhancement. In: Second international conference on intelligent computation technology and automation, 2009. ICICTA'09, vol 1. IEEE, pp 499–501
56. Zhang J, Yang J (2009) Finger-vein image enhancement based on combination of gray-level grouping and circular gabor filter. In: International conference on information engineering and computer science, 2009. ICIECS. IEEE, pp 1–4
57. Choi JH, Song W, Kim T, Lee SR, Kim HC (2009) Finger vein extraction using gradient normalization and principal curvature. Proc SPIE 7251:1–9
58. Lowe DG (1999) Object recognition from local scale-invariant features. In: Proceedings of the seventh IEEE international conference on computer vision (CVPR'99), vol 2. IEEE, pp 1150–1157
59. Yang J, Yang J (2009) Multi-channel gabor filter design for finger-vein image enhancement. In: Fifth international conference on image and graphics, 2009. ICIG'09. IEEE, pp 87–91
60. Rohr K, Fornefett M, Stiehl HS (1999) Approximating thin-plate splines for elastic registration: Integration of landmark errors and orientation attributes. In: Biennial international conference on information processing in medical imaging. Springer, pp 252–265
61. Maio D, Maltoni D, Cappelli R, Wayman JL, Jain AK (2004) FVC2004: third fingerprint verification competition. In: ICBA, vol 3072. Springer, pp 1–7
62. Zhang L, Zhang L, Zhang D (2009) Finger-knuckle-print: a new biometric identifier. In: 2009 16th IEEE international conference on image processing (ICIP). IEEE, pp 1981–1984
63. Yang W, Yu X, Liao Q (2009) Personal authentication using finger vein pattern and finger-dorsa texture fusion. In: Proceedings of the 17th ACM international conference on multimedia. ACM, pp 905–908
64. Hofbauer H, Uhl A (2016) Calculating a boundary for the significance from the equal-error rate. In: Proceedings of the 9th IAPR/IEEE international conference on biometrics (ICB'16), pp 1–4
65. Prommegger B, Kauba C, Uhl A (2018) Longitudinal finger rotation—problems and effects in finger-vein recognition. In: Proceedings of the international conference of the biometrics special interest group (BIOSIG'18), Darmstadt, Germany

Received: 22 September 2020 | Revised: 7 December 2020 | Accepted: 4 January 2021

DOI: 10.1049/bme2.12019

IET Biometrics

The Institution of Engineering and Technology WILEY

ORIGINAL RESEARCH PAPER

A fully rotation invariant multi-camera finger vein recognition system

Bernhard Prommegger | **Andreas Uhl**

Department of Computer Sciences, University of Salzburg, Jakob-Haringer-Str. 2, Salzburg, Austria

Correspondence

Bernhard Prommegger, Department of Computer Sciences, University of Salzburg, Jakob-Haringer-Str. 2, Salzburg, Austria.
Email: bprommeg@cs.sbg.ac.at

Funding information

FFG KIRAS project AUTFingerATM, Grant/Award Number: 864785; FWF project 'Advanced Methods and Applications for Fingervein Recognition', Grant/Award Number: P 32201-NBL

Abstract

Finger vein recognition systems utilize the venous pattern within the fingers to recognize subjects. It has been shown that the alignment of the acquired samples has a major impact on the recognition accuracy of such systems. Although a lot of work has been done in this field, there is still no approach that solves all kind of finger misplacements. In particular, longitudinal finger rotation still causes major problems. As the capturing devices evolve towards contactless acquisition, solutions to alignment problems become more important. As an alternative to rotation detection and correction, the problem can also be addressed by acquiring the vein pattern from different perspectives. This article presents a novel multi-camera finger vein recognition system that captures the vein pattern from multiple perspectives during enrolment and recognition. Contrary to existing multi-camera solutions that use the same capturing device for enrolment and recognition, the capturing devices for the proposed system differ in the configuration of the acquired perspectives. The cameras of the devices are positioned so that the recognition rates around the finger are high and that the number of cameras needed is kept to a minimum. The experimental results confirm the rotation invariance of the proposed approach.

1 | INTRODUCTION

Vascular biometric systems [1] have established themselves as a serious alternative to systems using traditional biometric traits such as fingerprint, face or iris. Especially, systems utilizing the structure of the blood vessels in the palm or fingers, commonly denoted as hand and finger vein biometrics, offer several advantages over traditional modalities. As the vein pattern is located inside the human body and it is only visible in near-infrared (NIR) light, vein images can hardly be acquired without the knowledge of the human subject and no latent variants of it exist [2]. As NIR videos exhibit the blood flow in the vessels, it is possible to apply liveness detection techniques to prevent presentation attacks [3,4].

The performance of finger vein recognition systems mainly depends on the quality and alignment of the acquired sample data. The quality of the vein images is influenced by the physical design and the configuration of the capturing device, whereas the alignment suffers from misplacements of the finger during the acquisition. The most typical finger misplacements are vertical or horizontal shifts, tilt, bending and longitudinal rotations. The problem of misaligned acquisition is not exclusive to finger vein recognition. Also other modalities suffer from it and apply different correction methods. In face recognition, the acquired images are registered towards the frontal view (face frontalization [5,6]). For fingerprint recognition pose-correction is particularly important when using contactless fingerprints [7,8]. In iris recognition, pose-correction is done implicitly by applying Daugmans rubber sheet model [9]. As there is a trend towards contactless acquisition in finger vein recognition systems [10–12], problems due to finger misplacements will get more important.

The negative effect of various types finger misplacements on the recognition rates and how its impact can be reduced or eliminated has been addressed in several publications. Lee et al. [13] utilized minutiae points of the vessel network of the finger for alignment. Huang et al. [14] reduced the influence of longitudinal finger rotation by normalizing the vein pattern assuming an elliptic finger shape. Kumar and Zhou [15] aligned the finger based on their boundary to correct in-planar translations and rotations. The feature-point based recognition system proposed by Matsuda et al. [16] introduces a finger-

shape model together with a non-rigid registration method. Yang et al. [17] introduce a system with an anatomy structure analysis based vein extraction algorithm and matching strategy. In [18], the authors proposed a recognition system which can handle different finger misplacements utilizing PCA-SIFT [19] together with bidirectional deformable spatial pyramid matching [20]. In [21], finger misplacements are detected by analysing the shape of the finger. The deformations are corrected using linear and non-linear transformations. Prommegger et al. [22] improved the resistance against longitudinal rotation by introducing additional comparisons to pre-rotated versions of the enrolment samples. In addition to these software-based solutions, there are also hardware-based ones which guides the subject to place the finger into the correct position in the first place (e.g. [23]). This way, finger misplacements are avoided during acquisition rather than correcting them afterwards in the processing pipeline. Another approach is to acquire the vascular pattern from multiple perspectives. For example Bunda [24] and Sonna Momo et al. [25] propose multi-camera systems that acquire vein images from three different perspectives. A system proposed by Kang et al. [26] applies finger vein recognition in the 3D space.

In [27], the authors presented two rotation invariant finger vein recognition systems. Contrary to traditional single-camera systems, both systems acquire the vein structure from multiple perspectives all around the finger for enrolment, while for recognition still only a single sample is captured. The first approach, *Multi-Perspective Enrolment* (MPE), compares the probe sample to all corresponding enrolment images. The final biometric comparison score is determined using a maximum rule score level fusion. The second approach, *Perspective Cumulative Finger Vein Templates* (PCT), uses the enrolment samples to generate a single template holding the vein information all around the finger. For recognition, the probe sample is compared to the generated template. The experiments confirmed the rotation invariance of both methods, although the recognition rates for MPE are better than those for PCT. In [28], an adopted version of MPE named *Perspective Multiplication for Multi-Perspective Enrolment* (PM-MPE) has been introduced. It effectively reduces the number of perspectives needed to be acquired during enrolment by introducing pseudo perspectives while the recognition rates are kept high. If enough perspectives are acquired during enrolment, negative effects of longitudinal finger rotation on the recognition performance can be inhibited for all three methods.

To counteract longitudinal finger rotation, a novel fully rotation invariant finger vein recognition system, *Combined Multi-Perspective Enrolment and Recognition* (MPER), is presented. Its rotational invariance is achieved by acquiring the vein pattern from several perspectives for both, enrolment and recognition. The final biometric candidate score is calculated using a maximum rule score level fusion (MaxSLF) of the individual comparison scores of each enrolment and recognition perspective. The idea of acquiring multiple perspectives for enrolment and recognition is not new. While existing solutions, for example [24–26], use the same capturing device for enrolment and recognition, for MPER the two devices are different in terms of the acquired perspectives. The two capturing devices are designed in such a way that the rotational distance between the closest enrolment and probe sample as well as the number of perspectives involved is kept to a minimum. The experiments analyse the recognition performance of MPER with respect to rotation invariance and its applicability for real-world applications. The performance achieved with its camera configuration is compared to the performance achieved by the state-of-the-art single-camera systems and by camera configuration of existing multi-camera finger vein recognition systems. The experiments are carried out using the *PLUSVein finger rotation data set* (PLUSVein-FR, [29]).

The reminder of this paper is organized as follows: Longitudinal finger rotation and the problems it causes for finger vein recognition systems are described in more detail in Section 2. Section 3 hold all details on MPER. The experimental set-up together with its results are described in Section 4. Section 5 discusses the design of the required capturing devices. Section 6 concludes the paper along with an outlook on future work.

2 | LONGITUDINAL FINGER ROTATION

Virtually all currently available commercially finger vein scanners acquire the vein images from a single finger using a single camera. Such capturing devices are prone to different misplacements of the finger, including in-planar shifts and rotation, bending, tilt and longitudinal finger rotation, during image acquisition. Misplaced fingers result in images that are misaligned or subject of certain deformations. There exist several countermeasures during acquisition (e.g. by adding support structures to the device for finger positioning) or processing (during pre-processing, feature extraction or comparison) to avoid or compensate certain misplacements, but especially longitudinal finger rotation is hard to prevent.

The acquisition of vein images corresponds to a projection of the blood vessels structure in the finger (3D space) onto a 2D plane. Rotating the finger along its longitudinal axis results in a change of the acquired vein pattern. Figure 1 tries to visualize this effect. The top row shows schematic cross sections of the same finger rotated from $-30°$ to $+30°$ in steps of 10°, the bottom row holds the corresponding vein patterns. It can be clearly seen that the vein pattern changes with the rotation of the finger. These changes follow a non-linear transformation and depend on the relative positioning of the veins to each other. In the worst case some veins can even disappear (merge). The vein pattern acquired at $-30°$, 0° and $+30°$ differ quite a lot. Obviously, this is a major problem for finger vein recognition systems. An analysis of publicly available finger vein data sets [31] showed that longitudinal finger rotation is a real problem. Depending on the acquisition setup (used capturing device and protocol), the examined data sets contain rotational distances of up to 77° between two samples of the same finger. In [30], it has been shown, that the

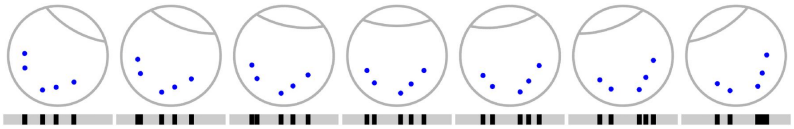

FIGURE 1 The problem of longitudinal finger rotation: The top row visualizes schematic cross sections of the same finger rotated from −30° (left) to +30° (right) in steps of 10°. The blue dots represent veins. The bottom row shows the corresponding vein pattern. The vein pattern changes depending on the positioning of the finger according to a non-linear transformation (originally published in [30])

performance of widely used recognition schemes suffer from such deformations. The negative effect for single camera systems can be reduced if appropriate countermeasures are taken [22]. There are also approaches, that is [24–28], that try to further reduce the negative influence of longitudinal finger rotations by acquiring multiple perspectives of the vein pattern.

3 | COMBINED MULTI-PERSPECTIVE ENROLMENT AND RECOGNITION

Combined Multi-Perspective Enrolment and Recognition (MPER) is a novel fully rotation invariant finger vein recognition method. It achieves its invariance against longitudinal finger rotation by acquiring multiple perspectives during enrolment and recognition. For every recognition attempt, the acquired probe samples are compared to the corresponding enrolment samples utilizing simple vein pattern based finger vein recognition approaches, for example as presented by Miura et al. in [32] combined with *Circular Pattern Normalization* (CPN) [22]. The final biometric candidate score is calculated using a MaxSLF of the individual comparisons. A downside of multi-perspective finger vein recognition is that the cost and complexity of the capturing devices increases with the number of perspectives involved. Multiple perspectives can be acquired by either using more than one camera (e.g. [24–26]), or by building the sensor in a rotating manner (camera and illumination module rotate around the finger, e.g. [29]). Since moving parts are susceptible to malfunction, it is assumed in the further course of the article that each perspective is acquired by a separate camera. Taking this into consideration, MPER was designed in a way that the number of perspectives a capturing device needs to acquire is kept to a minimum, while the rotational range, for which it delivers good results is maximized.

Contrary to existing multi-camera solutions, where the same capturing device is used for enrolment and recognition, for MPER the finger vein scanner used for recognition differs from the one used for enrolment. The n enrolment cameras are linearly spaced around the whole finger (360°). Distributing them evenly around the finger ensures that the vein pattern is captured from all sides. The rotational distance between two adjacent recognition perspectives is $\alpha = \frac{360°}{n}$. For the recognition device m cameras are arranged symmetrically with respect to the desired acquisition perspective. The distance between

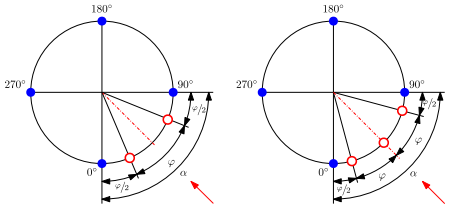

FIGURE 2 Camera positioning for MPER for a rotation distance of 90° between the enrolment perspectives and 2 (left) and 3 (right) recognition cameras. The filled blue dots are enrolment cameras, the red circles are recognition cameras and the red arrow in the bottom right corner represents the perspective acquired during recognition

adjacent perspectives φ depends on the distance between the enrolment cameras α and the number of acquired perspectives m. It is calculated as $\varphi = \frac{\alpha}{m}$. For devices with an odd number of cameras, the middle camera is positioned exactly in the acquisition direction. For those with an even number, the two cameras closest to the desired acquisition perspective are rotated by $\frac{\varphi}{2}$. By this arrangement, the distance between the closest enrolment and recognition perspective δ is always $\delta \leq \delta_{max} = \frac{\varphi}{2}$. If δ_{max} is kept smaller than the rotation the finger vein recognition system utilized by MPER can compensate, then MPER is invariant to longitudinal rotation.

Figure 2 depicts the principle of the positioning of the cameras for MPER for two different scenarios: Both scenarios acquire the same number of enrolment perspectives ($n = 4$, the cameras are visualized as filled blue dots) but a different number of recognition perspectives. The left side captures $m = 2$ recognition perspectives (visualized as red circles) and the right side $m = 3$, respectively. The enrolment cameras are distributed evenly around the whole finger. The rotational distance between two enrolment cameras is $\alpha_4 = \frac{360°}{4} = 90°$. As described, the finger vein scanner used for recognition differs from the enrolment one. The distance between two adjacent cameras φ is calculated as $\varphi = \frac{\alpha}{m}$. For $m = 2$ this results in a distance of $\varphi_{4,2} = 45°$, for $m = 3$ the distance is $\varphi_{4,3} = 30°$, respectively. The maximum distance between the closest enrolment and recognition camera is $\delta_{max} = \frac{\varphi}{2}$, that is $\delta_{max(4,2)} = 22.5°$ and $\delta_{max(4,3)} = 15°$. As all acquired probe perspectives are compared to all enrolment ones, the number of comparisons needed for one recognition attempt is $N_c = n \cdot$

TABLE 1 Details of different MPER settings: number of enrolment (n) and recognition perspectives (m), distances between enrolment (α) and recognition perspectives (φ), maximum distance between the closest enrolment and recognition camera (δ_{max}) and the number of comparisons for one recognition attempt (N_c)

Enrolment		Recognition					
		$m = 2$			$m = 3$		
n	α	φ	δ_{max}	N_c	φ	δ_{max}	N_c
6	60°	30°	15°	12	20°	10°	18
4	90°	45°	22.5°	8	30°	15°	12
3	120°	60°	30°	6	40°	20°	9
2	180°	-	-	-	60°	30°	6

m. Table 1 holds the details for all settings evaluated in the experiments of Section 4.

It is known that the shifts executed during the comparison of binary vein templates have a noticeable influence on the performance of vein pattern based recognition systems (cf. [28,31]). The horizontal shifts in the comparison step of MPER only needs to compensate the maximum distance between the closest enrolment and recognition perspective δ_{max}. The experiments showed that the shift can be calculated as

$$h_{shift} = 2 \cdot \frac{\delta_{max}}{360°} \cdot h = \frac{h}{n \cdot m} \tag{1}$$

where h is the height of the ROI image after applying CPN.

4 | EXPERIMENTS

The experiments of this article carry out a recognition performance analysis of the novel MPER approach with respect to its rotation in various acquisition camera configurations. Furthermore, it compares these results to those of state-of-the-art single-camera solutions and that of camera configurations of existing multi-camera recognition systems. In the last part of the experiments, a runtime analysis for MPER is carried out.

4.1 | Data set

Most available finger vein data sets were acquired using single-camera capturing devices. However, for the analysis of multi-perspective finger vein recognition systems the vein pattern must be available from several, well defined perspectives. Currently, there exist only a few devices, for example [24–26, 29], that are capable of doing so and not all of the data sets captured with these devices are available to the scientific community.

In the experiments, the performance of MPER all around the finger is analysed for different sensor configurations. Acquiring the data for each individual configuration separately using dedicated capturing devices is expensive in two ways: (1) the corresponding sensors have to be built, and above this, (2) the data must be acquired for a sufficient number of subjects and perspectives. The effort increases with each examined MPER configuration. For the planned evaluations (seven different configurations, cf. Table 1), this is unfeasible.

A viable alternative to building dedicated sensors is to acquire vein images all around the finger, and simulate different capturing devices by selecting images from the corresponding perspectives (only those a dedicated capturing device would acquire). This way all possible sensor configurations can be evaluated even though the data was acquired only once. The *PLUSVein Finger Rotation Data Set* (PLUSVein-FR) [29] was acquired with this idea in mind. It provides finger vein images all around the finger (360°) with a resolution of 1°.

The PLUSVein-FR contains finger images captured from 63 different subjects, four fingers per subject, which sums up to a total of 252 unique fingers. Each finger is acquired five times. This results in 1.260 images per perspective and 454.860 vein images for the whole data set (the data set contains 361 perspectives as 0° and 360° have been acquired separately). The experiments are carried out on a subset of the PLUSVein-FR containing perspectives in steps of 5°, resulting in 73 different perspectives (0° and 360° are acquired separately). For more details on the data set, the interested reader is referred to the authors previous publications [29,30].

4.2 | Recognition tool-chain

All experiments have been executed using an automated tool-chain. For MPER it consists of the following components:

1. *Finger region detection* and *finger alignment* are based on [33].
2. Similar to [14], the *region of interest* (ROI) is normalized to a fixed width.
3. In order to enhance the contrast between background and vein pixels *Circular Gabor Filter* (CGF) [34] and simple *CLAHE* (local histogram equalization) [35] are applied on the vein image during *pre-processing*.
4. The binary feature images are generated using the well-established vein pattern based *Maximum Curvature* (MC) method [32].
5. The comparison score between two feature images is evaluated using a correlation-based method. For this purpose, the probe samples are compared to shifted and rotated versions of the enrolment images [36].
6. The final biometric candidate score is calculated using a maximum rule score level fusion of the individual comparison scores of the previous step.

The single-camera performance results, except those for DFVR [18] and the CNN-based approach, have been taken from [22], those for MPE from [27] and those for PM-MPE from [28], respectively. The experiments of the remaining multi-camera systems [24–26] use the same tool-chain as MPER.

As there exists no publicly available implementation of DFVR, this method has been implemented for the experiments. For the implementation the code of *Deformable Spatial Pyramid Matching for Fast Dense Correspondences* proposed by Kim et al. [20] was extended by the vein based key-point selection, PCA-Sift [19] and bidirectional matching as described in [18]. The used CNN approach (Triplet-SqNet) was taken from [37]. It employs the *SqueezeNet* architecture [38] using the *triplet loss function* together with *hard triplet online selection* as described in [39]. All other experiments have been executed using the publicly available *PLUS OpenVein Finger- and Hand-Vein Toolkit* [40]. Download links for the *PLUS OpenVein Finger- and Hand-Vein Toolkit*, the DFVR implementation as well as the trained CNN model are provided on http://www.wavelab.at/sources/Prommegger20b.

4.3 | Evaluation protocol

The evaluation follows the FVC2004 test protocol [36]. For this protocol the evaluation of all possible genuine comparisons is required, while for the impostor scores only the comparisons between the first sample of a finger against the first sample of all other fingers are executed. MPER requires the acquisition of multiple perspectives for both, enrolment and recognition. Therefore two separate subsets are needed. The first subset, which is used for enrolment, contains the first two samples, the second one, used for recognition, contains the remaining three samples. This ensures, that every sample is used either for recognition or enrolment (but never for both). The split results in $63 \cdot 4 \cdot 3 \cdot 2 = 1.512$ genuine and $(63 \cdot 4) \cdot (63 \cdot 4 - 1) = 63.252$ impostor comparisons, which sums up to a total number of 64.764 comparisons. To assess the recognition performance of the examined recognition systems, the *equal error rate* (EER), the *receiver operating characteristics* (ROC) curve and the *area under the ROC curve* (AUC) are used.

4.4 | Performance evaluation for MPER

In this part of the experiments, the performance of the proposed method, MPER, with respect to its rotational invariance all around the finger (360°) is evaluated. In order to assess the performance of the proposed system, the recognition rates of every single (independent) perspective, the intra-perspective performance (IPP), serve as a reference. For the IPP, the 73 perspectives used in the experiments are evaluated independent from each other. This means that in principle every perspective represents its own single-camera system (only a single sample is acquired for enrolment and recognition using a single camera where ideally the finger is placed in the same manner). As a result of this, the results of the IPP, with respect to longitudinal finger rotation, are subject to the same limitations as presented in [30]. The IPP is calculated once without applying any rotation correction or compensation method and once applying CPN [22]. As MPER claims to be invariant against longitudinal finger rotation, recognition rates in the range of (or better than) IPP without rotation compensation can be accounted as good. Be aware that the IPP results are completely independent from each other, and therefore, although the results are presented together, no rotational independence can be concluded from them.

As described in Section 3, for MPER multiple probe samples are compared to multiple enrolment samples. The final score is calculated by fusing the scores of the different comparisons applying a maximum rule score level fusion. For these experiments seven different scenarios, which differ in the number of acquired enrolment and recognition perspectives, are evaluated. For enrolment, four different camera settings are used: six cameras ($\alpha = 60°$), four cameras ($\alpha = 90°$), three cameras ($\alpha = 120°$) and two cameras ($\alpha = 180°$). For recognition, the sensors are equipped with either two or three cameras. The actual rotational distance between the recognition cameras depend on the number of cameras m and the distance of the enrolment cameras α and is calculated by $\varphi = \frac{\alpha}{m}$. The details for the used sensor configurations can be found in Table 1.

The proposed method utilizes Maximum Curvature [32] features. This choice is based on the authors previous work on analysing the influence of longitudinal finger rotation on single-camera recognition systems [22] and (PM-)MPE [27,28,41]. The results in [22] showed that simple vein pattern based systems (e.g. [14,32,42]) in combination with rotation detection or compensation schemes (i.e. [14,21,22]) outperform more sophisticated recognition systems (i.e. [16,17,43]) with respect to their robustness to longitudinal finger rotation. The work on (PM-)MPE, especially [41], also indicated that vein pattern based methods should be preferred over other methods. In the course of this article, the evaluations of [22] were extended by two further recognition schemes ([18,37]) and CPN (cf. Section 4.5).

The trend of the resulting EERs are depicted in Figure 3. In addition, to MPER, also the intra perspective performance results for applying 'no correction' and CPN, respectively, are visualized. The performance of both intra perspective methods show akin trends, just at different EER levels: The best performance results are obtained in the palmar (0°, 360°) region followed by the dorsal (180°) region. The perspectives in between show inferior results, achieving the worst results around 90° and 270°. CPN outperforms 'no correction' over the whole range in average by a factor of two.

The top plot visualizes the results for the settings which use two cameras for recognition. The EERs for MPER-60°/2 and MPER-90°/2 are just above those of the intra perspective CPN results. The plot for both scenarios shows a noticeable drop in the recognition performance at those perspectives where the distance between the closest enrolment and recognition camera reaches its maximum δ_{max}. But they still achieve a better performance for almost all perspectives than IPP without rotation correction. For MPER-120°/2, the performance drops are more prominent. The reason for the high performance degradation is that MPER-120°/2 with

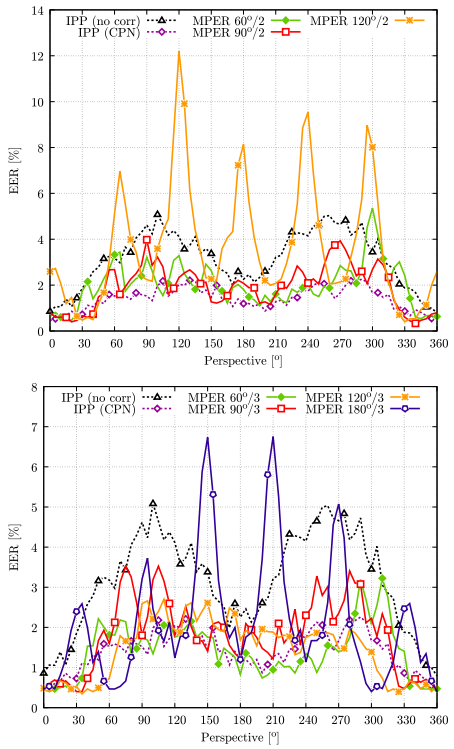

FIGURE 3 Performance results (EER) for MPER: The top plot holds settings for two recognition cameras, the bottom plot for three, respectively

$\delta_{max} = 30°$ brings the recognition system used (MC together with CPN) to its limits.

The bottom plot of Figure 3 shows the result for the three-camera recognition settings (please note the different scaling of the y-axis). All four evaluated scenarios again show the performance drop for those perspectives where the closest enrolment and recognition perspective are the farthest away from each other. However, the performance degradation is only striking for MPER-180°/3, where δ_{max} is again 30°, and thus can no longer be compensated.

The EER describes the behaviour of the system only for the single threshold where the false acceptance rate equals the false rejection rate. To describe the overall performance of the system, the ROC curve, where the system is evaluated for varying thresholds, can be used. The top row of Figure 4 shows the ROC curves for two selected MPER settings (MPER-90°/2 and MPER-120°/3). The evaluation of 73 perspectives for each MPER configuration results in 73 different ROC curves. For a good readability of the plot, only a few selected perspectives are highlighted with different colours, whereas the ROC curves for all other perspectives are shown using the same grey hue. The highlighted perspectives are 0° (palmar view), 45°, 90°, 135° and 180° (dorsal view). The ROC curves confirm the result of the EER values and affirm a good performance for all 73 perspectives. In order to better assess the results of the individual perspectives, a detailed view of the most interesting region (upper left corner, FAR in $[0, 0.1]$, TPR in $[0.9, 1]$) is shown. In this view, differences between the individual curves can be seen. These differences are determined by two factors: (1) the distance δ between the closest enrolment and recognition perspective, and (2) the performance at the examined perspective itself (cf. IPP performance). Table 2 holds the camera positions for enrolment and recognition, the evaluated perspective, the corresponding rotational distance δ and the EERs when applying MPER and IPP without any rotation correction, respectively.

For MPER-90°/2 δ is 22.5° for all five perspectives, which is the maximum δ can be for this setting. Therefore, the performance in relation to each another roughly corresponds to that of the IPP EER results: The best performance is achieved at the palmar view, the worst at 90°. The others are between these two curves. For MPER-120°/3 the situation is slightly different. There, δ differs for the highlighted curves. For 0° and 45° δ is quite small (0° and 5°). For 180° δ reaches its maximum of $\delta_{max} = 20°$. The experiments at 0° and 45° also give the best results. 90° ($\delta = 10°$) and 135° ($\delta = 15°$) perform worst.

In order to be able to better compare the different camera settings, this article uses the *area under ROC curve* (AUC) to aggregate the ROC curve into a single value. The AUC is equivalent to the probability that a randomly selected genuine comparison attempt is ranked higher than a randomly chosen imposter one. High AUC values (close to 1) are an indicator for well performing systems (a perfect system achieves an AUC of 1). The AUC plots in the bottom row of Figure 4 show the AUC values for all camera settings and perspectives. The trend of the curves confirms the results shown for the EER. Again, the worst results are achieved for those perspectives in which the distance between the closest enrolment and recognition perspectives, δ, approaches δ_{max}.

From the presented results it can be deduced, that rotational invariance is only given if the maximum distance between the closed enrolment and recognition camera is less than the angle the used recognition system (in these experiments: MC, CPN and Miura matcher) can compensate. Prommegger et al. showed in [22], that for the used recognition system, this angle should be $\delta_{max} < \pm 30°$ for simple vein pattern based systems. The aim of MPER is to find a camera setting, that maximizes the recognition rates across the entire range all around the finger while minimizing the number of used cameras. For the evaluations the intra-perspective recognition performance without rotation detection is defined as an indicator for good performance. As a result of this, all configurations that achieve recognition rates below the IPP without correction are rated as good. From the evaluated settings, MPER-90°/2 and MPER-120°/3 fulfil this aim best. Since

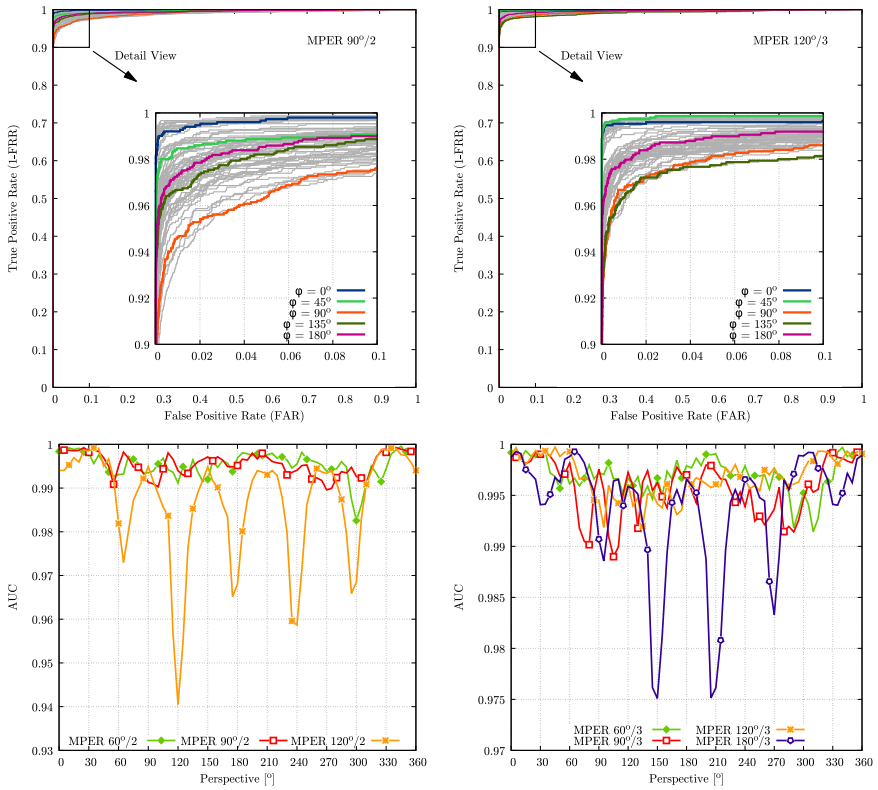

FIGURE 4 Performance results (ROC, AUC) for MPER, the left colon holds the results for two recognition results, the right one for three, respectively. The top row shows the ROC curve for the best performing setting (MPER-90°/2 and MPER-120°/3), the bottom row the AUC for all MPER camera settings

TABLE 2 Details of the highlighted perspectives of the ROC plots in Figure 4

Setting	Enrolment Camera Positions	Recognition Camera Offset	Evaluated Perspectives	Distance δ	EER	EER IPP No Corr
MPER-90°/2	0°	−22.5° 22.5	0°	22.5°	0.8%	0.9%
	90°		45°	22.5°	1.5%	2.8%
	180°		90°	22.5°	4.0%	4.6%
	270°		135°	22.5°	2.5%	4.1%
			180°	22.5°	2.1%	2.3%
MPER-120°/3	0°	−40° 0° 40°	0°	0°	0.5%	0.9%
	120°		45°	5°	0.4%	2.8%
	240°		90°	10°	2.6%	4.6%
			135°	15°	2.6%	4.1%
			180°	20°	1.7%	2.3%

there are usually fewer enrolment than recognition stations, the number of perspectives used for recognition should not exceed the number of enrolment cameras ($m \leq n$). Furthermore, it must be taken into account whether the proposed capturing devices can be built easily. Here, it is especially important to consider whether the illumination modules can be mounted for the proposed camera perspectives. More details on the required capturing devices can be found in Section 5.

4.5 | Comparison to single-camera recognition systems

In this part of the experiments the proposed system is compared to existing single-camera systems. Most of the performance results are taken from [22]. In addition to the methods evaluated in [22], two further recognition schemes, *Deformable Finger Vein Recognition* (DVFR) [18] and a CNN based system (Triplet-SqNet) [37], and *Circular Pattern Normalization* (CPN) [22] are evaluated. The added experiments follow the same protocol as described in [22]. Results taken from [22] are marked with an asterisk (*).

The experiments analyse the recognition performance of single-camera finger vein recognition schemes with respect to longitudinal finger rotation. The experiments intend to show, that with such traditional one-camera systems it is only possible to compensate longitudinal finger rotation to a limited extent. The evaluations include not only different recognition schemes, but also different state-of-the-art rotation correction and compensation methods. The recognition schemes under investigation are three simple vein pattern based recognition schemes, *Maximum Curvature* (MC) [32], *Principal Curvature* (PC) [42] and the *Wide Line Detector* (WLD) [14], where the biometric comparison score is calculated based on the correlation of the extracted binary feature images (as proposed in [44]), *Deformation-Tolerant Feature-Point Matching* (DTFPM) [16], *Finger Vein Recognition with Anatomy Structure Analysis* (ASAVE) [17], an approach based on classical *SIFT* [43] and a more recent scheme, *Deformable Finger Vein Recognition* (DFVR) [18], that uses SIFT features as well. The latter four of these methods claim to be rotation tolerant to a certain extent. The last method, Triplet-SqNet [37], employs the *SqueezeNet* architecture [38] using the *triplet loss function* together with *hard triplet online selection* [39].

The evaluated rotation compensation methods are *Known Angle Approach* [22], *Elliptic Pattern Normalization* (EPN) [14], *Circular Pattern Normalization* (CPN) [22], *Geometric Shape Analysis Based Finger Rotation Deformation Detection and Correction* (GADC) [21] and the *Fixed Angle Approach* proposed in [22]. The *Known Angle Approach* corrects the vein images based on the actual angle of rotation. Since the used PLUSVein-FR provides the actual angle of rotation, this method can be applied. EPN corresponds to a rolling of the finger. It assumes an elliptic finger shape and that the acquired veins are close to the finger surface. This way, non-linear deformations of the vein structure are reduced. CPN is very similar to EPN. The only difference is, that it assumes a circular finger shape instead of an elliptical one. GADC analyses the shape of the finger and based on this analysis, a decision is made for example whether a finger is rotated to the right or left and if so corrected accordingly. For the *Fixed Angle Approach*, the enrolment samples are rotated using a pre-defined angle in both directions. The probe sample is compared to all three enrolment images (the actual acquired one and the two rotated versions of it). The final biometric candidate score is determined using MaxSLF. By pre-rotation the input image, the rotational distance between the probe sample and the (rotated) enrolment samples should be reduced.

First, the behaviour of the single-perspective recognition systems with respect to longitudinal finger rotation is evaluated. The rotational range under investigation is ±45° from the palmar view. Figure 5 depicts the results. All simple vein pattern based methods, MC, PC and WLD, follow akin trends. At the palmar view, they achieve EERs below 1%. Up to a rotation of ±15°, the performance keeps quite stable. The performance drops sharply for larger rotation angles, hitting EERs close to 45% at ±45°. For the more sophisticated approaches, DFVR, DTFPM, SIFT and ASAVE, the performance at the palmar view is worse, but the performance degrades slower when the finger is rotated. The same holds true for the CNN based Triplet-SqNet. The best performance is achieved for DFVR.

Applying different rotation correction approaches can improve the recognition rates for the different recognition systems. As Prommegger et al. [22] showed, simple vein pattern based methods benefit most from rotation correction. Therefore, only one such system, that is using MC features, is evaluated. The results are presented in Figure 6. The line labelled *No Correction* corresponds to the MC line in Figure 5. The results show that the GADC approach (at least on the

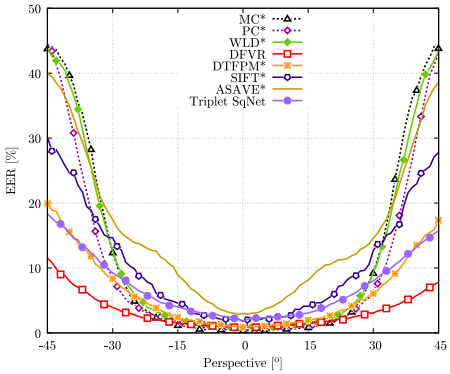

FIGURE 5 Trend of the EER for different single-camera recognition schemes across the rotation angles from −45° to 45° (0° corresponds to the palmar view)

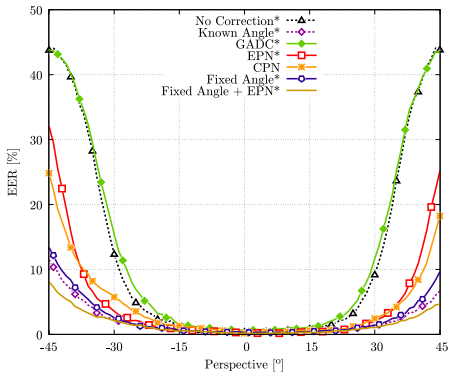

FIGURE 6 Trend of the EER across the different perspectives applying different rotation compensation approaches using MC

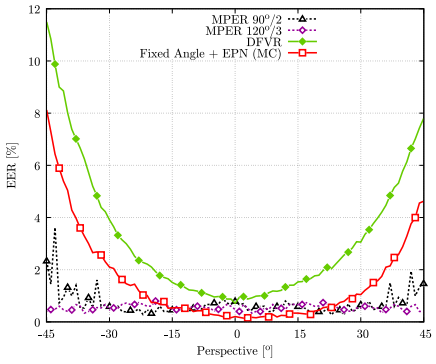

FIGURE 7 Comparison of performance results (EER) for single-camera recognition systems versus MPER

PLUSVein-FR) does not work. EPN and CPN improve results almost to the same extent. However, CPN is a bit better at larger rotation angles. The results of the *Fixed Angle* method are better than for CPN and almost match those of *Known Angle*. The overall best results are achieved if the *Fixed Angle* approach is applied together with EPN. For more details on results for single-perspective recognition systems, the interested reader is referred to the authors previous publication [22].

For the comparison of the proposed systems to classical single-perspective ones, the best recognition system, DFVR, and the best rotation compensation method, the *Fixed Angle* approach together with EPN, have been selected. The results are presented in Figure 7. As the single-perspective systems are tolerant to longitudinal rotation only to a certain extent, only the rotational range of ±45° is evaluated. All methods start with an EER <1% at the palmar view. As the rotation increases, the performance of the single-camera system drops. With DFVR an acceptable performance is achieved almost to ±20°. After that, the recognition rate drops rapidly. For the *Fixed Angle* Method with EPN (using MC features), this crucial point is reached at approximately ±25°. The multi-camera systems, and here in particular MPER-120°/3, achieve stable results across the entire range.

4.6 | Comparison to multi-camera recognition systems

The comparison to the camera configurations of other multi-camera recognition systems is split into two parts. In the first part MPER is compared to systems that enrol multiple perspectives only during enrolment, while in the second part it is compared to recognition systems, that utilize multiple perspectives for both, enrolment and recognition. This comparison should demonstrate the importance of the sensor configuration, that is how the positioning of the cameras, and thus also the selection of the perspectives acquired, influences behaviour of a recognition system. As the aim is to compare the different camera systems and not the whole recognition systems, the same processing chain (feature extraction and comparison) is used for all systems. This ensures that the results are not undermined by use different software.

In the first part the two systems MPE [27] and PM-MPE [28] are evaluated. The main difference between MPE and MPER is the sensor configuration. While MPER acquires multiple perspectives during enrolment and recognition, MPE captures multiple perspectives only during enrolment, and just a single view for recognition. For recognition, both methods compare the acquired probe sample(s) to the enrolled ones. The final biometric comparison score is calculated using a maximum rule score level fusion. PM-MPE is an adopted version of MPE. It still acquires multiple samples during enrolment and just a single one for recognition. The difference is that PM-MPE generates additional perspectives, so called pseudo-perspectives, by rotating the acquired enrolment samples in both directions by a defined rotation angle. During recognition, the probe sample is not only compared to the actual acquired enrolment images, but also to its rotated versions. This way the rotational distance between the closest enrolment sample (including the generated pseudo-perspectives) and the probe sample should be reduced. The results for this comparison are taken from the original publications for MPE [27] and PM-MPE [28]. The settings MPE 45° and PM-MPE 60° fulfil best this papers definition of good performance (EERs better than IPP without rotation correction with a minimum number of involved perspectives). Therefore, the comparison is done with respect to these two settings.

Table 3 lists the details of the configurations. All four methods require less than 10 cameras, the two MPER settings even only six. PM-MPE requires the most computing capacity because it has to calculate the pseudo perspectives during

TABLE 3 Details on the selected settings: Number of acquired enrolment samples (n), distance between enrolment perspectives (α), number of generated pseudo perspectives during enrolment (N_p), the number of recognition perspectives (m), the rotation angle that is used to generate the pseudo perspectives for PM-MPE (φ), the distance between the recognition cameras for MPER (φ), the maximum distance between the recognition and the closest enrolment perspective (δ_{max}), the number of comparisons for one recognition attempt (N_c) and the total number of cameras needed for one enrolment and one recognition device

	Enrolment			Recognition				
Method	n	α	N_p	m	φ	δ_{max}	N_c	**# Total Cameras**
MPER-90°/2	4	90°	-	2	45°	22.5°	8	6
MPER-120°/3	3	120°	-	3	40°	20°	9	6
MPE 45°	8	45°	-	1	-	22.5°	8	9
PM-MPE 60°	6	60°	12	1	20°	10°	18	7

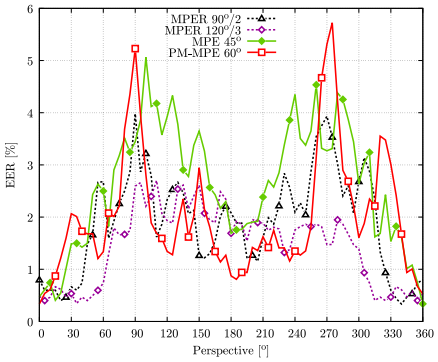

FIGURE 8 Comparison of performance results (EER) for MPER, MPE, PM-MPE

enrolment and executes most comparisons during recognition. With respect to the recognition performance, the most important factor is δ_{max}, the maximum distance between the closest enrolment and recognition perspective. δ_{max} must be smaller than the maximum distance which the used recognition scheme tolerates. In case of MC and CPN this is $\delta_{max} < 30°$. This condition is fulfilled for all four settings. The value of δ_{max} for PM-MPE 60° must be read differently. There, the pseudo perspectives generated for the enrolment sample are also taken into account. Therefore, the maximum distance to the closest actually acquired perspective is $3 * \delta = 30°$.

Figure 8 visualizes the performance results. The EERs of all four methods are in the same range. MPE 45° shows, with exception of a few spikes around 90°, 270° and 330° of PM-MPE, the worst recognition rates. The EERs for MPER-90°/2 are slightly better than for MPE and PM-MPE. The overall best results are achieved for MPER-120°/3. For this setting, the EERs are below 1% for the range between ±60° around the palmar view and less than 3% over the entire range (360°). All four methods can be considered as invariant against longitudinal finger rotation.

TABLE 4 Details of the capturing devices used in [24] (Twente), [25] (GlobalID) and [26] (SCUT): position of the enrolment cameras and offset of the cameras used for recognition

	Enrolment		Recognition			
Method	n	**Camera Positions**	m	**Camera Offset**	δ_{max}	N_c
Twente [24]	3	0°, 22.5°, 337.5°	3	−22.5°, 0°, +22.5°	-	9
GlobalID [25]	3	0°, 45°, 315°	3	−45°, 0°, +45°	-	9
SCUT [26]	3	0°, 120°, 240°	3	−120°, 0°, 120°	60°	9

The main disadvantage of (PM-)MPE is the complexity of their enrolment devices. For MPE 45° a device operating eight cameras is needed, for PM-MPE 60° it still needs six cameras. As a plus, the recognition devices are traditional single camera capturing devices. This might be beneficial if the number of recognition stations is much higher than the number of enrolment ones. The sensors used for the two MPER settings use four or less cameras.

Along to MPER, there are also other finger vein recognition systems that utilize multiple perspectives during enrolment and recognition. This part of the experiments tries to compare such existing multi-camera systems, that is [24–26], to MPER. Again, the main focus of this comparison is to show the influence of the configuration (arrangement of the cameras) of the acquisition devices. Therefore, the evaluation is reduced to a comparison of the camera systems itself. The experiments apply the same methodology as used for MPER: All relevant probe and enrolment samples are compared to each other combined with MaxSLF the get the final comparison score. Using the original algorithms/software as proposed in the original papers would even undermine the results of the intended analysis of the capturing devices. Anyway, for none of the three systems a reference implementation is provided. Therefore a comparison to the original systems would be a difficult task.

The systems taken into consideration are three 3-camera systems. The first one has been proposed by the *University of Twente* [24]. Its cameras are positioned towards the palmar view (0°) and under an angle of 22.5° in both directions from the palmar view. As the PLUSVein-FR data set provides only perspectives in steps of 1°, the cameras used in the experiments are placed at −22°, 0° and 23°. The second capturing device [25] is from *Global ID SA*, a commercial company. In principle the design of the sensor is identical to that of Twente. Only the distance between the cameras (45°) is larger than for the device from Twente (22.5°). The last capturing device was proposed by the *South China University of Technology* (SCUT) [26]. Its three cameras are positioned equally distributed around the finger which results in a rotational distance between two adjacent cameras of $\alpha = 120°$. Table 4 states the details of the three camera systems. For more information on the capturing devices, the interested reader is referred to the original publications.

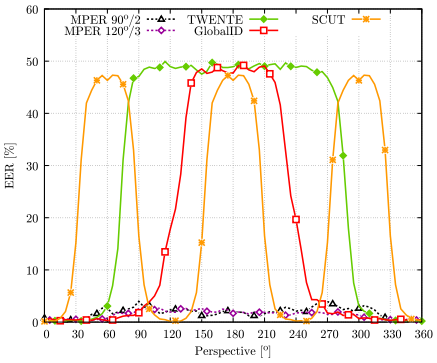

FIGURE 9 Comparison of performance results (EER) of other multi-camera recognition systems to MPER

Figure 9 shows the results for the three camera systems. The green line with filled diamonds depicts the results for the Twente sensor. Around the intended acquisition perspective (palmar view, 0° or 360°), this sensor configuration shows good recognition results with EER's below 0.5%. In the experiments, this performance keeps quite stable up to ±55°. Starting with this rotation angle, the performance starts to degrade. Around ±70° the recognition rate drops rapidly, arriving at EERs between 45% and 50% for rotations above ±85°. This is the expected behaviour. For a rotation of 70°, the distance of the closest enrolment and recognition camera is 25° (closest enrolment camera at 23°, recognition camera at 48°) which is, according to [22], close to the maximum rotation MC together with CPN can compensate.

The red line with the empty squared markers shows the results for the GlobalID sensor. Its behaviour is akin to the one of Twente. The difference is, that the range, in which it delivers good recognition results, is larger: For GlobalID, the performance degradation starts around 90° and drops rapidly beginning at 115°. The reason for this is the larger distance between the cameras. The chosen 45° is the largest possible distance the utilized recognition scheme (MC in combination with CPN) can handle.

The cameras of the SCUT sensor are positioned at the palmar view (intended acquisition perspective), 120° and 240°. Its results are visualized as ochre line with asterisks markers. Up to a longitudinal rotation of ±25° from the palmar view, the system shows good recognition rates. Starting at this angle the performance starts to degrade quickly, reaching EER's >40% between 40° and 80°. When the finger is rotated further towards 120°, the performance improves to the same level as achieved at 0°. That is the expected behaviour because the cameras are evenly distributed around the finger (0°, 120° and 240°), and thus for a finger rotation of 120° the same views as for 0° are acquired. The same behaviour can be observed at 240°.

It is obvious that none of the three camera systems achieve rotation invariance when applying the same methodology as used for MPER. The capturing devices proposed by the University of Twente [24], GlobalID [25] and SCUT [26], only show a good performance in the range that is covered by enrolment and recognition cameras while MPER-90°/2 achieves EERs below 4% and MPER-120°/3 even below 3% all around the finger. Again, please note that for the experiments only the capturing devices itself are evaluated using the same methodology as for MPER, and not the whole finger vein recognition systems as proposed in [24–26]. As a result of this, the comparison to the three capturing devices (Twente, GlobalID and SCUT) is not quite fair (the Twente and GlobalID sensors were not built with rotation invariance recognition all around the finger (360°) in mind and the SCUT sensor was developed for a different CNN based recognition system). But still, the results clearly show that the positioning of the cameras in the enrolment and recognition capturing devices is an essential factor for achieving rotation invariance in finger vein recognition. Especially the comparison to MPER-120°/3 is interesting: The sensors of Twente, GlobalID, SCUT and MPER-120°/3 use three cameras for both, enrolment and recognition, but only MPER-120°/3 (using a really simple recognition scheme: MC features, CPN and MaxSLF) achieves rotational invariance. The invariance for MPER-120°/3 is achieved by placing the cameras in a way that the maximum distance between the closest enrolment and recognition perspectives stays below the distance the recognition system can handle.

4.7 | Runtime analysis

As MPER introduces additional processing steps compared to simple single-camera systems, the runtime costs are relevant in a practical application. In this analysis the focus is set on the recognition step as this is more important to end users than enrolment (enrolment is executed only once whereas recognition is executed n times). The runtime of the best settings with respect to the recognition performance (MPER-90°/, MPER-120°/3, MPE 45° and PM-MPE 60°) are compared to single perspective systems with no correction, applying the *Fixed Angle* approach and the combination of EPN and the *Fixed Angle* method. As shown in [41], the systems like (PM-)MPE and MPER are applicable to all simple vein pattern based methods. Therefore, the runtime evaluation has been done for three such recognition schemes: MC, PC and WLD. Note that the implementations of the recognition algorithms used in these experiments are not optimized for runtime performance. Hence, the determined durations are only indicators for the additional costs imposed due to the evaluated approaches. As there are no reference implementations for [24–26] available, a runtime analysis for these systems is not possible.

The relevant processing steps to evaluate are pattern normalization (PN), pre-processing (PP), feature extraction (FE), comparison (CMP) and MaxSLF. While PN and MaxSLF are independent, the other three (PP, FE and CMP) are

TABLE 5 The average time of cost for recognition scheme dependent processing steps

Method	PP [ms]	FE [ms]	Comparison [ms]
MC	35.212	276.484	3.619
PC	36.903	5.779	3.339
WLD	24.435	26.843	3.253

dependent on the used recognition scheme. For the estimation of the runtime of every processing step, the average time needed for 1.260 repetitions (number of images of each perspective from PLUSVein-FR) has been calculated. For the scheme independent processing steps it is worth to mention, that CPN is more than 12 times faster than EPN (7 ms instead of 87 ms). The reason for this is, that the arc length of ellipses cannot be calculated directly. The MaxSLF is very fast, regardless of the number of scores involved (always < 0.001 ms). Table 5 lists the average processing times for the method dependent steps in the recognition tool-chain.

The number of times a processing step is executed varies between the different approaches. for example the fixed angle approach does not need any pattern normalization, whereas MPER-120°/3 needs to execute it three times (it acquires three samples for recognition). Table 6 lists how often each step needs to be executed for the different approaches. The runtimes determined for the different approaches are given in Table 7. The first line holds the results for a single perspective system without any rotation detection or compensation. One recognition attempt for PC and WLD needs only around 50 ms whereas for MC one try takes 315 ms. These results also serve as a reference for calculating the relative increase of the runtimes (RI) of the other methods. RI is calculated as

$$RI = \frac{t_{cur} - t_{ref}}{t_{ref}} \tag{2}$$

where t_{ref} is the execution time of the reference method (single-perspective system without rotation correction) and t_{cur} the time of the evaluated system, respectively.

The runtime for the fixed angle approach increases only minimally by two comparisons and the three scores MaxSLF. Combining the fixed angle approach with EPN adds another 78 ms, which more than doubles the execution time for PC and WLD. MPE 45° is slightly slower than *No Correction* and the *Fixed Angle* approach, but considerable faster than *Fixed Angle* combined with EPN. This is due to the additional comparisons and CPN (CPN is faster than EPN). PM-MPE 60° is, due to the additional comparisons to the pseudo perspectives, slower than MPE 45°, but still faster than *Fixed Angle* with EPN. As a result of the additionally captured probe samples, the two MPER setups, MPER-90°/2 and MPER-120°/3, are noticeably slower than the other approaches. However, MPER-90°/2 is still faster than *Fixed Angle* combined with EPN for PC and WLD.

All three multi-camera systems (MPE, PM-MPE and MPER) have the potential to improve their runtimes by means of parallelization. With the exception of the MaxSLF, all steps can be carried out in parallel. With (PM-)MPE, this affects only the comparison step, with MPER also the processing steps of the input images (CPN, PP, FE). Table 6 shows how often the work steps will be carried out simultaneously and therefore indicate the possible time savings. If the execution times are calculated without taking overhead costs into consideration, this would result for the same runtimes for all three approaches. The resulting runtime would be comparable to that of a single perspective system without rotation correction or the fixed angle approach. This clearly shows that all three approaches have the potential to be used in real-world applications.

TABLE 6 Number of times each single step needs to be executed for one recognition attempt of the different approaches

Method	PN	PP	FE	CMP	MaxSLF
No correction	-	1	1	1	-
Fixed angle	-	1	1	3	3
Fixed angle + EPN	1	1	1	3	3
MPE 45°	1	1	1	8	8
PM-MPE 60°	1	1	1	18	18
MPER-90°/2	2	2	2	8	8
MPER-120°/3	3	3	3	9	9

TABLE 7 The average time needed for a single comparison using the given recognition approaches. RI is the relative increase with respect to the single perspective approach without any rotation correction or compensation

	MC		PC		WLD	
Method	[s]	RI [%]	[s]	RI [%]	[s]	RI [%]
No correction	315.3	0.00	46.0	0.00	54.5	0.00
Fixed angle	322.6	2.30	52.7	14.52	61.0	11.93
Fixed angle + EPN	409.8	29.97	140.0	204.15	148.3	171.98
MPE 45°	347.6	10.25	76.4	66.01	84.3	54.59
PM-MPE 60°	383.8	21.73	109.8	138.57	116.8	114.24
MPER-90°/2	666.3	111.33	126.1	173.96	142.6	161.46
MPER-120°/3	988.7	213.55	179.1	289.17	204.1	274.30
Parallel processing	322.3	2.22	53.0	15.21	61.5	12.84

5 | DESIGN PROPOSAL FOR MPER CAPTURING DEVICES

Multi-perspective finger vein recognition systems require the acquisition of the vein pattern from different views of the finger. Currently, there exist only a few devices, for example [24–26,29], that are capable of doing so. The data used for the evaluation of MPER was not acquired using a dedicated

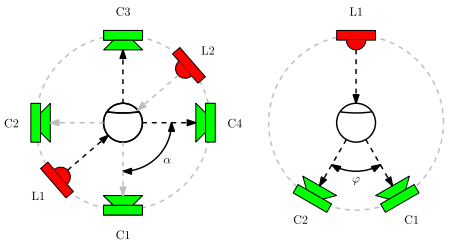

FIGURE 10 Possible multi-camera set-ups for MPER-90°/2. Left: The enrolment device consists of four cameras that acquire the vein pattern all around the finger. The cameras are spaced equally distanced all around the finger. Right: The two cameras of the recognition device cover the range between two enrolment cameras

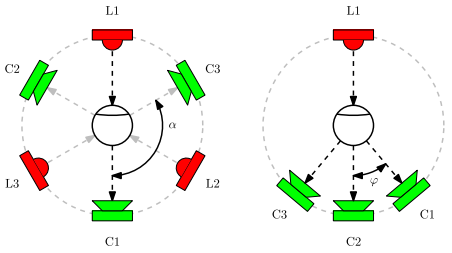

FIGURE 11 Possible multi-camera set-ups for MPER-120°/3. Left: The enrolment device consists of tree cameras that acquires the vein pattern all around the finger. The cameras are spaced equally distanced all around the finger. Right: The three cameras of the recognition device cover the range between two enrolment cameras

capturing device, but has been simulated by taking data from the PLUSVein-FR data set. However, in order to apply MPER in practise, appropriate capturing devices are required. In this section possible sensor designs for MPER are discussed.

MPER-90°/2 needs a four-camera device for enrolment and a two camera one for recognition, respectively. For MPER-120°/3 two three-camera devices are required. Figure 10 shows the possible sensor designs for MPER-90°/2. For the enrolment device (left), each of the four acquired perspectives has its own camera (*C1*–*C4*). They are placed equidistant with a rotational distance of 90° between each other. There is only one illumination module (*L1* and *L2*) for every two cameras. It is placed on the opposite side of the relevant cameras. *L1* illuminates the finger for *C3* and *C4* and *L2* for *C1* and *C2*, respectively. The angle of incidence from the illumination modules to the relevant cameras is $\frac{\alpha}{2}$. The recognition device on the right side consists of one illumination module and two cameras. The two cameras (*C1* and *C2*) are placed $\varphi = 45°$ from each other. The illumination module is positioned in a way, that the angle of incidence to both cameras is $\frac{\varphi}{2} = 22.5°$.

Possible designs of the sensors needed for MPER-120°/3 are visualized in Figure 11. For the enrolment device (left), the three cameras are positioned equally distanced with $\alpha = 120°$ at 0°, 120° and 240°. Every camera has its own illumination module which is placed on the opposite side of the finger. The recognition device on the right side consists of one illumination module and three cameras. One camera (*C2*) is placed opposite of the illumination module. The two other cameras (*C1* and *C3*) are rotated by $\varphi = 40°$ from *C2* to the right and the left. Similar devices have already been built: The enrolment device corresponds to that of SCUT [26] and the recognition device to the one of GlobalID [25], respectively.

6 | CONCLUSION

We presented the novel multi-camera finger vein recognition system MPER. The system acquires multiple perspectives for enrolment and recognition. The capturing devices used are designed in such a way that the rotational distance between the closest enrolment and recognition sample as well as the number of perspectives involved is kept to a minimum. As a result of this the two capturing devices differ. The experiments showed that rotation invariance can be achieved by using as little as three cameras in both devices. The processing steps are very simple. In the course of biometric recognition, the binarized vein pattern of all enrolment and probe samples are compared with each other. The final biometric candidate score is determined by applying a maximum rule score level fusion. The simplicity of the processing chain is also a strength of the proposed method. In contrast to other more sophisticated multi-camera recognition systems, for example [26], implementations for all processing steps (pre-processing, feature extraction and biometric comparison) are available (besides others also the one presented in [40]). The runtime analysis showed that MPER achieves comparable results with existing solutions and has the potential to be used in real-world applications.

The capturing devices for MPER were not actually built but have been simulated using the PLUSVein-FR dataset. This allowed us to evaluate a lot of different sensor configurations. Interestingly it turned out that for some of the configurations, sensors built for other recognition schemes could be used. For example, for MPER-120°/3 the sensor built by SCUT [26] can be used for enrolment and the one proposed by GlobalID [25] for recognition.

A drawback of multi-camera recognition systems compared to traditional single-camera systems is the increased cost and complexity of the capturing devices. Depending on the application, one has to decide which of the factors is more important. Systems that operate in a controlled environment, in which all users are cooperative and habituated, single-camera systems will be sufficient. The more freedom the user is given during acquisition (contactless, on-the-move), the more finger misplacements, including longitudinal finger rotation, will occur. In such environments, the added cost and complexity of using multi-camera systems will be justified.

Comparison with other multi-camera recognition systems shows how important the positioning of the cameras is.

Recognition systems that acquire multiple vein images for enrolment, but just a single one for recognition [27,28] achieve similar recognition rates all around the finger than MPER. The advantage of such a system is that the cost of the sensors used for recognition (using only a single camera) is kept low. However, the devices for enrolment (requiring at least six cameras) are complex and expensive. Comparison with capturing devices of recognition systems, which also use multi-camera devices for both, registration and recognition, shows the importance of the arrangement of the cameras. Like MPER-120°/3, all three investigated systems [24–26] use three cameras for both devices. When using the same methodology as proposed for MEPR for all sensors, only MPER-120°/3 achieves rotational invariance.

In our future work we plan to actually build the capturing devices needed for MPER-90°/2 and MPER-120°/3, and put the systems into operation. We will focus on the usability of the system, especially the time needed for a recognition attempt will be optimized for real world applications. Furthermore, we want to analyse existing multi-camera systems, using the originally proposed algorithms, with respect to their rotational invariance. Furthermore, motivated by the work of Kang et al. [26] and Xie and Kumar [45], we want to evaluate the rotation invariance of CNN-based recognition systems and, if they show good performance, whether such systems can help to simplify the required capturing devices (reduce the number of needed perspectives).

ACKNOWLEDGEMENT

This project was partly funded by the FFG KIRAS project AUTFingerATM under grant No. 864785 and the FWF project 'Advanced Methods and Applications for Fingervein Recognition' under grant No. P 32201-NBL.

ORCID

Bernhard Prommegger https://orcid.org/0000-0003-4002-2602

REFERENCES

1. Uhl, A., et al.: Handbook of Vascular Biometrics. Advances in Computer Vision and Pattern Recognition. Springer Nature Switzerland AG, Cham, Switzerland (2019)
2. Uhl, A.: State of the art in vascular biometrics. In: A., Uhl, et al. (eds.), Handbook of Vascular Biometrics, Chapter 1, pp. 3–61.Springer Nature Switzerland AG, Cham, Switzerland (2019)
3. Jin, Y., Suh, K.H., Lee, E.C.: Detecting fake finger-vein data using remote photoplethysmography. Electronics. 8(9), 1016 (2019).Bok
4. Raghavendra, R., Busch, C.: Exploring dorsal finger vein pattern for robust person recognition. In: 2015 International Conference on Biometrics (ICB), pp. 341–348, (2015)
5. Hassner, T., et al.: Effective face frontalization in unconstrained images. In: 2015 IEEE Conference on Computer Vision and Pattern Recognition (CVPR), pp. 4295–4304.(2015)
6. Yin, X., et al.: Towards large-pose face frontalization in the wild. In: 2017 IEEE International Conference on Computer Vision (ICCV), pp. 4010–4019 (2017)
7. Labati, R.D., et al.: Contactless fingerprint recognition: a neural approach for perspective and rotation effects reductionIn 2013 IEEE Symposium on Computational Intelligence in Biometrics and Identity Management (CIBIM), pp. 22–30.(2013)
8. Tan, H., Kumar, A.: Towards more accurate contactless fingerprint minutiae extraction and pose-invariant matching. IEEE Trans. Inf. Forensics Secur. 15, 3924–3937 (2020)
9. Daugman, J.: How iris recognition works. IEEE Trans. Circ. Syst. Video Technol. 14(1), 21–30 (2004)
10. Matsuda, Y., et al.: Walk through-style multi-finger vein authentication. In: 2017 IEEE International Conference on Consumer Electronics (ICCE), pp. 438–441, (2017)
11. Kauba, C., Prommegger, B., Uhl, A.: Combined fully contactless finger and hand vein capturing device with a corresponding dataset. Sensors, 19(22), 1–25 (2019)
12. Kuzu, R.S., et al.: On-the-fly finger-vein-based biometric recognition using deep neural networks. IEEE Trans. Inf. Forensics Secur. 15, 2641–2654 (2020)
13. Lee, E.C., Lee, H.C., Kang, R.P.: Finger vein recognition using minutia-based alignment and local binary pattern-based feature extraction. Int. J. Imag. Syst. Technol. 19(3), 179–186 (2009)
14. Huang, B., et al.: Finger-vein authentication based on wide line detector and pattern normalisation. In: 2010 20th International Conference on Pattern Recognition (ICPR), pp. 1269–1272.IEEE (2010)
15. Kumar, A., Zhou, Y.: Human identification using finger images. IEEE Trans. Imag. Process. 21(4), 2228–2244 (2012)
16. Matsuda, Y., et al.: Finger-vein authentication based on deformation-tolerant feature-point matching. Mach. Vis. Appl. 27(2), 237–250 (2016)
17. Lu, Y., et al.: Finger vein recognition with anatomy structure analysis. IEEE Trans. Circ. Syst. Video Technol.(1–1) (2017)
18. Chen, Q., et al.: DFVR: deformable finger vein recognition. In: 2017 IEEE International Conference on Acoustics, Speech and Signal Processing (ICASSP), pp. 1278–1282, (2017)
19. Yan, K., Sukthankar, R.: PCA-SIFT: a more distinctive representation for local image descriptors. In Proceedings of the 2004 IEEE Computer Society Conference on Computer Vision and Pattern Recognition, 2004. CVPR 2004., Vo. 2, pp. II. (2004)
20. Kim, J., et al.: Deformable spatial pyramid matching for fast dense correspondences. In 2013 IEEE Conference on Computer Vision and Pattern Recognition, 2307–2314 (June 2013)
21. Chen, Q., et al.: Geometric shape analysis based finger vein deformation detection and correction. Neurocomputing (2018).
22. Prommegger, B., et al.: Longitudinal finger rotation – deformation detection and correction. IEEE Trans. Biomet. Behav. Identity Sci. 1(2), 123–138 (2019).
23. Kauba, C., Prommegger, B., Uhl, A.: The two sides of the finger – an evaluation on the recognition performance of dorsal vs. palmar fingerveins. In: Proceedings of the International Conference of the Biometrics Special Interest Group (BIOSIG'18), Darmstadt (2018)
24. Bunda, S.: 3D point cloud reconstruction based on the finger vascular pattern. (B.S. thesis, University of Twente (2018)
25. Lambert Sonna, M., et al.: Method and device for biometric vascular recognition and/or identification. (2019)
26. Kang, W., et al.: Study of a full-view 3D finger vein verification technique. IEEE Trans. Inf. Forensics Secur, (2019)
27. Prommegger, B., Uhl, A.: Rotation invariant finger vein recognition. In: Proceedings of the IEEE 10th International Conference on Biometrics: Theory, Applications, and Systems (BTAS2019), Tampa (2019)
28. Prommegger, B., Uhl, A.: Perspective multiplication for multi-perspective enrolment in finger vein recognition. In: Proceedings of the 18th International Conference of the Biometrics Special Interest Group (BIOSIG'19), Darmstadt (2019)
29. Prommegger, B., Kauba, C., Uhl, A.: Multi-perspective finger-vein biometrics. In: Proceedings of the IEEE 9th International Conference on Biometrics: Theory, Applications, and Systems (BTAS2018), Los Angeles (2018)
30. Prommegger, B., Kauba, C., Uhl, A.: Longitudinal finger rotation – problems and effects in finger-vein recognition. In: Proceedings of the International Conference of the Biometrics Special Interest Group (BIOSIG'18), Darmstadt (2018)
31. Prommegger, B., Kauba, C., Uhl, A.: On the extent of longitudinal finger rotation in publicly available finger vein data setsIn Proceedings of the

12th IAPR/IEEE International Conference on Biometrics (ICB'19), Crete, Greece, pp. 1–8.(2019)
32. Miura, N., Nagasaka, A., Miyatake, T.: Extraction of finger-vein patterns using maximum curvature points in image profiles. IEICE Trans. Inform. Syst. 90(8), 1185–1194 (2007)
33. Lu, Y., et al.: Robust finger vein ROI localization based on flexible segmentation. Sensors. 13(11), 14339–14366 (2013).XiePark
34. Zhang, J., Yang, J.: Finger-vein image enhancement based on combination of grey-level grouping and circular gabor filter. In: ICIECS 2009. International Conference onInformation Engineering and Computer Science, pp. 1–4.IEEE (2009)
35. Zuiderveld, K.: Contrast limited adaptive histogram equalization. In: Heckbert, P.S. (ed.) Graphics Gems IV, pp. 474–485.Morgan Kaufmann (1994).
36. Maio, D., et al.: FVC2004: third fingerprint verification competition.In ICBA, volume 3072 of LNCS,pp. 1–7.Springer Verlag (2004)
37. Wimmer, G., Prommegger, B., Uhl, A.: Finger vein recognition and intra-subject similarity evaluation of finger veins using the CNN triplet loss. In Proceedings of the 25th International Conference on Pattern Recognition (ICPR), pp. 1–7, (2020)
38. Iandola, F.N., et al.: SqueezeNet: AlexNet-level accuracy with 50× fewer parameters and <1 mb model size. CoRR, abs/1602.07360, (2016)
39. Schroff, F., Kalenichenko, D., Philbin, J.: Facenet: a unified embedding for face recognition and clustering. In 2015 IEEE Conference on Computer Vision and Pattern Recognition (CVPR), pp. 815–823.(2015)
40. Kauba, C., Uhl, A.: An available open-source vein recognition framework. In A. Uhl, C. Busch, S. Marcel, and R. Veldhuis, editors, Handbook of Vascular Biometrics, Chapter 4, pp. 113–142.Springer Nature Switzerland AG, Cham, Switzerland (2019)
41. Prommegger, B., Uhl, A.: Advanced multi-perspective enrolment in finger vein recognition.In Proceedings of the 8th International Workshop on Biometrics and Forensics (IWBF'20), Porto, Portugal, pp. 1–6. (2020)
42. Choi, J.W., et al.: Finger vein extraction using gradient normalisation and principal curvature. Image Process. Mach. Vis. Appl. II, volume 7251, pages 7251 – 7251 – 9, 2009.
43. Kauba, C., Reissig, J., Uhl, A.: Pre-processing cascades and fusion in finger vein recognition.In: Proceedings of the International Conference of the Biometrics Special Interest Group (BIOSIG'14), Darmstadt, Germany (2014)
44. Miura, N., Nagasaka, A., Miyatake, T.: Feature extraction of finger-vein patterns based on repeated line tracking and its application to personal identification. Mach. Vis. Appl. 15(4), 194–203 (2004)
45. Xie, C., Kumar, A.: Finger vein identification using convolutional neural network and supervised discrete hashing. Pattern Recogn. Lett. 119, 148–156 (2019). Deep Learning for Pattern Recognition

How to cite this article: Prommegger B, Uhl A. A fully rotation invariant multi-camera finger vein recognition system. *IET Biom*. 2021;1−15. https://doi.org/10.1049/bme2.12019

4. Conclusion

Finger vein biometrics recognise human subjects based on the vascular pattern inside the finger. In almost all commercial and scientific systems, the vein structure is acquired only for a single finger using a single camera, preferably from the palmar view. There is very little work on other perspectives. This theses addresses this problem and examines all perspectives around the finger.

A general problem in biometrics is the availability of suitable data sets. For most modalities, large databases with high quality images are rarely available. This problem is even worse in finger vein biometrics since commercial sensors typically do not give access to the raw images, but only to already processed proprietary templates. Therefore, in the course of this theses, several finger vein capturing devices were built and used to acquire corresponding data sets. Particular attention was paid to being able to capture the vein pattern also from other perspectives than the commonly used palmar view as well as to contactless acquisition. The published data sets are: (1) The PLUSVein-FV3 data set consisting of palmar and dorsal finger vein images captured with the Laser and LED version of the *PLUS OpenVein Finger Vein Sensor*. For this sensor all information to build and operate the device, e.g. technical drawings, control board schematics or the capturing software, are available free of charge. (2) The PLUSVein-FR which provides vein images all around the finger in steps of 1°, and (3) the PLUSVein-CL consisting of hand and finger vein images captured in an contactless acquisition scenario. All acquired data sets are available to the scientific public free of charge.

The analysis of perspectives other than the typically used palmar view showed that it is also possible to use them for recognition. The best results are actually achieved for the palmar view followed by the dorsal region. Although the perspectives inbetween those two regions show inferior performance, they still deliver good enough results to perform recognition. The worst results are achieved when the finger is turned by $\pm 90°$ from the palmar view. In further analysis we showed that multi-perspective and multi-algorithm fusion as well as combinations of both significantly improve the recognition rates.

In order to show that longitudinal finger rotation in finger vein recognition is not only a scientific problem but also occurs in real systems, we examined four publicly available finger vein data sets for the extent to which they contain such rotations. The results showed that every data set contains longitudinal rotation and revealed rotational distances of up to 77° (!) between two samples of the same finger. The extent depends on the capturing device itself and the acquisition protocol (e.g. supervised vs unsupervised acquisition). These results show, that there is definitely a need for rotation tolerant recognition systems. As a result of this we proposed two different rotation correction and compensation schemes and compared their performance to state of the art systems. The first approach "*known angle*" improves the rotation tolerance by rotating the probe sample in direction of the enrolment sample using the actual angle of rotation. This method is only applicable if the actual angle of rotation is known. As this is not the case in normal acquisition scenarios, the rotation angle needs to be estimated. For this purpose we presented a CNN based rotation estimator. The second approach "*fixed angle*" reduces the rotational distance by rotating the enrolment sample in both direction using a pre-defined angle. Both methods are capable of increasing the tolerance to longitudinal rotations and outperform existing solutions. But still, for rotation angles larger than $\pm 30°$ recognition is not useful any more.

For finger vein recognition, especially in contactless acquisition scenarios, it would be desirable to get invariant to longitudinal rotation. We proposed four multi-camera systems that are capable of doing so. The first one, *Perspective Cumulative Finger Vein Templates* combines multiple perspectives acquired during enrolment to a single template to which a single probe image is compared. The other three methods, *Multi-Perspective Enrolment*, *Perspective Multiplication for Multi-Perspective Enrolment* and *Combined Multi-Perspective Enrolment and Recognition*, also acquire multiple finger vein images but evaluate them independent from each other. The final biometric candidate score is calculated using a *maximum rule score level fusion*. A major advantage of all four methods is that they use simple building blocks (preprocessing, vein pattern based feature extraction, correlation based comparison and score level fusion) for which implementations are publicly available. A runtime analysis showed, that the latter three methods can be applied in real-world applications.

4.1. Issues and open challenges

A general problem in biometrics is the availability of large high quality data sets. In finger vein recognition this problem is even worse as most commercial sensors to not provide access to the raw images. Therefore, we designed and built several finger vein sensors and acquired corresponding data sets. But this does not solve the problem completely as the size as well as the diversity (e.g. age and origin of the acquired subjects) of our data sets is still limited. If scientific institutions all over the world would acquire finger vein images with the same capturing device, then these independent data sets could be merged into a large global data set. With this idea in mind, we decided to publish all information necessary to build and operate our *PLUS OpenVein Finger Vein Sensor*. The task now is to get other organisations to acquire data using our sensor. The project already started by acquiring data at our University and as part of the PROTECT project.

Another problem is that currently available commercial (single camera) finger vein recognition systems are prone to performance degradations due to longitudinal finger rotations. It is possible to increase the rotation tolerance by introducing pattern normalisation or more sophisticated comparison algorithms, but the rotation angles that are tolerated by such systems are still limited. Essentially there are two possibilities to solve this problem: (1) by developing new or improving existing algorithms in order that they are more tolerant to rotation or (2) acquiring the vein pattern from multiple perspectives in order to get the vein information from a larger area. The development of new or improved methods is usually associated with an increased complexity of the algorithms. Multi-camera systems already achieve rotational invariance, but the work in this area still needs to be continued. For example, for some of the methods the capturing devices are still complex. One would need to evaluate if the complexity can be reduced by e.g. a different selection of the acquired perspectives, the use of different recognition toolchains or whether one can restrict the range in which such systems must be able to tolerate longitudinal rotation.

With regard to other recognition toolchains, only systems that are inherently more tolerant to longitudinal rotation than those evaluated up to now are suitable candidates. Given the promising results from our rotation detector, we believe that CNN-based systems can be a promising alternative. A problem with CNNs in finger vein recognition is, that many of the proposed systems use CNNs with in-built classifiers like e.g. SoftMax and therefore operate in a closed set environment [12, 51, 33]. Such systems show the potential of CNN based systems, but cannot be applied in practical biometric applications since theses systems are only able to identify classes that were including in the training set. If new subjects are added, the CNN needs to be re-trained. Contrary to this, CNN based finger vein recognition systems operating in an open

set environment do not directly classify the input images but compute a similarity measure between two samples. The similarity measure is than compared to a system wide threshold in order to determine whether the two input images are from the same class (genuine comparison) or not (impostor comparison) [18, 19, 56, 55]. It has been shown in e.g. [50] that the achieved recognition rates of experiments in an open set scenario are noticeably inferior to those in an closed set scenario.

When it comes to restricting the rotational range, in which a systems needs to be rotation tolerant, the application scenario itself is very important. If it operates in a controlled environment with cooperative and habituated users, even existing single-camera systems might be sufficient. But with increased degrees of freedom (e.g. contactless or on-the-move recognition), also the misplacements of the finger (including longitudinal finger rotation) will increase. For such systems added cost and complexity for capturing devices as well as more sophisticated algorithms can be justified.

It also needs to be noted that the data used in the experiments analysing the proposed multi-camera recognition systems was not acquired using dedicated capturing devices, but simulated using data from the PLUSVein-FR. For a final assessment of the proposed systems, the required capturing devices would have to be built and an evaluation performed using data acquired with these devices.

But rotational tolerance or invariance in not the only property that is of interest when developing next generation capturing devices. The trend in hand based vascular biometrics is towards contactless acquisition (e.g. [1, 25]), most probably in walk-through scenarios (e.g. [36, 33, 15]), and the use of mobile devices for data acquisition (e.g. [13, 16]). The greatest challenges in such scenarios will be achieving an uniform illumination of the object to be acquired, insensitivity to the varying NIR portion in the environmental light (e.g. from the sunlight), and misplacements due to the increasing number of freedom when presenting the hand or finger to the device. The current situation with the COVID-19 pandemic may further accelerate this trend [17].

Bibliography

[1] Datasheet: Fujitsu PalmSecure Contactless Biometric Authentication. https://www.fujitsu.com/global/Images/PalmSecure_Datasheet.pdf, 03 2011. Accessed 11 March 2021.

[2] Finger vein technology for Bank BPH (Poland). https://www.hitachi.eu/en/case-studies/finger-vein-technology-bank-bph-poland, 03 2013. Accessed 3 Feb 2020.

[3] Uk banking customers ready for finger biometrics authentication. *Biometric Technology Today*, 2014(9):3 – 12, 2014.

[4] Hitachi-Omron Terminal Solutions, Corp (2018) Taiwan's CTBC bank adopts finger vein authentication solution for ATMs - Hitachi News. https://www.hitachi-omron-ts.com/news/pdf/201607-001.pdf, 07 2016. Accessed 3 Feb 2020.

[5] M. S. M. Asaari, S. A. Suandi, and B. A. Rosdi. Fusion of band limited phase only correlation and width centroid contour distance for finger based biometrics. *Expert Systems with Applications*, 41(7):3367–3382, 2014.

[6] R. M. Bolle, J. H. Connell, S. Pankanti, N. K. Ratha, and A. W. Senior. *Guide to Biometrics*. Springer, New York, NY, 2004.

[7] S. Bunda. 3D point cloud reconstruction based on the finger vascular pattern. B.S. thesis, University of Twente, 2018.

[8] Q. Chen, L. Yang, G. Yang, and Y. Yin. Geometric shape analysis based finger vein deformation detection and correction. *Neurocomputing*, 2018.

[9] Q. Chen, L. Yang, G. Yang, Y. Yin, and X. Meng. DFVR: Deformable finger vein recognition. In *2017 IEEE International Conference on Acoustics, Speech and Signal Processing (ICASSP)*, pages 1278–1282, March 2017.

[10] J. H. Choi, W. Song, T. Kim, S.-R. Lee, and H. C. Kim. Finger vein extraction using gradient normalization and principal curvature. In *Image Processing: Machine Vision Applications II*, volume 7251, pages 7251 – 7251 – 9, 2009.

[11] R. Clarke. Human identification in information systems: Management challenges and public policy issues. *Information Technology & People*, 7(4):6–37, Dec. 1994.

[12] R. Das, E. Piciucco, E. Maiorana, and P. Campisi. Convolutional neural network for finger-vein-based biometric identification. *IEEE Transactions on Information Forensics and Security*, 14(2):360–373, Feb 2019.

[13] L. Debiasi, C. Kauba, B. Prommegger, and A. Uhl. Near-infrared illumination add-on for mobile hand-vein acquisition. In *2018 IEEE 9th International Conference on Biometrics Theory, Applications and Systems (BTAS)*, pages 1–9, 2018.

[14] P. Drozdowski, B. Prommegger, G. Wimmer, R. Schraml, C. Rathgeb, A. Uhl, and C. Busch. Demographic Bias: A Challenge for Fingervein Recognition Systems? In *2020 28th European Signal Processing Conference (EUSIPCO)*, pages 825–829, Amsterdam, The Nederlands, 2021.

[15] C. Galdi, J. Boyle, L. Chen, V. Chiesa, L. Debiasi, J.-L. Dugelay, J. Ferryman, A. Grudzień, C. Kauba, S. Kirchgasser, M. Kowalski, M. Linortner, P. Maik, K. Michoń, L. Patino, B. Prommegger, A. F. Sequeira, Łukasz Szklarski, and A. Uhl. Protect: Pervasive and user focused biometrics border project – a case study. *IET Biometrics*, 9(6):297–308, 2020.

[16] R. Garcia-Martin and R. Sanchez-Reillo. Vein biometric recognition on a smartphone. *IEEE Access*, 8:104801–104813, 2020.

[17] M. Gomez-Barrero, P. Drozdowski, C. Rathgeb, J. Patino, M. Todisco, A. Nautsch, N. Damer, J. Priesnitz, N. Evans, and C. Busch. Biometrics in the era of covid-19: Challenges and opportunities, 2021.

[18] H. G. Hong, M. B. Lee, and K. R. Park. Convolutional neural network-based finger-vein recognition using nir image sensors. *Sensors*, 17(6), 2017.

[19] Houjun Huang, S. Liu, H. Zheng, L. Ni, Yi Zhang, and W. Li. Deepvein: Novel finger vein verification methods based on deep convolutional neural networks. In *2017 IEEE International Conference on Identity, Security and Behavior Analysis (ISBA)*, pages 1–8, Feb 2017.

[20] B. Huang, Y. Dai, R. Li, D. Tang, and W. Li. Finger-vein authentication based on wide line detector and pattern normalization. In *Pattern Recognition (ICPR), 2010 20th International Conference on*, pages 1269–1272. IEEE, 2010.

[21] ISO/IEC JTC 1/SC 37 Biometrics. ISO/IEC 2382-37:2017(E). Information Technology - Vocabulary - Biometrics, 2017.

[22] W. Kang, H. Liu, W. Luo, and F. Deng. Study of a full-view 3D finger vein verification technique. *IEEE Transactions on Information Forensics and Security*, pages 1–1, 2019.

[23] C. Kauba, B. Prommegger, and A. Uhl. Focussing the beam - a new laser illumination based data set providing insights to finger-vein recognition. In *2018 IEEE 9th International Conference on Biometrics Theory, Applications and Systems (BTAS)*, pages 1–9, 2018.

[24] C. Kauba, B. Prommegger, and A. Uhl. The two sides of the finger - an evaluation on the recognition performance of dorsal vs. palmar finger-veins. In A. Brömme, C. Busch, A. Dantcheva, C. Rathgeb, and A. Uhl, editors, *BIOSIG 2018 - Proceedings of the 17th International Conference of the Biometrics Special Interest Group*, Bonn, 2018. Köllen Druck+Verlag GmbH.

[25] C. Kauba, B. Prommegger, and A. Uhl. Combined fully contactless finger and hand vein capturing device with a corresponding dataset. *Sensors*, 19(22)(5014), 2019.

[26] C. Kauba, B. Prommegger, and A. Uhl. *OpenVein—An Open-Source Modular Multipurpose Finger Vein Scanner Design*, pages 77–111. Springer International Publishing, Cham, 2020.

[27] C. Kauba, J. Reissig, and A. Uhl. Pre-processing cascades and fusion in finger vein recognition. In *Proceedings of the International Conference of the Biometrics Special Interest Group (BIOSIG'14)*, Darmstadt, Germany, sep 2014.

[28] J. Kim, H.-J. Kong, S. Park, S. Noh, S.-R. Lee, T. Kim, and H. C. Kim. Non-contact finger vein acquisition system using NIR laser. In E. Bodegom and V. Nguyen, editors, *Sensors, Cameras, and Systems for Industrial/Scientific Applications X*, volume 7249, pages 249 – 256. International Society for Optics and Photonics, SPIE, 2009.

[29] S. Kirchgasser, C. Kauba, and A. Uhl. *Towards Understanding Acquisition Conditions Influencing Finger Vein Recognition*, pages 179–199. Springer International Publishing, Cham, 2020.

[30] M. Kono, H. Ueki, and S. Umemura. Near-infrared finger vein patterns for personal identification. *Applied Optics*, 41(35):7429–7436, 2002.

[31] A. Kumar and C. Ravikanth. Personal authentication using finger knuckle surface. *IEEE Transactions on Information Forensics and Security*, 4(1):98–110, 2009.

[32] A. Kumar and Y. Zhou. Human identification using finger images. *IEEE Transactions on Image Processing*, 21(4):2228–2244, April 2012.

[33] R. S. Kuzu, E. Piciucco, E. Maiorana, and P. Campisi. On-the-fly finger-vein-based biometric recognition using deep neural networks. *IEEE Transactions on Information Forensics and Security*, pages 1–1, 2020.

[34] Y. Lu, S. Yoon, and D. S. Park. Finger vein identification system using two cameras. *Electronics Letters*, 50(22):1591–1593, 2014.

[35] Y. Matsuda, N. Miura, A. Nagasaka, H. Kiyomiu, and T. Miyatake. Finger-vein authentication based on deformation-tolerant feature-point matching. *Machine Vision and Applications*, 27(2):237–250, 2016.

[36] Y. Matsuda, N. Miura, Y. Nonomura, A. Nagasaka, and T. Miyatake. Walkthrough-style multi-finger vein authentication. In *2017 IEEE International Conference on Consumer Electronics (ICCE)*, pages 438–441, 2017.

[37] N. Miura, A. Nagasaka, and T. Miyatake. Extraction of finger-vein patterns using maximum curvature points in image profiles. *IEICE transactions on information and systems*, 90(8):1185–1194, 2007.

[38] B. Prommegger, C. Kauba, M. Linortner, and A. Uhl. Longitudinal finger rotation—deformation detection and correction. *IEEE Transactions on Biometrics, Behavior, and Identity Science*, 1(2):123–138, 2019.

[39] B. Prommegger, C. Kauba, and A. Uhl. Longitudinal finger rotation - problems and effects in finger-vein recognition. In A. Brömme, C. Busch, A. Dantcheva, C. Rathgeb, and A. Uhl, editors, *BIOSIG 2018 - Proceedings of the 17th International Conference of the Biometrics Special Interest Group*, Bonn, 2018. Köllen Druck+Verlag GmbH.

[40] B. Prommegger, C. Kauba, and A. Uhl. Multi-perspective finger-vein biometrics. In *2018 IEEE 9th International Conference on Biometrics Theory, Applications and Systems (BTAS)*, 2018.

[41] B. Prommegger, C. Kauba, and A. Uhl. On the extent of longitudinal finger rotation in publicly available finger vein data sets. In *2019 International Conference on Biometrics (ICB)*, pages 1–8, 2019.

[42] B. Prommegger, C. Kauba, and A. Uhl. *Different Views on the Finger - Score-Level Fusion in Multi-Perspective Finger Vein Recognition*, pages 261–305. Springer International Publishing, Cham, 2020.

[43] B. Prommegger and A. Uhl. Perspective multiplication for multi-perspective enrolment in finger vein recognition. In A. Brömme, C. Busch, A. Dantcheva, C. Rathgeb, and A. Uhl, editors, *BIOSIG 2019 - Proceedings of the 18th International Conference of the Biometrics Special Interest Group*, pages 107–117, Bonn, 2019. Gesellschaft für Informatik e.V.

[44] B. Prommegger and A. Uhl. Rotation invariant finger vein recognition. In *2019 IEEE 10th International Conference on Biometrics Theory, Applications and Systems (BTAS)*, pages 1–9, 2019.

[45] B. Prommegger and A. Uhl. Advanced multi-perspective enrolment in finger vein recognition. In *2020 8th International Workshop on Biometrics and Forensics (IWBF)*, pages 1–6, 2020.

[46] B. Prommegger and A. Uhl. A fully rotation invariant multi-camera finger vein recognition system. *IET Biometrics*, pages 1–15, 2021.

[47] B. Prommegger, G. Wimmer, and A. Uhl. Rotation detection in finger vein biometrics using cnns. In *Proceedings of the 25th International Conference on Pattern Recognition (ICPR)*, pages 1–7, 2020.

[48] R. Raghavendra and C. Busch. Exploring dorsal finger vein pattern for robust person recognition. In *2015 International Conference on Biometrics (ICB)*, pages 341–348, 2015.

[49] J. Rice. Method and apparatus for the identification of individuals. *WIPO (PCT) Patent*, (WO/1985/004088), 09 1985.

[50] R. Salih Kuzu, E. Maiorana, and P. Campisi. Loss functions for cnn-based biometric vein recognition. In *2020 28th European Signal Processing Conference (EUSIPCO)*, pages 750–754, 2021.

[51] J. M. Song, W. Kim, and K. R. Park. Finger-vein recognition based on deep densenet using composite image. *IEEE Access*, 7:66845–66863, 2019.

[52] L. Sonna Momo, L. Cerqueira Torres, S. Marcel, A. Anjos, M. Liebling, A. Shajkofci, S. Amoos, A. Woeffray, A. Sierro, P. Roduit, P. Ferez, and L. Bonvin. Method and device for biometric vascular recognition and/or identification, 08 2019.

[53] B. T. Ton and R. N. J. Veldhuis. A high quality finger vascular pattern dataset collected using a custom designed capturing device. In *2013 International Conference on Biometrics (ICB)*, pages 1–5, 2013.

[54] A. Uhl. *State of the Art in Vascular Biometrics*, pages 3–61. Springer International Publishing, Cham, 2020.

[55] G. Wimmer, B. Prommegger, and A. Uhl. Finger vein recognition and intra-subject similarity evaluation of finger veins using the cnn triplet loss. In *Proceedings of the 25th International Conference on Pattern Recognition (ICPR)*, pages 400–406, 2020.

[56] C. Xie and A. Kumar. Finger vein identification using convolutional neural network and supervised discrete hashing. *Pattern Recognition Letters*, 119:148 – 156, 2019.

[57] L. Yang, G. Yang, Y. Yin, and X. Xi. Finger vein recognition with anatomy structure analysis. *IEEE Transactions on Circuits and Systems for Video Technology*, pages 1–1, 2017.

[58] Y. Yin, L. Liu, and X. Sun. SDUMLA-HMT: a multimodal biometric database. *Biometric Recognition*, pages 260–268, 2011.

[59] L. Zhang, L. Zhang, and D. Zhang. Finger-knuckle-print: A new biometric identifier. In *2009 16th IEEE International Conference on Image Processing (ICIP)*, pages 1981–1984, 2009.

A. Appendix

A.1. Breakdown of Authors' Contribution

This section lists a breakdown of authors' contribution with respect to the papers included in this thesis. Andreas Uhl is/was the thesis advisor/project leader of Christof Kauba, Michael Linortner, Georg Wimmer and Bernhard Prommegger. Since the explicit contribution of an advisor/project leader cannot be stated for a single paper, it is omitted in the following breakdown.

Publication	Contribution (in %)			
	Bernhard Prommegger	Christof Kauba	Michael Linortner	Georg Wimmer
B. Prommegger, C. Kauba, and A. Uhl. Multi-perspective finger-vein biometrics. In *2018 IEEE 9th International Conference on Biometrics Theory, Applications and Systems (BTAS)*, 2018	70	30		
C. Kauba, B. Prommegger, and A. Uhl. Focussing the beam - a new laser illumination based data set providing insights to finger-vein recognition. In *2018 IEEE 9th International Conference on Biometrics Theory, Applications and Systems (BTAS)*, pages 1–9, 2018	20	80		
B. Prommegger, C. Kauba, and A. Uhl. Longitudinal finger rotation - problems and effects in finger-vein recognition. In A. Brömme, C. Busch, A. Dantcheva, C. Rathgeb, and A. Uhl, editors, *BIOSIG 2018 - Proceedings of the 17th International Conference of the Biometrics Special Interest Group*, Bonn, 2018. Köllen Druck+Verlag GmbH	50	50		
C. Kauba, B. Prommegger, and A. Uhl. The two sides of the finger - an evaluation on the recognition performance of dorsal vs. palmar finger-veins. In A. Brömme, C. Busch, A. Dantcheva, C. Rathgeb, and A. Uhl, editors, *BIOSIG 2018 - Proceedings of the 17th International Conference of the Biometrics Special Interest Group*, Bonn, 2018. Köllen Druck+Verlag GmbH	20	80		
B. Prommegger, C. Kauba, M. Linortner, and A. Uhl. Longitudinal finger rotation—deformation detection and correction. *IEEE Transactions on Biometrics, Behavior, and Identity Science*, 1(2):123–138, 2019	70	15	15	

Publication	Contribution (in %)			
	Bernhard Prommegger	Christof Kauba	Michael Linortner	Georg Wimmer
B. Prommegger, C. Kauba, and A. Uhl. On the extent of longitudinal finger rotation in publicly available finger vein data sets. In *2019 International Conference on Biometrics (ICB)*, pages 1–8, 2019	80	20		
C. Kauba, B. Prommegger, and A. Uhl. Combined fully contactless finger and hand vein capturing device with a corresponding dataset. *Sensors*, 19(22)(5014), 2019	50	50		
B. Prommegger and A. Uhl. Rotation invariant finger vein recognition. In *2019 IEEE 10th International Conference on Biometrics Theory, Applications and Systems (BTAS)*, pages 1–9, 2019	100			
B. Prommegger and A. Uhl. Perspective multiplication for multi-perspective enrolment in finger vein recognition. In A. Brömme, C. Busch, A. Dantcheva, C. Rathgeb, and A. Uhl, editors, *BIOSIG 2019 - Proceedings of the 18th International Conference of the Biometrics Special Interest Group*, pages 107–117, Bonn, 2019. Gesellschaft für Informatik e.V	100			
C. Kauba, B. Prommegger, and A. Uhl. *OpenVein—An Open-Source Modular Multipurpose Finger Vein Scanner Design*, pages 77–111. Springer International Publishing, Cham, 2020	50	50		
B. Prommegger, C. Kauba, and A. Uhl. *Different Views on the Finger - Score-Level Fusion in Multi-Perspective Finger Vein Recognition*, pages 261–305. Springer International Publishing, Cham, 2020	30	70		
B. Prommegger and A. Uhl. Advanced multi-perspective enrolment in finger vein recognition. In *2020 8th International Workshop on Biometrics and Forensics (IWBF)*, pages 1–6, 2020	100			
B. Prommegger and A. Uhl. A fully rotation invariant multi-camera finger vein recognition system. *IET Biometrics*, pages 1–15, 2021	100			
B. Prommegger, G. Wimmer, and A. Uhl. Rotation detection in finger vein biometrics using cnns. In *Proceedings of the 25th International Conference on Pattern Recognition (ICPR)*, pages 1–7, 2020	50			50